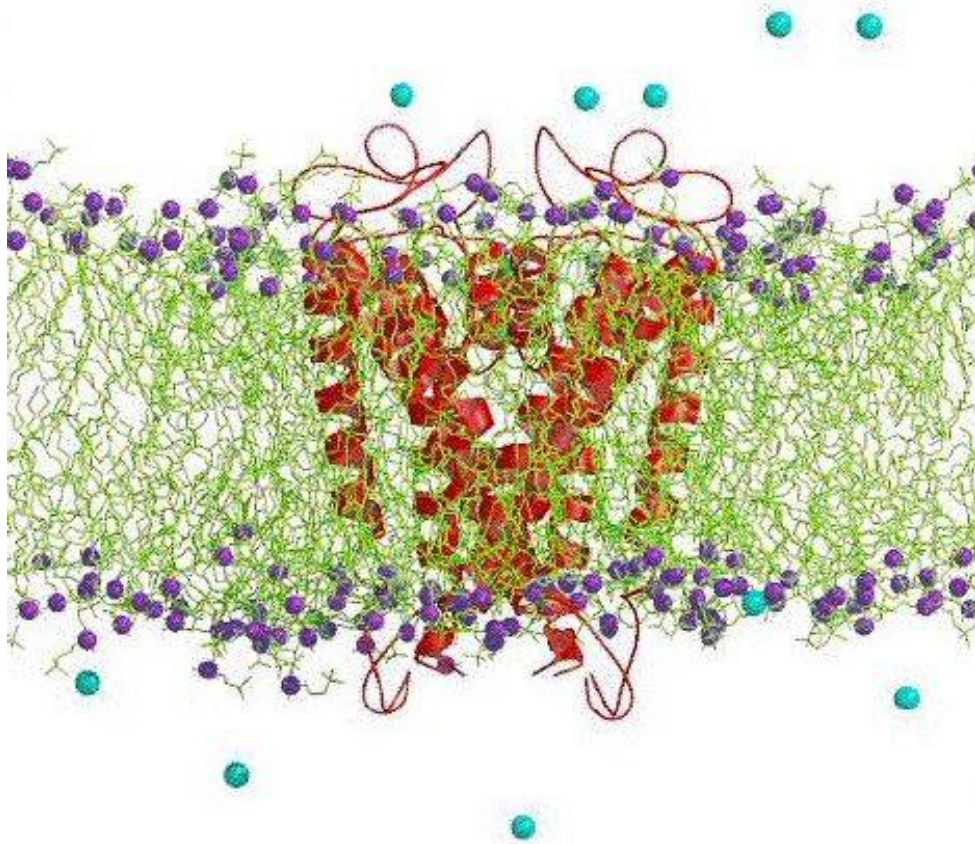# STRUCTURE-FUNCTION STUDIES OF INSECTICIDAL ATRACOTOXINS

PhD Thesis

SIMON GUNNING

UTS 2009

ABSTRACT

Part I

The κ-atracotoxins (κ-ACTXs, previously the Janus-faced atracotoxins) are a family of five insect-selective excitatory peptide neurotoxins containing 36-37 residues with four disulfide bonds. Toxins from this family were isolated from the venom of the Blue Mountains funnel-web spider (*Hadronyche versuta*) and Toowooba funnel-web spider (*Hadronyche infensa*). The NMR solution structure and primary sequence of the prototypic member κ-ATCT-Hv1c provided few clues as to the likely molecular target. In order to characterise the site of action and phylogenetic specificity of these toxins, whole-cell patch-clamp electrophysiology was employed using isolated DUM neurons from the American cockroach (*Periplaneta americana*). κ-ACTX-Hv1c had no effect on the gating or kinetics of I_{Na} or I_{Ca} at concentrations up to 1 μM. However, at the same concentration, κ-ATCT-Hv1c reduced K_v channel currents by 56 ± 7% (*n* = 5). Subsequent experiments in insect DUM neurons indicated that inhibition of the macroscopic I_K was due to a block of calcium-activated K_v (K_{Ca}) channels, with an IC_{50} of 2.3 nM and 2.9 nM for peak and late $I_{K(Ca)}$ respectively (*n* = 5), and not 'A-type' or delayed-rectifier K_v channels. Insect selectivity was confirmed by a lack of activity on rat dorsal root ganglion (DRG) neuron global I_K as well as $I_{K(Ca)}$ at doses up to 1 μM. κ-ACTX-Hv1c is a selective insect K_{Ca} (BK_{Ca}) channel pore-blocker, not a gating modifier, as inhibition of insect $I_{K(Ca)}$ occurred in the absence of any voltage-dependent actions on channel activation. Specificity for the insect BK_{Ca} channel was validated by κ-ACTX-Hv1c induced inhibition of $I_{K(Ca)}$ from the cloned insect K_{Ca} channel α-subunit (*pSlo*) expressed in HEK293 cells (IC_{50} of 240 nM). The 80-fold reduction in IC_{50}, most likely indicates that κ-ACTX-Hv1c interacts with the auxillary subunits that form part of the wild-type channel, in a manner similar to the BK_{Ca} blocker, charybdotoxin (ChTX), as previously reported. Phyletic selectivity of κ-ACTX-Hv1c was confirmed by the 9776-fold

increase in IC_{50} against *mSlo* channels. Interestingly κ-ACTX-Hv1c, like ChTX, failed to potently block the *dSlo* channel with the IC_{50} >10 μM.

Additional experiments on DUM neuron $I_{K(Ca)}$ using alanine mutants confirmed the pharmacophore of bioactive residues κ-ACTX-Hv1c comprises Arg^8, Pro^9, Val^{29} and Tyr^{31}, previously identified by acute toxicity tests in house flies (*Musca domestica*). Interestingly, the functionally critical Arg^8 and Tyr^{31} residues align extremelyç well with the Lys-Phe/Tyr diad conserved amongst structurally dissimilar K_v channel toxins, providing a possible basis for targeting of the toxin to K^+ channels. Using a panel of 8 mutants (R8E, R8Q, R8K, R8H, Y31W, Y31F, Y31L and Y31V) the mechanism of interaction was investigated further. The Arg^8 residue appears to interact with the channel via hydrogen bonding from the δ-guanido group to carbonyl groups on the extracellular surface of the channel, as evidenced by the high potency of the R8H mutant. The imidazole group of His is an adequate substitute for the δ-guanido group of arginine. In contrast the R8E, R8Q and R8K had reduced potency indicating that the positive charge of the amino group of Arg does not directly interact with the target nor is the alkyl group of Arg critical for binding to the target. The critically important Tyr^{31} interacts with the channel via non-specific hydrophobic interactions as substitution for an aromatic ring (Y31F & Y31W) maintains the potency of the toxin. In contrast substitution to small less hydrophobic side chains (Y31V, Y31L and Y31A) reduced potency. It appears therefore that Tyr^{31} in conjunction with IIe^2 and Val^{29}, that lie at either side of the primary pharmacophore, appear to act as 'gasket' residues to exclude bulk solvent from disrupting the Arg^8-channel interaction.

This study has identified κ-atracotoxins as potential lead compounds in the development of new biopesticides and validates insect BK_{Ca} channels as potential insecticide targets.

Part II

The second part of this thesis was to determine the target site for the 'hybrid' toxin FW178 from the venom of the Blue Mountains funnel-web spider (*H. versuta*). FW178 is a unique toxin that shares little homology to other known atracotoxins. In order to identify the site of action of this toxin, whole-cell patch-clamp electrophysiology was employed using isolated DUM neurons from the American cockroach (*Periplaneta americana*). FW178 failed to inhibit insect I_{Na}, $I_{K(DR)}$ or $I_{K(A)}$ at doses up to 1 µM. However, further studies demonstrated that η-ACTX-Hv1a blocks voltage-gated calcium (Ca_V) channel currents in DUM neurons as well as $K_{(Ca)}$ channel currents carried by *pSlo* channels with IC_{50} values of 409 nM and 671 nM, respectively. FW178 therefore blocks cockroach Ca_V currents with approximately the same potency as ω-ACTX-Hv1a, a known insect M-LVA and HVA Ca_V channel blocker, while it blocks cockroach *pSlo* channels with about a 4-fold lower potency than κ-ACTX-Hv1c.

Interestingly FW178 has an LD_{50} of 38 $\pm$ 3 pmol/g when injected into *M. domestica* as compared to the LD_{50} values for ω-ACTX-Hv1a (86.5 $\pm$ 1.3 pmol/g) and κ-ACTX-Hv1c (91 $\pm$ 5 pmol/g). This makes FW178 at least two-fold more potent than any other atracotoxin isolated from Australian funnel-web spiders. Despite this, FW178 only blocks cockroach Ca_V channels with a similar potency to ω-ACTX-Hv1a, and blocks cockroach $BK_{(Ca)}$ with 4-fold less potency than κ-ACTX-Hv1c. Therefore the striking potency of FW178 may result from a synergistic action to block insect Ca_V and $BK_{(Ca)}$ channels. Not surprising the pharmacophore of FW178 (refer section **4**.3) contains elements of the pharmacophore of both ω-ACTX-Hv1a and κ-ACTX-Hv1c. Thus FW178 directly block insect $K_{(Ca)}$ channels, but the toxin also enhances this action by indirectly reducing current through these channels by block of the transient inward flow of calcium through Ca_V channels. Therefore FW178 represents the first known dual-target, self-synergizing toxin and is an excellent lead compound for the development of a novel insecticide.

ACKNOWLEDGEMENTS

TABLE OF CONTENTS

LIST OF FIGURES AND TABLES

CHAPTER 1: INTRODUCTION

CHAPTER 2: ION CHANNELS AND ION CHANNEL TOXINS

CHAPTER 5: MATERIALS AND METHODS

CHAPTER 6: RESULTS

CHAPTER 7: RESULTS

CHAPTER 8: DISSCUSION

LIST OF ABBREVIATIONS

ACh	Acetylcholine
ACTX	Atracotoxin
AP	Action Potential
ATP	Adenosine tri-phosphate
α-BGT	α-Bungarotoxin
α-LTx	α-Latrotoxin
α-ScTX	α-Scorpion toxin
4-AP	4-amino pyridine
BAPTA	1,2-bis-(2-aminophenoxy)ethane-*N*,*N*,*N*,*N*-tetra acetate
BK_{Ca}	Large-conductance Ca^{2+}-activated K^+ channels
BTX	Batrachotoxin
β-Sctx	β-Scorpion toxin

CAMs	Cell adhesion molecules
CF-NIS	Ca^{2+}-free normal insect saline
CICR	Ca^{2+}-induced Ca^{2+}-release
ChTX	Charybdotoxin
CMF-PBS	Ca^{2+}-and Mg^{2+}-free phosphate buffered saline
DHP	Dihydropyridine
DRG	Dorsal Root Ganglion
DUM	Dorsal Unpaired Median
ET_{50}	Time to 50% paralysis/death
GABA	γ-aminobutyric acid
GSH	Glutathione
GST	Glutathione-S-transferase
HaTX-1	Hanatoxin-1
HEK293	Human embryonic kidney 293 cells
HpTX	Heteropodatoxin
HoTx	Hololenatoxin
IBX	Iberiotoxin
ICK	Inhibitory cystine knot
IFM	Hydrophobic triad of isoleucine, phenylalanine and methionine
Ig	Immunoglobulin
i.p	Intraperitoneal
$I_{Ca(tLVA)}$	Transient low voltage-activated calcium current
$I_{Ca(mLVA)}$	Maintained low voltage-activated calcium current
$I_{Ca(HVA)}$	High voltage-activated calcium current
$I_{Ca(r)}$	Calcium resting current
$I_{Cl(Ca)}$	Calcium-activated chloride current
$I_{K(A)}$	'A-like' potassium current
$I_{K(tCa)}$	Transient calcium-activated potassium current
$I_{K(mCa)}$	Maintained (or Late) calcium-activated potassium current
$I_{K(DR)}$	Delayed rectifier potassium current
$I_{K(IR)}$	Inward rectifier potassium current

$I_{K(r)}$	Potassium resting current
$I_{K(t)}$	Total (macroscopic) potassium current
$I_{K(Na)}$	Sodium-activated potassium current
I_{Na}	Sodium current
$I_{(mNa)}$	Maintained sodium current
$I_{(rNa)}$	Sodium resting (or background) current
LA	Local Anesthetics
MSG	Mushroom shaped accessory gland
NIS	Normal insect saline
NMR	Nuclear magnetic resonance
NPPB	5-nitro-2-(3-phenylpropylamino) benzoic acid
NSW	New South Wales
NVPs	Nucleopolyhedroviruses
PLTX	*Plectreurys* spider toxin
rp-HPLC	Reversed phase high performance liquid chromatography
SITS	4-acetamido-4'-isothiocyanostilbene-2,2'-disulfonic acid
SK_{Ca}	Small-conductance Ca^{2+}-activated K^+ channels
dSlo	*Drosophila* Slo-poke potassium channel
mSlo	Murine Slo-poke potassium channel
pSlo	*Periplaneta* Slo-poke potassium channel
STX	Saxitoxin
TAG	Terminal abdominal ganglion
TEA-Cl	Tetra ethyl ammonium chloride
TTX	Tetrodotoxin
VGCC	Voltage-gated calcium channels
VGKC	Voltage-gated potassium channels
VGSC	Voltage-gated sodium channels
VUM	Ventral Unpaired Median

PUBLICATIONS ARISING FROM THIS THESIS

PATENTS

[1]   King GF, Sollod McFarland B, Nicholson GM, Gunning SJ (2005) INSECTICIDAL POLYPEPTIDES AND METHODS OF USE THEREOF. United States Provisional Application Serial No. 11/267,815 filed on November 4, 2005

PUBLICATIONS IN REFEREED JOURNALS AND MONOGRAPHS

IF = 2006 Science Citation Index journal impact factor; Cites = Times Cited

[1]   Gunning SJ, Maggio FJ, Windley MJ, Valenzuela SM, King GF, Nicholson GM (2008) The Janus-faced atracotoxins are specific blockers of invertebrate K_{Ca} channels. *FEBS Journal*, 275, 4045-4059. (IF = 3.033; Cites = 0)

[2]   Birinyi-Strachan LC, Gunning SJ, Lewis RJ, Nicholson GM (2005) Block of voltage-gated potassium channels by Pacific ciguatoxin-1 contributes to increased neuronal excitability in rat sensory neurons. *Toxicology and Applied Pharmacology,* 204, 175-186. (4.722; Cites = 7)

[3]   Gunning SJ, Chong Y, Khalife AA, Hains PG, Broady KW, Nicholson GM (2003) Isolation of δ-missulenatoxin-Mb1a, the major vertebrate-active spider d-toxin from the venom of *Missulena bradleyi* (Actinopodidae). *FEBS Letters*, 554, 211-218. (3.372; Cites = 7)

PAPERS IN PREPARATION

[4]   Gunning S, Sollod BL, Wen S, Quinton L, Chamot-Rooke J, Escoubas P, Nicholson GM, King GF (2008) Evolution of a dual-target, self-synergizing ion channel toxin. *Science*, in preparation.

INTERNATIONAL CONFERENCE PROCEEDINGS

[1]   Nicholson GM, Gunning SJ, Maggio FJ, Windley MJ, Valenzuela SM, King GF (2008) Identifying novel insecticide targets using insect-specific spider toxins. 3rd International Congress on Natural Peptides to Drugs, Zermatt, Switzerland 14-17 April, 2008.

[2]   Sollod BL, Gunning S, Wen S, Nicholson GM, King, GF (2006) A dual-target, self-synergizing toxin from spider venom. 15th World Congress on Animal, Plant and Microbial Toxins, Glasgow, Scotland, 24-28 July, 2006

[3]   Gunning SJ, Maggio F, Valenzuela S, Broady KW, King GF, Nicholson GM (2006) Pharmacophore mapping of the κ-atracotoxins: selective insect potassium channel blockers that reveal a novel insecticide target. 15th World Congress on Animal, Plant and Microbial Toxins, Glasgow, Scotland, 24-28 July, 2006.

[4]   Gunning SJ, Maggio F, Valenzuela S, Broady KW, King GF, Nicholson GM (2005) Selective actions of □κ-atracotoxins on insect KCa channels: electrophysiological validation of the insect target and pharmacophore. 7th Asia-Pacific Congress on Animal, Plant and Microbial Toxins, Cebu City, Philippines, 25-28 October, 2005.

[5]   Sollod BL, Gunning SJ, Wen S, Nicholson GM, King GF (2005) Evolution of a dual target, self-synergizing toxin: implications for insecticide and pharmaceutical discovery. Venoms to Drugs 3, Heron Island, 28 August - 2 September, 2005.

[6]   Gunning SJ, Maggio F, Valenzuela S, Broady KW, King GF, Nicholson GM (2005) κ-Atracotoxins: Insect potassium channels blockers that reveal a novel insecticide target Venoms to Drugs 3, Heron Island, 28 August - 2 September, 2005.

[7]   Gunning SJ, Maggio F, King GF, Nicholson GM (2004) κ-Atracotoxins: Insect potassium channels blockers that reveal a novel insecticide target. 8th Symposium of the Pan-American Section of the International Society of Toxinology, Angra dos Reis, Brazil, 19-23 September 2004.

[8]   Gunning SJ, Chong Y, Khalife AA, Hains PG, Broady KW, Nicholson GM (2003) Discovery of a novel sodium channel neurotoxin δ-missulenatoxin-Mb1a from the venom of the Eastern mouse spider *Missulena bradleyi*. 14th World Congress on Animal, Plant and Microbial Toxins, Adelaide, 14-19 September 2003.

[9]   Gunning SJ, Maggio F, King GF, Nicholson GM (2003) Do insecticidal J-atracotoxins target insect potassium channels? 14th World Congress on Animal, Plant and Microbial Toxins, Adelaide, 14-19 September 2003.

[10]   Gunning S, Khalife A, Padula M, Smith R, Broady KW and Nicholson GM (2002) Modulation of sodium channel gating and kinetics by δ-missulenatoxin-Mb1a from the Australian eastern mouse spider *Missulena bradleyi*. 6th Asia-Pacific Congress on Animal, Plant and Microbial Toxins, Cairns, 8-12 July 2002

LOCAL CONFERENCE PROCEEDINGS

[1]   Gunning SJ, Maggio FJ, Valenzuela SM, King GF, Nicholson GM (2007) Mapping the insectophore of κ-atracotoxins: insect-selective BKCa channel blockers that reveal a novel insecticide target. Proceedings of the Australian Physiological Society, 38, 37P. Newcastle, 2-5 December, 2007

        RNSH

        RNSH

[4]   GunniXXIIIg SJ, Maggio F, Valenzuela, SM, King GF, Nicholson GM (2004) κ-Atracotoxins: Insect potassium channels blockers that reveal a novel insecticide target. 21th RNSH/UTS Scientific Meeting, Sydney, November 2004

[5]   Gunning SJ, Maggio F, King GF, Nicholson GM (2003) Do insecticidal J-atracotoxins target insect potassium channels? 20th RNSH/UTS Scientific Meeting, Sydney, November 2003

[6]   Gunning SJ, Chong Y, Khalife AA, Hains PG, Broady KW, Nicholson GM (2003) Discovery of a novel sodium channel neurotoxin δ-Missulenatoxin-Mb1a from the venom of the Eastern Mouse spider Missulena bradleyi. 20th RNSH/UTS Scientific Meeting, Sydney, November 2003

[7]   Gunning SJ, Khalife AA, Padula M, Smith R, Broady KW, Nicholson GM (2002) Isolation and pharmacological characterisation of the neurotoxin δ-Missulenatoxin-Mb1a from the Eastern Mouse spider Missulena bradleyi. 19th RNSH/UTS Scientific Meeting, Sydney, November 2002

CHAPTER 1

INTRODUCTION

The venoms of numerous aquatic and terrestrial animals contain rich cocktails of peptide toxins that specifically interact with, and alter the conductance properties of, ion channels. In addition to being highly potent, many of these toxins are also exquisitely specific, with some targeting only a single ion channel subtype over a highly restricted phylogenetic range. These properties make natural toxins attractive as neuropharmacological tools, proving invaluable for probing the diversity of ion channels and for identifying the myriad of ion channel subtypes. For example, two families of calcium channel toxins, the ω-conotoxins from *Conus* spp. (cone snails) and the ω-agatoxins from the American funnel-web spider *Agelenopsis aperta* (Adams *et al* 1990, Olivera *et al* 1994)*,* have become the defining pharmacology for various classes of these channels. Peptide toxins have also greatly facilitated molecular analysis of vertebrate voltage-gated sodium channels and structural comparisons of pharmacologically related (MacKinnon *et al* 1998) and unrelated ion channels (Li-Smerin and Swartz 2000).

More recently, peptide toxins such as ω-conotoxin MV11C (Ziconotide PRIALT[®]) have gained considerable attention as novel pharmaceuticals. The potency and specificity of many toxins, their resistance to proteolytic degradation, and their ease of chemical synthesis, are all attributes that make them attractive drug leads.

Insecticidal peptide toxins are also being used in the development of novel biopesticides. The evolution of insect resistance to commonly used chemical pesticides, along with growing community awareness of the environmental damage caused by many agrochemicals, has necessitated the development of new strategies to combat highly resistant insect species. This includes the release of insect-specific baculoviruses that have been engineered to express insecticidal neurotoxins. For these reasons the characterisation and structural analysis of toxins can provide invaluable information that can be beneficial in the development of lead compounds for the pharmaceutical and agricultural industries.

1.1: BIOPESTICIDES

1.1.1 The Global Pest Problem

Arthropods are undoubtedly the most widespread and diverse group of animals with an estimated 4-6 million species worldwide (Novotny *et al*, 2002). While only a small percentage of athropods are classified as pest species, they nevertheless cause major devastation to crops, destroying around 18% of the world annual crop production (Oerke and Dehne, 2004), contributing to the loss of nearly 20% of stored food grains (Bergvinson and Garcia-Lara, 2004) and causing around US$100 billion damage each year (Carlini and Grossi-de-Sa, 2002).

With the world population expected to increase by 40% by the year 2050, the world will have to produce more food in the next 50 years then it has since the onset of agricultural production approximately 10 000 yrs ago. This coincides with the fact that most of the world's fertile land is already in use and arable lands cannot be expanded significantly. For these reasons, the global challenge is to secure high and quality yields while ensuring agricultural production remains environmentally sustainable. Improvement in pest control strategies represents

one method to generate higher quality and higher quantity of agricultural products.

Many pest species particularly hemaophagous (blood-sucking) insects, act as vectors for the transmission of many current and re-emerging diseases. Certain disease vectors such as mosquitos, ticks and fleas are of public health importance and are of increasing concern to the general population. Consequently they pose a threat to productivity, health, and well-being of humans, livestock, companion animals and wild life (Brogdon and McAllister, 1998; Gubler 1998). Arthropod-borne diseases not only affect human populations but also affect global food production. In many areas of the world, particularly the tropics, these diseases compromise efficient production of livestock and poultry (Dryden *et al*, 1993).

This thesis is a small part of the search for novel insecticidal agents to replace those rapidly losing effectiveness, and replace them with a system that is much more selective, effective, economical, as well as having the potential to adapt to changing needs in the future.

1.1.2 Pesticide Usage

A number of factors have reduced the effectiveness of current pesticide usage. Firstly, prolonged application of chemical pesticides on agricultural crops has led to disruption of the natural ecosystem: non-target species sharing the same habitat (pollinators and predators) die as well as pest insects. Secondly, the evolution of resistance in target insects to conventional chemical pesticides such as pyrethroids, carbamates and endosulfan has reduced their efficacy of agrochemical application (Gunning and Easton 1994, Gunning *et al* 1992, Daly and Murray 1988). More importantly, overspraying has led to chemical residues in neighbouring crops and livestock. This contamination of food and bioaccumulation in animals not only decreases the marketability of the primary produce but also the increased level of harmful chemicals further devastates the

environment. Therefore there is a growing necessity for the development of safer and more effective insect pest management.

Recently scientists have begun producing new generations of pest control agents employing 'environmentally friendly' strategies to combat highly resistant insect species, such as bollworms (*Helicoverpa* spp*.*). One approach involves employing insect pathogens as biological insecticide agents (Bravo *et al*, 2007). These naturally occurring pathogens not only have innate ability to attack insect pests but their actions can be enhanced by genetic manipulation. Current aims are to produce species-selective insecticides, which are environmentally compliant, rapidly acting, have minimal environmental persistence and are relatively inexpensive.

Transgenic plants and recombinant baculoviruses that express insecticidal toxins are two such bioinsecticides which have been investigated and subsequently tested as biological pest control agents (Chakraborty 1999; Crawley 1999, Liu *et al* 1999). Since the mid 1990s several agrochemical companies have genetically engineered plants to incorporate and express a gene encoding an insecticidal δ-endotoxin derived from the spore-forming soil bacterium *Bacillus thuringiensis* (*Bt*). The *Bt* insecticidal activity is due to the formation of toxic crystals during sporulation, which are highly specific for certain insects (Chakraborty 1999). Upon ingestion, the crystals dissolve and release insecticidal proteins in the insect's gut resulting in death within 48 hours. Despite the slow response time, *Bt* produces paralysis that quickly stops insects feeding on the plant, hence preventing additional crop damage. In agricultural practice, plants expressing the *Bt* gene are widely employed against Lepidopteran larvae (caterpillars) such as cotton bollworm and tobacco budworm (*Helicoverpa* spp*.*), which are pests of cotton, corn and brassica crops (Chakraborty 1999, Wadman 1997).

1.1.3 Transgenic Plants

Two companies now market transgenic plants expressing biopesticides, which have been in commercial cropping operations since 1996: Monsanto, the developer of *Bt* cotton, and Novartis Seeds the major manufacturer of *Bt* corn (Wadman 1997). The major advantages claimed for these transgenic crops are increased target organism selectivity and a reduction in insect resistance. Only those pests that feed on the genetically transformed crop would be subject to the insecticidal action of the transgenic plant.

Despite these claims of reduced insecticide resistance with *Bt* plants, there are already signs of rapidly developing insecticide resistance in regions of extensive *Bt* planting (Chakraborty 1999; Liu *et al* 1999; Wadman 1997, Roush and Shelton 1997). To overcome this problem several strategies have been employed including the 'refuge strategy', where *Bt* resistant insects are encouraged to mate with non-resistant insects from adjacent fields containing non-*Bt* cotton. Therefore, ultimately, the resistance gene is 'drowned' in the larger gene pool (Liu *et al.*, 1999). Unfortunately, farmers have often subverted this by deliberately not planting refuge areas (usually 15-25% of their crop) in attempts to maximize their crop yield.

Another concern of transgenic plants is the risk of pollen distribution by wind to adjacent fields, affecting other non-target species (Losey *et al* 1999) or spreading the transgenic form to wild-type crops (Chamberlain and Stewart 1999). Most transgenic plants express the *Bt* toxin in large amounts in their pollen, and corn pollen has been reported to be dispersed over at least 60 metres by wind (Losey *et al* 1999). Consequently corn pollen is deposited on other plants near the corn fields and this can be consumed by non-target species that feed on these plants. Losey and coworkers (1999) found that larvae of the monarch butterfly, *Danaus plexippus,* raised on milkweed leaves dusted with pollen from *Bt* corn, ate less, had a retarded rate of development and suffered from higher mortality rates than larvae fed on leaves dusted with untransformed corn pollen or leaves without pollen. This is compounded by recent news that those insects that do develop

resistance mature more slowly than wild-type insects, and thus are more likely to mate with each other on emergence (Liu *et al* 1999).

1.1.4 Baculoviruses

Several alternative approaches are being investigated which avoid these problems. Other pathogens considered as bioinsecticides are the insect viruses of the Baculoviridae family, in particular the nucleopolyhedroviruses (NPVs) (Chakraborty 1999; Hoover *et al* 1996, McCutchen *et al* 1991). These are rod-shaped enveloped viruses containing a double-stranded circular DNA genome that can be manipulated to enhance their insecticidal activity. They are highly selective, efficient and environmentally friendly. Baculoviruses have been identified which selectively target particular species or genera in the insect Order Lepidoptera, which covers the major agricultural pests, as well others which target Coleoptera, Diptera, Hymenoptera, Trichoptera or the crustacean Order Decapoda. They are unique to these Orders and furthermore no baculoviruses have been found to affect plants, vertebrates, or invertebrates other than arthropods (Maeda & Hammock, 1993). Ingested viral polyhedrons dissolve in the insect's alkaline midgut, releasing virions that infect the gut and subsequently, other tissues, eventually killing the insect (Bonning and Hammock 1996; Hoover *et al* 1996). Dead insects release more infective viral polyhedra with variable environmental persistence.

Wild-type baculoviruses are cost effective and, more importantly, highly specific, usually attacking only one or several closely related species. For example, AcNPV, isolated from the alfalfa looper *Autographa californica*, has the broadest host range of any NPV of almost 40 lepidopteran species (Chakraborty 1999; Hoover *et al.,* 1996), yet this is a very narrow host range compared to chemical pesticides and thus would be less harmful to non-target species. Their narrow host range can be undesirable as some users might prefer an agent that has a different host range (Hoover *et al.,* 1996), but most farmers would have all their lepidopteran pests covered with one NPV.

However, the sole use of baculoviruses has certain limitations given that these viruses take several days to kill their hosts. In addition, the insufficiency of field persistence due to inactivation by ultra-violet light, which varies between 100% after the first day on plant surface to 75% after 5 years in soil (Hoover *et al,* 1996), can mean frequent reapplication. Also, as Chakraborty (1999) points out, these viruses require living host cells, therefore NPVs need to be produced in their larval hosts or in cell culture consequently posing limitations on commercial manufacture. Where labour is cheap and chemicals comparatively expensive, such as developing countries, this is less of a concern and baculoviruses are increasingly used, for example, in Brazil on soybean crops (Moscardi, 1999).

1.1.5 Recombinant Baculoviruses

Reducing the time to kill host insects and subsequent feeding capacity is the main target involving engineered baculoviruses (Bonning and Hammock 1996). Research in this area has involved the expression of genes coding for foreign proteins in baculovirus genomes, such as insect-specific toxins (arthropod venoms, *B. thuringiensis* toxins), insect hormones (diuretic and prothoracic hormones), juvenile hormone esterase (JHE), as well as ecdystroid UDP-glucosyltransferase (*egt*) (Bonning and Hammock 1996).

So far, the most promising results have been obtained with the toxin AaIT derived from the venom of the scorpion *Androctonus australis* (Maeda and Hammock 1993), and with the toxin TxPI from the mite *Pyemotes tritici* (Holly *et al* 1997). These baculovirus constructs have reduced the time-to-kill the host by 25%-40% in some selected insect species.

A recombinant baculovirus system presents a valuable area of study that has immense potential as an effective pest management system. The market for bioinsecticides is still rapidly expanding as evident by the commercial value sold in the United States during the early 1990s. This was estimated at US$95-147 million, that is, 1.3-2.4% of the total market for pest control agents (Chakraborty, 1999). The total replacement of chemical pesticides might be feasible in the

future as more biotechnology research and application is stimulated accompanied by the involvement of larger commercial companies. The flexibility of genetic manipulation allows introduction or deletion of multiple genes that are able to enhance the insecticidal potential or overcome the development of resistance. However, a major problem with current biopesticide management is the lack of well-characterised toxins from which to select new agents for incorporation into the baculoviral genome.

The venom of several spiders have been identified to have insecticidal peptides, for example venom from the trap door spider *Aptostichus schlingeri* (Skinner *et al* 1992) and Australian Funnel-web spiders (Atkinson *et al* 1996). Much work has been done on the isolation and biochemical characterization of the insect-specific peptides from Blue Mountains funnel-web spider venom *Hadronyche versuta* (Atkinson *et al* 1996; Fletcher *et al* 1997, Wang *et al* 1999, Wang *et al* 2000b). More studies are required, however, to investigate the pharmacological and structural aspects of the insecticidal components of the funnel-web spider venom to develop more efficacious agents or possibly develop non-peptidic foliar sprays. Knowledge of the three dimensional structure of the neurotoxin(s) is essential for assessing future biopesticide usage, in particular, the positions of critical and non-critical residue(s) that constitute the bioactive surface (pharmacophore) of the peptide.

1.2: AUSTRALIAN FUNNEL-WEB SPIDERS

Australian funnel-web spiders (Araneae: Mygalomorphae: Hexathelidae: Atracinae) are divided into 2 genera, *Atrax* and *Hadronyche,* containing more than 40 species (Gray 1987) (Fig **1**.**1**). The venom of these arachnids is highly suitable for investigation for novel neurotoxins because of several reasons. Firstly, these spiders belong to the suborder Mygalomorphae, or 'primitive spiders'. These ground-dwelling spiders were present before the evolution of flying insects; therefore they did not adapt to spin webs for prey capture. Instead, mygalomorph spiders depend upon the insecticidal nature of their venom as well as their physical size to immobilize their prey. Therefore, it is most likely that the venom of these spiders would possess a combination of novel insecticidal neurotoxins.

Australian funnel-web spiders are found predominately along the eastern coast extending from South-eastern Queensland to Tasmania, and in a small pocket of the Flinders Ranges in South Australia. The currently most studied funnel-web species in Australia, *H. versuta*, *occurs* throughout most of the Blue Mountains (Fig **1**.**2**). It is common in moist forest habitats.

Note the following figure **(Figure 1**.**1**: Partial taxonomy of Australian funnel-web spiders, with the classification of *Hydronyche versuta*, the Blue mountains funnel-web spider, highlighted) is shown at the end of the reference section.
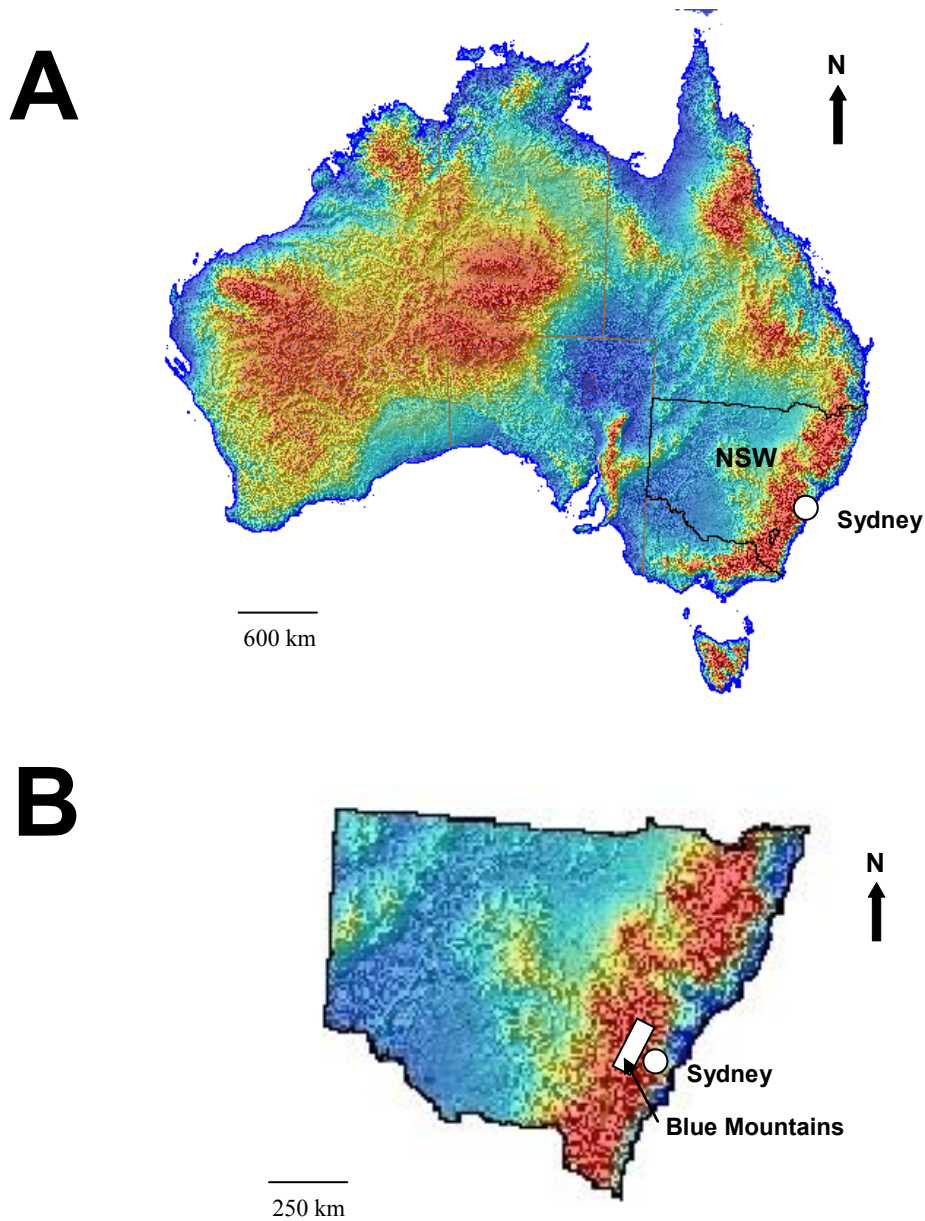
Figure 1.2: *Hadronyche versuta* is mainly distributed throughout the Blue Mountains region of New South Wales (NSW). (**A**) Elevation map of Australia (graded from blue to red in order of increasing elevation), indicating the state of NSW. (**B**) Map of NSW indicating the location of the Blue Mountains, west of Sydney.

Some distinct features of *H. versuta* are (i) large spinnerets at the end of the abdomen in which the terminal segment is longer than it is wide; (ii) teeth-like serrations on both margins of the fang grooves; (iii) peg-like spines on the labium; (iv) a strongly curved foveal groove on the carapace; (v) the male may have a blunt spur on the tibia of the second pair of legs (Brunet, 1996) (Fig **1**.**3**).
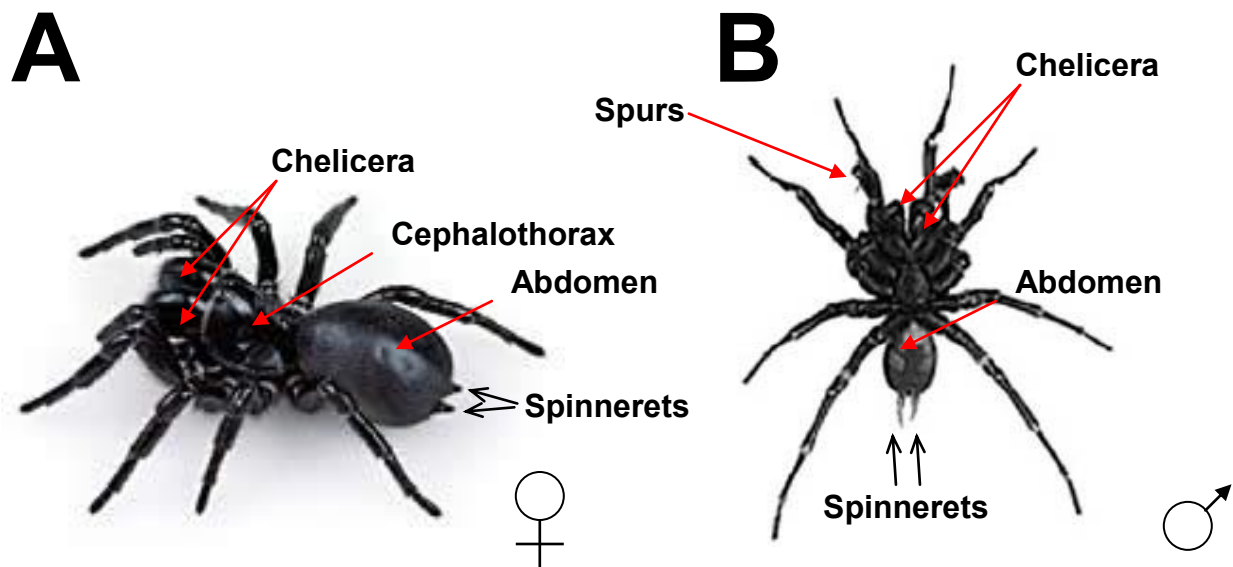
Figure 1.3: Adult female and male Blue Mountains funnel-web spiders (*Hadronyche versuta*). (**A**) Female and male (**B**) *H. versuta*, with major anatomical landmarks indicated.

1.3: AUSTRALIAN FUNNEL-WEB SPIDER TOXINS

1.3.1 Spider Venoms

Spider venoms are multicomponent biochemical systems of poorly understood complexity. In particular, the interactions between the various chemical classes present in the venoms and their respective role in the envenomation process has not been well defined. Spider venom components can be grouped into three major classes: low molecular mass organic molecules (M_r <1000 Da), polypeptides (M_r < 3000-10000 Da) and high molecular mass proteins (M_r > 10000 Da). Given the scope of this thesis, it will focus on the latter two groups. The main toxin arsenals of spiders are the polypeptides, which appear to mainly target various membrane ion channels.

1.3.2 Vertebrate-Selective Atracotoxins

Atkinson *et al*. (1996) screened venom from several different Australian spiders and demonstrated that funnel-web spider venom was the most potent against the economically important pest the cotton bollworm (*Helicoverpa armigera*). Previous work has already identified that funnel-web venom (*Atrax* and *Hadronyche* spp.) contain peptides called atracotoxins (ACTXs) that are toxic to both insects and/or vertebrates. Envenomation by the male Sydney funnel-web spider caused at least 14 human fatalities preceding the introduction of antivenom in 1980 (Sutherland 1990).

Most work has been performed on the venom of the Blue Mountains funnel-web spider *Hadronyche versuta*. The lethal neurotoxin from this venom, δ-ACTX-Hv1a, has been isolated and sequenced. This is a 42-residue peptide with eight cysteine residues that form four intramolecular disulfide bonds (Brown *et al* 1988).

Some investigations have also been performed on the venom of the Sydney funnel-web spider *Atrax robustus* to identify the active component responsible for the human envenomation syndrome. This led to the isolation and sequencing of another 42-residue peptide mammalian neurotoxin δ-ACTX-Ar1a (formerly known as robustoxin) by Sheumack *et al* (1985). δ-ACTX-Ar1a and δ-ACTX-Hv1a have 83% sequence homology (see Fig **1**.**4A**) and are also very similar in three-dimensional structure (Fig **1**.**4B**-**E**) (Pallaghy *et al* 1997*).* More recently, Nicholson *et al* (1994) revealed that δ-ACTX-Hv1a causes repetitive firing of action potentials by delaying the inactivation process of mammalian voltage-gated sodium channels. Interestingly, this is also very similar to the mechanism of action of scorpion α-toxins (Strichartz and Wang 1996). The mechanism of action of δ-ACTX-Ar1a is the same as δ-ACTX-Hv1a whereby the kinetics of the sodium channels are slowed, resulting in repetitive firing of action potentials (Nicholson *et al* 1998). At nanomolar concentrations δ-ACTX-Ar1a and δ-ACTX-Hv1a also completely inhibit the binding of the scorpion α-toxins Lqh II and Aah II to neurotoxin receptor site 3 on rat brain sodium channels (Little *et al.,* 1998a, 1998b). In addition they show moderate toxicity to insects (LD_{50} = 770 pmol/g in crickets) and compete for the same receptor site as the insect-selective toxin, LqhαIT on cockroach neuronal membranes (Little *et al* 1998b). It is clear that the δ-ACTXs are extremely potent and define a new class of toxins affecting both insect and mammalian sodium channels.

Recently, Szeto *et al* (2000) also isolated and sequenced another novel δ-atracotoxin; δ-ACTX-Hv1b (see Fig **1**.**4**), which is structurally similar to δ-ACTX-Ar1a and δ-ACTX-Hvla. This toxin also slows sodium channel inactivation but lacks insecticidal activity, as shown by the lack of effect when large doses (2000 pmol/g) are injected into crickets. The lack of insecticidal activity might be due to the lack of charged residues at positions 4 and 5 of δ-ACTX-Hv1b (see figure **1**.**4A**), (Szeto *et al* 2000). These characteristics of the toxin allow the possibility of manipulating key residues, thus enabling the construction of a δ-ACTX that is

insect-selective without vertebrate activity. The product would be highly desirable as a bioinsecticide given the potential high selectivity and potency.

Figure 1.4: Structural characteristics of the δ-ACTX family. (**A**) Comparison of the primary sequence of δ-ACTX-Ar1a with currently known members of the δ-ACTX family. Identical residues are boxed in yellow and conservative substitutions are in italicised red text. The red arrows indicate suspected key residues important for bioactivity. (**B**) & (**C**) Stereo schematic view of the structures of δ-ACTX-Ar1a (PDB file 1VTX) and δ-ACTX-Hv1a (PDB file 1QDP) showing the location of β-strands (cyan arrows) and C-terminal 310-helix (green and yellow). These disulfides bridges form an ICK motif and are shown as red tubes. (**D**) Stereo view of the ICK motif of δ-ACTX-Hv1a. The Cys^{14}–Cys^{31} disulfide pierces a 14-residue loop formed by the Cys^{1}–Cys^{15} and Cys^{8}–Cys^{20} disulfides (red) and the intervening sections of the polypeptide backbone (green). (**E**) Stereo view of an overlay of the backbone of gurmarin (green, PDB file 1C4E), δ-ACTX-Hv1a (red), and μ-agatoxin I (blue, PDB file 1EIT). Adapted from King *et al*, 2002.

1.3.3 Insect-Selective Atracotoxins

This class of atracotoxins provides the best tools for use in transgenic plants and recombinant baculoviruses given their innate insect selectivity. ω-Atracotoxin (ACTX)-Hv1a, a specific antagonist of insect voltage-gated calcium channels, isolated from the Blue Mountains funnel-web spider *Hydronyche versuta*, is a 37-residue peptide toxin which contains three intramolecular disulphide bonds (Chong *et al*, 2007, Wang *et al* 1999). It is lethal to cotton bollworms, cockroaches, mealworms, blowflies and locusts (Fletcher *et al* 1997; Atkinson *et al* 1993; Atkinson *et al* 1996), but is harmless to newborn mice at doses up to 2.5 mg.kg^{-1} (Atkinson *et al* 1993). Subsequently, a further five ω-atracotoxin-1 toxins from *H*. versuta venom (ω-ACTX-Hv1b-f) have been isolated and sequenced. Most of these toxins differ by only 1-3 residues and they have very similar insecticidal potencies (Wang *et al* 1999). In contrast, ω-ACTX-Hv1f differs by up to 10 residues from the other toxins, and has markedly reduced insecticidal activity. This has enabled identification of key functional residues that are non-conservatively substituted in ω-ACTX-Hv1f. Another class of insect-specific toxins from *H*. *versuta* venom include the Janus-faced atracotoxins (J-ACTX-Hv1a-c). Both the ω-atracotoxin and Janus-faced atracotoxin families are discussed in more detail in chapter 4.

CHAPTER 2

ION CHANNELS AND ION CHANNEL TOXINS

Ion permeation concerns the nature of the pathway that allows ions to cross through the lipid membrane. Hodgkin and Huxley (1952) made it clear that membranes could distinguish Na^+ from K^+ ions and could alter their permeability to either ion in a millisecond or less. What was the identity of the structure that catalyzed ion movement through the lipid bilayer? Hodgkin and Huxley considered both pores and carriers as possible transport mechanisms, perhaps favouring the latter on the grounds that selectivity was somewhat easier to imagine for a carrier. Experimental evidence however, using radioactive tracers demonstrated a "long pore" effect, which could be interpreted as the name implies, to mean that the conducting path was a pore, occupied simultaneously by at least two ions that could not pass each other in the pore. This gave rise to the modern concept of ion-selective channels.

2.1: Na_V CHANNELS

Sodium channels are transmembrane proteins responsible for the voltage-dependent increase in sodium permeability that initiates action potentials (Hodgkin and Huxley, 1952). Voltage-gated sodium (Na_V) channels are present

in a variety of electrically excitable cells, including neurons and muscle cells where they are crucial for action potential initiation, propagation and muscle cell contraction. In addition, Na_V channels are the molecular targets for several groups of neurotoxins, which bind strongly to specific receptors located on the channel, thus an understanding of the structure, function and kinetics of Na_V channels remains crucial for an investigation such as this. Biochemical studies of sodium channels have been greatly facilitated by the use of a number of neurotoxins that bind with high affinity and specificity to Na_V channels and alter their gating properties. The actions of these neurotoxins have been well described in previous reviews (Narahashi 1974; Catterall 1980, Cestèle and Catterall 2000).

Essentially all models for the structure of the voltage-gated ion channels include a transmembrane pore forming α subunit of 220-260 kDa associated with auxiliary subunits: $\beta1$, $\beta2$ and $\beta3$ (Fig **2.1**). The α-subunit normally consists of four homologous domains (I-IV), each containing six transmembrane segments (S1-S6), and one re-entrant segment (SS1/SS2) connected by internal and external polypeptide loops (Cestèle and Catterall 2000; Catterall, 2001). The four domains fold together in a clockwise orientation such that domains I and IV are brought into close proximity to form the outer pore vestibule.

In most tissues and species the α-subunit of Na_V channels is non-covalently associated with a smaller $\beta1$ subunit of 30-40 kDa (Gordon 1997). In mammalian brain, the Na_V channels (mainly $Na_V1.2$) consist of a heterotrimeric complex of α (260 kDa), $\beta1$ (36 kDa) and a disulphide linked $\beta2$ (33 kDa) subunits (Hartshorne and Catterall 1981; Hartshorne *et al* 1982). The purified *Electroplax* Na_V channel is functional with only a single α-subunit, indicating that it contains most, if not all, of the functional domains of the channel (Catterall 1992; Barchi 1988; Cohen and Barchi 1993).

Voltage-gated sodium channels comprise a single family of nine related functional α-subunits, which appear to have arisen by gene duplication (Catterall 2000). The primary sequence of the α-subunit contains about 2000 amino acid residues and is comprised of contiguous repeats of four internally homologous domains called repeats I-IV (Catterall 2000). Structural modeling of sodium channel α-subunits has indicated that the channel is formed by a pseudo-symmetrical assembly of the four repetitive homologous domains (pseudo-subunits) (Guy and Conti 1990; Noda *et al* 1984; 1986) and as such all four repeats are required for the formation of functional Na_V channels (Stühmer 1991). These four internally homologous domains form a single, voltage-gated aqueous pore (Wood *et al* 2001).

Each α-subunit repeat contains six potential transmembrane segments, S1 to S6, of sufficient length to span the membrane as an α-helix. The largest degree of homology exists in the putative transmembrane regions, with a few charged residues, in S2, S3 and S4 being strictly conserved among all voltage-gated channels (Gordon 1997).

The sodium channel β-subunit family ($Na_V\beta1$, $Na_V\beta2$, $Na_V\beta3$ and $Na_V\beta4$) are transmembrane proteins with type I topology: containing an extracellular amino-terminus, a single transmembrane segment, and an intracellular carboxyl terminus (Isom 2001). All four subunit molecules contain extracellular immunoglobulin (Ig) domains that are structurally homologous to the V-set of the Ig superfamily that includes cell adhesion molecules (CAM"s) (Isom and Catterall 1996). β-Subunits of the sodium channel appear to have dual functions-modulation of channel gating and cell-cell interaction.

Just as the high affinity and specificity of neurotoxins led to discovery of the sodium channel protein, the pore blockers tetrodotoxin (TTX) and saxitoxin (STX) also led directly to identification of the outer pore and selectivity filter (Catterall 2000). Ion transport mediated by Na_V channels is among the most rapid protein-

mediated processes (Conti *et al* 1975; Sigworth 1980). On the basis of the selectivity of the pore for organic cations, the limiting region (ion selectivity filter) was proposed to be approximately a 3.1 A° × 5.1 A° rectangular orifice lined by oxygen atoms, which act as hydrogen bond acceptors during transport of organic cations and hydrated metal cations, but exclude similarly sized ions having non-hydrogen-bonding substituents, like methyl groups.

Na_V channels open and inactivate in response to a depolarisation of the resting membrane potential. When these channels open, an influx of sodium occurs, depolarising the membrane, and generating the upstroke phase of the action potential (Hodgkin and Huxley, 1952). Inactivation (closing) of sodium channels halts the sodium influx, preventing a permanent depolarisation of the resting membrane potential. Recovery from inactivation coupled with activation of voltage-gated potassium (K_V) channels causes repolarisation thus allowing the cell membrane to regain its resting excitable properties (Hodgkin and Huxley, 1952).

The voltage dependence of activation of the Na_V channel derives from the outward movement of gating charges in the membrane electric field (Hodgson and Huxley 1952; Armstrong 1981). Recent studies indicate that ~12 electronic charges in the sodium channel protein move across the membrane electric field during activation (Hirschberg *et al* 1995). The S4 transmembrane segment of the α-subunit is the most characteristic structure shared by members of this superfamily. It contains a positively charged residue at every third position followed by two hydrophobic residues, potentially creating a cylindrical α-helix with a spiral ribbon of positive charge around it (Guy and Conti 1990; Noda *et al* 1986; Stühmer 1991). The first evidence in favor of the S4 segments as voltage sensors came from mutagenesis studies which found that neutralization of the positively charged residues in the S4 segment of domain I was found to reduce the steepness of voltage-dependent gating, as expected for a reduction in gating charge, and to shift the voltage dependence along the voltage axis (Stühmer *et al*

1989a). These findings have led to the helical screw model of gating and proposes that these positively charged amino acid residues in the S4 segment are stabilised in the transmembrane environment by forming ionic pairs with negatively charged residues in adjacent transmembrane segments (Guy and Seetharamulu 1986). Depolarization of the membrane releases the S4 segments to move outward along a spiral path, initiating a conformational change that opens the pore resulting in the rapid movement of sodium ions down an electrochemical gradient resulting in further depolarisation of the cell membrane. (Armstrong, 1981).

Inactivation of the ion conductance activity of the Na_V channel is terminated within a few milliseconds after opening resulting in partial repolarisation of the cell membrane. This is a critical feature of Na_V channel function because persistent opening of the Na_V channels would depolarize excitable cells leading initially to prolonged action potentials and if sufficient sodium ion flux occurs, prolonged inexcitablity may result, since persistent depolarisation can lead to steady-state inactivation of Na_V channels (Catterall, 1998; Bezanilla and Armstrong, 1977). The voltage-dependence of fast inactivation of the Na_V channel is coupled to voltage-dependence of activation. In addition, the inactivation process can be specifically prevented by treatment of the intracellular surface of the Na_V channel with proteolytic enzymes (Armstrong, 1981). These results led to the proposal of an autoinhibitory gate with a „ball-and-chain" or „hinged-lid" structure for Na_V channel inactivation in which an inactivation particle tethered on the intracellular surface of the Na_V channel (the ball) diffuses to a receptor site in the intracellular mouth of the pore (Catterall, 1998) (Fig **2.1**). Mutagenesis studies of this region revealed a hydrophobic triad of isoleucine, phenylalanine, and methionine (IFM) that is critical for fast inactivation (West *et al* 1992), and peptides containing this motif can serve as pore blockers and can restore inactivation to Na_V channels having a mutated inactivation gate (Eaholtz *et al* 1994). These results support a model in which the IFM motif serves as a tethered pore blocker that binds to a receptor in the intracellular mouth of the

pore. Inactivation is impaired in proportion to the hydrophilicity of amino acid substitutions for the key phenylalanine residue (F1489), suggesting that it forms a hydrophobic interaction with an inactivation gate receptor during inactivation (Kellenberger *et al* 1997). Evidently, multiple peptide segments form a complex inactivation gate receptor into which the inactivation gate inserts to occlude the channel pore.

Scorpion α-toxins and sea anemone toxins uncouple activation from inactivation by binding to a receptor site at the extracellular end of the IVS4 segment and preventing its normal gating movement (Sheets *et al* 1999), thus trapping it in a position that is permissive for activation but not for fast inactivation. The IIIS4 and IVS4 segments, detected by covalently incorporated fluorescent probes, are specifically immobilised in the outward position by fast inactivation, arguing that their movement is coupled to the inactivation process (Cha *et al* 1999). Together, these results provide strong evidence that outward movement of the S4 segment in domain IV is the signal to initiate fast inactivation of the Na_V channel by closure of the intracellular inactivation gate.
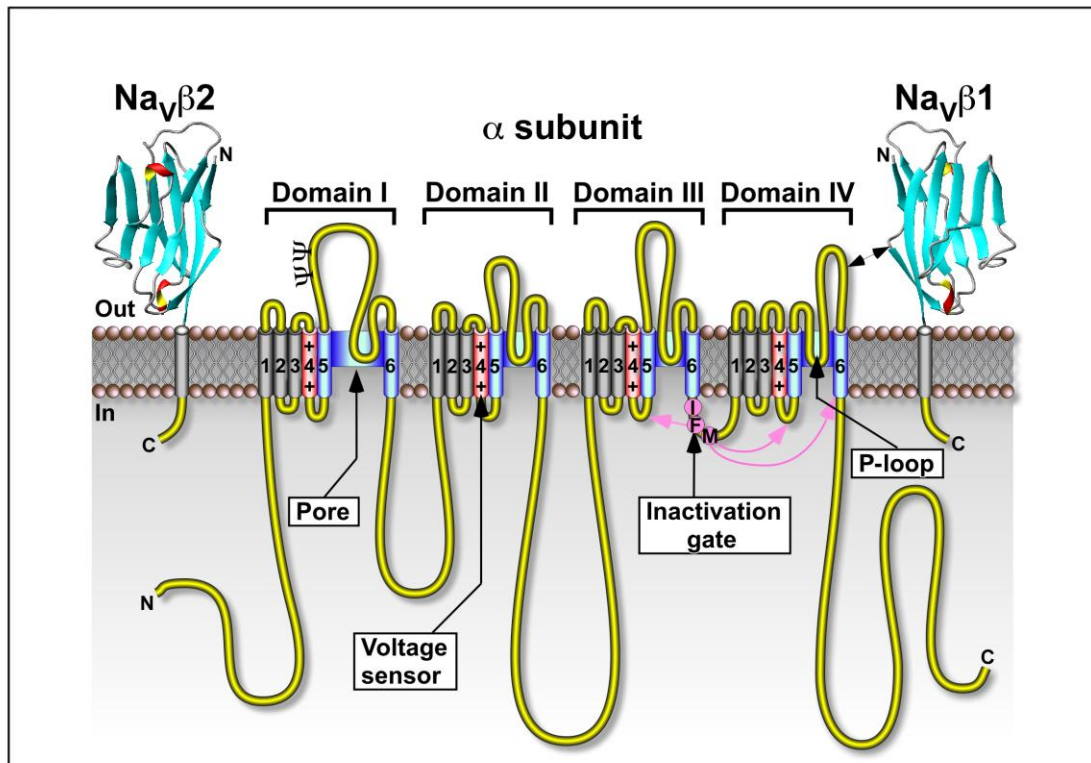
Figure 2.**1**. Schematic representation of the molecular structure and membrane topology of Na_V channels. The pore-forming α-subunit (centre) comprises four homologous domains designated I-IV. Within each domain, the putative transmembrane α-helical segments (S1-S6) are represented by cylinders, with the S4 voltage-sensor shown in red. The pore-lining segments S5 and S6 and the intervening P loop that form the walls of the ion-conducting pathway are shown in blue. The Na_V channel inactivation gate (magenta) is represented by the inactivation particle (hydrophobic residues IFM in mammals) with magenta arrows indicating the sites thought to form the inactivation gate receptor. The extracellular domains of the $\beta1$ and $\beta2$ subunits are represented as immunoglobulin-like folds similar to myelin protein P_0. ψ indicates sites of probable *N*-linked glycosylation. Adapted from Nicholson, 2007.

2.1.1 Insect Na$_V$ channels

Despite the discovery of at least 18 genes encoding Na$_V$-like channels cloned from invertebrate species very few have been functionally expressed (Goldin, 2002). The first putative insect Na$_V$ channel gene *para* (encoding the α-subunit of the DmNa$_V$1 channel) was isolated from the fruit fly *Drosophila melanogaster* (Ramaswami and Tanouye, 1989). The overall domain organization and amino acid sequence of DmNa$_V$1 is highly homologous to that of the mammalian Na$_V$ channel α-subunits. The structural features critical for mammalian Na$_V$ channel function, including the D, E, K, A residues in the pore regions of domains I-IV that are crucial for sodium selectivity are conserved in DMNa$_V$1 (Loughney *et al*, 1989). RNA editing of the *para* gene has been described by Reenan *et al*, thereby adding to the molecular and functional diversity of *para* gene products (Hoopengardner *et al*, 2003). An additional *D, melanogaster* subunit, the product of the temperature-induced paralysis (*tip-E*) locus has been found. Although quite different in sequence from the rat brain sodium channel β2 subunit, the polypeptide encoded by the *tip-E* gene appears to play a similar role. Although the product of the *para* gene alone will express to yield channel activity, a functional insect Na$_V$ channel has been generated by co-expression of α-like subunits PARA and TIP-E resulting in channels with increased current amplitude and rate of channel inactivation without altering the timecourse and voltage-dependence of the sodium channel. In addition the para/tip-E heteromer is sensitive to TTX, resembling in these aspects many native insect sodium channels (Raymond-Delpech *et al*, 2005).

More recently the orthologous channels MdNa$_v$1 from the house fly *Musca domestica* and BgNa$_V$1 from the German cockroach *Blattella germanica* have been identified and functionally expressed (Dong, 1997). In contrast, the *para*-type Na$_V$ channel sequence has very low levels of identity (typically 50-60 %) with various types of mammalian Na$_V$ channels. This explains why a high degree

of phylogenetic specificity can be achieved with both Na_V channel toxins and insecticides that target Na_V channels.

In contrast to mammals, insects rely upon extensive alternative splicing and RNA editing of a single *para* Na_V channel gene to provide channels with different functional properties. To date, a total of nine alternative splice sites (a, b, c/d, I, j, e, f, h, l/k) have been identified in *para* genes that potentially generate >100 different tissue/cell type-specific distinct insect Na_V channels (Song *et al,* 2004; Tan *et al*, 2002). Although multiple isoforms and variants are now know, the molecular basis for this functional diversity remains to be determined.

The significant primary structure differences between mammalian and insect Na_V channels are reflected in complex differences in the affinity for, or the allosteric modulation of, Na_V channels, as well as phyletically selective actions of certain Na_V channel toxins. As a result, insect Na_V channels are often more or less sensitive to the actions of particular Na_V channel toxins (Warmke *et al*, 1997; Gordon *et al*, 2002).

2.1.2: Na_V CHANNEL TOXINS AND TOXIN BINDING SITES

Sodium channels are the molecular targets for several groups of neurotoxins, which strongly alter channel function by binding to specific receptor sites. Consequently, localisation of the neurotoxin receptor sites gives unique information on the structure-function relationship of the Na_V channel. Electrophysiological and neurochemical binding studies of Na_V channels indicate that neurotoxins act at seven distinct receptor sites (The four principal sites are shown in Fig **2.2**) and have primary effects on either ion permeation or voltage-dependent gating. The orphan receptor sites at which neurotoxins affect gating were found to be allosterically coupled, suggesting that conformational changes induced by neurotoxin binding alter the equilibrium between the open and the

closed/inactivated states and also alter conformation and toxin binding affinity at other neurotoxin receptor sites (for a review see Cestèle and Catterall, 2000). Receptor site 1 is occupied by two different groups of toxins: the water-soluble heterocyclic guanidines tetrodotoxin (TTX) and saxitoxin (STX) and the peptidic μ-conotoxins. TTX is isolated from the tissues of at least 40 species of puffer fish (Fuhrman 1967), but it is also found in molluscs, crabs, octopi and Central American frogs (Yamasuto *et al*, 1986; Mebs and Schmidt 1989; Hwang *et al* 1991). STX is produced by a variety of marine dinoflagellates including *Gonyaulax catenella* and *Gonyaulax tamarensis* and can also be found in certain clams and mussels that feed on the dinoflagellates (Schantz 1986). μ-Conotoxins are isolated from the venom of *Conus geographus* and related cone snails (Cruz *et al* 1985; Sato *et al* 1983).

These toxins bind to receptor site 1 on the extracellular side of the membrane and thus block sodium conductance. Localization of the TTX/STX receptor site has been investigated by site directed mutagenesis, indicating that the receptor site is formed by two rings of amino acid residues localized in segment SS2 on the N-terminal side of the S6 transmembrane segment in each of the four domains of the channel (Noda *et al* 1989; Terlau *et al* 1991). Although binding experiments have shown that μ-conotoxins inhibit TTX/STX binding competitively (Moczydlowski *et al* 1986; Yanagawa *et al* 1986), some of the mutations which affect TTX/STX affinity do not alter μ-conotoxins binding, suggesting that these two groups of toxins share an overlapping but not identical receptor site.

Lipid-soluble grayanotoxins (found in rhododendron and other plants of the family *Ericaceae*), the alkaloids, veratridine (from *Liliaceae*), acontine (from the plant *Acontinum napellus*) and batrachotoxin (from the skin of the Columbian frog *Phyllobates aurotaenia*) bind to receptor site 2. These toxins bind preferentially to the activated state of the channel and cause persistent activation at resting membrane potentials via an allosteric mechanism that leads to block of Na_V channel inactivation and shift of the voltage-dependence of activation to more

negative potentials (Catterall 1977; Narahashi *et al* 1964; Albuquerque *et al* 1971; Chahine *et al* 1995). Photolabelling experiments using batrachotoxin have shown that mutation of amino acid residues (I433, N434 and L437) in transmembrane segment IS6 impair batrachotoxin binding and action (Wang and Wang 1998). In addition mutations of amino acid residues F1579 and N1584 in transmembrane IVS6 of the skeletal muscle Na_V channels (Wang and Wang 1999), as well as I1760 and F1764 of the rat brain Na_V channels (Linford *et al* 1998), prevent batrachotoxin binding, indicating that these residues also play an important role in the formation of the batrachotoxin receptor site (Cestèle and Catterall 2000). Involvement of IS6 and IVS6 transmembrane segments in the formation of receptor site 2 suggests that these toxins conform to a domain-interface allosteric model of ligand binding and action. It is postulated that the block of inactivation induced by this group of toxins is due to their interaction with the IVS6 transmembrane segment that is required for fast inactivation and may allow the toxins to alter the voltage-dependent movement of the adjacent IVS6 voltage-sensor and thereby affecting both activation and coupling of activation to inactivation (Linford *et al* 1998).

Neurotoxin receptor site 3 of sodium channels is occupied by several groups of polypeptide toxins: Scorpion α-toxins, sea anemone toxins and some spider toxins. These toxins slow or block Na_V channel inactivation (Narahashi 1974; Catterall 1979; Eitan *et al* 1990; Nicholson *et al* 1994; 1998). Scorpion α-toxin binding affinity is decreased by depolarization on rat brain Na_V channels (Catterall *et al* 1976; Courand *et al* 1978), thus the voltage-dependent binding correlates closely with the voltage dependence of channel activation (Catterall 1979). These findings indicate that the specific action of these toxins on inactivation implies that membrane potential affects the structure of receptor site 3 and that this region of the channel is important for coupling of activation and inactivation, and that toxin binding prevents the conformational change required for fast inactivation (Catterall 1979). Using scorpion α-insect toxins receptor site 3 on insect Na_V channels has been identified. In contrast to the binding of scorpion α-toxins on mammalian sodium channels, the binding of insect-selective

α-scorpion toxins is not voltage-dependent (Gordan and Zlotkin 1993; Cestèle *et al* 1997). Scorpion α-toxins and sea anemone toxins bind to IVS3-S4 through electrostatic interactions with E1613 for rat brain Na_V channels (Rogers *et al* 1996), D1612 for cardiac Na_V channels (Benzinger *et al* 1998) and D1428 for skeletal Na_V channels (Ma *et al* 2000). Location of neurotoxin receptor site 3 just on the extracellular side of the transmembrane segment IVS4 suggests a molecular mechanism for toxin action (Rogers *et al* 1996). Scorpion α-toxins and sea anemone toxins are proposed to slow Na_V channel inactivation by preventing the movement of the IVS4 voltage-sensor transmembrane segment, thereby preventing conformational changes that are necessary for fast inactivation (Rogers *et al* 1996). Prolonged depolarization forces the outward movement of the IVS4 segment and causes voltage-dependent dissociation of the scorpion α-toxins (Catterall 1977; 1979). This mechanism of action is supported by recent evidence that scorpion α-toxins prevent a component of outward gating charge movement that is associated with inactivation of the channel (Sheets *et al* 1999).

Neurotoxin receptor site 4 is occupied by another group of scorpion toxins: the scorpion β-toxins. These toxins induce both a shift in the voltage dependence of sodium channel activation in the hyperpolarizing direction and a reduction of the peak sodium current amplitude (Jover *et al* 1980; Cahalan 1975; Jonas *et al* 1986). Binding of these toxins to receptor site 4 is dependent on the activated conformational state of the toxin receptor site, and the binding is disturbed by mutation of amino acid G845N on the extracellular end of the IIS4 segment (Cestèle *et al* 1998). The proposed mechanism of action of scorpion β-toxins, therefore involves their interaction with the extracellular end of the IIS4 segment in activated channels through binding to the S3-S4 loop. Since the IIS4 segment moves outward during depolarisation, it is proposed that the toxins bind to newly accessible residues in the IIIS3-S4 loop and the extracellular end of the IIIS4 segment during conditioning prepulses. Scorpion β-toxins are thought to trap and stabilize the IIS4 segment in its outward, activated position thus enhancing channel activation in response to subsequent depolarization and therefore

causes the negative shift in the voltage dependence of activation (Cestèle *et al* 1998).

The lipid-soluble brevetoxins and ciguatoxins isolated from the dinoflagellates *Ptychodiscus brevis* and *Gambierdicus toxicus*, respectively, bind to receptor site 5, resulting in enhanced sodium channel activity and causing a shift in activation to more negative membrane potentials, and block inactivation (Benoit *et al* 1986; Huang *et al* 1984; Lombet *et al* 1987; Birinyi-Strachan 2002).   Photoaffinity labelling experiments have identified transmembrane segments IS6 and IVS5 as participating in the formation of receptor site 5. How the binding of these toxins to segments IS6 and IVS5, alter sodium channel kinetics have yet to be fully understood.

The polypeptide toxin conotoxin-TxVIA isolated from the venom of the cone snail *Conus textile* led to the identification of receptor site 6. This toxin causes a marked prolongation of action potentials, due to specific inhibition of sodium current inactivation (Hasson *et al* 1993). Although conotoxin-TxVIA has the same physiological effects on sodium current as toxins binding to receptor site 3, its binding is not voltage-dependent and allosteric modulation by toxins binding to other receptor sites is different (Fainzilber *et al* 1994).
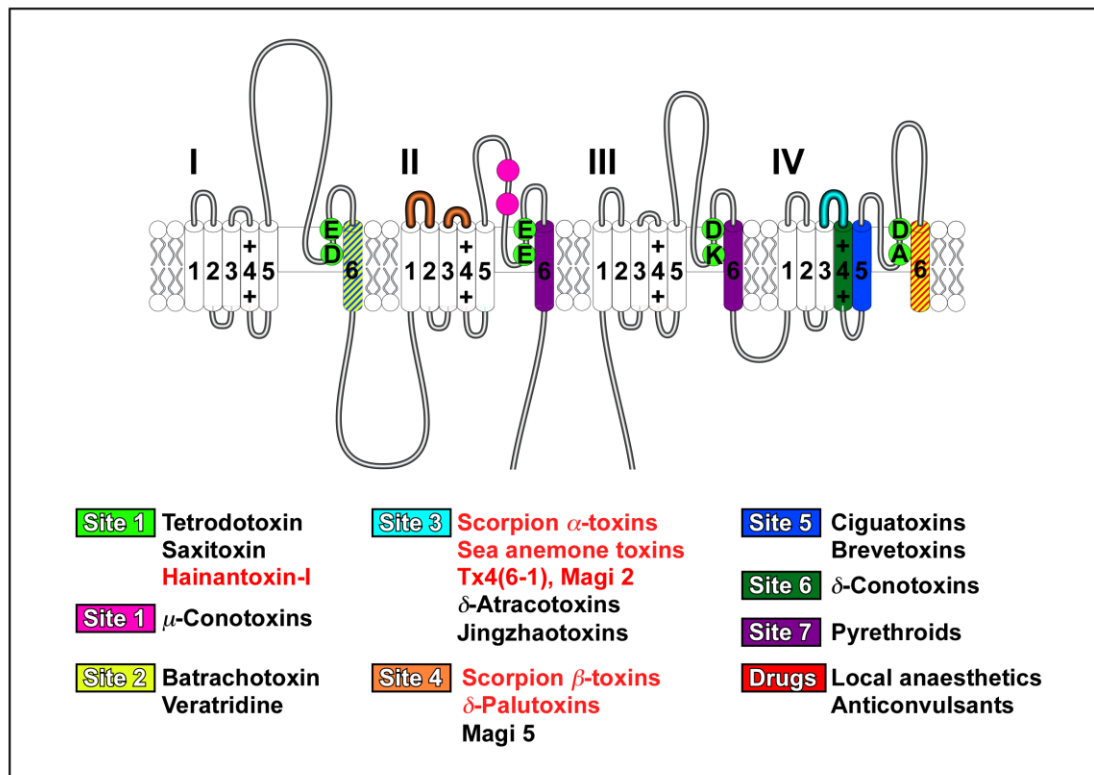
Figure 2.2: Localization of known neurotoxin receptor sites on Na$_V$ channels. Green circles represent the outer (EEDD) and inner (DEKA) rings of amino acid residues that form the ion selectivity filter and the proposed neurotoxin receptor site-1 for the water soluble guanidinium toxins, tetrodotoxin (TTX) and saxitoxin (STX). Some μ-conotoxin binding sites overlap with those of TTX and are omitted for clarity. In the case of receptor sites 3 and 4, only areas where mutagenesis of key residues leads to a more than five-fold decrease in binding affinity are highlighted. Insect-selective toxins are highlighted in red text. Adapted from Céstele and Catterall, 2000).

2.2: K_V CHANNELS

The movement of potassium ions through the voltage-gated potassium (K_V) channel underlies many fundamental biological processes, including electrical signalling in the nervous system. These channels are small in size compared to their molecular cousins, the Na^+ and Ca^{2+} channels, and indeed the major protein unit of the Na_V and Ca_V channels looks very much like four K^+ channels strung in tandem. All K_V channels show a selectivity sequence for $K^+ \approx Rb^+ > Cs^+$, whereas permeability for the smallest alkali metal ions Na^+ and Li^+ is immeasurably low. Potassium channels also share a constellation of permeability characteristics that is indicative of a multi-ion conduction mechanism (Doyle et al 1998): The flux of ions in one direction shows high-order coupling to flux in the opposite direction, and ionic mixtures result in anomalous conduction behaviour (Hodgkin and Keynes 1955). Because of these properties, K_V channels are classified as "long pore channels", invoking the notion that multiple ions queue inside a long, narrow pore of 45 Å in single file (Doyle *et al* 1998).

A K_V channel subunit and a single domain of a Na_V or Ca_V channel have similar hydropathy profiles, which highlight six possible transmembrane segments (S1-S6) (Mackinnon 1991). The fourth putative transmembrane segment, S4, is very atypical because the hydrophobic sequence is interrupted by a cationic residue (arginine or lysine) at every third or fourth position. This unusual motif, thought to be a voltage sensor (Stühmer *et al* 1989b), is very conserved: all of the voltage-activated K^+ subunits have one of these activated peculiar sequences while Na_V and Ca_V channels have four (one in each domain). A second structural class of potassium channels, which includes the inward rectifier and K_{ATP} channels, contains two putative transmembrane segments (M1 and M2) and a pore-forming P-region (Nichols and Lopatin 1997).

When the Shaker „A-type" K^+ channel gene was first cloned, its size relationship to Na_V channels immediately suggested that a functional K_V channel may be

formed by the coassembly of independent subunits (Tempel *et al* 1987). Evidence for multiple subunits was first proven by experiments in which two K_V channels with distinct properties were coexpressed in the same cell (Christie *et al* 1990). A fraction of the resulting channels displayed a unique blend of properties and exhibited currents that could not be explained by the expression of the parent channels alone (Christie *et al* 1990). These findings point to the formation of hybrid K_V channels and provide clear evidence that the functional channel is a multimeric protein. Later experiments studying the interaction of a scorpion toxin inhibitor, charybdotoxin (ChTX), with coexpressed wild-type and toxin-resistant mutant Shaker A-type K_V channels revealed that the mutant channel subunits were coexpressed along with the wild-type in known ratios (MacKinnon *et al* 1990). By measuring inhibition of the channels at high toxin concentrations, the fraction of channels containing only mutant subunits was determined. This fraction is a measure of the subunit stoichiometry since, for a given mixture ratio, it is related in a simple binomial way to the subunit number. For the Shaker A-type K_V channel, the subunit number was found to be four concluding that the complete K_V channel is tetrameric, and in this respect is very similar to the Na_V and Ca_V channels (MacKinnon *et al* 1990).

A
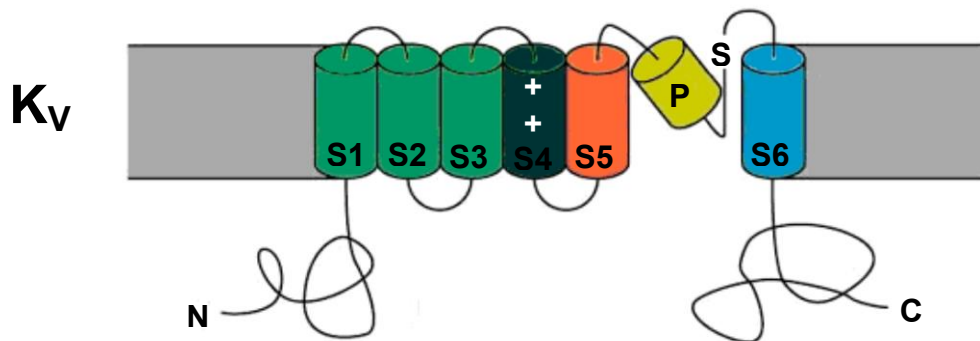
B
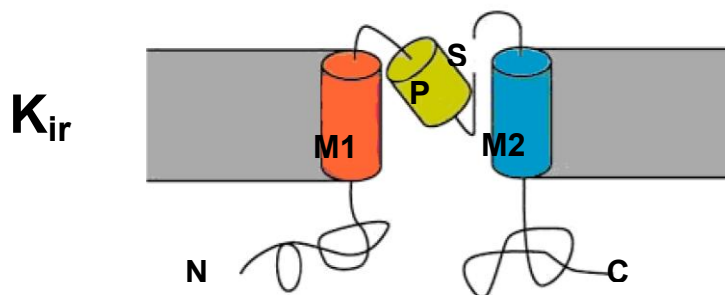
Figure 2.3: Membrane topologies and main features of K_v and K_{ir} potassium channel subtypes. Schematic representation of the membrane topologies of K_v channels (**A**) and K_{ir} channels (**B**). Note that one subunit of the tetrameric structure is shown. Transmembrane helices are numbered S1-S6 in K_v channels and M1 and M2 in K_{ir} channels; P, pore helix; S, signature sequence; N, amino terminus; C, carboxyl terminus. The extracellular side is towards the top of the page.

The selectivity filter is the central structural element that defines a K_v channel; its amino-acid sequence is conserved in all K_v channels throughout nature (also

called the signature sequence). In the filter, four strands of sequence TVGYG, one contributed by each of the four subunits, are arranged with their carbonyl oxygen atoms pointed inward towards the ion conduction pathway (Morais-Cabral *et al* 2001). When an ion enters the selectivity filter, it evidently dehydrates. To compensate for the energetic cost of dehydration, the carbonyl oxygen atoms must take the place of the water oxygen atoms, come in very close contact with the ion and act like surrounding water (Benzilla and Armstrong 1972) (Fig **2.4**). This arrangement creates four potential ion-binding sites into which a K^+ ion can bind in an essentially dehydrated state, surrounded by eight oxygen atoms from the protein (Morais-Cabral *et al* 2001).

As a first approximation, K_V channels can be subdivided into four general categories: (a) voltage-gated channels; (b) Ca^{2+}-activated channels; (c) receptor-coupled channels; and (d) ATP-sensitive channels. Some representatives of the first two channel types are blocked with high affinity by specific toxins. Although no toxin inhibitors have been identified for members of categories (c) and (d), antidiabetic sulfonylurea drugs are potent inhibitors of ATP-dependent K^+ channels present in pancreatic β-cells (Garcia *et al* 1991). Given the focus of this review only the K_V channels of catergories (a) and (b) will be discussed.

The voltage-gated K_V channels are a heterogenous group of proteins that can be subdivided into noninactivating or "delayed," and rapidly inactivating or "transient", outward current carriers based on their biophysical properties (Hille 1984). Delayed rectifying channels differ greatly in their inactivation kinetics among various tissues, and are found in most nerve and muscle cells. Their primary function is to repolarize the cell membrane during the late phase of the action potential (Garcia *et al* 1991). There are two main criteria used to consider K_V channels as delayed rectifiers. The first is that the macroscopic current through these channels is similar in overall kinetic behaviour and voltage-depedence to the K^+ current described by Hodgkin and Huxley. The second criterion is one of exclusion. K_V currents activated by membrane depolarization that are distinct from typical „A"-type currents and which are not activated by a

rise in the internal Ca^{2+} concentration are called delayed-rectifiers. However „A‟ currents and Ca^{2+}-activated K_V currents can produce delayed rectification; and may also participate in action potential repolarization (see below).

The transient rapidly inactivating („A-type‟) K_V channel (K_A) has been observed in many cell types (Rogawski 1985). This channel rapidly activates and then inactivates upon membrane depolarization. It is believed to regulate the firing frequency of neurons (Connor and Stevens 1971a). More information about this type of K_V channel is available because of the successful cloning and functional expression of the *Drosophila shaker* gene (Tempel *et al*,1987; Timpe *et al*,1988). Mutations at the *shaker* locus affect rapidly inactivating K^+ currents in *Drosophila*, and mRNA transcribed from *Shaker* cDNA clones induces functional A-type K_V channels when expressed in frog oocytes (Timpe *et al* 1998). Subsequent studies of A-type K^+ currents in molluscan neurons have identified characteristics that further distinguish this current from other K^+ currents (Connor and Stevens 1971a; 1971b). A-type K^+ currents activate and inactivate quickly compared to other K^+ currents. Steady state inactivation is complete near resting potential (-40mV) and the threshold for activation is more hyperpolarized then that for other K^+ currents. Thus, this current operates in the subthreshold region for action potential generation, opening transiently with small depolarisations, which start from hyperpolarized potentials (Rudy 1988). Such properties enable this current to regulate the frequency of repetitive firing when a neuron is spontaneously active or fires repetitively in response to tonic depolarisation. The hyperpolarization that follows an action potential removes the steady-state inactivation of A-type K_V channels, which open transiently. The resultant transient outward current slows down the return of the membrane potential toward action potential threshold (Rudy 1988). As a result the interspike interval is prolonged (Rudy 1988). The channels described previously, delayed-rectifiers and „A-type‟, are voltage-dependent channels, that is, they are gated by the membrane potential.

In a class of K_V channels to be now considered, channel opening and closing depends on the Ca^{2+} activity in the cell‟s cytoplasm. In these channels an

increase in the concentration of Ca^{2+} inside the cell leads to channel opening. Although in some cases there may be also voltage-dependent gating, for one of the Ca^{2+}-activated channels (the BK, slo, maxi-K^+ channels or $K_{Ca}1.X$), the observed voltage-dependence of channel opening (e-fold increase in conductance per 10-15 mV at all Ca^{2+} concentrations) is the result of voltage-dependent Ca^{2+} binding to the channel (Moczydlowski and Latorre 1983). In addition increasing concentrations of internal Ca^{2+} causes a shift in the voltage dependence of activation along the voltage axis toward more hyperpolarized potentials.

In whole cells, the Ca^{2+}-activated K^+ currents show a voltage-dependence derived from the gating of voltage-dependent Ca_V channels and the ensuing Ca^{2+} entry. Ca^{2+}-Activated K^+ channels (K_{Ca}) are found in a variety of electrically excitable and nonexcitable cells (Schwartz and Passow 1983; Blatz and Magleby 1986). Channel conductance, calcium sensitivity, voltage dependence and pharmacological properties have all been used to distinguish between different channels in this family. Since channel conductances range from a few to several hundred picosiemens (pS), K_{Ca} channels have been subdivided according to this property (Garcia *et al* 1991). High-conductance K_{Ca} channels also known as BK_{Ca} (big) or maxi-K^+ channels because of their large conductance (130-300pS), are the best studied K_{Ca} channels. These channels are widely distributed in neurons, striated and smooth muscle cells, endocrine and exocrine glands, (Latorre *et al* 1989). Topological analysis of the BK_{Ca} α-subunit has revealed that the channel possess seven transmembrane domains, rather than six transmembrane domains found in voltage-gated K_V channels; the extra domain (S0) is located at the amino terminus of the protein (Fig **2.4**, Meera *et al*, 1997). The α-subunit also contains the P-loop (or the pore-forming loop P between S5 and S6 domains, and the four hydrophobic segments (S7-S10) at the large intracellular carboxyl (C) terminus. The C-terminal region consists of a regulator of conductance for potassium (RCK) domain (Jiang *et al*, 2001), connected by a non-conserved linker to the tail domain (Wei *et al*, 1994). The C-terminal contains

the "Ca bowl" motif, several leucine zipper domains for protein-protein interactions (Tian *et al*, 2003) and multiple phosphorylation sites for cAMP- and cGMP-dependent protein kinases (Zhou *et al*, 2001).

The site on the α subunit where Ca^{2+} binds „the Ca^{2+} bowl" appears to be located towards the long carboxyl terminus (Ghatta *et al*, 2005). Voltage, by itself, will also activate BK_{Ca} channels in the absence of calcium (Cui *et al* 1997; Meera *et al* 1996), consistent with the presence of a voltage sensor in the S4 region of this protein, similar to Na_V and Ca_V channels. These channels provide a pathway for cell repolarization subsequent to membrane depolarization. Consequently, they have been implicated in regulation of neuroendocrine secretion and muscle contractility. High conductance can be explained by postulating that the channel is a multi-ion pore, which contains fixed negative charges in its mouth.
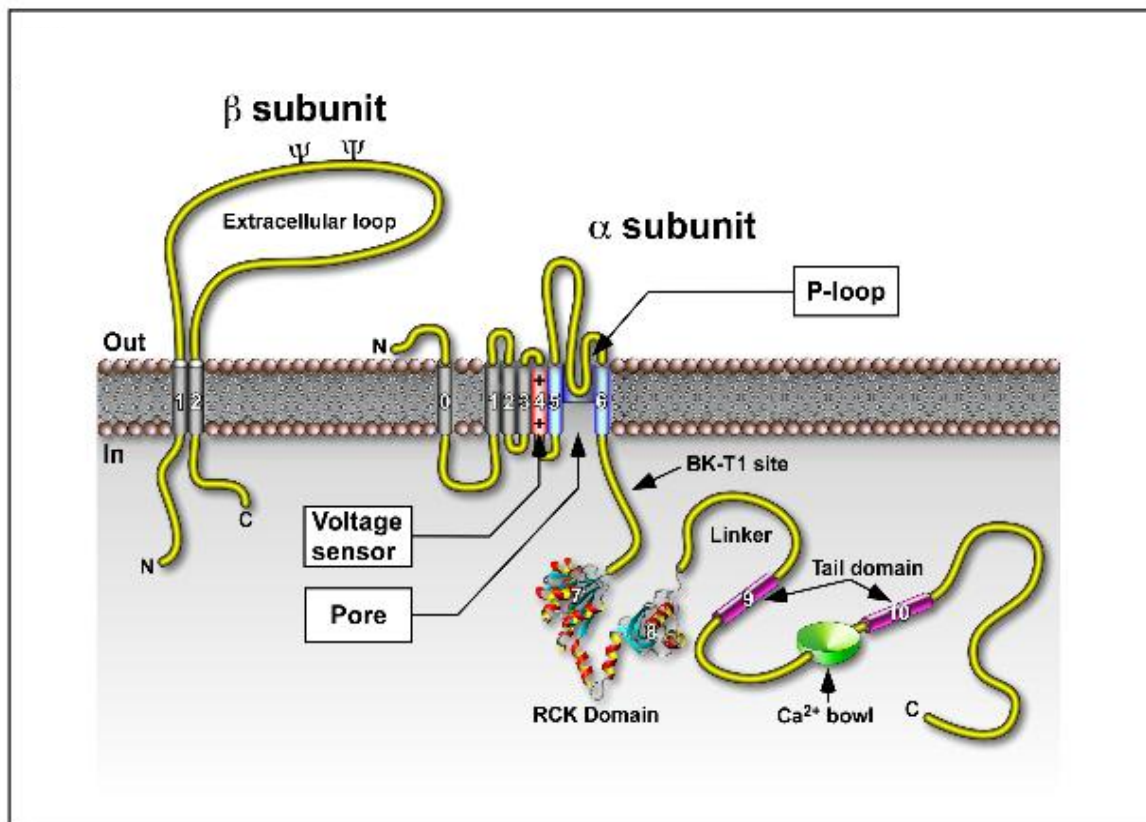
Figure 2.4: Schematic representation of the molecular structure and membrane topology of the α- and β-subunits of BK$_{Ca}$ channels. The central portion of the figure shows the extracellular portion of the □-subunit with the putative transmembrane α-helical segments (S0–S6) represented by cylinders and the S4 voltage sensor shown in red. The pore-lining segments S5 and S6 and the intervening P loop that form the walls of the ion-conducting pathway are shown in blue. The intracellular portion of the channel comprises the S7-S10 domains, including the RCK domain (S7 and S8; PDB code 2AEF), the tail domain (S9 and S10; magenta) including the calcium bowl (green), and the long C-terminus of the α-subunit. Functional channels are formed by the assembly and tetramerization of appropriate channel monomers which are mediated by the association domain (BK-T1) from each monomer. The left-hand portion of the figure shows the regulatory β-subunit comprising two putative transmembrane units (TM1 and TM2) connected by an extracellular loop. ψ indicates sites of probable glycosylation. Adapted from Ghatta *et al*, 2005.

Small-conductance Ca^{2+}-activated K^+ channels also known as SK_{Ca} channels ($K_{Ca}2.X$), are in general very sensitive to internal Ca^{2+}, and can be divided into two different categories: voltage-dependent SK_{Ca} channels, such as those present in *Aplysia* and *Helix* neurons, and voltage-independent SK_{Ca} channels that are found in muscle, olfactory neurons and erythrocytes (Garcia *et al* 1991). The SK_{Ca} channel in rat skeletal muscle displays a conductance of 12 pS and possess the properties necessary to account for the after-hyperpolarization in myotubes (Blatz and Magleby 1986), this result has identified the role that SK channels play in after-hyperpolarization during action potentials. Unlike strictly voltage-dependent channels, limited structural information is available for K_{Ca} channels. This may suggest that although some pharmacological characteristics are similar for both classes of channels, significant differences in primary structure do exist.

2.2.1 INSECT K_V CHANNELS

Insect K_V channels can be grouped into three main structural classes according to the number of transmembrane segments, i.e. 2, 4 and 6TM (Wei *et al*, 1996). The domain consisting of 2 TM segments is the simplest protein motif, which can form the core of an ion channel. The pore domain of the 2TM protein is homologous to that between S5 and S6 in 6TM channel-proteins. This group of channels form the family of „inward rectifiers" interestingly K_{IR} channels have yet to be identified in *Drosophila* (Nasonkin *et al*, 1999), although K_{IR}-like sequences are found in the *Drosophila* gene bank. In the genome of *C. elegans* there are two genes, which code for 2TM channels. They appear to be more closely related to each other than to any of the vertebrate genes (Wei *et al*, 1996).

The 4TM channel α subunit consists of two 2TM segments, which are linked by an intracellular loop, and thus contains two P-domains. The extracellular loop

between M1 and M2 is notably large, as it bears in most cases a cysteine residue. Formation of a disulfide bridge between the corresponding cysteines of two 4TM subunits can link them together to a functional channel (Lesage *et al*, 1996). ORK1, the sole presently characterized example found in insects, is an open rectifier K$^+$ channel coded by a gene in *Drosophila* (Goldstein *et al*, 1996). Of interest in *C. elegans*, the 4TM family constitutes the largest K$^+$ channel family – there are over 50 genes.

The large 6TM superfamily comprises four families of Shaker-type voltage-gated K$^+$ channels (K$_V$), the family KCNQ channels, three families of EAG-like channels and three families of Ca^{2+}- dependent K$^+$ channels. Some of these channels are not voltage-gated, e.g. SK$_{Ca}$ channels. The BK$_{Ca}$ channels are included in this superfamily despite having an additional TM segment (S$_0$). Notably in *drosophila* for each of these families there is just one gene. Unlike in mammals it is therefore possible to eliminate an entire family of K$^+$ channels with a mutation to a single gene (Tsunoda and Salkoff, 1995).

2.2.2: K$_V$ CHANNEL TOXINS

The first K$_V$ channel toxin identified in *Leiurus quinquestriatus hebraeus* scorpion venom and probably the most extensively studied member in this series, was named charybdotoxin (ChTX) by Miller *et al* (1985). This group found that ChTX blocks large-conductance BK$_{Ca}$ channels when added to the membrane surface opposite from that at which Ca^{2+} activates the channel (i.e., at the external side). ChTX block of channel activity is characterized by silent periods, during which time no activity is observed, separated by "bursts" of typical channel activity (Miller *et al* 1985). Within such a burst, channel gating kinetics, as well as unitary conductance, are identical to those observed under control conditions. Silent periods of activity have been interpreted as time intervals during which a molecule of toxin is bound to the channel and ion conduction is blocked (Miller *et al* 1985). Purification of ChTX has been achieved using a combination of ion

exchange and reversed-phase chromatography (Gimenez-Gallego *et al* 1988; Valdivia *et al* 1988; Strong *et al* 1989). The complete amino acid sequence has been elucidated (Gimenez-Gallego *et al* 1988) and later confirmed (Strong *et al* 1989). This 37 amino acid peptide contains six cysteine residues. Its N-terminal amino group is cyclised in the form of pyroglutamate, but treatment of the toxin with pyroglutamate amino-peptidase cleaves the residue allowing the unblocked peptide to be sequenced.

Interestingly, ChTX has a high content of positively charged residues (i.e., 4 Lys, 3 Arg and His), which gives the peptide a net charge of +5. Since the discovery and purification of ChTX, a number of investigators have studied the effects of this toxin on different types of K_V channels. It is well known that ChTX does not affect Na^+ or Ca^{2+} channels (Miller *et al* 1985; Hermann and Erxleben 1987). However, its selectivity as an inhibitor of high-conductance BK_{Ca} channels has been questioned (Schweitz *et al* 1989), and there is accumulating evidence that ChTX blocks several different types of K_V channels (Garcia *et al* 1991). In bullfrog ganglion B neurons, ChTX prolongs action potential duration consistent with blockade of the voltage-and calcium-dependent K_V channels known to control membrane repolarization in these cells (Goh and Pennefather 1987). ChTX was also found to block non Ca^{2+}-activated K_V channels in human and murine T-lymphocytes (Chandy *et al* 1986). In human quiescent peripheral blood T cells of both helper ($CD4^+$) and suppressor type ($CD8^+$) phenotype, ChTX blocks voltage-gated K_V channels with a K_d of 0.3 nM (Price *et al* 1989). Of interest ChTX also blocks rat K_V1.3 channels with a comparatively high K_d value of 0.17 nM. Perhaps, one of the most interesting findings for ChTX is the observation that *Drosophila shaker* (K_V1.1) channels, expressed in either *Xenopus* oocytes (insect) or mammalian cells are sensitive to inhibition by the toxin, with a K_d of 120 nM (Possani *et al*, 1999). Similarly ChTX inhibits the *shaker*-like vertebrate channels K_{Ca}1.1 from rats and human K_{Ca}3.1 with K_d values of 2.1 and 0.17 nM, respectively (Possani *et al*, 1999, Rauer *et al*, 2000).

The toxin does not alter the time course of K_V channel activation or inactivation, and it binds to the closed channel since full block is observed within the first few

milliseconds of the activating pulse. Subsequent studies have shown that ChTX blocks the α-subunits of BK channels from the American cockroach, (*Periplaneta Americana* , pSlo) murine (mSlo) and human (hSlo). Interestingly, channels with biophysical properties similar to the *shaker* channel are present in several other preparations, but are not inhibited by ChTX (Gimenez-Gallego *et al* 1988), for example dSlo from *Drosophila melanogaster* (Derst *et al*, 2003). However, the K_{Ca} current eliminated by *slo* in adult *Drosophila* muscle is sensitive to ChTX (Elkins *et al*, 1986). Although ChTX is not an insect/mammalian-specific toxin, it remains the most widely used and understood scorpion toxin to understand K_V channel function.

The observation that ChTX is not a selective K_V channel probe has spurred research efforts to find a specific modulator of BK_{Ca} channels. Investigation of the venom from the scorpion *Buthus tamulus* revealed a 4.3 kDa protein with a 70% homologous primary sequence to ChTX (Galvez *et al* 1990). This toxin called iberiotoxin (IbTX) has been subsequently shown to be highly selective for high-conductance BK_{Ca} channels, reversibly inhibiting channel activity by causing long silent periods (Garcia *et al* 1991). In addition, IbTX is a noncompetitive inhibitor of [^{125}I]ChTX binding in smooth muscle, suggesting that it interacts at a unique site on the receptor (Garcia *et al* 1991). To date, the high-conductance BK_{Ca} is the only target sensitive to this toxin, making IbTX a unique tool with which to investigate the physiological role of BK_{Ca} in different tissues. IbTX consists of a single 4.3kDa polypeptide chain, with 68% sequence homology with ChTX (Galvez *et al* 1990). However, IbTX possesses 4 more acidic and 1 less basic residue than does ChTX, making this toxin much less positively charged then ChTX. In single channel recordings IbTX reversibly blocks BK_{Ca} in excised membrane patches from bovine aortic smooth muscle (Galvez *et al* 1990). It acts exclusively at the outer face of the channel and has an IC_{50} of about 250 pM (Galvez *et al* 1990).

New BK channel blockers that are isolated have tremendous potential as pharmacological tools for the study of the diverse physiological role of BK

channel subtypes in different tissues and organisms. Of particular interest is the 31 residue toxin, BmBKTx1 (BmK) from the venom of the Asian scorpion *Buthus martensi* (Xu *et al,* 2004).   BmK was shown to block the α-subunits of BK channels of the fruit fly (*Drosophila melanogaster*, *dSlo*) and the American cockroach (*Periplaneta americana*, *pSlo*) with IC_{50} values of 194 nM and 82 nM, respectively. In contrast BmK failed to inhibit the α-subunit of the human BK channel (hSlo) at concentrations as high as 10 µM. Furthermore BmK only partially inhibits rat SK_2 channels at doses up to 1 µM. These results indicate that BmK is an insect selective BK channel blocker, and the first reported toxin active on the *Drosophila* Slo channel *dSlo*.

2.3: Ca_V CHANNELS

Voltage-gated calcium (Ca_V) channels are essential for the normal physiological function of excitable cells. These integral membrane proteins sense surface membrane depolarization and subsequently control the entry of extracellular calcium into the cytoplasm. Calcium entry alters membrane voltage and regulates a variety of physiological activates such as muscle contraction, neurotransmitter release, hormone secretion and gene expression. Structurally calcium channels are multimeric proteins consisting of a pore forming α_1 subunit (175 kD) and some combination of auxiliary β (54kd), α_2 (143 kD), δ (27 kD) and γ (30 kD) subunits (De Waard *et al* 1996; Catterall *et al* 1988). Multiple genes encode each of the subunits. The varied biophysical and pharmacological properties of calcium currents recorded in different cells result from the differential expression of the α_1 and auxiliary subunits.

Insect Ca_V channels can be divided into two families based on their voltage-dependence of activation: low-voltage-activated (LVA) Ca_V channels and HVA (high-voltage-activated) LVA currents are those, which activate around –60 mV whereas HVA currents activate around –30 mV. This distinction is purely phenomenological.

The Ca_V α_1 subunit is comprised of ~2000 amino acid residues and like the Na_V channel, the Ca_V α_1 subunit can by itself give rise to voltage-dependent currents (Stühmer 1991). The Ca_V α_1 subunit is organized in four repeat domains (I-IV), each with six transmembrane segments (S1-S6), and a membrane-associated re-entrant loop between S5 and S6 (Fig **2.5**). The quaternary structure of HVA Ca_V channels typically comprises 4-5 subunits: (i) a pore-forming α_1 subunit of 170-250 kDa: (ii) an extracellular α_2 subunit; (iii) a transmembrane δ-subunit that is covalently linked to α_2 via a disulfide bond to form an 170 kDa α_2-δ complex; (De Jongh *et al*, 1990) (iv) an intracellular 50-78 kDa β subunit; and (v) in some cases, a transmembrane γ-subunit of 25-78 kDa (Catterall, 2000b).

While the identity of the α_1 subunit determines many of the functional characteristics of the expressed channel, the auxiliary subunits are known to modulate voltage dependency, kinetics and current density (Chu *et al* 2001).

In HVA Ca_V channels, the α_2-δ, β and γ subunits modulate properties of the α_1 subunit such as activation/inactivation kinetics and the voltage-dependence of activation (Doering and Zamponi, 2003; Feng *et al*, 2003). The β subunit additionally helps traffic the α_1-subunit to the plasma membrane (Dolphin, 2003). Some toxins from predatory marine snails and spiders are selective calcium channels blockers and may therefore be used to identify distinct types in native cells (e.g Olivera *et al* 1994).

By comparison of the amino acid sequence of the three α_1 subunits produced by *Drosophila melanogaster*, designated Dmca1D, Dmca1A and Ca-α_{IT}, insect calcium channels can be classified broadly as Ca_V1-, Ca_V2- and Ca_V3-, respectively. However the pharmacological agents used to functionally define the various subtypes of vertebrate Ca_V channels cannot be used to classify invertebrate Ca_V channels. For example, insect Ca_V channels are less sensitive to dihydropyridines and ω-conotoxin-GVIA, which are used to distinguish vertebrate L-type (Ca_V1) and N-type (Ca_V2) channels, respectively (Wicher and Penzlin, 1997). Of interest is that even when the variable N- and C- terminal cytoplasmic regions of the α_1 subunit are excluded from amino acid comparisons,

the level of identity between insect Ca_V channels and their closest human ortholog is only 66% (King, 2007).
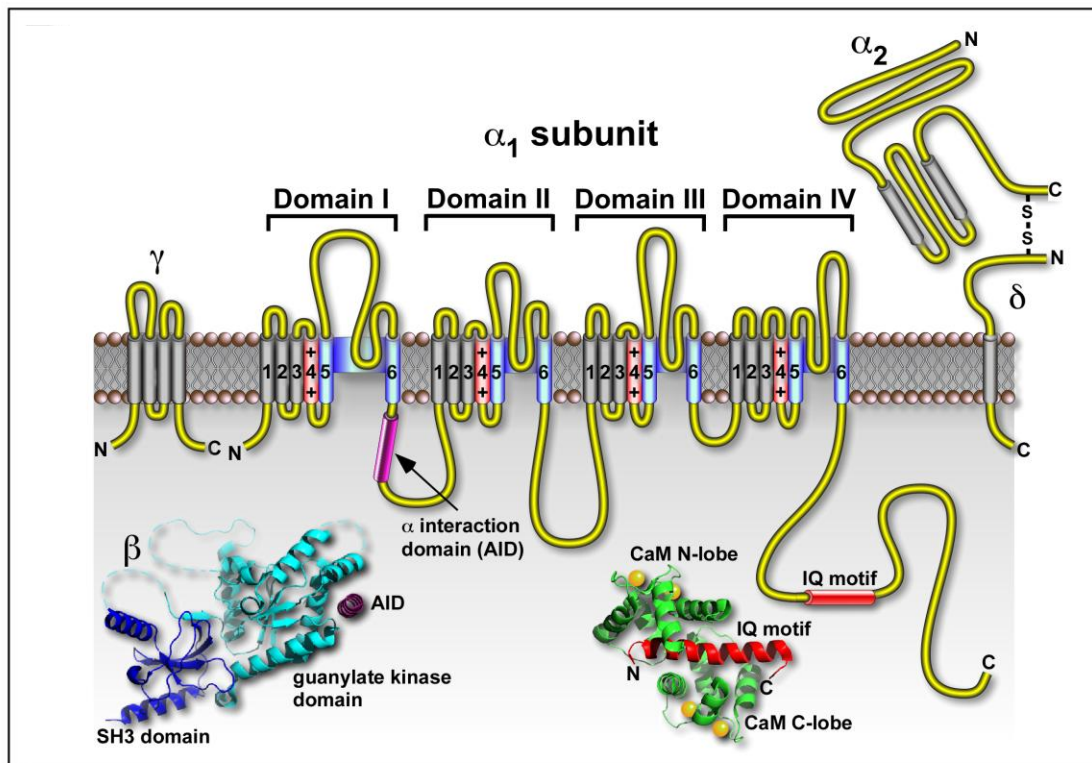
Figure 2.5: HVA Ca_V channels typically comprise a single copy of each of the α_1, α_2-δ, β and γ subunits, whereas LVA Ca_V channels consist of only the pore-forming α_1 subunit. The intracellular β subunit comprises an N-terminal SH3 domain (blue) and a C-terminal guanylate kinase domain (cyan). The guanylate kinase domain binds the α interaction domain (AID; purple) located in the cytoplasmic loop linking domains I and II of α_1, and this interaction modulates the rate of channel inactivation (Chen *et al* 2004; Van Petegem *et al* 2004). Calmodulin (CaM) interacts with Ca_V1 and Ca_V2 channels via a conserved sequence motif (the "IQ motif") located in the cytoplasmic C-terminal region of α_1. The N- and C-terminal lobes of CaM (green) bind the IQ domain (red) at different sites and with different affinities, making this interaction sensitive to both global calcium levels and the concentration of calcium in the vicinity of the Ca_V channel

pore. Calcium ions bound to CaM in the CaM-IQ complex are indicated by orange spheres. Adapted from King, 2007.

2.3.1: INSECT Ca$_V$ CHANNELS

Insects have a much smaller repertoire of Ca$_V$ channels then vertebrates (King, 2007). For example, whereas human genome encodes 10 pore-forming α_1 subunits, 4 β subunits, 4 α_2-δ complexes and 7 γ subunits, the genome of *D. melanogaster* appears to encode only 3 α_1 subunits, a single β subunit, 3 α_2-δ complexes and a single γ subunit (Littleton and Ganetsky, 2007). However, insects are able to expand their array of functional Ca$_V$ channels through alternative splicing and RNA editing (King, 2007). Amino acid sequence comparisons indicate that the 3 α_1 subunits produced by *D. melanogaster*, designated Dmca1D, Dmca1A and Ca-α_{1T}, can be classified as Ca$_V$1, Ca$_V$2 and Ca$_V$3-type channels, respectively (King, 2007). Given that insects express only a single ortholog of each channel subtype might explain why loss-of-function mutations in the genes encoding Dmca1D and Dmca1A are embryonic lethal. This indicates that these ion channels have distinct physiological roles that cannot be complemented by other Ca$_V$ channel subtypes.

When the variable N- and C-terminal cytoplasmic regions of the α_1 subunit are excluded from amino acid sequence comparison, the level of identity between insect Ca$_V$ channels and their closest human ortholog is only ~60% (King, 2007). This would explain why many of the pharmacological agents used to define vertebrate Ca$_V$ channel subtypes are not as useful for characterising insect Ca$_V$ channels (King *et al*, 2008).

2.3.2: INSECT-SELECTIVE Ca_V CHANNEL TOXINS

Toxins from spiders and predatory marine snails (ω-toxins; Olivera *et al* 1994) are very potent and selective blockers ω- conotoxin GVIA (ω-CgTx GVIA) and ω-agatoxin IVA (ω-Aga-IVA) – which in mammals are highly selective for N- and P-type channels, respectively; Venema *et al* 1992 - as well as depress calcium currents in insect neurons.

A number of features are common to all ω-conotoxins. The natural peptides are found in *Conus* venoms, and specifically target voltage-dependent calcium channel subtypes (Olivera *et al* 1994). The characteristic arrangement of cysteine residues –C....C......CC......C- is called the "four-loop Cys scaffold" of the conotoxins (Olivera *et al* 1991). ω- Conotoxin GVIA is the prototypic blocker of vertebrate $Ca_V2.1$ (N-type) channels. In contrast, ω- conotoxin GVIA has much weaker effects on insect Ca_V channels. In cockroach DUM neurons ω- conotoxin GVIA is a very weak blocker of HVA currents ($ED_{50} > 1\mu M$) (Wicher and Penzlin, 1997). Similarly ω- conotoxin MVIIC is a high-affinity blocker of vertebrate $C_V2.1$ and $Ca_V2.2$ (N-type) channels but has little effect on HVA currents in cockroach DUM neurons (Wicher and Penzlin, 1997;Chong *et al*, 2007). Due to their limited potency, ω- conotoxin GVIA and ω- conotoxin MVIIC are likely to have limited value in the study of insect Ca_V channels.

The ω-agatoxins of *Agelenopsis aperta* venom are a heterogenous group of polypeptides varying in molecular mass from 5 to 10 kDa. The earliest accounts of the ω-agatoxins described their block of presynaptic calcium channels at the insect neuromuscular junction (Bindokas and Adams 1989; Adams *et al* 1990; Bindakos *et al* 1991). ω-Aga-IVA despite becoming the defining pharmacology for vertebrate P/Q-type ($Ca_V2.1$) channels, also blocks Ca_V currents in a number of insect neurons with equal or higher potency than its effects on vertebrate Ca_V

channels. The effect of ω-Aga-IVA on insect Ca_V currents is highly variable, for example of the two HVA Ca_V currents observed in embryonic cockroach neurons, one is potently blocked by ω-Aga-IVA (IC_{50} = 9 nM) whereas ω-Aga-IVA has only a minor effect on the other (IC_{50} = 900 nM) (Benquet *et al*, 1999). In bee brain neurons ω-Aga-IVA potently blocks the MVA current (IC_{50} = 10 nM) in a way that is very similar to that observed for block of the ω-Aga-IVA-sensitive HVA current in embryonic cockroach neurons. However, the HVA Ca_V currents in cockroach DUM neurons are completely insensitive to ω-Aga-IVA, while the MVA Ca_V currents in the same neurons are mildly affected (IC_{50} = 100 nM) (Wicher and Penzlin, 1997). As mentioned Ca_V2 channels are the only subtype in insects that have a canonical ω-Aga-IVA binding site, and therefore the target for ω-Aga-IVA in insect neurons must be Ca_v2 channels. The varying effects of ω-Aga-IVA are likely due to different insect neurons expressing different isoforms of Ca_v2 channels.

Neurotoxins that also affect neuromuscular transmission in *Drosophila* have been identified and purified from *Plectreurys* spider venom (PLTX). These toxins have been highly purified and are peptides of about 7 kDa in molecular weight (Branton *et al* 1987). Inhibition of calcium channels by these toxins has been identified in *Drosophila* neurons using the prototypic member PLTX-II, that blocks both the inactivating and non-inactivating components (Leung *et al* 1989). Biochemical analysis of PLTXs has identified that fatty acylation of the C-terminal is crucial for the calcium channel specificity of the *Plectreurys* toxins. As such cleavage of the *O*-palmitoyl ester from the native toxin by base treatment results as expected in a drop of potency by at least two orders of magnitude (Branton *et al* 1993).

CHAPTER 3

DORSAL UNPAIRED MEDIAN NEURONES

Dorsal unpaired median (DUM) neurons from the terminal abdominal ganglia of the adult American cockroach (*Periplaneta americana*) are an ideal neuronal cell type to use when determining the specific activity of insect-selective neurotoxins. The diverse array of well-characterised ion channels present in this cell type, provide numerous and distinct target sites for insect-selective toxins to interact. Indeed, two types of Na_V channel (TTX-S and TTX-R) currents, five types of K_V channel ($K_{(Ca)}$, $K_{(A)}$, $K_{(DR)}$, $K_{(Na)}$ and $K_{(IR)}$) currents and four different types of Ca_V channel (tLVA, mLVA, MVA and HVA) currents, can be evoked in DUM neurons. Furthermore, DUM neurons are important electrophysiologically because they differ from other insect neurons in their complex membrane properties, like endogenous pacemaker properties, even in the absence of rhythmic somatic input (Lapied *et al*, 1989;93). Given these reasons DUM neurons were deemed the most suitable insect neuronal cell-type to use in this investigation to determine the target site(s) of the unknown insect-selective neurotoxins J-ACTX-Hv1c and the 'hybrid' toxin FW178.

3.1: CHARACTERISTICS OF DORSAL UNPAIRED MEDIAN NEURONS FROM AMERICAN COCKROACHES *PERIPLANETA AMERICANA*

The DUM cells in the cockroach *Periplaneta americana* have been studied in the metathoracic ganglion by Crossman *et al* (1971), Tanaka and Washio (1988), and Elia and Gardner (1990). There is also a population of DUM cells on the dorsal surface of the terminal abdominal ganglion (TAG) of the cockroach; these DUM cells have morphological and electrophysiological properties similar to those of the metathoracic ganglion (Crossman *et al* 1971, Dymond and Evans 1979) (Fig **3.1**). Three clusters of octopamine (OA)- immunoreactive (OR-ir) DUM neurones have been described by Eckart *et al* (1992) in the TAG of *P. americana*. The TAG, composed of the fused 7th to 11th neuromeres, contains three clusters of octopamine-immunoreactive (ir) midline somata, each comprising 12 DUM cells (both sexes) and 2 ventral somata, probably VUM cells. These three clusters appear to be confined to the 7th, 8th and 9th neuromeres, respectively (Eckert *et al* 1992). Those of the 7th neuromere in females probably correspond to identified DUM and VUM neurons, which innervate the oviduct muscle (Stoya *et al* 1989).
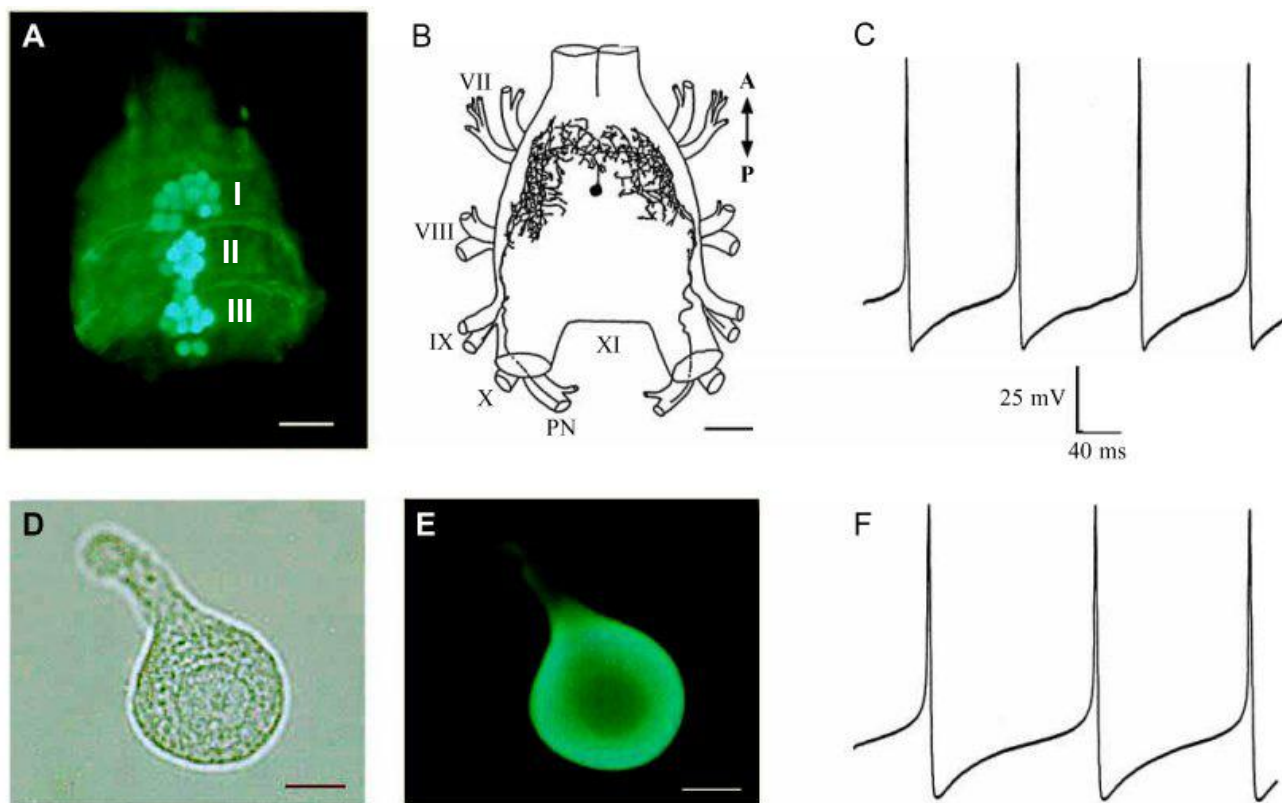
Figure 3.1: DUM neurons of the terminal abdominal ganglion (TAG) of the cockroach *Periplaneta americana*. (**A**) Photomicrograph showing octopamine-like immunoreactive DUM neurons revealed on the dorsal surface of the TAG. Clusters I to III are indicated. Scale bar 200 μm. (**B**) A dorsal-view c*amera lucida* drawing of the general morphology of DUM neurons revealed by anterograde cobalt staining performed on a soma located along the midline of the TAG. Scale bar 200 μm, A, anterior, P, posterior, VII, VIII, IX segmental nerves; X and XI, cercal nerves; PN phallic nerves. (**C**) Spontaneous overshooting action potentials recorded using an intracellular microelectrode in a DUM neuron *in situ*. The scale bar also applies to **F**. (**D**) Light micrographs of an isolated DUM neuron cell body maintained in short-term culture and treated with a polyclonal antibody directed against octopamine (**E**). Scale bars 25 μm. (**F**) Spontaneous electrical activity recorded using the patch-clamp technique (whole-cell recording configuration) in a single DUM neuron cell body. Adapted from Grolleau and Lapied 2000.

3.1.1 Basic Electrophysiological Characteristics

The somata of efferent DUM neurons in *P. americana* are, in contrast to those of many other insect neurons, capable of generating repetitive all-or-nothing action potentials (Hoyle and Dagan 1978). The discharge pattern observed in such preparations is very regular, yet in intact animals this is the exception rather than the rule. In the last decade many ionic currents important for spiking in cockroach TAG DUM neurons have been characterized (Lapied *et al* 1990a, 1990b, 1999; Grolleau and Lapied 1995a & b, 1996; Wicher and Penzlin 1994, 1997, 1998; Heine and Wicher 1998). Presently, octopaminergic cockroach TAG DUM neurons are among the electrophysiologically best characterized insect nerve cells and offer interesting opportunities to study modulatory mechanisms.

In the absence of excitatory and inhibitory input, repetitive, regular spiking requires an intrinsic pacemaking process that drives the membrane potential towards the action potential threshold as well as mechanisms, which repolarise the membrane or even lead to a transient hyperpolarization. In cockroach DUM neurons, several ionic currents might be involved in pacemaking (Figure **3.2**): (1) A background Na^+ current (Lapied *et al* 1999); (2) a background Ca^{2+} current (Wicher and Reuter 1993, Wicher *et al* 1994); (3) the voltage-activated Na^+ current (Lapied *et al* 1990); and (4) low voltage-activated Ca^{2+} currents (Grolleau and Lapied 1996). These currents as well as other related components will be discussed further in the following sections.
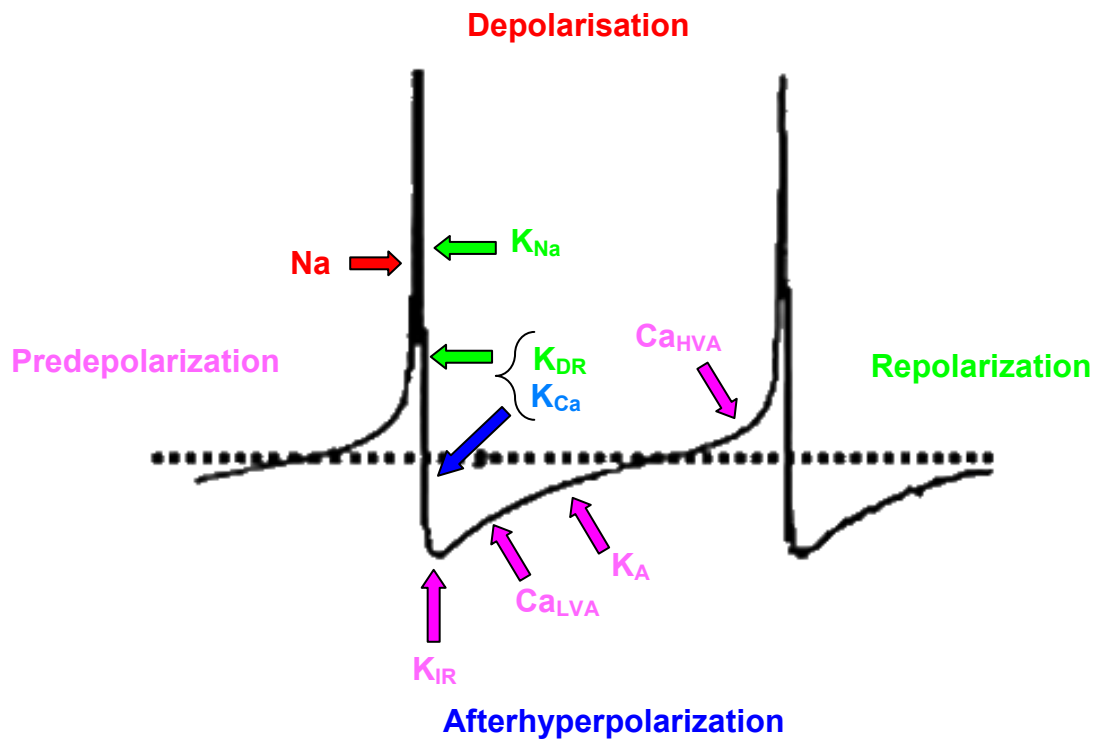
Figure 3.2: Intrinsic spontaneous electrical activity in DUM neuron somata *in vitro*. A model representing currents thought to be involved in the generation of the different phases of the beating pacemaker activity. Refer to the list of abbreviations on page xi. Adapted from Grolleau and Lapied 2000.

3.1.2: SODIUM CURRENTS

Na_V channels in TAG DUM neuron cell bodies have been localized by immunocytochemistry using antibodies directed against a synthetic peptide corresponding to the highly conserved SP19 segment of the rat brain type I voltage-dependent Na^+ channel α-subunit (Amat *et al* 1998). Light microscopy has revealed that voltage-dependent Na^+ channels are heterogeneously distributed in TAG DUM neuron somata (Grolleau and Lapied 2000). Voltage-clamp experiments provide further insight into the biophysical properties of the cockroach DUM neuron inward Na^+ current. When the concentration of extracellular Na^+ is varied, the reversal potential of the inward current shifts as expected from the Nernst equation, confirming that the inward current is highly selective for Na^+ (Lapied *et al* 1990b). This inward current is very sensitive to TTX. The concentration of half-maximal current inhibition (IC_{50}) varies somewhat among different preparations between 2 nM (Lapied unpublished observations) and 10.5 nM (Wicher and Penzlin 1998). This current is also partially blocked by external veratridine, ω-agatoxin-IVA, ω-conotoxin-MVIIC and ω-atracotoxin-Ar1a which reduces the time constant of inactivation (Wicher and Penzlin 1998; Chong *et al*, 2007). The voltage-dependent Na^+ current activates at potentials more positive than –40 mV (e.g. –35 mV) corresponding to the threshold of spontaneous action potentials (Lapied *et al* 1989), and reaches a current maximum at approximately –10 mV (Lapied *et al* 1990b, Wicher and Penzlin 1998). The Na^+ current exhibits sigmoidal voltage-dependent activation kinetics, and both activation and inactivation of the current become faster with strong depolarization. The voltage-dependence of steady-state inactivation and activation indicate that the Na^+ channels are half-inactivated at approximately –40 mV and half-activated near –25 mV. The inactivation and activation curves cross at approximately –75 to +10 mV. This suggests the existence of a large

steady-state window current, indicating that some of the channels activated are never inactivated in this potential range (Lapied *et al* 1990b).

In addition to this transient inward current, an unexpected maintained voltage-dependent Na$^+$ current has also been characterized in TAG DUM neurons (Lapied *et al* 1990b). This Na$^+$ current, also sensitive to TTX, is biophysically isolated from the other current by its negative threshold for activation (approximately –70 mV). This suggests the existence to two distinct voltage-dependent Na$^+$ currents in TAG DUM neurons (Table **3**.**1**). However no more information is available about the precise biophysical properties and physiological role of this low-threshold current in DUM neuron electrical activity (Grolleau and Lapied 2000).

The Na$^+$ resting current was first described in locust metathoracic ganglion DUM neurons (Goodman and Spitzer 1981a). This study reported that DUM neurons hyperpolarized by over 10 mV when Na$^+$ was replaced by Tris or choline, suggesting that the participation of the resting conductance of Na$^+$ is essential in maintaining the resting membrane potential near –60 mV. Similar observations were made both *in situ* and in isolated cockroach TAG DUM neurons (Lapied *et al* 1989). It was shown that the resting membrane potential was dependent on the external Na$^+$ concentration. The hyperpolarization observed in a reduced external Na$^+$ concentration was mimicked by external application of saxitoxin or TTX, indicating that most of the resting Na$^+$ current passed through TTX-sensitive Na$^+$ channels. Whole-cell experiments indicate that application of LqhαIT (an insect specific Na$^+$ channel blocker) to spontaneously active TAG DUM neurons stimulates a transition from rhythmic activity to burst firing. This bimodal flexibility is the consequence of an alteration in the behaviour of the resting Na$^+$ current (Lapied *et al* 1999). These results indicate that the Na$^+$ resting channels are necessary not only to drive the membrane potential of TAG DUM neurons to threshold for firing spontaneous action potentials (Lapied *et al* 1989) but are also essential in determining the firing pattern. In other words, these Na$^+$ channels are essential in maintaining rhythmic pacemaker activity at the normal range of resting membrane potential.

Table 3.1: Sodium currents in cockroach DUM neurons.

	I_{Na}	$I_{Na(m)}$	$I_{(rNa)}$
Description	Inward depolarisation-activated sodium current	Inward maintained sodium current	Inward sodium resting or maintained current
Sensitivity	TTX, Saxitoxin Partially blocked by ω-conotoxin MVIIC, ω-agatoxin-IVA, ω-atracotoxin-Ar1a veratridine and scorpion α-toxins.	TTX, Saxitoxin	TTX, Saxitoxin
Non-sensitivity	K^+ channel blockers	K^+ channel blockers, ω-conotoxin MVIIC, ω-agatoxins, veratridine and scorpion α-toxins.	Unknown
Activation Range	-35 mV	-75 mV	NA
Inactivation Range	Intrinsic Inactivation (<3 ms)	Slow or none	NA
Role in AP	AP depolarization	Unknown	Threshold for firing and determining firing pattern

Adapted from Grolleau and Lapied, 2000.

3.1.3: POTASSIUM CURRENTS

Electrophysiological and pharmacological investigations performed under voltage-clamp conditions revealed an unexpected diversity of K^+ channels underlying the electrical activity of the DUM neuron. Earlier studies performed using patch-clamp technique (cell-attached configuration) had revealed the existence of at least three types of outward current in cockroach metathoracic DUM neurons distinguished by their unitary conductance (11, 34 and 110 pS) (Dunbar and Pitman 1985). Although the ionic properties of these channels were not determined, two of these channels (with conductances of 11 and 34 pS) were shown to conduct K^+. Whole-cell voltage-clamp experiments have allowed the identification of at least five distinct types of K^+ channel in isolated cockroach TAG DUM neurons (Table **3**.**2**) (Grolleau and Lapied 1994, 1995a; Wicher *et al* 1994). These K^+ channels can be classified into two groups, the first type activated by voltage and intracellular ions and the second type only by voltage. Two distinct K^+ currents activated by intracellular ions have been characterized. The Na^+-activated K^+ current is one of the most unexpected currents (Dryer 1994) since usually K^+ currents are directly studied electrophysiologically in the presence of Na^+ channel blockers. However, it has been demonstrated in both the TAG DUM neuron (Grolleau and Lapied 1994) and the fifth abdominal ganglion (A5) DUMIa neuron (Gundel *et al* 1996) that a portion of the global outward current was sensitive to TTX. Tail current analysis, used to determine the ionic selectivity of this outward current, has confirmed that it is carried by K^+. The progressive activation of the Na^+-activated K^+ current is well correlated with the activation of the inward Na^+ current, indicating that this K^+ current is activated by the entry of Na^+ into the DUM neuron. Since there is no selective blocker of this current available the physiological significance of such currents in DUM neurons is unknown. Nevertheless, it is suggested that this current could limit the action potential duration by increasing the rate of repolarization of the action potential (Grolleau and Lapied 1994).

The second type of K^+ channel activated by intracellular ions is the more commonly found Ca^{2+}-activated K^+ channel (Rudy 1988). Electrophysiological experiments performed on cockroach TAG DUM neurons have indicated that they are also voltage-dependent (Thomas 1984, Wicher *et al* 1994, Grolleau and Lapied 1995a, Achenbach *et al* 1997). The Ca^{2+}-activated K^+ current of the TAG DUM neuron activates rapidly at potentials more positive than –50 mV and then inactivates in two phases. Both the transient and late components of the current are sensitive to extracellular TEA-Cl, inorganic blockers such as Cd^{2+} and Ni^{2+} and to different scorpion toxins (CTX and IbTX) known to block Ca^{2+}-activated K^+ currents (Garcia *et al* 1991). The biphasic aspect of this current together with the different steady-state holding potential sensitivity of the two components, led to the suggestion of the existence of to two separate Ca^{2+}-activated K^+ currents in TAG DUM neurons. However this hypothesis has never been proven since none of the specific Ca^{2+}-activated K^+ current blockers tested allows discrimination between the fast transient and late components. Ca^{2+}-activated K^+ currents have different physiological implications for the electrical activity of the DUM neuron. The prolongation of the falling phase of action potentials associated with a suppression of the afterhyperpolarization observed in the presence of Ca^{2+}-activated K^+ channel blockers (Lapied *et al* 1989) indicates that these currents play an important role in spike repolarization (i.e. in the regulation of action potential duration) and in the regulation of the repetitive discharge frequency of the TAG DUM neuron.

Besides K^+ currents activated by intracellular ions, three additional K^+ currents activated by voltage have also been characterized in cockroach TAG DUM neurons. Using biophysical and pharmacological approaches, it has been possible to dissect the ion-independent K^+ currents into three further voltage-dependent K^+ currents identified as an 'A-like' current, a delayed outward rectifier K^+ current (Grolleau and Lapied 1995a) and an inward rectifier K^+ current (Raymond and Lapied 1999).

The 'A-like' current, also termed the fast transient K^+ current, was first described in invertebrates and in gastropod neural somata (Connor and Stevens 1971a).

Because the A-current is selectively blocked by 4-aminopyridine (4-AP) in TAG DUM neurons, it has been isolated by subtracting the residual current after treatment with 4-AP from the global voltage-dependent K^+ current. This current activates at depolarising potentials more positive than –70 mV and exhibits rapid time-dependent activation and inactivation. Half-maximal steady-state inactivation occurs at approximately –65 mV and unlike the classical A-current of other neurons (Hille 1992), this current inactivates with complex inactivation kinetics (Grolleau and Lapied 1995a). Steady-state activation and inactivation curves cross at approximately –53 mV, resulting in a region of activation/inactivation overlap that extends from approximately –70 to –30 mV. This indicates that these channels conduct only within a window of negative potentials. In cockroach TAG DUM neurons, the physiological implication of the A-current has been demonstrated using 4-AP under current-clamp conditions (Grolleau and Lapied 1995a). These results indicate that the A-current is not involved in the repolarization and afterhyperpolarization of the action potentials. In contrast, the 4-AP-induced increase in action potential frequency indicates that the A-current, which is activated when the membrane is hyperpolarized beyond the resting level, regulates the behaviour of the TAG DUM neuron repetitive discharge firing.

The delayed outward rectifier K^+ current described in both excitable and non-excitable preparations (Rudy 1988, Pelhate *et al* 1990, Hille 1992), activates slowly and follows a sigmoidal time course to reach its steady-state value. This current shows no inactivation during the course of a maintained depolarization. It activates at potentials more positive than –50 mV and is completely blocked by a high external TEA-Cl concentration. On the basis of its time course of activation, it is postulated that the delayed rectifier outward K^+ current contributes to the repolarising phase of the action potential (Grolleau and Lapied 1995a).

The final type of voltage-dependent K^+ current, the hyperpolarized-activated inward current, is also heavily involved in regulating spontaneous neuronal electrical activity. The electrophysiological properties of this current characterized in TAG DUM neurons (Raymond and Lapied 1999) closely resemble those of

inward rectifier K^+ currents in many other cells (Rudy 1988, Hille 1992). This inward current activates at potentials near –80 mV, is half-activated at 109 mV and does not show time-dependent inactivation in normal saline solution. This current is not dependent on external Na^+ concentration and is sensitive to CsCl, $BaCl_2$ and TEA-Cl, but at high concentrations (Raymond and Lapied 1999). Under current-clamp conditions, injection of a long hyperpolarizing current pulse into the cell body induces a time-dependent rectification seen as a depolarising sag in the electrotonic potential. The very negative potential range in which the current is activated indicates that it does not affect DUM neuron excitability at or near the resting membrane potential. However it may act as an important depolarising mechanism that prevents TAG DUM neurons from becoming unresponsive when they are excessively hyperpolarized.

Table 3.2: Potassium and chloride currents in cockroach DUM neurons

	$I_{K(Ca)t}$	$I_{K(Ca)m}$	$I_{K(A)}$	$I_{K(DR)}$
Description	Transient IbTX-sensitive outward K^+ current	Late IbTX-sensitive outward K^+ current	Transient 4-AP sensitive outward K^+ current	Late ChTX- and 4-AP-resistant outward K^+ current
Sensitivity	ChTX, IbTX CdCl$_2$, Slightly TEA-sensitive	Slightly TEA-sensitive, ChTX, IbTX, CdCl$_2$	4-AP	TEA
Insensitivity	4-AP	4-AP	Ca^{2+} ChTX, IbTX, CdCl$_2$, Ext MgCl$_2$ TEA	Ca^{2+} ChTX, IbTX, CdCl$_2$, Ext MgCl$_2$ and 4-AP
Activation Range	-80 to –35 mV	Around –35 mV	~ –65 mV	~ –50 mV
Inactivation Range	Transient fast inactivation	No inactivation	Rapid	Very slow inactivation
Role in AP	Spike repolarization, Regulates AP duration Regulate Ca^{2+} entry	Action potential afterhyperpolarization and repolarization	Regulates firing frequency	Spike repolarization, role in sustained depolarisation seen after cholinergic transmission

Table 3.2 (Con't) Adapted from Grolleau and Lapied, 2000.

	$I_{K(Na)}$	$I_{K(IR)}$	$I_{Cl(Ca)}$
Description	Transient Na^+-sensitive K^+ current	Hyperpolarization activated inward K^+ current	Calcium-dependent outward chloride current
Sensitivity	Ext. Tris-HCl (replace Na^+), Declines as potentials reach Na^+ reversal potential. TTX (below +60 mV)	Ba^{2+}, Cs^{2+} TEA-Cl	$ZnCl_2$ (ext) SITS (int) DIDS (int) BAPTA
Insensitivity	$CoCl_2$, $CdCl_2$ TTX (above + 60mV). Li^+ as charge carrier	$ZnCl_2$ (ext) SITS (int) DIDS (int) BAPTA	Altering Na^+ or K^+ conc (ext) TEA-Cl
Activation Range	~ –30 mV	< –80 mV	< –60 mV
Inactivation Range	Slow inactivation	Slow inactivation	Slow inactivation (>3 sec)
Role in AP	Slow predepolarization allows repetitive firing at low frequencies, spike repolarization. Reduces AP duration	Underlies inward rectification following hyperpolarization	Limits excessive hyperpolarization by exogenous neurotransmitters.

3.1.4: CALCIUM CURRENTS

Ca^{2+} influx through voltage-activated Ca_V channels plays a central role in shaping spontaneous neuronal electrical activity since internal $[Ca^{2+}]$ itself not only controls the activation of other ionic channels (e.g. $K_{(Ca)}$ channels) but also controls the inactivation of the Ca_V channel. Furthermore, Ca^{2+} entry into nerve cell bodies through Ca_V channels is generally accepted as an important step in the sequence of events underlying the synthesis and release of secretory products.

Previous current-clamp investigations indicated the existence of Ca_V channels in the soma membrane of DUM neurons (Goodman and Heitler 1979, Bindokas and Adams 1989, Lapied *et al* 1989). Under normal conditions overshooting action potentials recorded in adult TAG DUM neuron somata resulted from a combination of voltage-activated Na^+, K^+, and Ca^{2+} currents. Under appropriate conditions (in the presence of Na^+-free saline and/or K^+ channel blockers), TAG DUM neurons can generate long-duration Ca^{2+} spikes that are blocked by the addition of Co^{2+} or ω-agatoxin-I (Goodman and Heitler 1979, Bindokos and Adams 1989). As a result, the three effects on action potentials (i.e. an increase in action potential duration, a reduction in the afterhyperpolarization and a positive shift of the threshold of the action potential), also indicates that TAG DUM neurons contained somatic Ca_V channels (Table **3.3**). Voltage-activated Ca_V channels have been classified using a variety of criteria including ionic selectivity, voltage and ionic sensitivity, pharmacological profile and sensitivity to physiological ligands (e.g. nicotine, octopamine and neurohormone D). Accordingly, it has been possible to define several distinct classes of Ca_V channels including LVA and HVA Ca_V channels (section **2 5**).

In cockroach DUM neurons the LVA and HVA Ca_V currents differ from each other not only on the basis of their sensitivity to different Ca_V channel blockers, but also in their voltage-dependence of activation and inactivation. Activation at very negative membrane potentials (between –70 mV to –60 mV), measured at

physiological Ca^{2+} concentrations (Grolleau and Lapied 1996), is the main characteristic of the LVA Ca^{2+} currents in neuronal preparations (Kostyuk 1999). In cockroach TAG DUM neurons, the global LVA Ca^{2+} current has been further dissociated by means of the sensitivity to nickel chloride, the time constant of deactivation and the kinetics of inactivation into transient LVA (tLVA) and maintained LVA (mLVA) Ca^{2+} currents (Grolleau and Lapied 1996). The tLVA current resembles the classical LVA Ca^{2+} current described previously (Kostyuk 1999). This current activates at a potential more positive than –80 mV and inactivated completely during a prolonged depolarising pulse. It is completely blocked by a low concentration of nickel chloride (<100 μM) and the kinetics of its inactivation is independent of Ca^{2+} influx through the channel. The potential at which half the tLVA channels are inactivated is approximately –60 mV. In contrast the mLVA Ca^{2+} current is easily distinguished from the tLVA current by its slow kinetics of inactivation (it does not completely inactivate during the course of the depolarising pulse), by its activation threshold (10 mV more positive then tLVA currents) by its decreased sensitivity to nickel chloride (> 100 μM) and by its Ca^{2+}-sensitive inactivation. The mLVA current becomes completely inactivated by any means that increases or reduces the intracellular Ca^{2+} concentration (Grolleau and Lapied 1996). Furthermore the voltage-dependence of inactivation displays an unexpected U-shaped curve. This is consistent with the existence of a complex inactivation mechanism controlled by both voltage and intracellular Ca^{2+} concentration (Grolleau and Lapied 2000).

The HVA Ca^{2+} current characterized in TAG DUM neurons (Grolleau and Lapied 1996, Wicher and Penzlin 1997) activates at potentials more positive than
–40 mV. During the depolarizing pulse, the current reaches a peak then declines as channels inactivate. However, on return to the initial membrane potential, open channels close and the current deactivates, indicating the existence of incomplete inactivation (Grolleau and Lapied 2000). The value of half-maximal steady-state inactivation is estimated to be –45 mV. TAG DUM neuron HVA currents are carried by Ca^{2+} or Ba^{2+} through Ca^{2+} channels and are blocked by cadmium and nickel (estimated IC_{50} values are 5 μM for cadmium chloride and

40 μM for nickel chloride). HVA currents are reduced by verapamil and diltiazem (Wicher and Penzlin 1997), which are regarded as non-selective blockers (Triggle 1999), and by octopamine (100μM) (Achenbach *et al* 1997). In contrast, HVA Ca^{2+} currents are not affected by dihydropyridines, such as nifedipine and Ca^{2+} agonists such as the racemic BAYK 8644, which is often used to identify dihydropyridine-sensitive Ca^{2+} channels. In TAG DUM neurons HVA Ca^{2+} channels are also sensitive to ω-conotoxin GVIA in the concentration range 0.1-1 μM (Grolleau unpublished observations, Wicher and Penzlin 1997).

It has been postulated that the functional significance of both the LVA and HVA Ca^{2+} currents is to play a key role in the control of the afterhyperpolarizing phase *via* the modulation of the Ca^{2+}-activated K^+ current (Lapied *et al* 1989). In contrast, it has been demonstrated that the two distinct LVA Ca^{2+} channels have specialized functions in the generation of spontaneous electrical activity. (Grolleau and Lapied 1996). In pacemaker neurons, spontaneous activity results from a typical phase of their action potential, the slow depolarization. During this phase, the membrane slowly depolarizes following the termination of an action potential until the threshold for a new action potential is reached. Because LVA Ca^{2+} currents can be activated when the membrane is hyperpolarized beyond the resting level, they are one of the most suitable candidates to promote this predepolarization. In spontaneously active TAG DUM neurons, it has been demonstrated pharmacologically that LVA Ca^{2+} currents contribute to the predepolarizing phase (Grolleau and Lapied 1996). The transient LVA currents are essential for initiating the first part of the predepolarization whereas mLVA Ca^{2+} currents plays a determinant role in the last two-thirds of the pacemaker potential. These mLVA Ca^{2+} currents, which are controlled by intracellular Ca^{2+} concentration, influence both the shape of the predepolarization and also the spontaneous firing frequency since complete inactivation of this current by changes in internal Ca^{2+} concentration induces an important reduction in the frequency of spontaneous action potentials.

The first experimental evidence revealing the existence of a Ca^{2+} resting current in TAG DUM neurons came from experiments performed with neurohormone D,

which elevated intracellular Ca^{2+} concentration *via* the potentiation of a putative Ca^{2+} resting current (Heine and Wicher 1998). The resting Ca^{2+} current in TAG DUM neurons is voltage-independent and flows at the resting membrane potential. In addition the current-voltage relationship indicates that the size of the current increases when the membrane is hyperpolarized to levels more negative than –50 mV (Wicher and Reuter 1993). This current is strongly reduced by cadmium chloride (0.1 mM), non-selective cation current blockers such as 5-nitro-2-(3-phenylpropylamino) benzoic acid (NPPB), mefenamic acid and when external Ca^{2+} concentration is reduced (Grolleau and Lapied 2000). The resting Ca^{2+} current seems to play a physiological role in the control of TAG DUM neuron spike frequency (Wicher *et al* 1994) and also in the regulation of intracellular Ca^{2+} concentration *via* a Ca^{2+}-induced Ca^{2+}-released (CICR) mechanism, involving ryanodine-sensitive channels, rather than inositol trisphosphate channels (Heine and Wicher 1998).

*Note: The following table **3**.3: (Calcium currents in cockroach DUM neurons), on page 68, is attached following the reference section.

Table 3.3: Calcium currents in cockroach DUM neurons

	$I_{Ca(tLVA)}$	$I_{Ca(mLVA)}$	$I_{Ca(HVA)}$	$I_{Ca(r)}$
Description	Peak Current	Maintained Current	Peak Current	Maintained Current
Sensitivity	$CdCl_2$ $NiCl_2$ (<100 µm) ω-conotoxin MVIIC ω-agatoxin IVA	$CdCl_2$ $NiCl_2$ (>100 µm) ω-conotoxin MVIIC ω-agatoxin IVA	$CdCl_2$ $NiCl_2$ ω-conotoxin-GV1a verapamil, diltiazem	$CdCl_2$ NPPB Mefenamic acid
Insensitivity	Equimolar (Na+) Choline Choride K^+ channel blockers	Equimolar (Na+) Choline Choride K^+ channel blockers	Nifedipine BAY K 8644 K^+ channel blockers	Unknown
Activation Range	>–80 mV Depolarisation activated Max at –10 mV?	~–65 mV Depolarisation activated Max at –10 mV?	>–40 mV Maximal at +10 mV	N/A
Inactivation Range	Completely inactivates	Does not completely inactivate	Incomplete inactivation	Voltage independent
Role in AP	Slow depolarisation Repolarization and afterhyperpolarization via $I_{K,Ca}$	Slow depolarisation Firing frequency Repolarization and afterhyperpolarization via $I_{K,Ca}$	Repolarization and afterhyperpolarization via $I_{K,Ca}$	Spike frequency Regulate $[Ca^{2+}]_i$ via CICR

CHAPTER 4

ATRACOTOXINS

4.1: JANUS-FACED ATRACOTOXINS

The janus-faced atracotoxins (J-ACTXs), comprise a five-member family of insect-selective excitatory neurotoxins containing 35-37 amino acid residues and four disulfide bonds (Wang 2000a) (Fig **4**.**1**). The janus-faced atracotoxins (J-ACTX-Hv1a-c) were first isolated using reverse-phase HPLC from the crude venom of the Blue Mountains funnel-web spider, *Hadronyche versuta* (*H. versuta*) and the Toowoomba funnel-web *Hadronyche infensa* (*H. infensa*). Curiously, the concentrations of these peptides are highly variable between batches of venom, and they are sometimes absent, suggesting a temporal or locale-specific variation in expression. Recently J-ACTX-Hf1a-b, were discovered from the venom of the tree-dwelling funnel-web spider, *H. infensa*, and represent the only members of this toxin family, so far, found in another member of the Hexathelidae spider family.

The primary sequence of these peptides (J-ACTX,a-c) has revealed an unusual CCPCCP motif and they show no homology with any sequences in the protein and DNA sequence databases.

4.1.1 Toxicity of J-ACTX Family

Insect toxicity testing using the prototypic family member J-ACTX-Hv1c found that it was lethal (at 2 μg/100mg) in house crickets (*Acheta domesticus* LD_{50} = 167 $\pm$ 10 pmol/g), fall armyworm (*Spodoptera frugiperda* LD_{50} = 3070 $\pm$ 154 pmol/g) and tobacco budworm (*Heliothis virescens* LD_{50} = 3195 $\pm$ 160 pmol/g) (Wang 2000a). These tests confirm the lethality of J-ACTXs to the coleopteran, lepidopteran and orthopteran orders. Further testing of J-ACTX-Hv1c revealed lethality against houseflies (*Musca domestica* LD_{50} = 91.5 $\pm$ 5 pmol/g) and fruit flies (*Drosophila melanogaster*) both members of the important dipteran order (flies and mosquitoes) (Maggio and King 2002a). J-ACTX-Hv1c had no effect on the Deer tick (*Ixodes scapularis*), which is also a member of the Phylum Arthropoda. Hence, the toxin displays some degree of specificity within related invertebrate Orders. In addition the J-ACTX family are inactive in vertebrate neuromuscular junction preparations (chick biventer cervicis and rat vas deferens at concentrations up to 1 μM), as well as newborn BALB/c mice (Wang *et al* 2001)

A

| | 1 | | 5 | | | | | | | | | | | | 15 | | | | 20 | | | | | 25 | | | | | 30 | | | | | 35 |
J-ACTX-Hv1a   T I C T G A D R P C A A C C P C C P G T S C Q G P E S N G V V Y C R N F
J-ACTX-Hv1b   T I C T G A D R P C A A C C P C C P G T S C Q G P E P N G V S Y C R N D
J-ACTX-Hv1c   A I C T G A D R P C A A C C P C C P G T S C K A G E S N G V S Y C R K D E P
J-ACTX-Hi1a S P T C T G A D R P C A A C C P C C P G T S C K G P E P N G V S Y C R N
J-ACTX-Hi1b S P T C T G A D R P C A A C C P C C P G T S C K G P E P N G V S Y C R N D

B

C
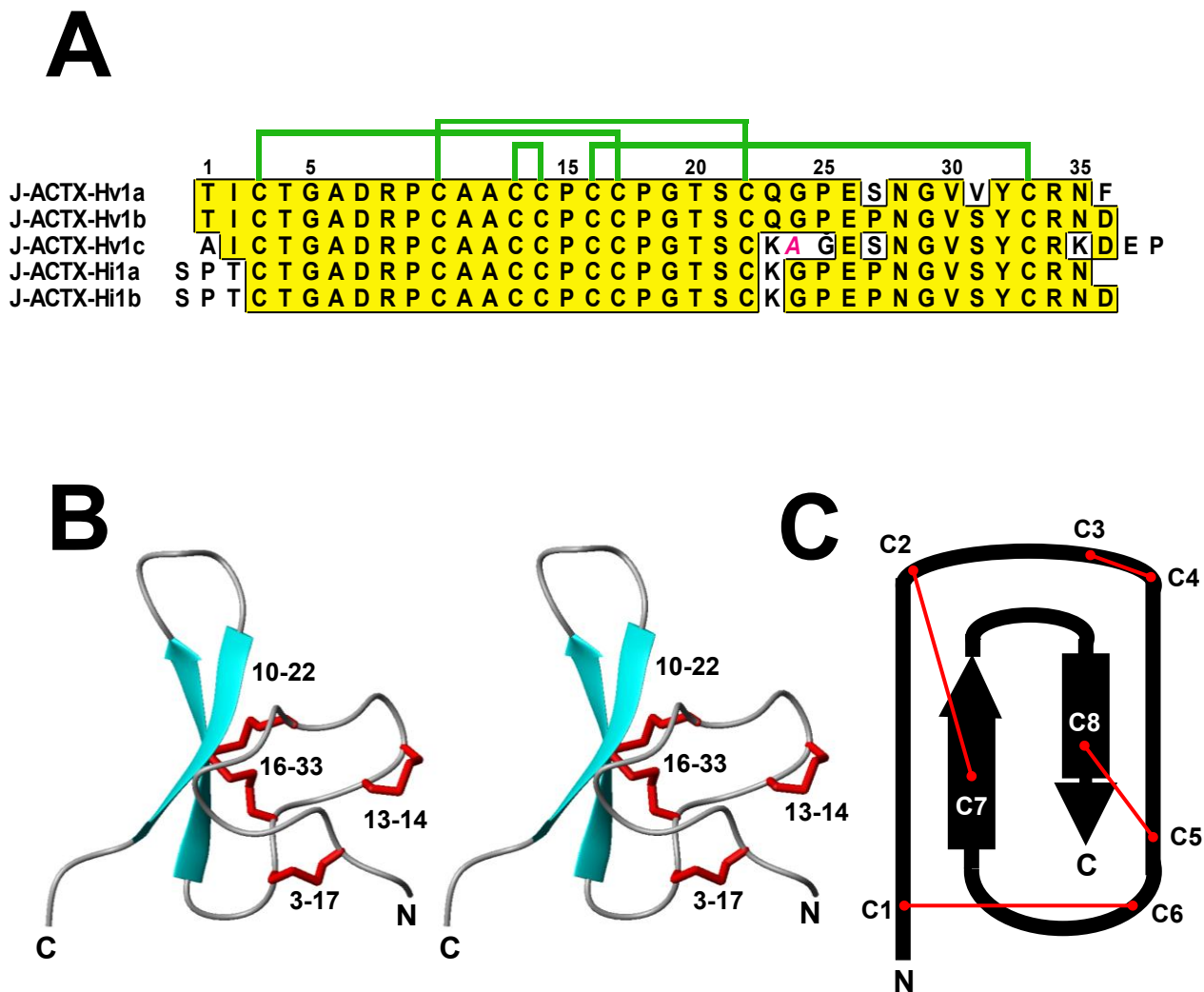
Figure 4.1: Structural characteristics of the J-ACTX-1 family. (**A**) Primary sequences of the J-ACTX-1 family. Homologous residues are boxed in yellow and the disulfide bonding arrangements for J-ACTX-Hv1c is shown above the sequences (Wang *et al* 2001). (**B**) Stereo view of the 3D structure of J-ACTX-Hv1c (PDB file 1DLO) (Wang *et al* 2001). Arrows represent β-strands, while the red tubes indicate the location of the 4-disulfide bonds. (**C**) Schematic representation showing the location of the 8 cysteine residues and the disulfide bonding arrangement for J-ACTX-Hv1c (no: 1-8 in order of appearance in the primary sequence). Models were drawn using MOLMOL (Koradi *et al*, 1996).

4.1.2 Structure of J-ACTX-Hv1c and Pharmacophore Mapping

In an attempt to elucidate the mode of action and key functional residues of the toxin, a recombinant expression system for J-ACTX-Hv1c was developed (Maggio and King 2002b). This was achieved by transfecting *E. coli* with the pGEX-2T vector encoding J-ACTX-Hv1c fused to glutathione *S*-transferase with an intervening thrombin cleavage site (Maggio and King 2002b). The periplasmic Dsb system found in *E. coli*, which normally catalyses disulfide isomerization ensured the correct folding and disulfide bond formation of the toxin. Following cell lysis, the fusion product could be quantitatively bound to a GSH-agarose affinity column. On-column thrombin cleavage liberates the recombinant toxin, which can then be eluted from the column with buffer (Maggio and King 2002b).

To determine the pharmacophore of the toxin, alanine-scanning mutagenesis was employed to determine the functional relevance of almost every residue in J-ACTX-Hv1c. Alanine scanning mutagenesis allows for the identification of the pharmacophore of the toxin, which may provide clues as to the molecular target of the toxin. Specifically, this technique involves mutating each non-alanine residue to alanine. Cysteine residues are also excluded from the scan because they typically form the disulfide bridges that define the three-dimensional structure of the toxin.

As previously determined, deletion of the N-terminal residue (Ala[1]) and the two C-terminal residues (Glu[36] and Pro[37]) does not affect toxin function (Maggio and King 2002a), consequently scanning mutagenesis was restricted to residues 2-35. In addition, residues Cys[3], Cys[10], Cys[16], Cys[17], Cys[22] and Cys[33] were excluded from the mutational analysis because their side chains are involved in disulfide bonds that form the cystine knot that is critical to the structure of the toxin (Wang *et al* 2000a). The two cysteine residues that form the unusual vicinal disulfide (Cys[13] and Cys[14]) have previously been shown to be critical for function as mutation to an isosteric Ser-Ser bond renders J-ACTX-Hv1c inactive even at

doses up to 60 times the LD_{50} of the native toxin (Wang *et al* 2000a). Mutation of the cysteine residues that comprise the vicinal disulfide were also excluded as mutation of either residue was certain to be highly deleterious. Finally the remaining 22 non-alanine residues were mutated to alanine, whereas the four alanine residues were mutated to serine. Alanine is generally chosen for scanning mutagenesis because it can be accommodated in most types of secondary structure (β-sheet, α-helix and β-turn), thus minimizing the chances that the point mutation will induce major structural perturbation. To confirm this, the far UV CD spectra of all mutants were compared to the wild-type toxin and those in which a minor structural perturbation was suspected were discarded (A6S and R33A were not pursued further). This left a panel of 23 first round mutants for biological assay. For the 23 alanine scan mutants, the *in vivo* activity of each of them was analyzed relative to recombinant (wildtype) toxin by comparison of their LD_{50} values in houseflies. A 5-fold or lower decrease in activity was exhibited by 18 of the 23 mutants indicating that these 18 residues are not critical to toxin activity. Thus, including the vicinal disulfide residues, there are seven residues that had significant decreases in activity (>5-fold) when mutated. Of the seven residues deemed critical for function, Ile^2 and Val^{29} were least affected when mutated to alanine. I2A and V29A caused a 6.6- and 13-fold respective decrease in activity. It appears these residues are important but not absolutely critical for toxin function.

A recent survey of protein-protein binding interfaces revealed that most interfaces consist of a central hot spot surrounded by residues whose primary role is to occlude water from the critical interacting residues; in other words, these peripheral residues act like a gasket to seal off the 'hot-spot' from bulk solvent (Bogan and Thorn 1998). This may explain why mutation of Ile^2 to Ala caused only a 7-fold drop in activity, whereas shown previously deletion of Ile^2 led to a substantial 70-fold drop in insecticidal potency. Given its location at the opposite end of the hotspot, Val^{29} might also be a gasket residue that helps to prevent bulk solvent penetrating into the binding site.

The major hits from the scanning mutagenesis were (excluding the vicinal disulfide Cys^{13}-Cys^{14}), Arg^8, Pro^9, and Tyr^{31}. Changing these residues caused very significant reductions in activity (98–423-fold). These five residues are clearly responsible for most of the insect-specific neurotoxic activity of κ-ACTX-Hv1c. This limited number of functionally significant residues parallels scanning mutagenesis results obtained for other disulfide-rich toxins. Scanning mutagenesis of the potassium channel blocker BgK also uncovered five key residues (Alessandri-Haber *et al*, 1999) and mutagenesis studies of the N-type calcium channel blockers ω-conotoxin GVIA and ω-conotoxin MVIIA revealed a small number of critical residues as well (Lew *et al* 1997). In contrast to ω-conotoxin GVIA for which the key residues are arbitrarily distributed on multiple faces of the structure, the key residues of κ-ACTX-Hv1c lie on a single face of the protein forming a bipartite surface patch. The spatial restriction of these residues should allow the successful design of a small molecule mimetic of the toxin pharmacophore. The pharmacophore side-chains of κ-ACTX-Hv1c display very little flexibility (as defined by the extremely low RMSD values) (Maggio, 2006), with the exception of Arg^8, which extends into the solvent. This structural property of the pharmacophore is highly suggestive that these residues form the target binding surface rather then being involved in other functions such as delivery to the target site, evasion of the insect immune system, or some other *in vivo* role. Shape complementarity is the foremost determinant for protein-protein interaction and specificity (Young *et al*, 1994). The taut nature of the κ-ACTX-Hv1c pharmacophore should pack appropriately into the corresponding surface of the binding partner, thus conferring specificity and affinity for target binding.
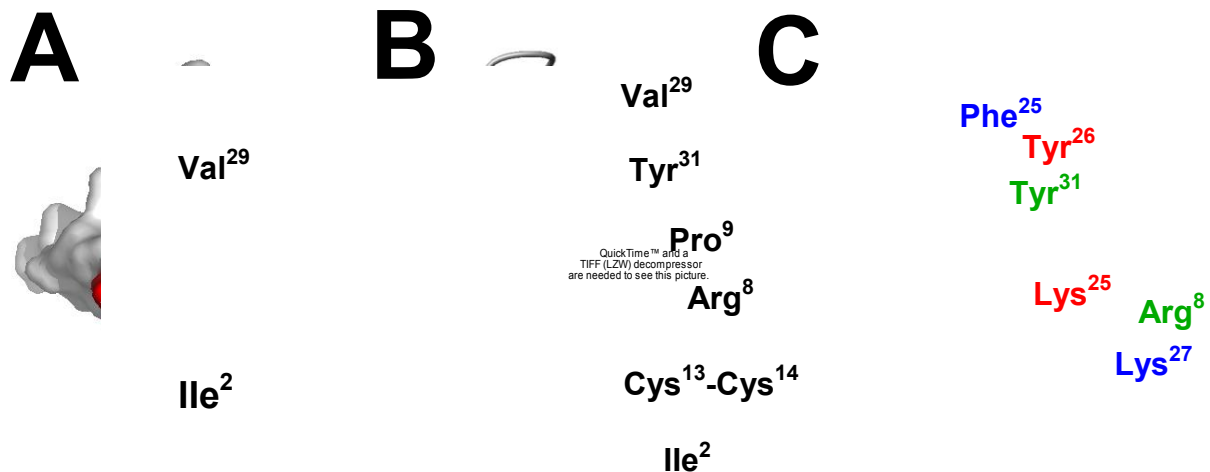
Figure 4.2: The bioactive surface of J-ACTX-Hv1c. (**A**) Molecular surface of J-ACTX-Hv1c (PDB file 1DLO) (Wang *et al* 2000), illustrating the key functional residues (Arg[8], Pro[9], Tyr[31], Cys[13] and Cys[14] coloured red) and two 'gasket residues' (Ile[2] and Val[29] coloured yellow) identified using alanine-scanning mutagenesis. These residues form two closely apposed patches on one face of the toxin. (**B**) 3-dimensional ribbon structure of J-ACTX-Hv1c highlighting the side-chains for the five critical residues (green) and two 'gasket' residues' (coloured yellow). The four-disulfide bonds are coloured red and the anti-parallel beta sheets are coloured cyan. (**C**) Superposition of the side chains of the functionally critical Arg[8] and Tyr[31] residues of J-ACTX-Hv1c (green) on the Lys-Tyr/Phe dyad of the K^{+} channel blockers agitoxin 2 (blue; PDB file 1AGT) and BgK (red; PDB file 1BGK). The three-dimensional folds of these toxins are very different and thus, for the sake of clarity, only the backbone of J-ACTX-Hv1c is shown (thin green tube, except for the arrows representing the two β-strands). Structures were drawn using MOLMOL or PyMOL.

4.1.3 What Is the target of J-ACTX-Hv1c?

The three-dimensional fold of cystine knot toxins generally provides little insight into their mode of action; the cystine knot simply provides the structural framework onto which diverse functional motifs can be grafted (Fig **4.3**, King *et al* 2002; Norton and Pallaghy 1998; Craik *et al* 2001). However, for cystine knot and other disulfide-rich ion channel toxins, the topological disposition of key functional residues, regardless of three-dimensional scaffold, is often informative of function.

Figure 4.3. Inhibitory Cystine knot motif (ICK). The cystine knot commonly found in conotoxins and atracotoxins. The backbone is shown in green and disulfides in red. The central disulfide pierces a ring formed by the other disulfide bridges and the intervening sections of the polypeptide backbone.
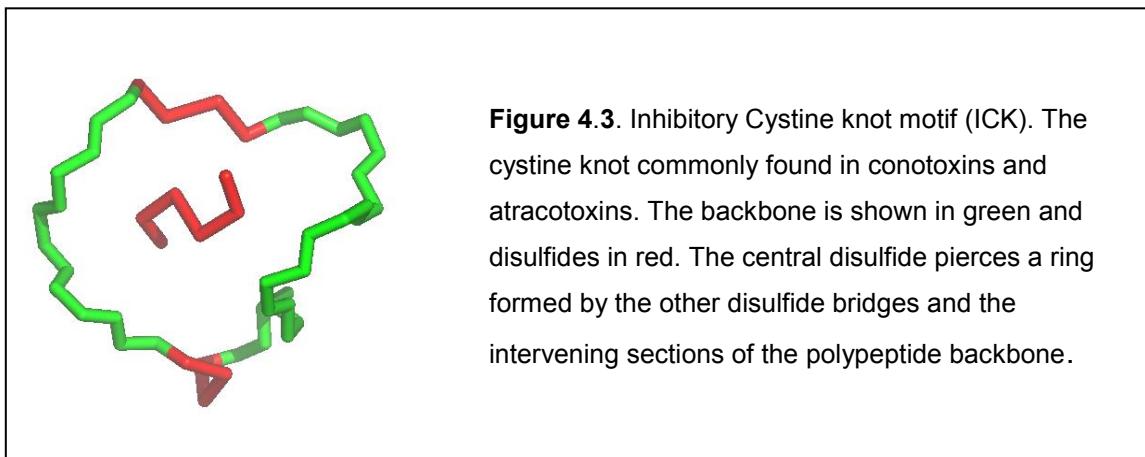
The ICK fold is an evolutionary conserved structural motif shared by a large group of polypeptides with diverse sequences and functions. Although found in different phyla (animal, plant and fungus), ICK peptides appear to be most prominent in venoms of cone snails and spider (Zhu *et al*, 2003). Almost all ICK peptides have a net positive charge, with the animal-derived peptides generally being more highly charged than those originating from plants. The peptides range in size from 26 to 48 residues. Toxins containing the cystine knot motif exhibit a range of biological activities from antimicrobial to anti-HIV to ion-channel blockade. This wide range of activities opens the possibility that some of these molecules may be useful leads in drug design applications. Examples of known ICK peptide toxins are detailed in the table **4**.**2**.

Table **4.1** Sources and biological activity of cystine knot peptides.

	Peptide	No. of amino acids	Source	Biological activity
Fungi	AVR9	28	*C. fulvum*	Race-specific elicitor
Plants	Kalata B1	29	*O. affinis*	Anti-microbial
	Gurmarin	35	*G. sylvestre*	Sweet taste-suppressing
Marine Molluscs	GVIA	26	*C. geographus*	Ca_V (N-type) channel blocker
	κ-PVIIA	27	*C. purpurascens*	K_V channel blocker
Spiders	Huwentoxin-1	33	*S. huwena*	nAChR blocker
	ω-Agatoxin IVA	48	*A. aperta*	Ca_V (P-type) channel blocker

Voltage-gated sodium channel peptide toxins bind to a number of pharmacologically and apparently topologically distinct sites (refer to chapter **2**, section **2**). Mutagenesis of μ-conotoxins (μ-CTXs) has revealed that the key residue for blockage of vertebrate voltage-gated sodium channels is an arginine (Arg[13] in μ-CTX GIIIA) that projects into the pore of the channel (Sato *et al* 1991). However, in striking contrast to J-ACTX-Hv1c, the critical arginine is surrounded by an array of positively charged residues (Arg[1], Lys[11], Lys[16] and Arg[19] in μ-CTX GIIIA) that also interact with the channel according to mutant cycle analyses (Li *et al* 2001). In addition, scorpion α-toxins bind to a different locus on sodium channels than μ-CTXs, however the bioactive surface also comprises a critically positive residue (Lys[8] in the insecticidal α-toxin LqhαIT), surrounded by several important positively charged residues (Zilberberg *et al* 1997). Sea anemone toxins contain chemically diversified bioactive surfaces, with both positively and negatively charged residues as well as hydrophobes being important in binding to voltage-gated sodium channels (Khera *et al* 1991, Dias-Kadambi *et al* 1996). Therefore, if J-ACTX-Hv1c interacts with insect sodium channels, it must do so by an entirely different mechanism to that seen for μ-CTXs, sea anemone toxins and α-scorpion toxins.

Mutagenesis studies have revealed that N-type calcium blockers such as ω-CTX GVIA (Lew *et al* 1997), ω-CTX MVIIA (Nadasdi *et al* 1995) and Ptu1 (Bernard *et al* 2001) contain a functionally critical Lys/Tyr dyad. The lysine, but not the tyrosine residue is conserved in the recently discovered L-type calcium channel blocker ω-CTX TxVII (Kobayashi *et al* 2000). The Lys and Tyr residues in the N blocker dyad are separated by a considerable distance and are located on opposite faces of the toxin, bearing no resemblance to the J-ACTX-Hv1c pharmacophore. In addition, the blockage of calcium channels is inconsistent with the excitatory phenotype induced in insects by J-ACTX-Hv1c (Wang *et al* 2000).

The functionally critical Arg[8] and Tyr[31] residues in J-ACTX-Hv1c (Fig **4**.**2C**) align extremely well with the Lys-Phe/Tyr dyad conserved amongst structurally dissimilar potassium channel blockers such as BgK, agitoxin 2, charybdotoxin and κ-conotoxin PVIIA (Jocobsen *et al* 2000, Krezel *et al* 1995, Terlau *et al* 1999). The excitatory phenotype induced by J-ACTX-Hv1a in insects is consistent with a potassium channel blocking activity. Indeed prior to death, the fruit flies exhibit a leg shaking phenotype that is reminiscent of that induced by conditional mutants of *Drosophila* K^+ channels such as EAG and *Shaker* (Ganetzky 2000). Thus, the topological arrangement of key functional residues, rather than the three-dimensional structure *per se*, allows speculation that J-ACTX-Hv1c most likely targets invertebrate potassium channels.

4.2: ω-ATRACOTOXINS

4.2.1 Structure and Function of the ω-ACTX-Hv1 Family

The ω-atracotoxin-1 (ω-ACTX-1) family comprises 36-37 residue peptide neurotoxins isolated from a variety of Australian funnel-web spider venoms (Atkinson *et al* 1993). These toxins block insect, but not mammalian, Ca_V channels (Fletcher *et al* 1997b). Furthermore, these toxins have no effect on insect macroscopic K_V currents and only a modest effect on insect Na_V channels (18 % block in cockroach DUM neurons at a toxin concentration of 1 µM) (Chong *et al*, 2006).

These peptides contain six strictly conserved cysteine residues that form three disulfide bonds. There are also no homologs of these peptides in the protein or DNA databases. A single species of spider may contain six or more variants of the toxin, with some variants differing by only a single conserved residue substitution (Wang *et al* 1999); for example, ω-ACTX-Hv1c differs from ω-ACTX-Hv1b only by the substitution of Phe for Tyr at position 24 (Fig **4.4A**).

The ω-ACTX-1 family of toxins are lethal to a wide range of insects, including members from the orders Coleoptera, Orthoptera, Lepidoptera and Diptera, but they are harmless when injected at high doses into newborn mice (Atkinson *et al* 1993, Fletcher *et al* 1997b and Tedford *et al* 2001). Injection of toxin into American cockroaches (*Periplaneta americana*), causes a loss of locomotion, high frequency twitching of limbs with loss of righting reflexes, followed by paralysis and death (Fletcher *et al* 1997b). These peptides can therefore be classified as depressant neurotoxins. Electrophysiological studies revealed that the phylogenetic specificity of the toxins derives from their ability to block insect, but not vertebrate, Ca_V channels (Fletcher *et al* 1997b). At 1 µM concentration, ω-ACTX-Hv1a partially blocks HVA Ca_V channel currents in voltage-clamped cockroach neuronal somata, but it has no effect on calcium currents in rat trigeminal neurons (Fletcher *et al* 1997b). Recently the effect of ω-ACTX-Hv1a on DUM neurons from the American cockroach (*P. Americana*) indicated that ω-ACTX-Hv1a blocks HVA Ca_V currents with an IC_{50} value of 768 nM, without affecting activation or inactivation kinetics (Chong *et al* 2006). The toxin did not alter the voltage-dependence of activation, and the block was voltage-independent indicating that ω-ACTX-Hv1a acts as a pore blocker rather than a gating modifier (Chong *et al* 2006).

The 3D structure of the prototypic family member, ω-ACTX-Hv1a revealed a structurally disordered N-terminus (residues 1-3), a disulfide rich globular core (residues 4-21), and a finger-like β-hairpin (residues 22-37) that protrudes from the globular domain (Fig **4.4B** and **C**). The three disulfide bonds form a cystine knot in which the Cys^{17}-Cys^{36} disulfide passes through a 13-residue ring formed by the Cys^4-Cys^{18} and Cys^{11}-Cys^{22} disulfide bridges and the intervening sections of polypeptide backbone. The structure of ω-ACX-Hv1a is not closely related to that of other Ca_V blockers such as ω-agatoxin-IVA or ω-conotoxin-GIVA.
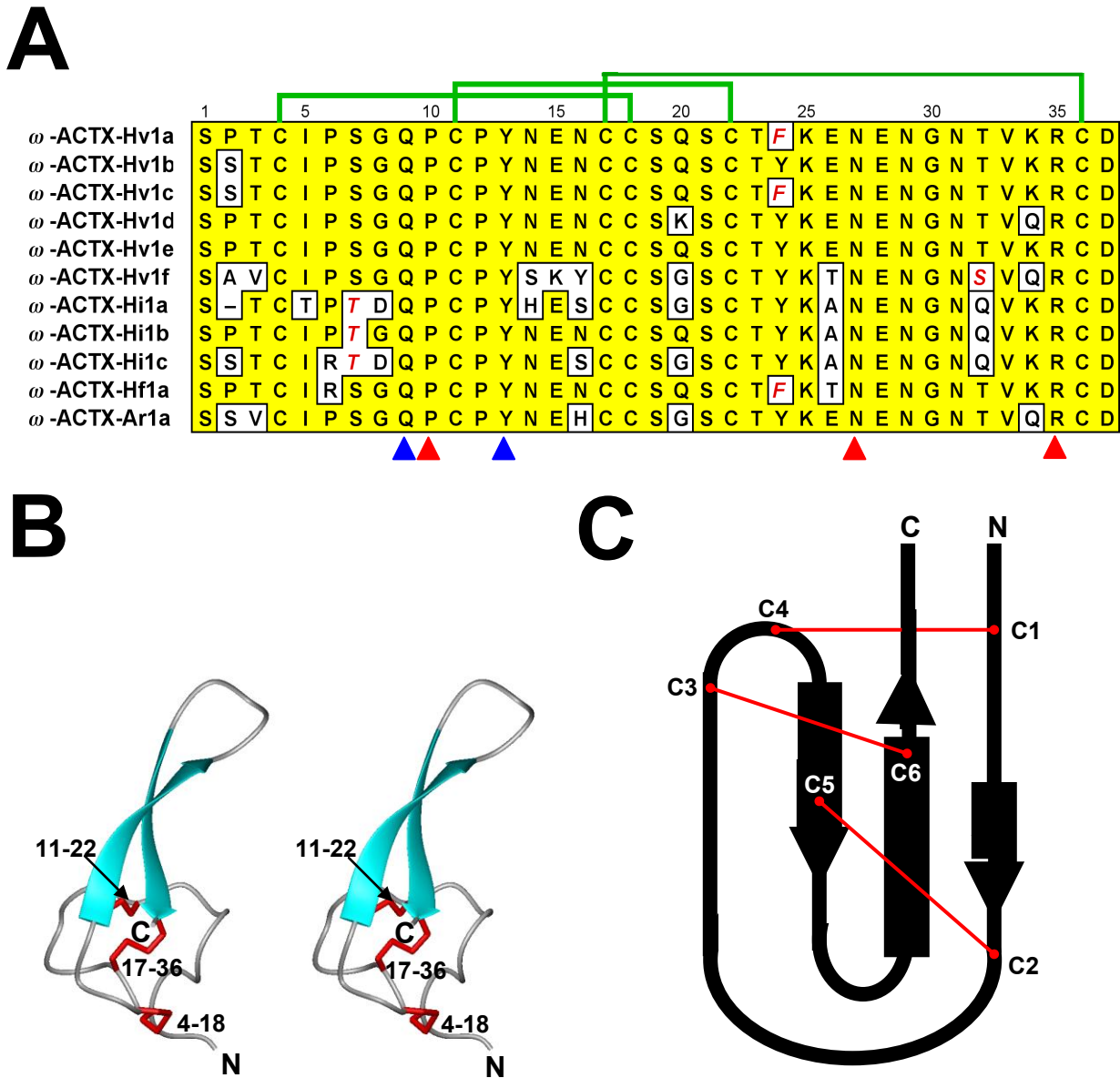
Figure 4.4: (**A**) Comparison of the primary structures of currently available members of the ω-ACTX-1 family. The toxins are from *H. versuta* (Hv), *H. infensa* (Hi), *H. formidabilis* (Hf) and *A. robustus* (Ar) (Chong *et al*, 2007, Atkinson *et al*, 1998; Wang *et al*, 1999). Identities are boxed in yellow, conservative substitutions are shown in red italics, and disulfide bonds are indicated by green lines connecting pairs of Cys residues. The red arrowheads below the sequences indicate the primary pharmacophore and the secondary pharmacophore in blue, as judged by alanine-scanning mutagenesis (Tedford et al., 2001) and bioassays using synthesised truncates (see text) (Wang et al., 1999). (**B**) Stereo view of the structure of ω-ACTX-Hv1a (PDB file 1AXH)

(Fletcher et al., 1997b). β-Strands are represented by blue arrows, while the red tubes indicate the location of the three disulfide bonds. (**C**) Schematic representation showing the location of the 6-cysteine residues and the disulfide bonding arrangement for ω-ACTX-Hv1a (no: 1-6 in order of appearance in the primary sequence). Models were drawn using MOLMOL (Koradi *et al*, 1996).

4.2.2 Insectophore mapping of ω-ACTX-Hv1a

The solution structure of ω-ACTX-Hv1a shows a similar overall fold to the N- and P/Q-type calcium channel antagonists ω-conotoxin (24-29 residues) and ω-agatoxins (48 residues), despite the fact that the only common sequence motif is the relative arrangement of Cys residues. In order to shed light on the molecular mechanism of action of ω-ACTX-Hv1a and to facilitate its use as a lead compound for insecticide development, a combination of protein engineering and site-directed mutagenesis was employed. The C-terminal β-hairpin of ω-ACTX-Hv1a is highly conserved, and thus a prominent structural feature distinguishes it from other calcium channel blocking toxins such as the ω-conotoxins in which the loops tethered to the cystine knot scaffold are considerably smaller (Olivera *et al* 1994). A ω-ACTX-Hv1a mutant lacking this C-terminal β-hairpin, was devoid of insecticidal activity, thus confirming that the β-hairpin was indispensable for ω-ACTX-Hv1a activity (Wang *et al* 2001). Examination of conserved residues found within all members of the ω-ACTX-Hv1 family and contained within the β-hairpin region, identified two residues Asn[27] and Arg[35]. These residues not surprisingly were the most functionally critical residues as determined by site-directed mutagenesis of ω-ACTX-Hv1a. An N27A, R35A double mutant toxin folds properly but is completely devoid of insecticidal activity. Analysis of the structure of ω-ACTX-Hv1a revealed that these two residues form a contiguous patch on the surface of the molecule (Fletcher *et al* 1997b) (Fig **4**.**5A**). Analysis of the N27D and R35E mutants indicated that this interaction most likely comprises a hydrogen bond interaction between the side chain amine group of Asn[27] and a hydrogen bond acceptor on the channel and an electrostatic interaction between the side chain guanido group of Arg[35] and a

negatively charged residue on the channel (Wang *et al* 2001). Asp^{37} and Asn^{29} flank the main Asn^{27}/Arg^{35} interaction site (Fig **4.5B**) and potentially extend the channel interaction surface. However the N29A mutation only marginally reduced insecticidal potency (2.24 fold), also a D37K mutation reduced insecticidal potency by 8.94 fold, suggesting that Asp^{37} makes an electrostatic interaction with a positively charged residue on the channel.
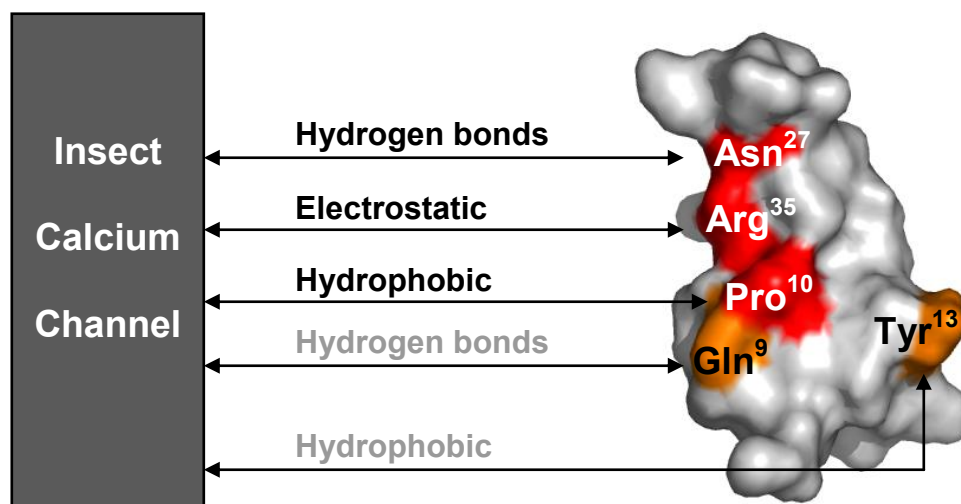
Figure 4.5: Molecular surface of ω-ACTX-Hv1a illustrating the proposed interaction between residues in the β-hairpin and insect Ca_V channels. The side chains of the key interacting residues form a contiguous patch (shown in red) on the surface of the hairpin, and this patch is flanked by two residues (shown in yellow) that are proposed to be important, but not critical, for the toxin-channel interaction. Modified from Wang *et al* 2001.

4.2.3 Structure and Function of the ω-ACTX-2 Family

A second family of ω-ACTXs that specifically block insect Ca_V channels was recently reported (Wang *et al* 2001). These toxins contain 41-45 residues with six conserved cysteines that form three disulfide bonds (Fig **4.6A**). The sequences are unrelated to the ω-ACTX-1 toxins and there are no homologs in the protein/DNA sequence databases. These toxins cause a prolonged but reversible paralysis in a range of insects including dipterans. At moderate to high doses the

paralysis is sustained for ~6h in house crickets (*Acheta domesticus*) and ~10h in flies (*Musca domestica*) (Wang *et al* 2001).

The prototypic family member ω-ACTX-Hv2a, inhibits bee brain calcium currents with an EC_{50} of ~130 pM, whereas it has virtually no effect on calcium currents in rat trigeminal neurons at a concentration of 1 μM (Wang *et al* 2001). This indicates not only that they have exceptional phylogenetic specificity, with at least a 10,000-fold preference for bee brain versus rat brain Ca_V channels. Another remarkable feature of ω-ACTX-Hv2a is the extent of current blocked in bee brain neurons. Even at very high concentrations (1 μM), ω-ACTX-Hv1a only caused ~50% blockage of whole-cell calcium currents in cockroach neurons (Fletcher *et al* 1997b), whereas ω-ACTX-Hv2a gave ~70% inhibition in bee brain calcium currents at a concentration of 10 nM (Wang *et al* 2001). This suggests that ω-ACTX-Hv2a has broad specificity for the various subtypes of insect Ca_V channels or that bee brain neurons are enriched in a specific subtype for which ω-ACTX-Hv2a has high affinity. The extent to which ω-ACTX-Hv2a binds to different Ca_V channel subtypes should be further explored using cockroach TAG DUM neurons as a model.

The 3D NMR structure of ω-ACTX-Hv2a (Fig **4**.**6B** and **C**) revealed that the disulfide-rich region of the toxin is organized into a compact globular domain containing a short 3_{10} helix (residues 13-17), β-hairpin comprising residues 23-30, and several well defined β-turns (Wang *et al* 2001). The three disulfide bridges form a cystine knot in which the Cys[17]-Cys[29] disulfide pierces a 15-residue ring formed by the two other disulfide bridges and the intervening sections of polypeptide backbone. Unlike most other ICK toxins, which are exemplars of economical protein engineering, the two N-terminal residues and the entire C-terminal region of ω-ACTX-Hv2a are completely disordered in solution (Wang *et al* 2001).

A


```
                        5        10       15       20       25       30       35       40       45
ω-ACTX-Hv2a  L L A C L F G N G R C S S N R D C C E L T P V C K R G S C V S S G P G L V G G I L G G I L
ω-ACTX-Hi2a  G V L D C V V N T L G C S S D K D C C G M T P S C T L G I C A P S V G G I V G G L L G R A L
ω-ACTX-Hi2b  G V V D C V L N T L G C S S D K D C C G M T P S C T L G I C A P S V G G L V G G L L G R A L
ω-ACTX-As2a  L L D C V L S R V - C S P D A N C C G L T P I C K M G L C V P K V G G L L G G L L G G I L
ω-ACTX-As2b  L L D C V L S R V - C S S D A N C C G L T P T C K M G L C V P K V G G L L G G L L G G I L
```

B   **C**

Disordered C-terminal tail SS-rich core

Figure 4.6: (**A**) Comparison of the primary structures of currently available members of the ω-ACTX-2 family. The toxins are from *H. versuta* (Hv), *H. infensa* (Hi), and an uncharacterised *Atrax* sp. from the Illawarra region of New South Wales (Aus). The ω-ACTX-Hv2a sequence was derived from protein sequencing, whereas the other primary structures were inferred from cDNA analyses (Wang et al., 2001). Identities are boxed in yellow, conservative substitutions are in red italics, and disulfide bonds are indicated by green lines connecting pairs of Cys residues. (**B**) Ensemble of 10 solution structures of ω-ACTX-Hv2a (PDB file 1G9P; Wang et al., 2001). The toxin structure can be divided into an N-terminal disulfide (SS)-rich core, and a structurally disordered C-terminal tail. β-Strands are represented by blue arrows, the single turn of 3_{10}-helix is shown as a red and yellow ribbon, and the green tubes indicate the location of the three disulfide bonds. (**C**) Schematic representation showing the location of the 6 cysteine residues and the disulfide bonding arrangement for ω-ACTX-Hv2a (no: 1-6 in order of appearance in the primary sequence) Models were drawn using MOLMOL (Koradi *et al*, 1996).

4.2.4 Homology with ω-Agatoxin-IVA and possible mode of action

There are no close structural homologs of ω-ACTX-Hv2a in the protein database but the toxin has certain structural, chemical and functional similarities with ω-agatoxin-IVA from the unrelated American funnel-web spider *Agelenopsis aperta*, vis: 1) the core ICK regions of the two toxins can be superimposed so that the central disulfide bridges and the β-strands overlay reasonably well (Fig **4**.**7**); 2) both toxins contain a highly disordered, lipophilic C-terminal extension that protrudes from the globular domain; 3) both toxins target VGCCs; 4) deletion of the disordered C-terminal tail from either toxin completely abolishes their ability to block VGCCs (Wang *et al* 2001, Kim *et al* 1995). A C-terminal truncation mutant of ω-ACTX-Hv2a comprising only residues 1-32 of the toxin neither blocks invertebrate VGCCs nor competitively inhibits the wild-type toxin; this implies that the lipophilic C-terminal tail is essential for interaction with VGCCs and that it initiates toxin binding. Hence, it has been suggested (Wang *et al* 2001), that the lipophilic tails of ω-ACTX-Hv2a and ω-agatoxin-IVA initiate toxin binding by penetrating the membrane either adjacent to the channel or, perhaps more likely, by intercalation between transmembrane segments of the channel protein (Fig **4**.**7**). Anchoring of the C-terminal tail in the membrane might alter the channel conformation sufficiently to reveal an otherwise cryptic high-affinity binding site for the disulfide-rich core region of the toxin.
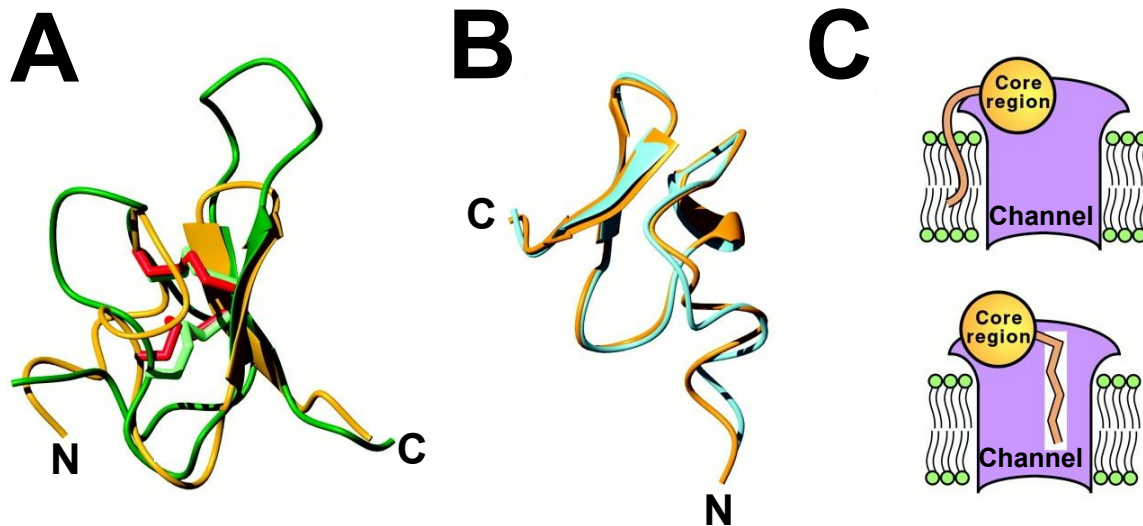
Figure 4.**7**: Structural similarities between ω-ACTX-Hv2a and ω-agatoxin IVA. (**A**) Overlay of ω-ACTX-Hv2a (gold) on ω-Aga-IVA (green; PDB file 1OAW Kim *et al* 1995), the core disulfide bridges of each toxin are shown as red and sage tubes, respectively. A similar comparison can be made with ω-Aga-IVB (PDB file 1AGG Riley *et al* 1995). The folds are homologous, but loops 1 and 3 are more highly elaborated in ω-Aga-IVA/B. The molecules are rotated ~180° around the long axis of the β-hairpin relative to the view in (**B**), the mean 20 CT-Hv2a structure (cyan) superimposed for best fit over the backbone of residues 3-32 of the mean ω-ACTX-Hv2a structure (gold). (**C**) Hypothetical models of the mechanism of action of ω-ACTX-Hv2a and ω-Aga-IVA in which the lipophilic C-terminal tail (orange) penetrates the lipid bilayer either adjacent to the channel (top panel) or by intercalation between transmembrane segments of the calcium channel (bottom panel). In either case, this positions the disulfide-rich core (shaded sphere) for direct interaction with the extracellular surface of the channel (adapted from Wang *et al* 2001).

4.3: THE 'HYBRID' TOXIN FW178

The 'hybrid' toxin FW178 is the prototypic member of the 'hybrid toxin family' that consists of up to nine family members (Sollod, 2006). FW178 is comprised of 36 amino acid residues, with very little homology to any other known atracotoxins (Fig **4**.**8**).

This unique family of toxins got this name because members contain elements of the pharmacophore of the ω-ACT-1 and J-ACTX-1 families even though they have little overall sequence homology with these toxins. Interestingly none of the hybrid toxins were discovered in routine venom screens. This might be due to low levels of expression, or possibly the toxin is only expressed by the spider at certain stages of its life cycle (Kalapothakis, et al 1998). In order to undertake functional and structural studies of these hybrid toxins, a bacterial expression system for the overproduction of the prototypic hybrid member FW178 was developed. In a similar procedure to that used for the production of recombinant κ-ACTX-Hv1c, FW178 was expressed by transforming *E. coli* with plasmid pBLS1, which contains an in-frame fusion of a synthetic *fw178* gene to the C-terminus of *S. japonicum* glutathione S-transferase (GST), with a thrombin cleveage site present between the *gst* and *FW178* coding regions. With a large supply of recombinant FW178, insect toxicity testing and alanine scanning mutagenesis could be undertaken.
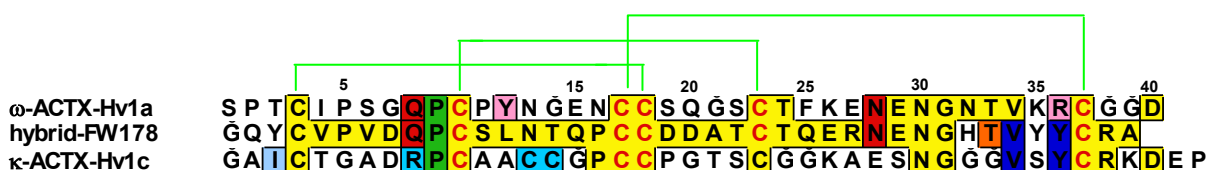
Figure 4.**8**: Comparison of the mature toxin sequences of ω-ACTX-Hv1a, κ-ACTX-Hv1c and FW178. Red shading shows pharmacophore residues of ω-ACTX-Hv1a (Tedford *et al*, 2001; 2004) that are also found in FW178. Residues highlighted in pink are additional residues that are part of the pharmacophore of ω-ACTX-Hv1c. The blue shading highlights key functional residues of κ-ACTX-Hv1c (Maggio *et al*, 2002) including those that are also found in FW178. Residues highlighted in cyan are additional residues that are part of the pharmacophore of κ-ACTX-Hv1c.

Orange highlighting represents part of the pharmacophore of FW178 (Sollod, 2006). Residues highlighted in green are part of the pharmacophores of both ω-ACTX-Hv1a and κ-ACTX-Hv1c and these residues are also found in FW178. Conserved Cys residues are shown in red. Green lines represent the disulfide-bonding pattern for FW178.

4.3.1 Toxicity of the 'hybrid' toxin FW178

FW178 the prototypic 'hybrid' toxin family member represents the most potent insecticidal atracotoxin currently known, as assessed by injection into the housefly, *Musca domestica*. The LD_{50} for FW178 is 38 ± 3 pmol/g (Sollod 2006), as compared to 91 ± 5 pmol/g and 86.5 ± 1.3 pmol/g for J-ACTX-Hv1c and ω-ACTX-Hv1a respectively (Maggio and King 2002a, Tedford *et al*, 2004). This makes FW178 at least two-fold more potent than any other atracotoxin isolated from Australian funnel-web spiders.

Given the highly insecticidal nature of FW178 coupled with its compact, tightly folded and resilient structure, FW178 may represent a perfect lead compound for development as a non-peptidic mimetic for use as an insecticide. For this to be realised further studies on the long-term stability and bioavailability of FW178 are required. Of critical importance, the molecular target(s) of FW178 need to be identified and will be undertaken as part of this project.

4.3.2 Structure of FW178 and Pharmacophore Mapping

The 3D NMR structure of FW178 comprises a C-terminal β hairpin that is held close to the core of the structure by the Cys^{10}-Cys^{23} and Cys^{17}-Cys^{37} disulfide bonds. The three disulfide bonds form a cystine knot motif in which a ring formed by the Cys^{3}-Cys^{18} and Cys^{10}-Cys^{23} disulfide bands and the intervening sections of polypeptide backbone are pierced by the third Cys^{17}-Cys^{37} disulfide (Fig **4.9**, Sollod, 2006). The arrangement of the disulfides results in four intercysteine loops.

Figure 4.9: Ribbon representation of FW178 hybrid toxin (PDB code 2H1Z). β Strands are shown in cyan. The three disulfide bonds (shown in red and the four intercysteine loops are labelled. Model was drawn using MOLMOL (Karadi *et al*, 1996)
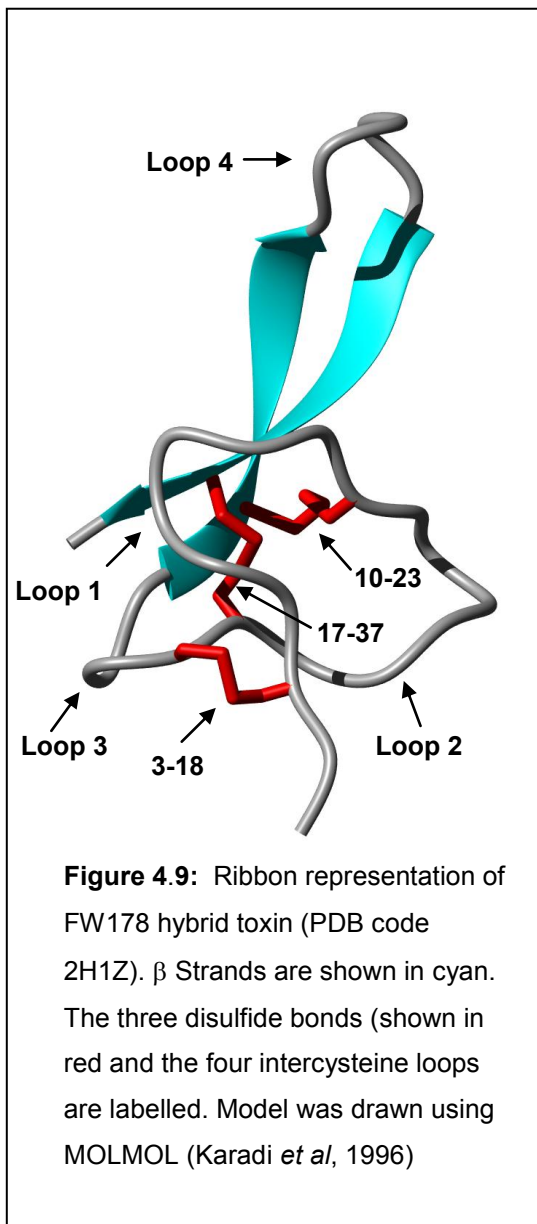
When compared to the structures of ω-ACTX-Hv1a and J-ACTX-Hv1c, the 3D folds are very similar; all three toxins contain a C-terminal β-hairpin, and the three conserved disulfides form an inhibitory cystine knot motif that results in four intercysteine loops. When the 3 structures are overlayed, there is significant variability in loops 1-3. Loop 1 of FW178 is very similar to that of ω-ACTX-Hv1a while loops 2 and 3 are significantly different to the corresponding loops in both ω-ACTX-Hv1a and J-ACTX-Hv1c. Thus, the structure provides little insight into the likely molecular target.

Alanine scanning mutagenesis of FW178 created a panel of 26 alanine-scan mutants (E26A and L12A were excluded) that were not structurally perturbed as determined by a chemical shift in the far UV CD spectra from the native toxin.

The insecticidal potency of each of the mutants was examined by comparison of their LD_{50} values in houseflies with that of the wild-type recombinant toxin.

Only those residues that produced a greater than five-fold increase in insecticidal activity were considered to be critical for toxin activity. Therefore 20 of the 26 mutants were deemed not critical. Of the remaining 6 residues, four residues- Gln^8, Pro^9, Asn^{28} and Val^{34} are the primary determinants of toxin function. Thr^{33}

and Tyr^{36} make important, but less critical, contributions to insecticidal activity, and form the secondary pharmacophore.

Remarkably, those four residues critical for toxin function (Gln^8, Pro^9, Asn^{28} and Val^{34}) plus Tyr^{36} form a contiguous patch of one face of FW718 (Fig **4.10B**). It is presumed, therefore that this epitope corresponds to the binding site for the toxin's primary *in vivo* molecular target.
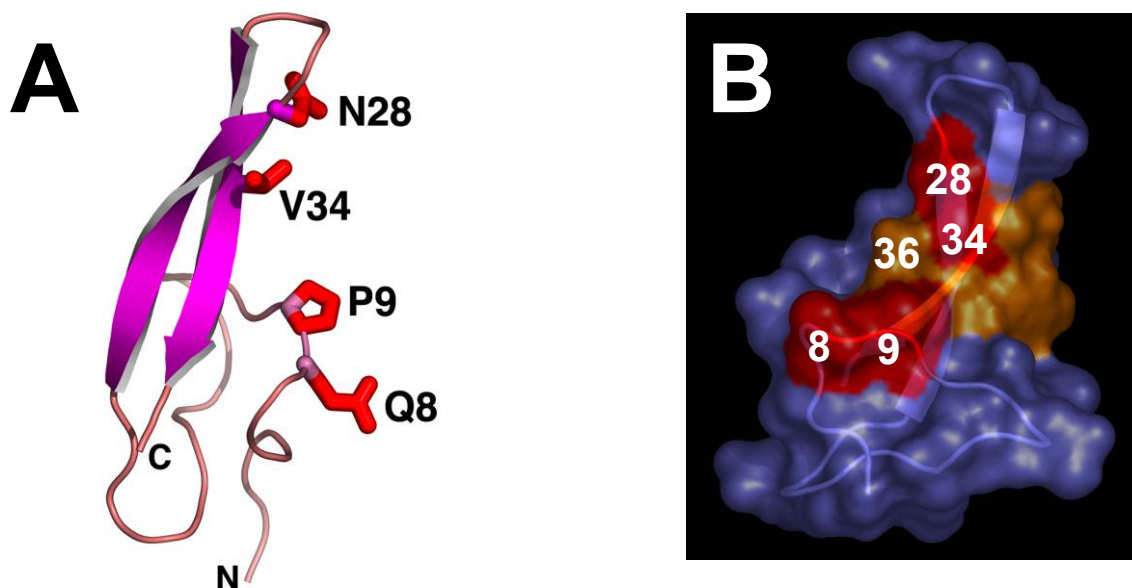
Figure 4.10: Pharmacophore of FW178. (**A**) Ribbon representation of the structure of FW178. The sidechains of the key functional residues are shown as red tubes and are labelled. (**B**) Molecular surface of FW178 highlighting the key functional residues (Gln^8, Pro^9, Asn^{28} and Val^{34} in red and Tyr^{36} in orange), which form a contiguous epitope on one face of the toxin. The ribbon structure of FW178 is superimposed onto the 3-D structure.

4.3.3 What is the target of the 'hybrid' toxin Fw178?

The limited set of key functional residues delineated for FW178 is similar in scope to the pharmacophore of other disulfide-rich toxins. For instance, mutagenesis studies of the N-type calcium channel blockers ω-conotoxin MVIIA and ω-conotoxin GIVA revealed that only a few residues are critical for function

(Nadasdi *et al*, 1995), similarly the pharmacophores of κ-ACTX-Hv1c and ω-ACTX-Hv1a comprise only a few residues that form spatially restricted epitopes on one face of the toxin (Maggio and King, 2002, Tedford *et al*, 2004). Remarkably, the pharmacophores of κ-ACTX-Hv1c and ω-ACTX-Hv1a, and FW178 can be overlaid with a high degree of superposition of key functional residues, despite the variations in tertiary structure. The Pro^9 residue, that forms part of the pharmacophore of all three toxins overlays almost perfectly (Group 2 in Fig **4**.**11B**). The Gln^8 residue that forms part of the pharmacophore of both FW178 and ω-ACTX-Hv1a overlays well, and these residues have the same spatial disposition as the Arg^8 residue which forms part of the pharmacophore of κ-ACTX-Hv1c (Group 1 in Fig **4**.**11B**). The Asn^{27} and Asn^{28} residues, which form part of the pharmacophores of ω-ACTX-Hv1a and FW178, respectively, have a very similar spatial location in the structure of the respective toxins (Group 4 in Fig **4**.**11B**). The Arg^{35} residue that forms part of the pharmacophore of ω-ACTX-Hv1a overlays well with the Tyr^{31} residue that forms part of the pharmacophore of κ-ACTX-Hv1c, despite both residues having diverse functions (Group 3 in Fig **4**.**11A** and **B**). In FW178, this spatial location is filled by the critical residue Val^{34} and less critical Tyr^{36}. Note that the pharmacophore of κ-ACTX-Hv1c does not contain a residue that corresponds to the group 4 residues in ω-ACTX-Hv1a and FW178. The pharmacophore of κ-ACTX-Hv1c does, however contain a vicinal disulfide; there are no corresponding residues in the pharmacophore of ω-ACTX-Hv1a and FW178.
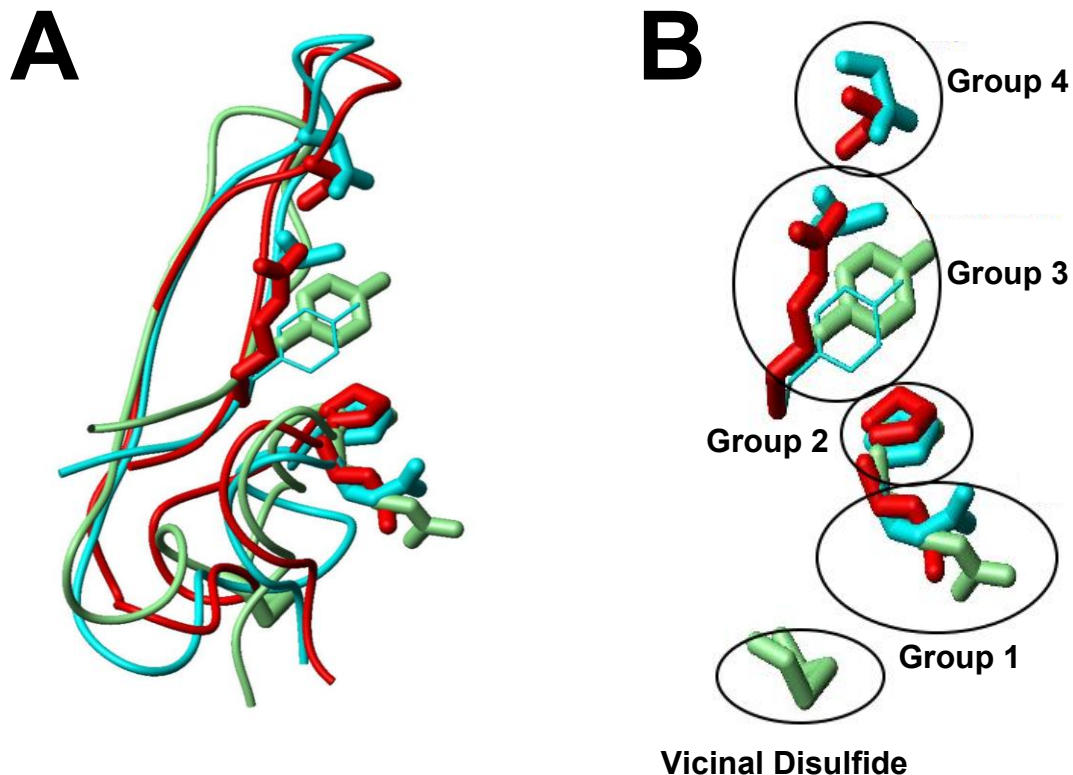
Figure 4.11: Overlay of the pharmacophores of ω-ACTX-Hv1a, κ-ACTX-Hv1c and FW178. (**A**) Overlay of the backbone and side chain pharmacophore residues of ω-ACTX-Hv1a (red), κ-ACTX-Hv1c (lime green) and FW178 (cyan). (**B**) Enlarged view showing only the side chains of the pharmacophore residues. Colours are as for in (**A**). Circles enclose pharmacophore residues that have the same spatial position.

The pharmacophore of FW178 remains unique and as such provides little insight into the molecular target of the toxin. Interestingly, though, the pharmacophore of FW178 does form a spatially restricted contiguous surface patch that has similarities with both κ-ACTX-Hv1c and ω-ACTX-Hv1a. Could this indicate that FW178 will share the same, as yet unknown, target as κ-ACTX-Hv1c or the insect calcium channel like ω-ACTX-Hv1a or both? Likewise does FW178 have an entirely unique function?

4.4: THESIS AIMS & OBJECTIVES

PART I

As previously discussed in section **4.1.3**, the molecular target for the Janus-faced atracotoxins has yet to be elucidated. Despite obtaining the complete primary sequence and gene sequence for the prototypic family member J-ACTX-Hv1c, no homology with any sequences in the protein and DNA sequence databases is observed. Furthermore, in spite of obtaining the three-dimensional fold of J-ACTX-Hv1c, inhibitory cysteine-knot toxins generally provide little insight into their mode of action; the cysteine-knot simply provides the structural framework onto which diverse functional motifs can be grafted (King *et al* 2002, Norton and Pallaghy 1998 and Craik *et al* 2001). Therefore the overriding aim of this project was to determine the molecular target of the Janus-faced atracotoxin family using the prototypic family member J-ACTX-Hv1c by whole-cell patch-clamping of cockroach dorsal unpaired median (DUM) neurons. Discovery of a novel insecticidal target, distinct from the established classical insecticide targets, would minimize the potential for cross resistance and provide a lead for high throughput screening for new insecticidal toxins.

J-ACTX-Hv1c was isolated from the Blue Mountains funnel-web spider *Hadronyche versuta* and has been shown to be lethal (at 2 µg/ml) upon injection to house crickets (*Acheta domesticus*), mealworms (*Tenebrio molitor*) and cotton bollworms (*Helicoverpa armigera*) (Wang 2000a). These tests confirm the lethality of J-ACTXs to the coleopteran, lepidopteran and orthopteran orders. Further testing of J-ACTX-Hv1c revealed lethality against house-flies (*Musca domestica*) and fruit flies (*Drosophila melanogaster*) both members of the important dipteran order (flies and mosquitoes) (Maggio and King 2002a). In addition the J-ACTX family are inactive in vertebrate neuromuscular junction

preparations (chick biventer cervicis and rat vas deferens), as well as newborn BALB/c mice (Wang *et al* 2001).

Specific Aims of this Thesis (Part I)

The specific aims of this thesis were to:

1. Identify the specific molecular target for J-ACTX-Hv1c using whole-cell patch clamping of dorsal unpaired median (DUM) neurons from the American cockroach *Periplaneta americana*. This involves testing for activity of the toxin against a range of ion channel currents known to be present in this cell type. These include voltage dependent sodium, calcium and potassium channels. In addition the study aimed to test for activity against a range of K_V channel subtypes including delayed rectifier ($K_{(DR)}$), 'A-type' ($K_{(A)}$) and calcium-activated ($K_{(Ca)}$). Once the target channel has been identified we will further examine the actions of the toxin by testing against the target insect channel in isolation. This can be achieved by using recombinant expression of the channel or major functional subunit of the channel in HEK293 cells. This technique may also allow for the testing against other homologous insect ion channels eg. the fruit fly (*Drosophila melanogastor*).

2. Confirm the insect selectivity of the toxin by using whole-cell patch-clamping of dorsal root ganglion (DRG) neurons from newborn rats. Once the specific molecular target of the toxin is identified we endeavour to compare this to the vertebrate equivalent ion channels using rat DRG neurons and by recombinant expression of vertebrate equivalent ion channels in HEK293 cells.

3. Determine how the critical residues of the toxin interact with the target channel. Firstly we will confirm the pharmacophore of the toxin. This will involve testing a panel of alanine mutants using whole-cell patch clamping against the identified target channel. Secondly by using the non-functional mutants R8A, Y31A, P9A and V29A we will confirm the importance of the

residues Arg^8, Tyr^{31}, Pro^9 and Val^{29} and validate that the reduction in lethality with these alanine mutants is not due to alterations in bioavailabilty. Further probing of the interaction of J-ACTX-Hv1c and its target can be achieved by using an extended panel of mutants. To investigate the interaction of the side-chain for the critical residue Arg^8 with the target, we will use the panel of mutants R8K, R8H, R8E and R8Q. Furthermore, investigation of the interaction of the side-chain for the critical residue Tyr^{31} with the target will be achieved using the mutants Y31F, Y31W, Y31L and Y31V. Importantly the determination of the key functional residues of the toxin and their specific contribution to target binding are essential to the design of any small molecule mimetics as novel chemical insecticides.

PART II

The recently identified 'hybrid' toxin Fw178 shows minimal sequence similarity to the ω-ACTX-1 and κ-ACTX-Hv1 families of toxins that are present in the same superfamily (Sollod *et al* 2006). Interestingly, however, this toxin does posses some of the key functional residues from the mapped pharmacophore of the Ca$_V$ channel blocker ω-ACTX-Hv1a (Tedford *et al* 2004) and κ-ACTX-Hv1c (Maggio and King, 2002). Therefore it appears superficially that this toxin may contain a hybrid of the pharmacophores of ω-ACTX-Hv1a and κ-ACTX-Hv1c. As discussed in section **4**.**3**, NMR structural studies of FW178 indicated that the overall 3D fold, is at least in part, very similar to ω-ACTX-Hv1a and κ-ACTX-Hv1c. Particularly the three disulfides form a cysteine-knot motif, and the major secondary structure element is the C-terminal β-hairpin. Significant differences do however occur in the intercysteine loops between these toxins. As such the overall structure provides no direct insight into the likely molecular target of FW178. It will be interesting therefore to determine if the molecular target of

FW178 is unique or if it targets one, or both, of the same channel targets as ω-ACTX-Hv1a or κ-ACTX-Hv1c.

Specific Aims of this Thesis (Part II)

The specific aim of this part of the thesis is to:

1. Identify the molecular target(s) of the 'hybrid' toxin FW178. This will be achieved by using whole-cell patch clamping of DUM neurons from the American cockroach *Periplaneta americana* as described previously. This involves testing for activity of the toxin against a range of ion channel currents including voltage dependent sodium, calcium and potassium channels. Once the target channel has been identified we will further examine the actions of the toxin by testing against the target insect channel in isolation. This can be achieved by using recombinant expression of the channel or major functional sub-unit of the channel in HEK293 cells.

CHAPTER 5

MATERIALS AND METHODS

5.1: INSECT ELECTROPHYSIOLOGICAL EXPERIMENTS

To determine the insecticidal target site(s) for the toxins used in this study, the patch-clamp recording technique in the whole-cell configuration was employed (Hamil *et al*, 1981). This technique allows the highly sensitive recording of ionic currents and voltage changes of high temporal resolution (s). These electrophysiological experiments were performed on voltage-gated sodium, potassium and calcium channels of acutely dissociated cockroach dorsal unpaired median (DUM) neurons.

5.1.1 Research animals

Adult American cockroaches (*Periplaneta americana*) were obtained as required from breeding facilities within the Department of Medical and Molecular Biosciences, UTS. The animals were kept in a temperature-controlled room (25°C) in large plastic rubbish bins. They were fed dog biscuits and water *ad libidum*. Between 5-37 cockroaches were used in each preparation.

5.1.2 Dissection of DUM neurons

The dissections and tissue culture methods described in the following sections are modifications of the techniques first employed by the group at Université d' Angers (France). Adult cockroaches were selected for dissection on the afternoon prior to an electrophysiological experiment. Cockroaches were immobilised by placing them into a - 20°C freezer for 5 minutes. All procedures hereafter were performed in a laminar flow cabinet (Model 1687-0200 Email-Westinghouse®) using aseptic techniques, where possible. Each cockroach was pinned dorsal side up onto a sylgard coated glass petri dish. Using surgical scissors the dorsal cuticle, underlying muscle and fatty tissue were removed to reveal the ventral nerve cord. The terminal abdominal ganglion (TAG) was identified as described in chapter **3**, section **1**. The TAG was then removed from the spinal cord and placed into a sterile petri dish containing Ca^{2+}-free normal insect saline (CF-NIS) and penicillin/streptomycin (2U/ml). NIS is composed of (in mM); NaCl 200, KCl 3.1, $CaCl_2$ 5, $MgCl_2$ 4, sucrose 50 and HEPES 10, pH was balanced to 7.4 with NaOH. Each TAG in turn was then desheathed using fine forceps and iris scissors.

5.1.3 Enzyme treatment of DUM neurons

Once the ganglia were desheathed, they were treated with the enzyme collagenase (Type 1A) to weaken the capsule of connective tissue surrounding each ganglion. Using a sterile Pasteur pipette the ganglia were transferred from the small petri dish to a 15 ml graduated centrifuge tube (Falcon 2095) containing 2 ml CF-NIS to which had been added penicillin/streptomycin (2U/ml) and 2 mg/ml collagenase (Type 1A). The ganglia were then incubated in a water bath at 37°C for 15 minutes. A strict incubation period was employed to weaken the encapsulating tissue without damaging the neurons inside the ganglia.

After the enzyme treatment was completed the ganglia were centrifuged at 500 rpm for approximately 30 seconds using a bench centrifuge (ICH HN-SII Model) to pellet the ganglia, and the supernatant was removed by aspiration. The ganglia were washed four times with NIS-containing foetal calf serum (FCS) (5% v/v) and penicillin/streptomycin (2U/ml). The ganglia were centrifuged as before and the supernatant was removed again by aspiration. After the final wash the ganglia were re-suspended in 3 ml of the remaining NIS-containing FCS (5% v/v) and penicillin/streptomycin (2U/ml) ready for mechanical trituration.

5.1.4 Trituration and tissue culture of DUM neurons

The third and final step of the isolation process was the trituration and subsequent plating of the DUM neurons. The purpose of the trituration was to gently free the neurons from the surrounding support tissue. This was accomplished by passing the ganglia in and out of a sterile Pasteur pipette that had been heat polished to progressively narrowing diameters. The first trituration procedure was performed using minimal occlusion of the pipette tip. Trituration was stopped as soon as the solution appeared cloudy to the eye. The neuronal debris and remaining ganglion were allowed to settle before the supernatant containing dissociated DUM cells were evenly dispersed, drop-wise into 3 wells of a prepared 24 well tissue culture plate (between 2-3 ganglia per well).

Each well on these plates contained a 12 mm (round) glass cover slip, which had been previously coated with 2 mg/ml concanavalin-A (see section **5.1.5**) to ensure adequate adhesion of the neurons. The tissue culture plate was incubated overnight (25°C and 100% humidity) to allow the isolated neurons to settle and adhere to the coverslips. Cells were used the next day (between 14-24 hours) for electrophysiological experiments. This short-term culture of dissociated DUM neurons ensures neurite outgrowth is limited and as a result cells retain a smooth surface and spherical shape. This enables effective patch clamping to be employed with minimal space clamp issues.

5.1.5 Preparation of tissue culture plates

The tissue culture plates employed to incubate DUM neurons required pre-prepared concanavalin-A coated coverslips for easy cell adhesion. Using aseptic techniques a single autoclaved, 12 mm-diameter glass coverslips (Lomb scientific®, Taren Point, NSW) was placed in each well of a 24-well sterile tissue culture plate (Limbro®). A solution of concanavalin-A (2 mg/ml) was made on the day prior to use by adding 8 mg of concanavalin-A to 4 ml of sterile distilled H_2O. This solution was gently warmed to aid solubility of the concanavalin-A. The solutions were then filtered using a 0.2 µm syringe filter attached to a sterile 15 ml syringe. Approximately 1 ml of solution was then added to each well containing a coverslip. Once the coverslips were covered with the concanavalin-A solution, they were left under UV light in the laminar flow cabinet for at least 1 hour. After a minimum of 6 hrs, the concanavalin-A solution was aspirated using a sterile Pasteur pipette attached to a suction pump. Each well was then washed three times with ~1 ml of sterile distilled H_2O and the coated plates were left to dry in the laminar flow cabinet.

5.1.6 Electrophysiological whole-cell patch-clamp setup

Electrophysiological experiments employed the patch-clamp recording technique in whole-cell configuration to measure sodium, potassium and calcium currents from cockroach DUM neurons. This is a modification of the whole-cell recording procedure originally used on chromaffin cells, as described by Hamil *et al* (1981). The apparatus utilised to record currents included a phase contrast microscope (Lietz Labovert FS), which was used for visualisation of the cells and positioning of the pipette electrode. A ~1 ml glass-bottomed perfusion chamber, in which the coverslips and their attached neurons were placed, was mounted on the microscope stage. The neurons were bathed in an iso-osmotic external solution applied via a pressurized fast perfusion system (Automate Scientific®), in which

the flow rate was maintained at 1 ml/min using a Gilmont (F-1100) flowmeter. All experiments were performed at room temperature.

A recording microelectrode holder (Axon instruments, CA, USA) containing a silver (Ag) wire and pellet which was coated with Ag/AgCl, provided the interface between the electrolyte solution and head-stage (Axon Instruments CV201) input. A Huxley-style micromanipulator (Sutter instruments, CA, USA) held the electrode and head-stage at 45 degrees to the plane of the bath, allowing for correct positioning of the electrode in the absence of any drift. The manipulator and microscope were mounted on a vibration isolation workstation (Newport Series 3036) in order to provide effective isolation from mechanical vibrations above 5 kHz. In addition, radio frequency and 50 Hz mains interference was minimised by isolating the apparatus in a Faraday cage and electrically grounding all equipment.

Recording of ionic currents was achieved using an ultra-low noise Axopatch 200A amplifier connected to a CV201 head-stage. The signal was acquired at 10-15 kHz depending on the type of current being recorded. The amplified signal was then sent to a Macintosh^{TM} personal computer via an ITC-16 channel A/D converter (Instrutech Corp$^{®}$,FL, USA) or Dell personal computer via a hard disk. Finally, a digitising oscilloscope which received the amplified signal (Textronix 2210, OR, USA) was used for displaying waveforms for visual signal interpretation.

5.1.7 Microelectrodes and bath electrodes

Microelectrodes for patch-clamp experiments were pulled just prior to use from borosilicate glass capillary tubing (Corning 7052; Warner Corp, USA; 1.5 mm external diameter and 1.1 mm internal diameter), using a Flaming/Brown flatbed electrode puller (Sutter Model P-87). The puller fabricated glass electrodes that were of consistent tip diameter and resistance. An electrode tip resistance of 0.8

to 3 MΩ was required for the patch clamp technique; with a 2.5 MΩ tip resistance being the optimum for our experiments (for recording of rat DRG neurons, the tip resistance was between 0.8-2 MΩ). Heat polishing of the electrodes was also undertaken using an MF-83 model electrode polisher (Narishige, Tokoyo, Japan). This ensured the tips had a steep taper and were evenly rounded to provide long lasting giga-ohm seals. Bath reference electrodes were made from polyethylene tubing, with a 1.5 mm outer diameter (A-M systems Inc, WA, USA) and filled with 3 M KCl agar salt bridges. The bath electrodes were fitted to an electrode holder (World Precision instruments, Inc, FL, USA), which contained an Ag/AgCl half-cell moulded into its base. The holder was filled with 3 M KCl and a new bath electrode was used on each day of an electrophysiological experiment.

5.1.8 Electrophysiological solutions

Two solutions, an internal and external solution, were required for whole-cell patch-clamp recordings. The contents of both the internal and external solutions were varied according to the type of recording procedure undertaken and also the particular ion channel of interest. The pH was adjusted to 7.35 and 7.4 for the internal and external solutions using KOH (1 M) or NaOH (2 M) respectively. Osmolarity was set to 380 mOM for all solutions used. The contents of all internal and external solutions used in voltage-clamp electrophysiological experiments are detailed in Tables **5.1**, **5.2**, **5.3**.

5.1.9 External and internal solutions for recording Na$^+$, K$^+$ and Ca^{2+} currents from DUM neurons

Solutions for recording sodium (I_{Na}), potassium (I_K) and calcium currents (I_{Ca}) are shown in Tables **5.1, 5.2** and **5.3**. In order to block TTX-S sodium currents 150 nM TTX was added to the external solution, while cells displaying any resistant sodium currents were discarded.

Table 5.1: Composition of external and internal solutions used for electrophysiological recordings of sodium currents from DUM neurons.

	Solution Number	Constituents (mM)
Voltage clamp		
External solution	1	NaCl **130**, CsCl **5**, CaCl$_2$ **1.8**, TEA-Cl **20**, 4-AP **5**, HEPES **10**, verapamil.HCl **0.01**, NiCl$_2$ **0.1**, CdCl$_2$ **1**
I_{Na} internal solution	2	CsF **135**, MgCl$_2$ **1**, NaCl **20**, HEPES **10**, EGTA **5**

Table 5.2: Composition of external and internal solutions used for electrophysiological recordings of potassium currents from DUM neurons.

	Solution Number	Constituents (mM)
Voltage Clamp		
External solution	1	NaCl **100**, KCl **3.1**, CaCl$_2$ **5**, MgCl$_2$ **4**, HEPES **10** glucose **10**, TTX **150** nM
$I_{K(Total)}$ solution	2	Same as 1 but KCl ext **30** mM
$I_{K(DR)}$ solution	3	Same as 1 + **30** nM CTX, **1** mM Cd^{2+} and **5** mM 4-AP
$I_{K(A)}$ solution	4	Same as 1 + **30** nM CTX, **1** mM Cd^{2+}
$I_{K(Ca)}$ solution	5	Same as 1 but KCl int **75** mM and ext KCl **10** mM + **5** mM 4-AP
Complete block of I_K	6	Same as 1 + **30** nM CTX, **1** mM Cd^{2+}, **5** mM 4-AP and **50** mM TEA-Cl
Internal solution	7	KCl **135**, KF **25**, NaCl **9**, ATP-Mg$_2$ **3**, MgCl$_2$ **1**, CaCl$_2$ **0.1**, EGTA **1** and HEPES **10**

;
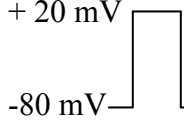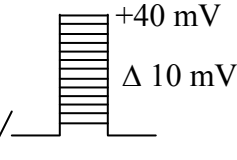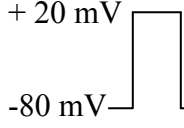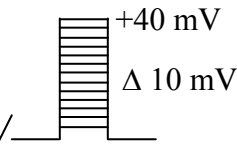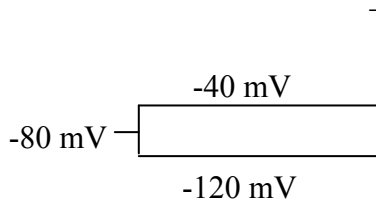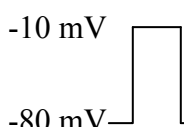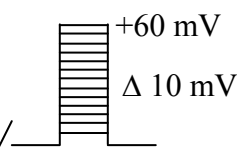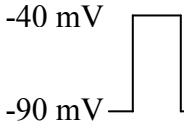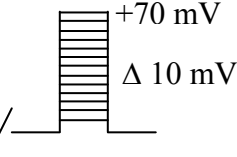
Table 5.3: Composition of external and internal solutions used for electrophysiological recordings of calcium currents from DUM neurons.

	Solution Number	Constituents (mM)
Voltage clamp		
External solution	1	CaCl$_2$ **5**, TEA-Br **30**, HEPES **10**, Na-acetate **160**
Internal solution	3	CsCl **110**, CaCl$_2$ **0.5**, Na-acetate **10**, HEPES **10**, TEA-Br **50**, ATP-Na$_2$ **2,** EGTA **10**

Abbreviations: HEPES, N-[2-Hydroxyethyl]piperazine-N'-[2-ethanesulfonic acid]; TEA-Br tetraethyl-ammonium bromide; TEA-Cl tetraethyl-ammonium chloride;

CTX charybdotoxin; 4-AP 4-aminopyridine; EGTA ethylene glycol-bis(β-aminoethylether)-*N,N,N'N'*-tetraacetic acid.

5.1.10 Voltage-clamp protocols

	Sweep	I/V	Conditions

A) $I_{K(Ca)}$ — + 20 mV, -80 mV; +40 mV, Δ 10 mV; Table 5.2, Solutions 4 + 7

B) $I_{K(DR)}$ — + 20 mV, -80 mV; +40 mV, Δ 10 mV; Table 5.2, Solutions 2 + 7

C) $I_{K(A)}$ — + 40 mV, -40 mV, -80 mV, -120 mV; +40 mV, Δ 10 mV; Table 5.2, Solutions 3 + 7

D) I_{Na} — -10 mV, -80 mV; +60 mV, Δ 10 mV; Table 5.1, Solutions 1 + 2

E) I_{Ca} — -40 mV, -90 mV; +70 mV, Δ 10 mV; Table 5.3, Solutions 1 + 3

5.2: IDENTIFICATION OF DUM NEURONS

To confirm the presence and location of viable adult DUM neurons by using the techniques described above, neutral red staining was performed. This technique selectively highlights amine-containing cells (Stuart *et al* 1974). Tissues were dissected free from the animal and stained intact in freshly prepared solutions of neutral red (0.01 mg/ml) in normal insect saline. The solution was filtered (Whatman no 1) immediately before use and tissues were incubated for 3 hrs at room temperature. No stained cells were used in electrophysiological analysis. The following tissues/isolated cells were allowed to adhere to glass coverslips as described in section **5**.**1**.**5**.
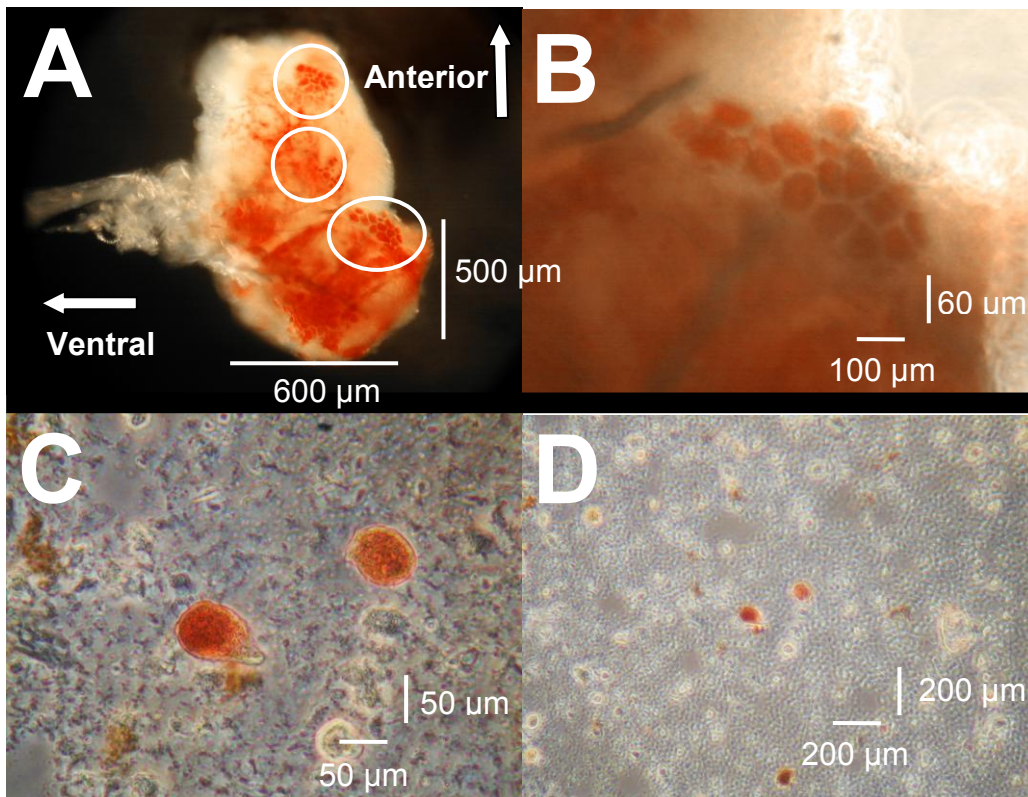
Fig 5.1 Light micrographs of DUM neurons stained with neutral red. (**A**) Staining of an isolated desheathed terminal abdominal ganglia, reveals three clusters of amine-containing cells located along the dorsal-midline of the tissue. These clusters appear to correspond to the octopamine (OA)- immunoreactive (OR-ir) DUM neurones described by Eckart *et al* (1992) in the TAG of *P*.

americana. (**B**) Closer examination of the inferior cluster reveals 12-14 amine-containing cells. As is evident non-specific staining does make distinct identification of individual cells difficult. (**C**) Isolated DUM neurons show a distinct tear-drop shape and large somata (40-60 µM) as compared to surrounding cells. (**D**) Low power light micrograph of cells isolated from (**A**) reveal both amine-containing cells surrounded by large numbers of smaller non-amine containing cells.

5.3: MAMMALIAN ELECTROPHYSIOLOGICAL EXPERIMENTS

To determine the effect of the toxin on the activation and inactivation kinetics of mammalian voltage-gated potassium channels, modified whole-cell voltage-clamp recording techniques developed by Hamil *et al* (1981) were employed. Voltage clamp recordings were made from mechanically dissociated dorsal root ganglion (DRG) neurons isolated from 5-14 day-old Wister rat pups. Newborn rats were obtained from Gore Hill Research Laboratories, University of Technology (UTS), Sydney, and were housed in sawdust-lined holding cages within a light and temperature controlled facility within the department of Medical and Molecular Biosciences. The rats were fed rodent pellets and water *ad libidum*. The Animal ethics protocol for the handling and euthanasia of rats was approved by the joint UTS/RNSH Animal care and ethics committee.

5.3.1 Preparation of Tissue Culture Plates

In preparation for the short-term culture of DRG neurons, single autoclaved round glass coverslips (12mm diameter) (Lomb Scientific, Taren Point, NSW) were coated in poly-*D*-lysine and transferred to 4 x 6-well tissue culture plates (Linbro, Aurora Ohio, USA) using aseptic techniques.

5.3.2 Dissection and isolation of Dorsal Root Ganglion (DRG) Neurons

Newborn rats were transferred to a glass anaesthetic chamber containing 1 ml isoflurane (Fluothane®, Abbot Australasia Pty Ltd, Kurnell, NSW). A sufficient level of anaesthesia was reached when the rat was unable to evoke a withdrawal reflex upon gently squeezing the hind limb using a pair of forceps. Subsequent procedures were performed using aseptic techniques in a laminar flow hood. Using surgical scissors the rat was rapidly decapitated and the vertebral column dissected away and placed in a petri dish containing sterile Ca^{2+} - and Mg^{2+} -free phosphate buffered saline and 0.6% w/v glucose (CMF-PBS-glucose). The vertebral column was then dissected longitudinally through both ventral and dorsal walls, producing two hemisections and exposing the spinal cord. After removal of the spinal cord, individual DRG capsules were removed from the intervertebral lumen under a low power microscope, and transferred into a small petri dish containing CMF-PBS-glucose.

5.3.3 Enzyme treatment of DRG Neurons

In order to free the ganglia from the connective tissue surrounding them, the DRG capsules were enzyme treated with trypsin (Type XI, Sigma-Aldrich®, Castle Hill, NSW). Before each rat dissection was performed, 25 mg of trypsin was dissolved in 8.0 ml of CMF-PBS-glucose and filtered (0.22 μm) into a 15 ml centrifuge tube and pre-incubated at 37°C. The dissected DRG capsules were then transferred into the centrifuge tube and the volume topped up to 10 ml and allowed to incubate at 37°C for between 19-45 min depending on the age of the animal (ref Table **5.4**). The trypsin solution was then removed from the centrifuge tube by aspiration and the DRG capsules were then resuspended in Dulbecco′s Modified eagles Medium (DMEM) containing newborn calf serum (10% v/v) and gentamycin (0.08 mg/ml). The resuspended ganglia were then spun at 500 rpm

for 30 seconds and the supernatant was removed and replaced with DMEM. This washing procedure was repeated three times. The ganglia pellet was finally suspended in 2 ml of DMEM.

Age of Animal (days)	Incubation time in 2.5mg/ml trypsin (min)
2	18
3	19
4	21
5	23
6	25
7	27
8	29
9	31
10	34
11	37
12	40

Table 5.4: Trypsin incubation times for newborn rats.

5.3.4 Trituration and Plating of DRG Neurons

Mechanical trituration was performed in order to rupture the capsule (already weakened by trypsin) surrounding the DRG and to separate the cell body from its axon. The DRGs were passed in and out of a fire polished sterile glass Pasteur pipette until the DMEM solution became turbid indicating the liberation of large numbers of neurons. Once the capsule debris had settled under gravity the turbid supernatant was evenly distributed drop wise amongst 8 wells of a pre-incubated tissue culture plate containing 1.0 ml DMEM/well. Upon completion the tissue culture plate was incubated overnight at 37°C (10% CO_2, 90% O_2, 100%

humidity) allowing the neurons to settle and adhere to the poly-*D*-lysine coated coverslips. Refer to **5**.**1**.**6** and **5**.**1**.**7** for whole-cell patch-clamp set-up.

5.3.5 External and Internal solutions for recording K$^+$ currents from DRG neurons

Table 5.5: Composition of external and internal solutions used for electrophysiological recordings of potassium currents from DRG neurons

	Solution Number	Constituents (mM)
Voltage Clamp		
External solution	1	TMA-Cl **120**, KCl **5**, NaCl **30**, CaCl$_2$ **1.8**, MgCl$_2$ **1**, HEPES **5** glucose **25**, 4-AP **5** and TTX **200** nM
$I_{K(Ca)}$ solution	2	Same as 1 + 4-AP **5**
$I_{K(A)}$ solution	3	Same as 1 + CdCl$_2$ **1**, CTX **100** nM and TEA-Cl **25**
$I_{k(DR)}$ solution	4	Same as 1 + **1** mM CdCl$_2$, CTX **100** nM and 4-AP **5**
Internal Solution	5	KF **80**, TMA-Cl **50**, glucose **5**, EDTA **5**, and HEPES **5**
Internal Solution	6	KCl **140**, TMA-Cl **50**, CaCl$_2$ **0.1**, EGTA **1**, glucose **5** and HEPES **5**

Abbreviations: TMA-Cl tetramethyl ammonium chloride;

5.3.6 Voltage-clamp protocol

	Sweep	**I/V**	**Conditions**
$I_{K(Ca)}$	+ 20 mV ⎍ -80 mV	+20 mV ⋀ 10 mV	**Table 5.4 Solutions 2 + 6**
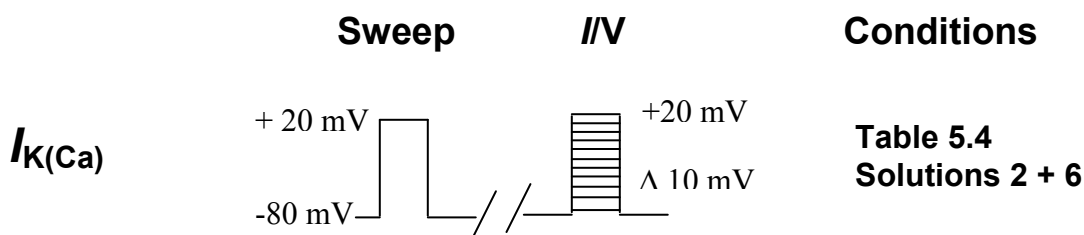
5.4: *SLO*-CHANNEL ELECTROPHYSIOLOGICAL EXPERIMENTS

Whole-cell *Slo* currents were measured using the same conditions as described in sections **5**.**1**.**6** and **5**.**1**.**7** with tip resistances of 2-4 MΩ.

5.4.1 *Slo* channel expression in HEK293 cells

HEK293 cells (American Type Culture Collection, Bethesda, MD, USA) used in the following experiments were maintained in Dulbecco's Modified Eagle's Medium (DMEM/High Modified, JRH Biosciences, Lenexa KS, USA) supplemented with 10% bovine calf serum. Eukaryotic expression of *pSlo*, *dSlo* and *mSlo* were performed by transfection of the HEK293 cells with a construct containing the *pSlo*, *dSlo* or *mSlo* coding region cloned into the expression vector pcDNA3.1 which also carries the G418 resistance gene (Invitrogen BV, San Diego, CA, USA). HEK293 monolayers in 35 mm^2 dishes were transfected using 9 µl Lipofectamine Reagent (Gibco, BRL) and 1 µg DNA. Stably transfected cells were then selected with 1000 µg ml^{-1} G418 (Gibco, Grand Island, NY, USA), These cells were maintained in the normal growth media described above and cultured on sterile glass coverslips to be used for the patch clamping experiments.

5.4.2 External and internal solutions for recording $I_{K(Ca)}$ currents from transfected HEK293 cells.

Table 5.6: Composition of external and internal solutions used for electrophysiological recordings of $I_{K(Ca)}$ currents from transfected HEK293 cells.

	Solution Number	Constituents (mM)
Voltage Clamp		
Physiological external solution	1	NaCl **135**, KCl **5**, CaCl$_2$ **1**, MgCl$_2$ **1**, NaHPO$_4$ **0.33**, HEPES **10** and glucose **10**
Internal Solution	2	KCl **140**, NaCl **4**, Na$_2$-ATP **2**, CaCl$_2$ **0.6** and HEPES **10**

5.4.3 Voltage-clamp protocols

	Sweep	***I/V***	**Conditions**
$I_{K(Ca)}$	+40 mV ... -80 mV	+40 mV Δ 10 mV	**Table 5.5 Solutions 1 + 2**
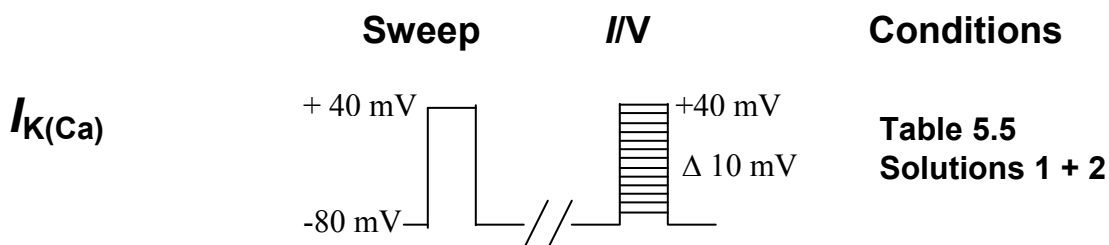
5.5: ACUTE VERTEBRATE TOXICITY TESTING

5.5.1 Chick Biventer Cervicis Nerve-Muscle Bioassay

To confirm the insect-selective toxicity of neurotoxins, a vertebrate neurotoxicity bioassay was performed. This involved the use of an isolated chick biventer cervicis nerve- muscle preparation. The nerve-muscle preparation was dissected from male Australorp chicks, 1-7 days-old (S.F. Barter and Sons, Huntingwood, Australia). Chicks were first anaesthetised by placing them into a sealed

container filled with 100% CO_2 according to the protocol approved by the joint RNSH/UTS animal care and ethics committee. Once fully unconscious, the chick was removed from the container and an incision was made into the mid-thoracic region of the chick, using sharp scissors, and the abdominal aorta was cut. The dissection was carried out according to the procedure outlined in Ginsborg and Warriner (1960). Once the muscle, with attached nerve, was removed from the chick it was bathed in Krebs-Henseleit solution (in mM): NaCl 118.4, KCl 4.7, $MgSO_4$ 1.2, KH_2PO_4 1.2, $NaHCO_3$ 25.0, D-glucose 11.1, $CaCl_2$ 2.5, pH 7.4. The proximal and distal ends of the muscle were tied with cotton threads and mounted in an 8 ml water-jacketed organ bath. The dissected chick biventer cervicis muscle was then maintained at $34°C$ by a Thermomix$^®$M (Braun, Melsungen, Germany) water pump and heating system. The muscle was constantly carbogenated with 95% O_2 and 5% CO_2 and maintained under 1 gram of resting tension. The motor nerve of the neck muscle was electrically stimulated using supramaximal (10-20 V) square wave pulses of 0.05 ms duration at 0.1 Hz via silver electrodes connected to an A-M Systems Isolated Pulse Stimulator (Model 2100 SDR Clinical Technology, Middle Cove, NSW). An isometric force transducer was used to measure the change in tension of the muscle and the measurements were displayed on a Neotrace Neomedix Systems chart recorder (Dee Why West, NSW). The measurements were also sent to a MacLab/4s (ADInstruments, Castle Hill, NSW) A/D converter connected to a Centris 650 Macintosh computer where tension traces were displayed, stored and analysed off-line. Once the muscle was mounted in the organ bath, the muscle was electrically stimulated for at least 20 minutes to allow for the muscle to equilibrate before application of the test toxins.

5.6: DATA ANALYSIS

Mathematical curve fitting algorithms available in Prism$^®$ v4.0c for Macintosh using a non-linear least-squares method were used. The curve fits for the I/V data were obtained using the following equation:

$$I = g_{max}\left(1 - \frac{1}{1 + \exp[(V - V_{1/2})/s]}\right)(V - V_{rev})$$
(1)

where I is the amplitude of the peak (either I_K, I_{Na} or I_{Ca}) at a given test potential, V, g_{max} is the maximal ion conductance, $V_{1/2}$ is the voltage at half-maximal activation, s is the slope factor and V_{rev} is the reversal potential.

IC_{50} values were determined by fitting the dose-response curves with the equation outlined below.

$$y = \frac{1}{1 + \left([x]/Dose_{50}\right)^{n_H}}$$
(2)

where x is the toxin dose, n_H is the Hill coefficient (slope parameter), and $Dose_{50}$ is the median inhibitory dose causing block of membrane currents.

On-rates were determined by fitting time-course data with the following single exponential decay function:

$$y = Ae^{-kx} + C$$
(3)

where x is time, A is the normalized current value (usually 1.0) before application of toxin, and C is the final normalized current value following block by the toxin. The on-rate (τ_{on}) was determined from the inverse of the rate constant k.

Off-rates were determined by fitting time-course data with the following single exponential association function:

$$y = C + A(1 - e^{-kx})$$
(4)

where x is time, A is the normalized current value after washout of the toxin (usually 1.0 if complete washout occurred), and C is the normalized current value

prior to washout of the toxin. The off-rate (τ_{off}) was determined from the inverse of the rate constant k.

Comparisons of two sample means were made using a Wilcoxon signed-rank test or paired Student's t-test. A test was considered to be significant when $p<0.05$. Data, when quantified, was expressed as mean $\pm$ standard error of the mean (SEM).

5.7: SUPPLY OF CHEMICALS

Unless otherwise specified all chemicals were of analytical grade and supplied by Sigma$^{®}$ Chemicals (Castle Hill, NSW, Australia) unless otherwise specified. TTX was supplied by Alamone Labs (Jerusalem, Israel), while charybdotoxin was supplied by Bachem AG$^{®}$ (Bubendorf, Switzerland). J-ACTX-Hv1c (κ-ACTX-Hv1c; including mutant constructs) and FW178 (η-ACTX-Hv1a) were supplied by Professor Glenn King (University of Connecticut, Farmington Connecticut, USA). *PSlo* (splice form AAAA$\triangle$), was supplied by Prof. Dieter Wicher and Dr Christian Derst (Saxon Academy of Sciences, Res. Grp. Neurohormonal Mechanisms, Jena, Germany), *dSlo* (splice form A1/C2/E1/G3/IO), was provided by Prof. Irwin Levitan (Department of Pharmacology & Chemical Biology, University of Pennsylvania, Philadelphia USA) and *mSlo* (splice form mB2), was provided by Assoc. Prof. Andy Braun (Department of Pharmacology & Therapeutics, University of Calgary, Calgary, Canada).

CHAPTER 6

RESULTS

6.1: DETERMINATION OF THE TARGET SITE FOR J-ACTX-Hv1c

Til now the target site for the neurotoxin J-ACTX-Hv1c has remained enigmatic. Based upon the topological arrangement of key functional residues, speculation points to invertebrate potassium channels as the most likely target. Given that the key functional residues of J-ACTX-Hv1c align extremely well with the Lys-Phe/Tyr diad that is conserved across structurally dissimilar potassium channel toxins, and the excitatory phenotype induced by J-ACTX-Hv1c in insect bioassays, is consistent with potassium channel blocking activity.

In contrast, the critical arginine (Arg[8]) of J-ACTX-Hv1c identified in the alanine mutant scan (Maggio and King 2002b) is not surrounded by an array of positively charged residues unlike that seen for the sodium channel toxins, μ- and δ-conotoxins that bind to site 3 & 1 respectively. In addition the bioactive surface of J-ACTX-Hv1c does not possess the conserved lysine residue critical for α-scorpion toxin blockade of Na_V channels. Despite the 3D structure of J-ACTX-Hv1c closely resembling the Na_V channel modulator δ-ACTX-Hv1a (Fletcher *et al*, 1997a), Na_V channels are unlikely to be the primary target of J-ACTX-Hv1c as it is active against the nematode *Caenorhabditis elegans* (Glenn King, personal communication), which does not possess Na_V channels (Bargmann, 1998).

Mutagenesis studies have revealed that N-type calcium channel blockers such as ω-CTX-GVIA (Lew *et al* 1997), ω-CTX-MVIIA (Nadasdi *et al* 1995), contain a functionally critical Lys-Tyr diad, located on opposite faces of the toxin. This diad does not resemble the pharmacophore of J-ACTX-Hv1c. In addition, the excitatory phenotype induced by J-ACTX-Hv1c in insects is inconsistent with a blockade of calcium channels.

Despite the indications for a selective blockade of insect potassium channels it is necessary to confirm any lack of activity on insect sodium and calcium ion channels. The aim of this section of the project is to identify the site and mode of action of J-ACTX-Hv1c.

6.1.1 Effect of J-ACTX-Hv1c on insect Na_V channels

Sodium currents were recorded under voltage-clamp conditions in acutely dissociated dorsal unpaired median (DUM) neurons of the American cockroach *Periplaneta americana*, as described in chapter **5**, section **1**. By stepping the membrane potential from –80 mV to –10 mV a large inward rapidly inactivating sodium current was observed (Fig **6**.**1A**). All currents were recorded in the presence of known calcium channel blockers Cd^{2+} (1 mM), verapamil (0.01 mM) and $NiCl_2$ (0.1 mM), as well as known potassium channel blockers TEA-Cl (20 mM) and 4-AP (5 mM) (Grolleau and Lapied, 1995a). Addition of 150 nM TTX always totally abolished this current thus confirming it was carried by sodium. In contrast, addition of 1 µM J-ACTX-Hv1c failed to significantly alter peak amplitude ($p > 0.05$, paired Student's *t*-test, $n = 5$). To confirm the apparent lack of activity by J-ACTX-Hv1c on insect sodium currents the effects of the toxin were examined at a range of voltages from –80 mV to +70 mV using 10 mV steps. This procedure elicits families of sodium currents at voltages between –40 mV and +70 mV, recorded in both the absence and presence of 1 µM J-ACTX-Hv1c (Fig **C** and **D**). The peak current for each voltage step (*I*/*V*) was then plotted both in the absence (○) and presence (●) of the toxin as seen in Fig **6.1B**. The equation for this curve fit is detailed in chapter **5**, section **6**. As seen there is no

significant differences in peak current amplitude between control and toxin at any of the voltages tested ($p > 0.05$, paired Student's t-test, $n = 5$). In addition, no shift in the voltage dependence of activation (or activation threshold), was observed between control and in the presence of the toxin.

In order to maximise sodium current amplitude the external sodium concentration was increased to 130 mM, while the internal concentration was 20 mM (refer to table **5.2** for the composition of both external and internal solutions). This allowed currents up to 18 nA to be observed at −10 mV (the voltage at which peak current flowed was between −10 mV and 0 mV). In addition, this gave a calculated reversal potential (V_{rev}) for sodium of +49.6 mV (by the Nernst equation). This compared to the measured values of +52.2 ± 1.1 mV and +51.6 ± 2.0 mV ($p > 0.05$, paired Student's t-test, $n = 5$) in the absence and presence of the toxin respectively, indicates that the toxin does not alter sodium channel ion selectivity (Fig **6**.**1B**).

Fig 6.1: Effects of J-ACTX-Hv1c on Na_V channels in cockroach DUM neurons. (**A**) Superimposed typical current traces showing typical lack of effect of 1 µM J-ACTX-Hv1c. I_{Na} currents were obtained by a 50 ms step to +10 mV from a holding potential of –80 mV. The inset shows an enlarged view of the peak current in the presence (**b**) and absence (**a**) of the toxin. This current could be completely abolished by addition of 150 nM TTX, thus proving the current was carried by Na_V channels (*n* = 5) (**B**) The *I*/*V* relationship is shown in both the presence (O) and absence (●) of 1 µM J-ACTX-Hv1c. This curve was plotted using equation **1,** section **5.6**. Data is expressed as mean ± SEM. As seen, there is no shift in the threshold of activation or reversal potential (V_{rev}) by addition of the toxin. (**C**-**D**) Families of currents were obtained by 10 mV steps in the absence (**C**) and presence (**D**) of 1µM J-ACTX-Hv1c from a holding potential of –80 mV (*n* = 5) (see methods for further details).

6.1.2 Effect of J-ACTX-Hv1c on insect Ca_V channels

Similar to sodium currents, calcium currents were recorded under voltage-clamp conditions as described in chapter **5**, section **1**. By stepping the membrane potential from –90 mV to –10 mV a large inward current is elicited. This current has an initial peak (or transient) component followed by a slowly inactivating (or maintained) component still present at the end of the 100 ms test pulse (Fig **6**.**2A**). All currents were recorded in the presence of the sodium channel blocker TTX (150 nM), whilst any potassium current was absent due to the lack of potassium in either the external or internal solutions and substitution by Cs^{2+}.

Addition of 1 mM $CdCl_2$ always totally abolished this current thus confirming it was carried by calcium ions. In contrast, addition of 1 µM J-ACTX-Hv1c failed to significantly inhibit peak current (*p*< 0.05 paired Student's *t*-Test, *n* = 4). To confirm the apparent lack of activity by J-ACTX-Hv1c on insect calcium currents the effects of the toxin was assessed at a range of voltages from –90 mV to +50 mV using 10 mV steps. This procedure elicits families of calcium currents at voltages between –60 mV and +50 mV, recorded in both the absence (Fig **6.2C**) and presence of 1 µM J-ACTX-Hv1c (Fig **6.2D**). The normalized peak current for each voltage step (*I*/*V*) was then plotted both in the absence (●) and presence

(○) of the toxin as seen in Fig **6**.**B**. The equation for this curve fit is detailed chapter **5**, section **6**. As seen there is no significant differences in peak current amplitude between control and toxin at any of the voltages tested ($p > 0.05$, paired Student's t-test, $n = 5$). In addition there are no significant shift in the voltage dependence of activation (or activation threshold) between control currents and those recorded in the presence of the toxin.

Furthermore, the calculated reversal potential (V_{rev}) for calcium (under the conditions described in table **5.3**) was +56.2 mV (by the Nernst equation). This was not significantly different compared to the measured values of +50.2 ± 2.2 mV and +52.6 ± 2.4 mV ($p > 0.05$, paired Student's t-test, $n = 5$) in the absence and presence of the toxin respectively, indicating that the toxin does not alter calcium channel ion selectivity (Fig **6.2B**).

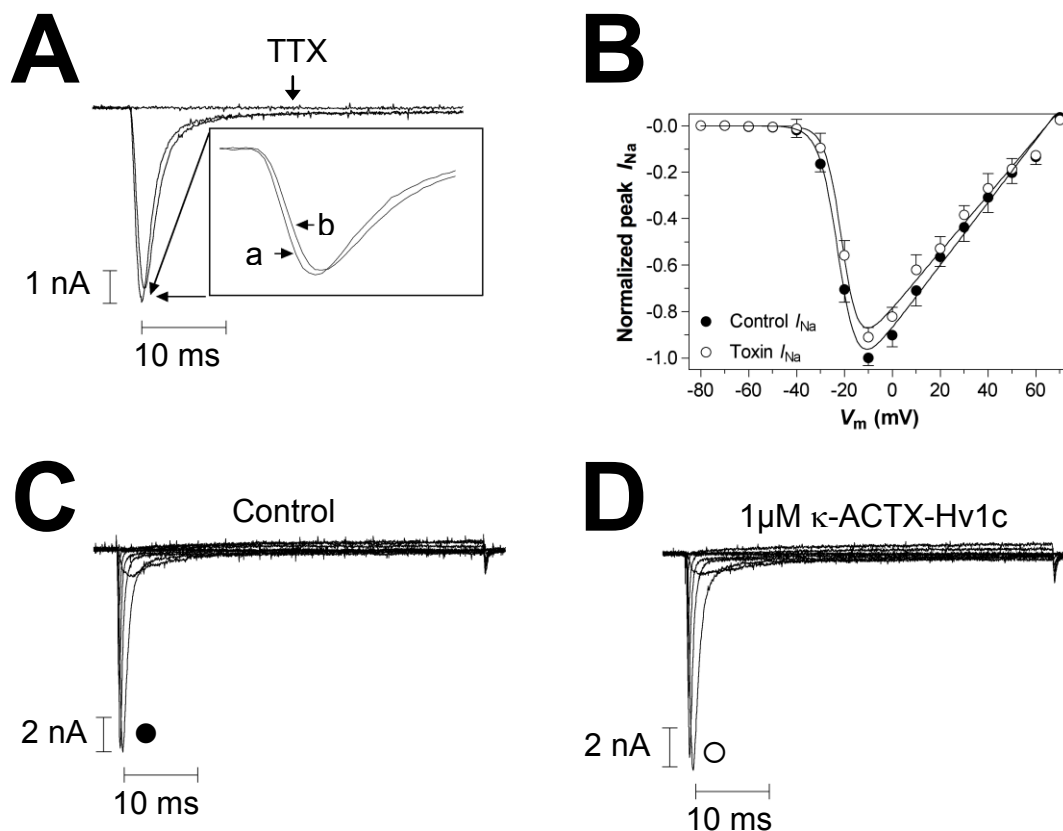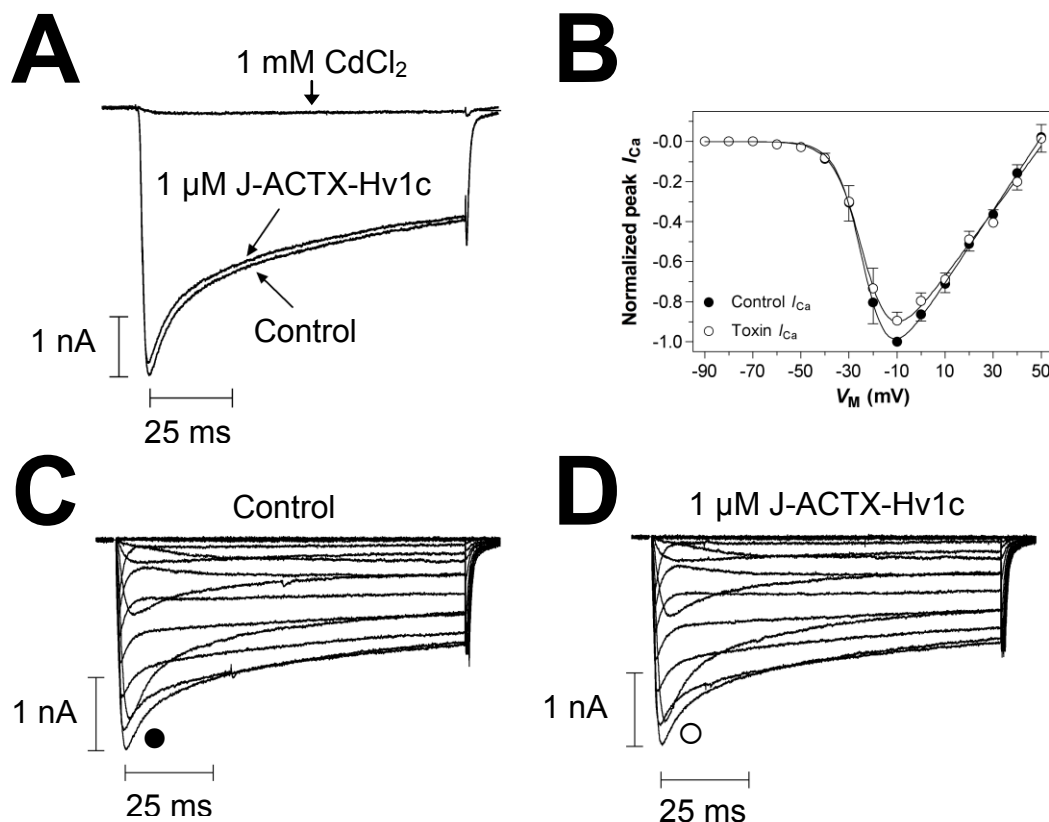**Fig 6.2**: Effects of J-ACTX-Hv1c on Ca_V channels in cockroach DUM neurons. (**A**) Superimposed typical current traces showing typical lack of effect of 1 µM J-ACTX-Hv1c on I_{Ca} currents were

obtained by a 50 ms step to -10 mV from a holding potential of −90 mV. This current could be completely abolished by addition of 1 mM Cd^{2+}, thus proving the current was carried by Ca_V channels (n = 5). (**B**) The *I/V* relationship is shown in both the presence (○) and absence (●) of 1 μM J-ACTX-Hv1c. This curve was plotted using equation **1** section **5.6**. Data is expressed as mean ± SEM. As seen, there is no shift in the threshold of activation or reversal potential (V_{rev}) by addition of the toxin. (**C**-**D**) Families of calcium currents were obtained by 10 mV steps from a holding potential of −90 mV (n = 5) (see methods for further details).

6.1.3 Effect of J-ACTX-Hv1c on macroscopic insect K_V channels

Given the key functional residues of J-ACTX-Hv1c align extremely well with the Lys-Phe/Tyr diad that is conserved across structurally dissimilar potassium channel toxins (Dauplais *et al* 1997) and the excitatory phenotype induced by J-ACTX-Hv1c in insect bioassays, our hypothesis was J-ACTX-Hv1c is an insect selective potassium channel blocker. This was supported by the fact that J-ACTX-Hv1c fails to display activity against isolated insect sodium or calcium currents. Therefore we examined the effects of 1 μM J-ACTX-Hv1c on macroscopic potassium currents from cockroach (DUM) neurons as discussed in chapter **5**, section **1**.

DUM neurons have previously been shown to possess four outward potassium channel subtypes; the 'A-type' ($K_{(A)}$), delayed rectifier ($K_{(DR)}$), calcium-activated ($K_{(Ca)}$) and sodium-activated ($K_{(Na)}$) potassium channels. Stepping the voltage from a holding level of −80 mV to +40 mV elicits a large outward current, with an initial peak (or transient) component followed by a non-inactivating (or maintained) component that persists until the end of the depolarising test pulse (Fig **6.3A**). This current was recorded under the recording conditions provided in table **5**.**1**. The only channel-blocking agent used for these experiments was the sodium channel blocker TTX (150 nM), note that no calcium channel antagonists were included thus allowing the calcium-activated potassium current to remain. Addition of 1 μM J-ACTX-Hv1c inhibits total late (as determined by the current remaining at conclusion of the 100 ms test pulse) I_K by 56 ± 7 % (n = 5). Furthermore addition of the antagonists; TEA-Cl (50 mM), 4-AP (5 mM), charybdotoxin (30 nM) and $CdCl_2$ totally abolished all outward current (n = 4, FIG

6.**3A**). This indicates that the observed current was carried only by potassium and calcium ions.

Families of outward currents were obtained by increasing the voltage from a holding level of –80 mV to +40 mV in 10 mV increments, in both the absence (Fig **6**.**3C**) and presence (Fig **6.3D**) of 1 µM J-ACTX-Hv1c (*n* = 5). The normalized peak (Fig **6.3E**) and late (Fig **6.3F**) *I*/*V* relationship was then plotted in both the absence (λ)(v) and presence (O)($\blacklozenge$) of 1 µM J-ACTX-Hv1c. As is evident, presence of the toxin consistently inhibited both peak (circles) and late current (squares) at voltages tested within the range of –50 mV to + 40 mV (*p* = 0.01 at +40 mV, *n* = 5). The equation for this curve fit is detailed in section **5**.**6**. In contrast no change in the voltage-dependence of activation is seen for either peak or late current in the presence of the toxin (*n* = 5).

J-ACTX-Hv1c therefore represents the first atracotoxin that selectively blocks voltage-gated potassium channels. As a result J-ACTX-Hv1c has been renamed κ-ACTX-Hv1c in accordance with the nomenclature previously described for Australian funnel-web spider toxins (Fletcher *et al*, 1997) to reflect its ability to inhibit I_K. The next step in this project was to identify which subtype(s) are inhibited by κ-ACTX-Hv1c and thus underlie the inhibition of macroscopic I_K.
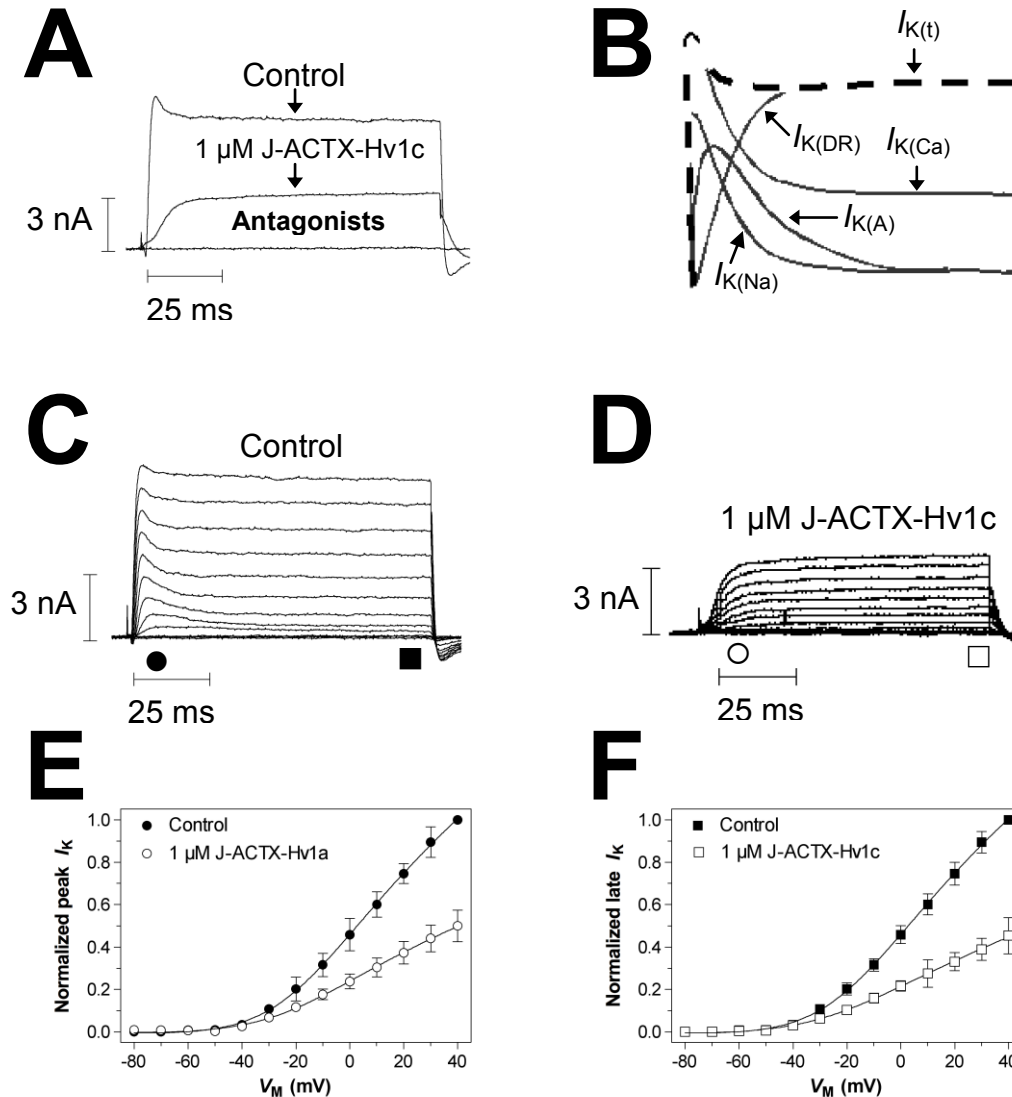
Fig 6.3: Effects of J-ACTX-Hv1c on K_V channels in cockroach DUM neurons. (**A**) Superimposed typical current traces showing the blockade by 1 µM J-ACTX-Hv1c on I_K currents that were obtained by a 100 ms step to +40 mV from a holding potential of –80 mV. Addition of the toxin inhibited $I_{K(Total)}$ by 56 ± 7 %, indicating that J-ACTX-Hv1c targets at least one of the four distinct K^+ channel subtypes that have been identified in DUM neuron somata. This current could be completely abolished by addition of 1 mM Cd^{2+}, 5 mM 4-AP and 50 mM TEA (data not shown) thus proving the current was carried by K_V channels (*n* = 4). (**B**) Diagrammatic representation of I_K subtypes elicited upon depolarisation of DUM neurons. $I_{K(Total)}$ is shown by a dashed line. Given the presence of TTX in these experiments, $I_{K(Na)}$ is not seen. (**C**-**D**) Families of currents were obtained by 10 mV steps from a holding potential of –80 mV (*n* = 4). (**E**-**F**) The *I*/*V* relationships

for both peak (circles) and late (squares) I_K are shown in both the presence (O or ◆), and absence (● or ■) of 1 µM J-ACTX-Hv1c respectively. This curve was plotted using equation **2**, section **5**.**6**. Data is expressed as mean ± SEM. As seen, currents are inhibited by 1 µM J-ACTX-Hv1c at each potential tested however was there a shift in the threshold of activation ($n = 4$).

6.1.4 Effect of κ-ACTX-Hv1c on insect $K_{(DR)}$ channels

Isolation of $IK_{(DR)}$ required the use of a range of sodium (Na_V), calcium (Ca_V) and other potassium channel inhibitors. These included the sodium channel and sodium-activated potassium channel blocker; TTX (150 nM), Ca_V channel blocker $CdCl_2$ (1 mM) the selective 'A-type' potassium ($K_{(A)}$) channel blocker 4-AP (5 mM) and selective calcium-activated potassium channel blocker, charybdotoxin (30 nM). The correct concentration to block $K_{(CA)}$ was determined in separate experiments (see section **6**.**1**.**6**). Under these conditions (table **5**.**1**) a non-inactivating (or maintained) current occurred by stepping from a holding potential of −80 mV to +40 mV. This current remained throughout the duration of the 100 ms test pulse and was not inhibited by addition of 1 µM κ-ACTX-Hv1c $I_{K(DR)}$ (Fig **6**.**4A** $n = 5$). Furthermore, families of outward currents were obtained by increasing the voltage from a holding level of −80 mV to +40 mV in 10 mV increments, in both the absence (Fig **6**.**4C**) and presence (Fig **6**.**4D**) of 1 µM κ-ACTX-Hv1c ($n = 5$). The normalized late I/V relationship was then plotted in both the absence (v) and presence ( ) of 1 µM κ-ACTX-Hv1c (Fig **6**.**4E**). As is evident, 1 µM κ-ACTX-Hv1c failed to significantly block $I_{K(DR)}$ at any voltages tested ($p < 0.05$, Paired Student T-test, $n = 5$). In addition no shift in the voltage-dependence of activation is seen. This result confirms that the blockade of total I_K by 1 µM κ-ACTX-Hv1c is not due to a blockade of $I_{K(DR)}$.
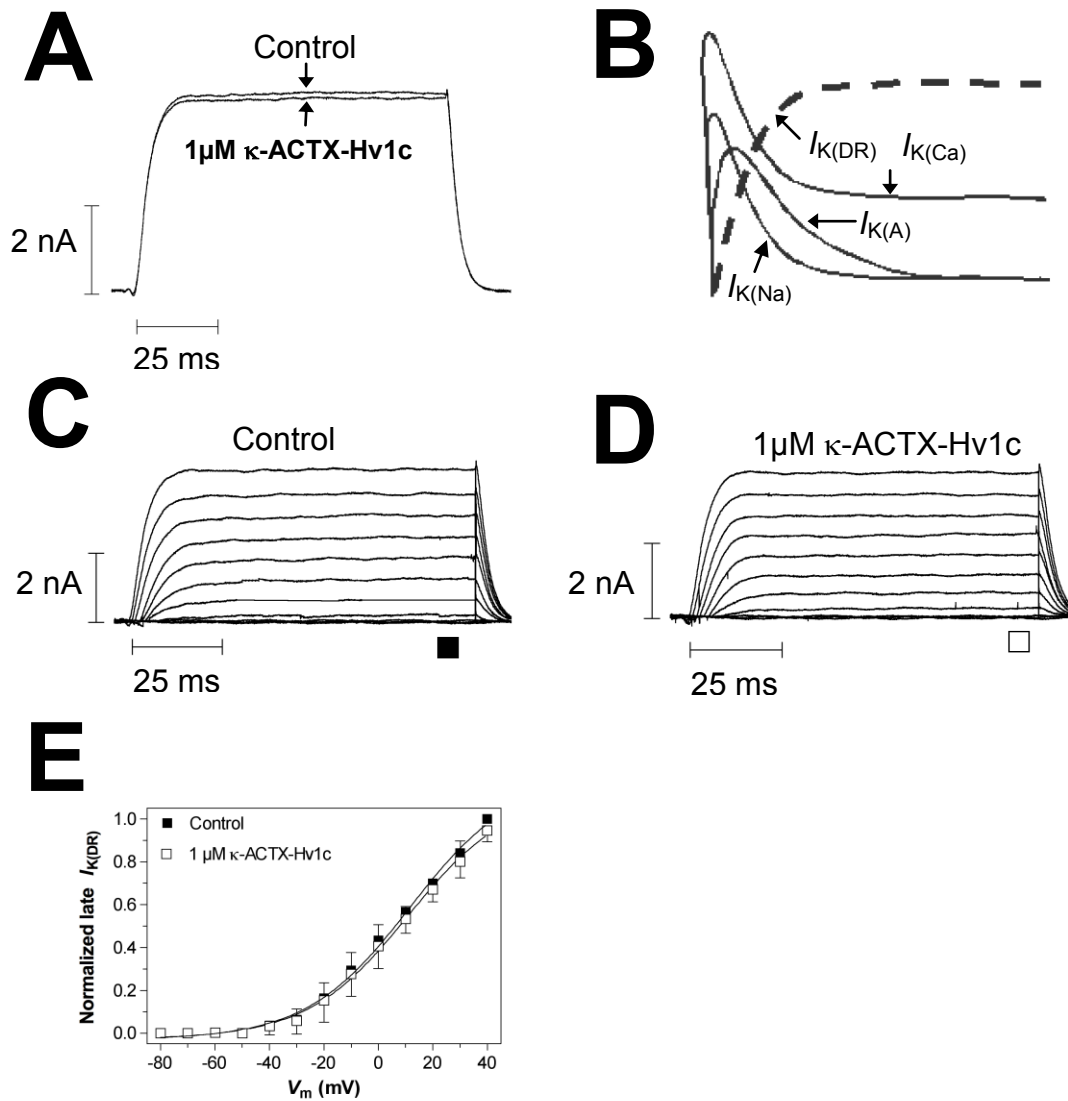
Fig 6.**4**: Effects of κ-ACTX-Hv1c on $K_{(DR)}$ channels in cockroach DUM neurons. (**A**) Superimposed current traces showing typical lack of effect of 1 μM κ-ACTX-Hv1c on $I_{K(DR)}$ currents that were obtained by a 100 ms step to +40 mV from a holding potential of –80 mV. $I_{K(DR)}$ currents were isolated by the addition of 1 mM Cd^{2+} (blocks I_{Ca}), 5 mM 4-AP (blocks $I_{K(A)}$) and 30 nM ChTX (blocks $I_{K(Ca)}$). This current could be completely abolished by addition of 50 mM TEA (data not shown) (*n* = 5). (**B**) Diagrammatic representation of I_K subtypes elicited upon depolarisation of DUM neurons. $I_{K(DR)}$ is shown by a dashed line. Given the presence of TTX in these experiments, $I_{K(Na)}$ is not seen. (**C**-**D**) Families of currents were obtained by 10 mV steps from a holding potential of –80 mV (*n* = 5). (**E**) The *I/V* relationship for late $I_{K(DR)}$ (measured at the end of the 100 ms test pulse), are shown in both the presence ( ) ,and absence (■) of 1 μM κ-

□

ACTX-Hv1c respectively. This curve was plotted using equation **2** section **5.6**. Data is expressed as mean ± SEM. As seen, currents were not inhibited by 1 μM κ-ACTX-Hv1c at each potential tested nor was there a shift in the threshold of activation (n = 5).

6.1.5 Effect of κ-ACTX-Hv1c on insect $K_{(A)}$ channels

The 'A-type' current ($I_{K(A)}$) is characterised by rapid activation, that contributes to the peak current seen in total I_K and subsequent rapid inactivation (Fig **6**.**5A**). This current is elicited in the presence of TTX (150 nM, to block I_{Na} and $I_{K(Na)}$) $CdCl_2$ (1 mM to block I_{Ca}) and charybdotoxin (30 nM to block $I_{K(Ca)}$). TEA-Cl and 4-AP are not included as both antagonists were found to block $I_{K(A)}$ (Grolleau and Lapied, 1994; data not shown).

Total current was elicited by stepping the voltage from a holding potential of –80 mV to +30 mV following a 1 second pre-pulse to either –120 mV or –40 mV. The –120 mV prepulse removes steady-state inactivation and elicits a large outward current with both an initial peak followed by a non-inactivating (or maintained) current. This represents both $I_{K(A)}$ and $I_{K(DR)}$. By using a –40 mV prepulse, $I_{K(A)}$ is abolished as $K_{(A)}$ channels are inactivated at voltages above –65 mV (Grolleau and Lapied 1994). The remaining current that is seen therefore represents only $I_{K(DR)}$. Subtraction of currents recorded in the presence of the –40 mV prepulse ($I_{K(DR)}$) from currents recorded in the presence of the –120 mV prepulse ($I_{K(A)}$ and $I_{K(DR)}$) reveals $I_{K(A)}$ in isolation. Refer to section **5.1.9** & table **5.1** for further details of the recording conditions.

Addition of 1 μM κ-ACTX-Hv1c significantly inhibits $I_{K(A)}$ by 14.3 ± 4.6 % at voltages above +30 mV (Fig **6.5B**, p < 0.05, paired Student's t-test, n = 5). Families of $I_{K(A)}$ were elicited in both the absence (Fig **6.5C**), and presence (Fig **6.5D**), of 1 μM κ-ACTX-Hv1c by increasing the voltage in 10 mV steps from a holding potential of –80 mV to + 30mV following a 1 second prepulse to either – 120 mV or –40 mV. Analysis of the subsequent I/V relationship (Fig **6.5B**) indicates that the presence of 1 μM κ-ACTX-Hv1c does not significantly inhibit

$I_{K(A)}$ at voltages below + 30 mV, nor is there a shift in the voltage-dependence of activation (activation threshold) ($p < 0.05$, paired Student's *t*-test, $n = 5$).

Although κ-ACTX-Hv1c at doses above 1 μM does inhibit $I_{K(A)}$ at voltages above + 30 mV, it does not explain the large voltage-independent blockade of both the peak and maintained components of total I_K. Therefore the molecular target (or specific K_V channel subtype) of κ-ACTX-Hv1c is unlikely $K_{(A)}$ channels.
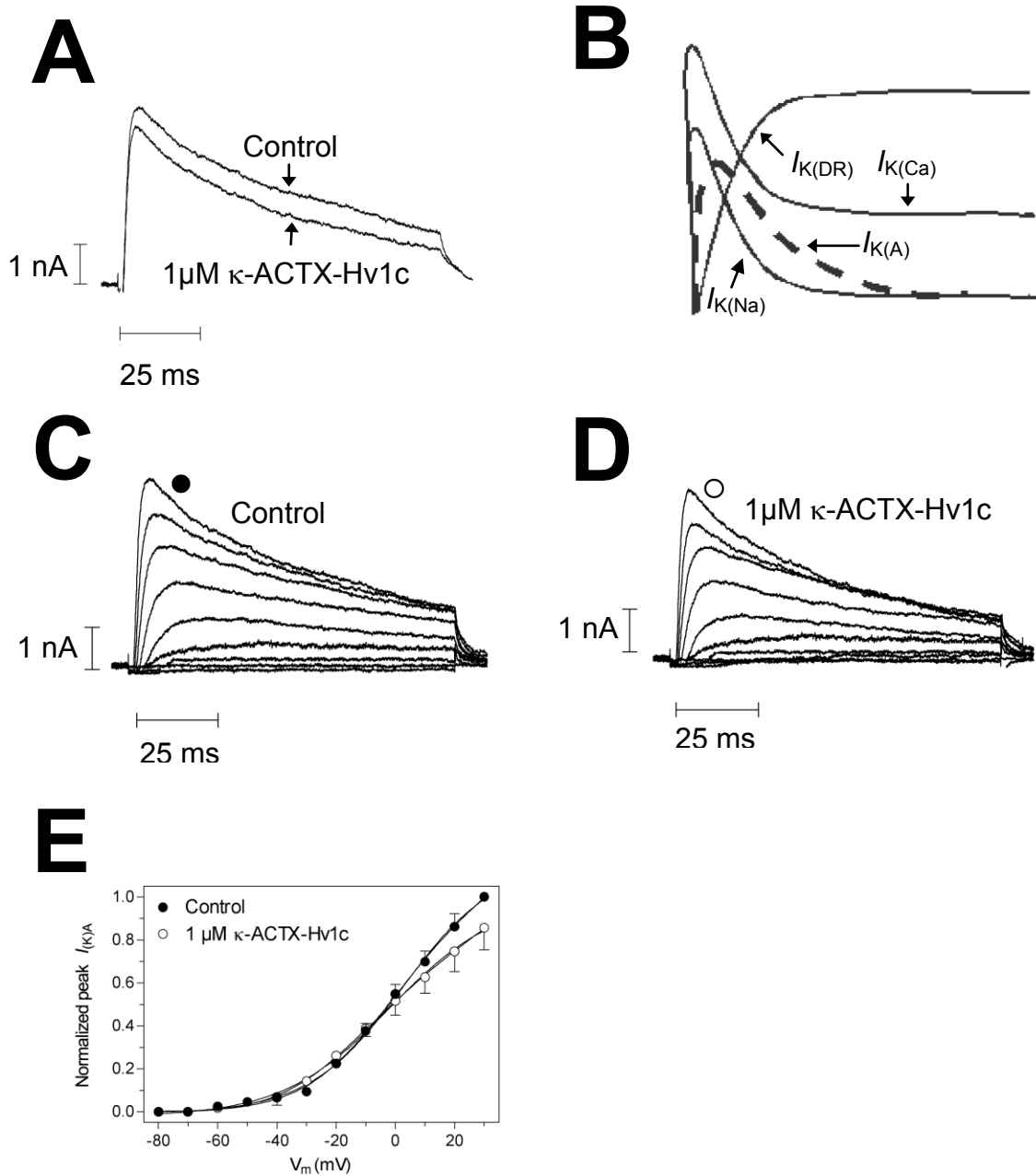
Fig 6.5: Effects of κ-ACTX-Hv1c on K(A) channels in cockroach DUM neurons. (**A**) Superimposed typical current traces showing a significant block of 14.3 ± 4.2 % by 1 µM κ-ACTX-Hv1c on $I_{K(A)}$ currents that were obtained by current subtraction routines following prepulse potentials of −120 and −40 mV (see sections **5.1.9** & **5.1.10**; $p < 0.05$, $n = 5$). $I_{K(A)}$ currents were isolated by the addition of 1 mM Cd^{2+} and 30 nM ChTX (blocks I_{Ca} and $I_{K(Ca)}$). This current could be completely abolished by addition of 5 mM 4-AP (data not shown) ($n = 5$). (**B**) Diagrammatic representation of I_K subtypes elicited upon depolarisation of DUM neurons. $I_{K(A)}$ is shown by a dashed line. Given

the presence of TTX in these experiments, $I_{K(Na)}$ is not seen. (**C-D**) Families of $I_{K(Ca)}$ were obtained by 10 mV steps following subtraction routines using 1 second prepulse potentials of –120 and –40 mV from a holding potential of –80 mV. (**E**) The I/V relationship for peak $I_{K(A)}$ are shown in both the presence (O) ,and absence (●) of 1 μM κ-ACTX-Hv1c respectively. This curve was fitted using equation **2** chapter **5**, section **6**. Data is expressed as mean $\pm$ SEM (n = 5). As seen, currents were not significantly inhibited by 1 μM κ-ACTX-Hv1c at each potential tested except at test potentials of +30 mV, and there was no shift in the threshold of activation ($p < 0.05$, n = 5).

6.1.6 Isolation of insect K$_{(Ca)}$ channels using charybdotoxin (ChTX)

In order to determine the effects of κ-ACTX-Hv1c on insect calcium-activated potassium (K$_{(Ca)}$) channels it was necessary to isolate $I_{K(Ca)}$ from other K$_V$ channel subtypes present in DUM neurons. Under control conditions, 4-AP (5 mM) was included to inhibit $I_{K(A)}$, as was the Na$_V$ channel blocker TTX (150 nM) and the Ca$_V$ channel blocker CdCl$_2$ (1 mM). However to remove the $I_{K(DR)}$ component proved difficult as TEA-Cl is not specific for K$_{(DR)}$ channels, and indeed also inhibits $I_{K(Ca)}$ potassium channels (Grolleau and Lapied, 1994). Therefore it was necessary to isolate $I_{K(Ca)}$ by using a subtraction routine. This involved, firstly recording $I_{K(DR)}$ and $I_{K(Ca)}$ in combination (control current) using a 100 ms test pulse to +40 mV from a holding potential of –80 mV. At this time toxin was applied for a period of 10 minutes, followed by a 10-minute washout period with toxin-free solution. By then completely blocking $I_{K(Ca)}$ with CdCl$_2$ and ChTX would leave $I_{K(DR)}$ in isolation. This remaining $I_{K(DR)}$ when subtracted from the previous currents would leave only $I_{K(Ca)}$ in isolation.

For this technique to work it was necessary to identify the optimum concentration of the selective $I_{K(Ca)}$ channel blocker ChTX to totally block $I_{K(Ca)}$. Indeed, once this was determined, then $I_{K(DR)}$ could be isolated by simply including the optimum concentration of charybdotoxin in the external solution at all times.

Large outward potassium currents were elicited by stepping the voltage from a holding potential of –80 mV to +40 mV under the conditions described in sections **5**.**1**.**9** & **5**.**1**.**10**. The addition of ChTX (1-100 nM) irreversibly inhibits a portion of

I_K (n = 5) (Fig **6.6A**, **C** and **D**). Analysis of the dose-response curve (Fig **6.6B**) indicates a concentration-dependent inhibition of the peak and late I_K that reaches a maximum at 30 nM. At doses above 30 nM no further inhibition of current occurs indicating that the current remaining is charybdotoxin insensitive, namely $I_{K(DR)}$ (given that K_A and K_{Na} were blocked by the presence of 4-AP and TTX, respectively). Considering that $CdCl_2$ (1 mM) was also present in the external solution indicates that blockade of Ca_V channels was not sufficient to fully inhibit $I_{K(Ca)}$. This is no doubt due to the presence of internal Ca^{2+} (0.1 mM) in the internal solution, the release of calcium from internal stores or that there is a calcium-independent activation of $K_{(Ca)}$ channels, that is sufficient to elicit $I_{K(Ca)}$. Families of currents were elicited by 10 mV steps from –80 mV to +40 mV recorded in the absence (Fig **6.6E**), and presence (Fig **6.6F**), of 30 nM charybdotoxin (n = 5). The I/V analysis (Fig **6.6G**) revealed an irreversible blockade of late I_K as well as no significant shift in the voltage dependence of activation ($p < 0.05$, paired Student's t-test, n = 5). To further determine if the blockade of I_K was voltage-dependent, the normalized $I_{K(ca)}$ block was plotted against membrane potential (Fig **6.6H**). This revealed that indeed as the voltage increased a significant increase in blockade resulted ($p < 0.05$, paired Student's t-test, n = 5), indicating that ChTX inhibits I_K in a voltage-dependent manner.

In summary these results indicate that in order to completely inhibit $I_{K(Ca)}$ it was necessary to include both $CdCl_2$ (1 mM) and charybdotoxin (30 nM) in the external solution. This combination would therefore be required to isolate $I_{K(DR)}$ and $I_{K(A)}$ as well as $I_{K(Ca)}$ (by subtraction).
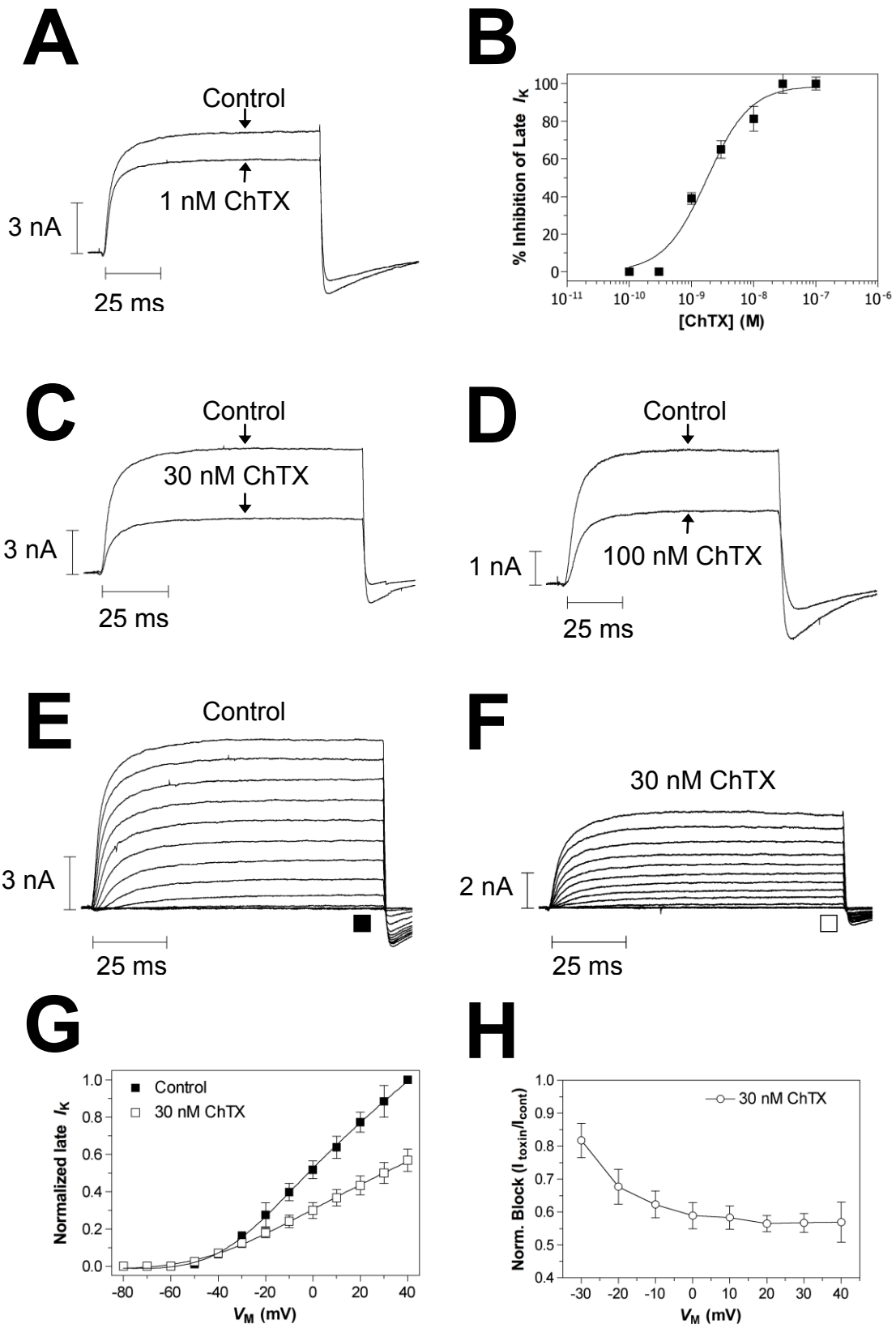
Fig 6.6: To record $I_{K(Ca)}$ in isolation from other K_V channel currents a current subtraction routine following perfusion with the K_{Ca} channel blockers ChTX and $CdCl_2$ was used. (**A,C-D**) Superimposed current traces were obtained by stepping the voltage to +40 mV from a holding potential of –80 mV. Addition of ChTX in the presence of $CdCl_2$ (1 mM) and 4-AP (5 mM) produced a dose-dependent block of the remaining outward current despite the presence of the Ca_V channel and K_A channel blockers respectively. (**B**) A plot of the concentration-response curve indicates that maximum block of the remaining outward current could be achieved at concentrations above 30 nM. As a consequence $I_{K(Ca)}$ was isolated by subtraction both prior to and following application of the toxin following addition of ChTX (30 nM) and $CdCl_2$ (1 mM) at the conclusion of the experiment. Families of currents were obtained by 10 mV steps in the absence *(E),* and presence (**F**), of 30 nM ChTX from a holding potential of –80 mV (n = 5).

(**G**) The *I/V* relationship is shown in both the presence (◆) and absence (■) of 30 nM ChTX. As seen, there is no shift in the threshold of activation by addition of the toxin (n = 5). (**H**) The fractional block by 30 nM ChTX (●) as compared to control was not consistent at all test potentials indicating that ChTX block of $I_{K(Ca)}$ is voltage-dependent (p = 0.08, n = 5). Refer to section **5**.6 for the equations for dose-response and *I/V* analysis. Data is expressed as mean ± SEM.

6.1.7 Effect of κ-ACTX-Hv1c on insect K_{Ca} channels

As previously discussed (chapter **3**, section **3**) DUM neurons from the American cockroach *Periplaneta americana* contain both a fast-activating/inactivating and non-inactivating (or maintained) $I_{K(Ca)}$. Both components are voltage-dependent and require the presence of internal Ca^{2+}, this can be done by directly including Ca^{2+} in the internal solution, by the voltage-dependent release of Ca^{2+} from internal stores, or by the influx of Ca^{2+} via Ca_V channels.

Stepping the voltage from a holding potential of –80 mV to +40 mV elicits a large outward current with both an initial peak (transient) component along with a late (maintained) component that persists until termination of the voltage step. This current is recorded in the presence of TTX (150 nM, to block I_{Na}) and 4-AP (5 mM, to block $I_{K(A)}$). Given that TEA-Cl has previously been shown to inhibit $I_{K(Ca)}$ it was necessary to isolate $I_{K(Ca)}$ by subtraction. This was done by subtracting the current remaining after addition of ChTX (30 nM) and $CdCl_2$ (1 mM) from the control current. As discussed in section **6**.**1**.**6** this combination of agents

completely inhibits $I_{K(Ca)}$ thus the current remaining after the subtraction was only $I_{K(Ca)}$ in its entirety.   Refer to sections **5**.**1**.**9** & **5**.**1**.**10** for further details of the voltage protocols and solutions used for this procedure. Given that κ-ACTX-Hv1c at doses up to 1 μM failed to inhibit I_{Ca} or $I_{K(DR)}$ (see previous sections), any inhibition of the outward current in the presence of the toxin following current subtraction is attributed to a selective block of $I_{K(Ca)}$. This current also activated at membrane potentials greater than –50 mV consistent with BK_{Ca} currents recorded previously in DUM neurons (Grolleau and Lapied, 1995).

Addition of 3 nM κ-ACTX-Hv1c inhibits with partial reversibility both the initial peak and late component of $I_{K(Ca)}$ by 53 ± 7.4 % and 52.4 ± 4.3 % respectively. (Fig **6.7A**, n = 5). Examination of the dose-response curve reveals that blockade of current is concentration-dependent with IC_{50} values for the peak and late components of 1.8 and 2.1 nM respectively (Fig **6.7B**). Families of currents were elicited by stepping the voltage from –80 mV to +40 mV in 10 mV steps both in the absence (Fig **6.7C**) and presence (Fig **6.7D**) of 3 nM κ-ACTX-Hv1c (n = 5). I/V analysis of both normalized peak (Fig **6.7E**) and late (Fig **6.7F**) components, revealed a consistent degree of block of $I_{K(Ca)}$ at all voltages tested thus indicating that inhibition of $I_{K(Ca)}$ by κ-ACTX-Hv1c is not voltage-dependent. Furthermore partial reversibility was seen at all voltages tested for both the peak and late components. The voltage dependence of activation (activation threshold) was also unaffected for both the peak and late components by the presence of 3 nM κ-ACTX-Hv1c (p < 0.05, paired Student's t-test, n = 5). These results indicate that κ-ACTX-Hv1c likely acts to block $I_{K(Ca)}$ by occluding the extracellular pore of the channel rather then altering the voltage-dependence of activation of the channel as seen with toxins that interact with the channels voltage-sensor eg Hanatoxin (Swartz and MacKinnon, 1997). Plotting the normalized late current remaining in the presence of 3 nM κ-ACTX-Hv1c versus time revealed a τ_{on} value of 104.8 ± 6.4 seconds (n = 5). In addition, the remaining current was measured during a washout period with toxin-free solution (indicating reversibility of the toxin-channel interaction), that revealed a τ_{off} value

of 217.3 ± 7.8 seconds (Fig **6**.**7H**, *n* = 5). However this current failed to return to control levels despite a washout period of up to 10 minutes (data not shown).

κ-ACTX-Hv1c therefore inhibits insect macroscopic potassium current (I_K) by the specific inhibition of $I_{K(Ca)}$ similar to charybdotoxin and iberiotoxin. This validates insect K_{Ca} channels as a potential target for bio-pesticides, and κ-ACTX-Hv1c as a likely lead compound.
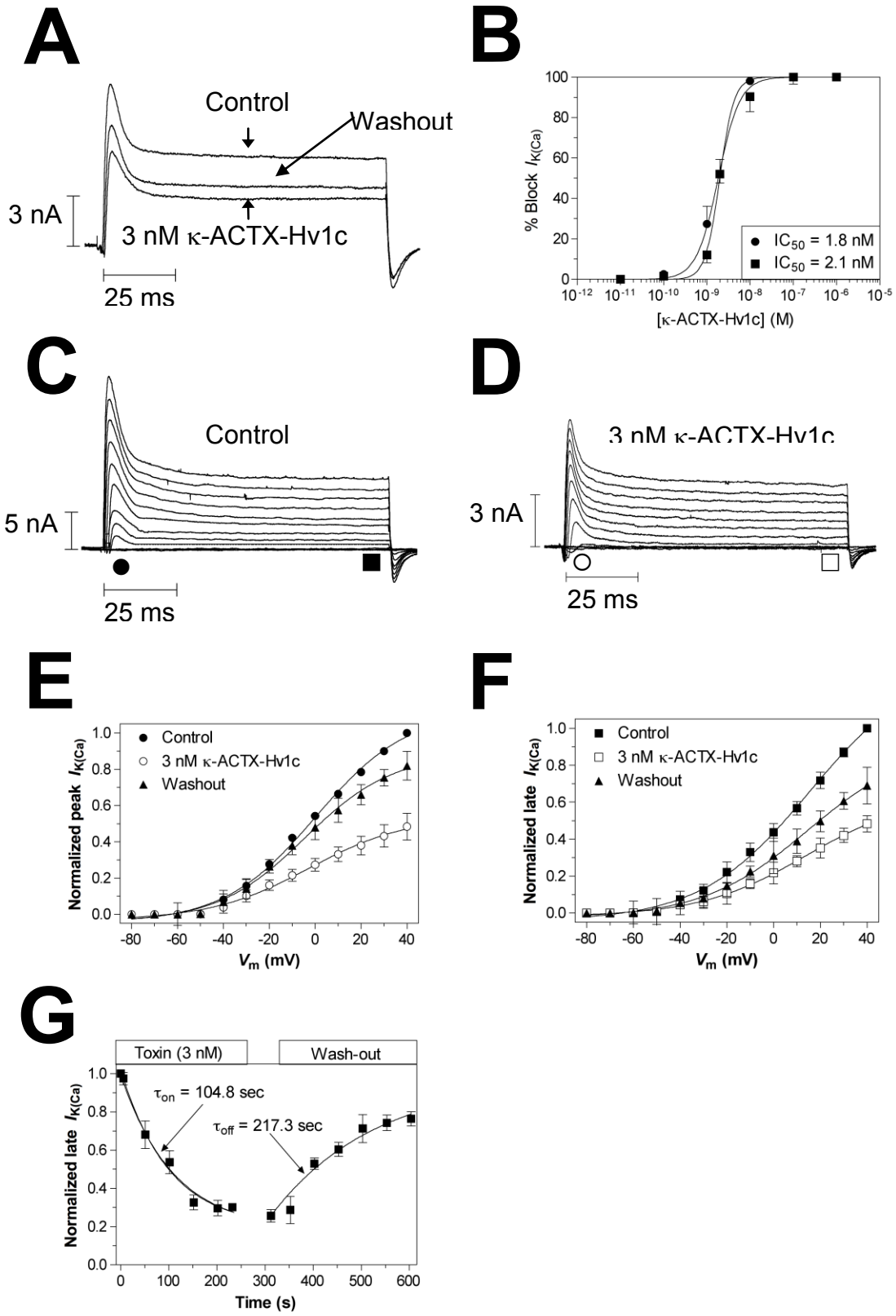
Fig 6.7: κ-ACTX-Hv1c blocks K_{Ca} channels in cockroach DUM neurons. (**A**) Addition of 3 nM κ-ACTX-Hv1c inhibits both peak and late $I_{K(Ca)}$ by 53 ± 7.4 % and 52.4 ± 4.3 %, respectively with only partial reversibility ($n = 5$). Currents were induced by stepping the potential to +20 mV from a holding potential of –80 mV. (**B**) The concentration-response curve for inhibition of both peak ($\bullet$), and late ($\blacksquare$), $I_{K(Ca)}$ revealed IC_{50} values of 2.3 and 2.9 nM, respectively. Families of currents were elicited by 10 mV depolarisation steps from –80 to +40 mV, in both the absence (**C**), and presence (**D**), of 3 nM κ-ACTX-Hv1c ($n = 5$). As shown by the peak (**E**), and late (**F**), I/V relationships, 3 nM κ-ACTX-Hv1c inhibits these currents at all potentials tested with only partial washout observed. Data is expressed as mean $\pm$ SEM. (**G**) A plot of the time-course for inhibition of $I_{K(Ca)}$ by 3 nM κ-ACTX-Hv1c revealed values for τ_{on} and τ_{off} as 104.8 ± 6.7 and 217.3 ± 18.6 seconds respectively ($n = 5$). Refer to section **5**.6 for the equations for fitting concentration-response curves, I/V analysis and determining τ_{on} and τ_{off} values.
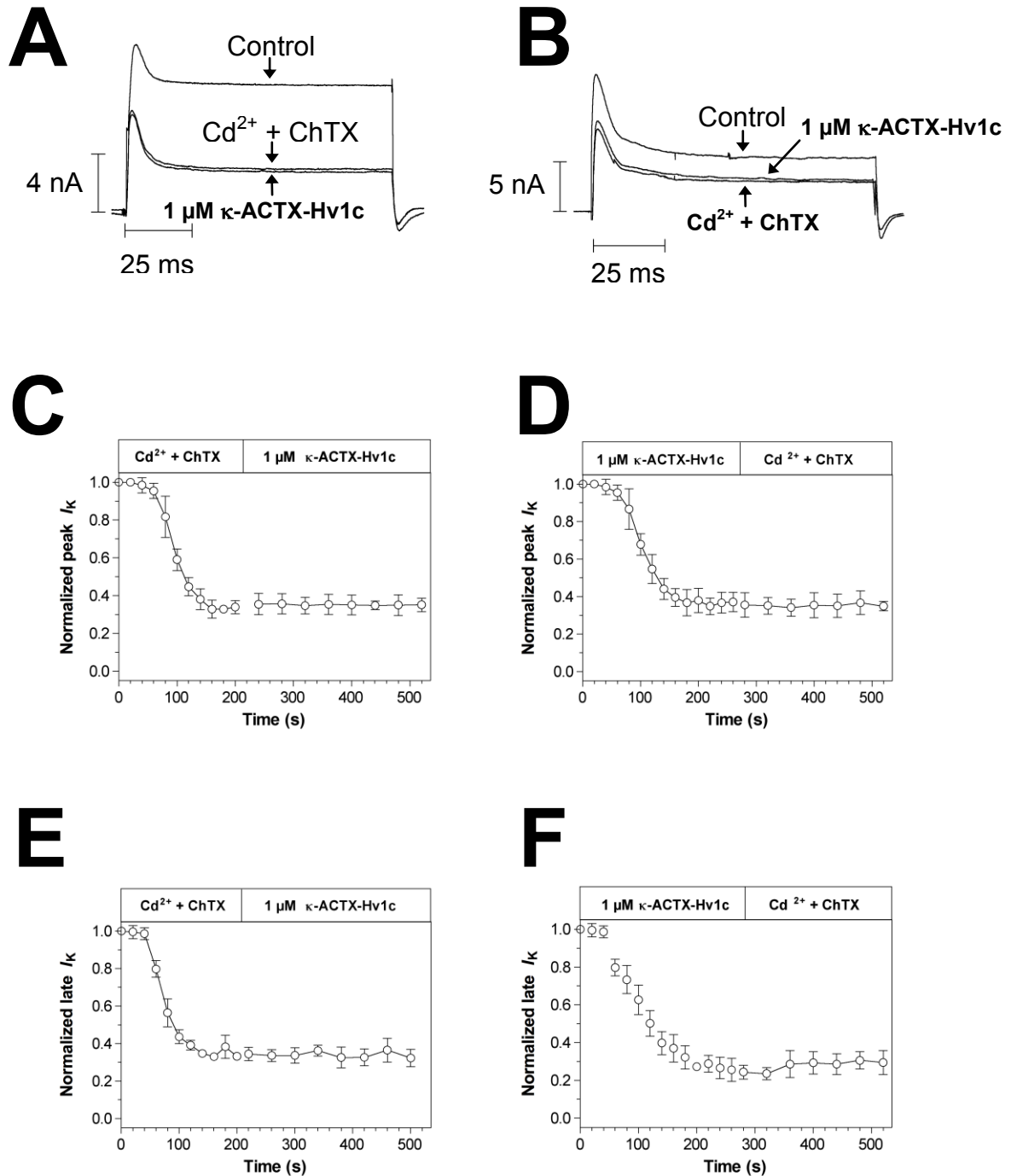
Fig 6.8: κ-ACTX-Hv1c and charybdotoxin share the same insecticidal target. (**A**, **C** & **E**) Addition of Cd^{2+} (1 mM) and ChTX (30 nM) inhibits both peak and late total I_K by 61.3 ± 4.6 % and 58.4 ± 6.2 %, respectively (n = 3). Subsequent addition of 1 μM κ-ACTX-Hv1c fails to further inhibit total I_K despite prolonged exposure (n = 3). No reversibility is seen. (**A**, **C** & **E**) Addition of 1 μM κ-

ACTX-Hv1c inhibits both peak and late I_K by 54.3 ± 4.6 % and 53.4 ± 6.2 %, respectively. Subsequent addition of Cd^{2+} (1 mM) and ChTX (30 nM) fails to further inhibit I_K (B, D & **F, n** = 3). All currents were recorded in the presence of 4-AP (5 mM) to block $I_{K(A)}$.

6.1.8 Effect of κ-ACTX-Hv1c on mammalian $K_{(Ca)}$ channels

$I_{K(Ca)}$ were recorded from acutely dissociated dorsal root ganglion neurons from 5-12 day-old Wister rats as discussed in section **5.3**. Control currents were elicited by stepping the voltage from a holding level of −80 mV to +20 mV in the presence of TTX (200 nM) and 4-AP (5 mM). Upon 10-minute perfusion of 1 μM κ-ACTX-Hv1c no significant inhibition of current occurred (Fig **6.9A**, p < 0.05, paired Student's t-test, n = 4). In contrast, perfusion with $CdCl_2$ (1 mM) and ChTX (100 nM) inhibited total current by 69.5 ± 3.5% (n = 4). When this remaining current (Fig **6**.9A, *2*), was subtracted from the control current (Fig **6**.9A, *1*) an outward current with both an initial peak and late component is seen (Fig **6.9B**). This provides evidence that the control current was composed of both $I_{K(DR)}$ (*2*) and $I_{K(Ca)}$ (*1-2*). When the subtraction was performed following perfusion with 1 μM κ-ACTX-Hv1c no significant inhibition of $I_{K(Ca)}$ was seen (Fig **6.9B**, p < 0.05, paired Student's t-test, n = 4). Families of currents were elicited both in the absence (Fig **6.9C**) and presence, of 1 μM κ-ACTX-Hv1c (Fig **6.9D**). These currents were subtracted from the control currents following perfusion with $CdCl_2$ (1 mM) and ChTX (100 nM). The I/V analysis for peak current (FIG **6.9E**) revealed no significant blockade of current at any of the voltages tested despite the presence of 1 μM κ-ACTX-Hv1c (p > 0.05, paired Student's t-test, n = 4). In slight contrast to this a statistically significant blockade of late $I_{K(Ca)}$ was seen at voltages above +10 mV (p < 0.05, paired Student's t-test, n = 4). The voltage dependence of activation was unaltered for both peak and late $I_{K(Ca)}$ despite the presence of 1 μM κ-ACTX-Hv1c.

These results provide evidence that κ-ACTX-Hv1c is the first spider toxin that is an insect-selective blocker of K_{Ca} channels. This novel action lends weight to κ-

ACTX-Hv1c being an ideal lead compound for the development of novel bioinsecticides.
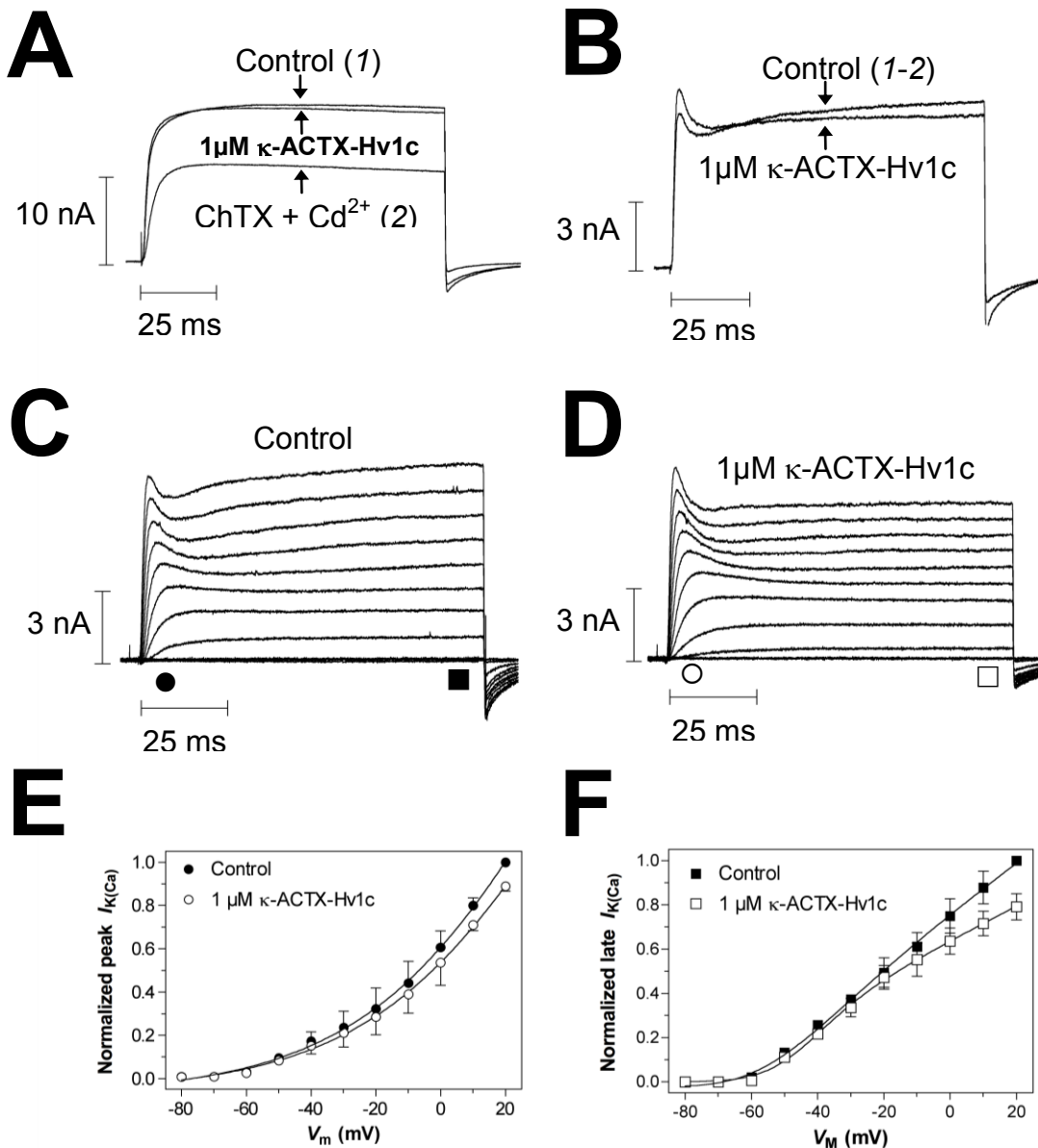
Fig 6.9: κ-ACTX-Hv1c failed to inhibit K_V channels in rat DRG neurons. (**A**) Superimposed typical current traces showing typical lack of effect of 1 μM κ-ACTX-Hv1c on I_K currents were obtained by a 100 ms step to +20 mV from a holding potential of –80 mV. In contrast the addition of ChTX (100 nM) and $CdCl_2$ (1 mM) inhibited total current by 69.5 ± 3.5%. By subtraction of the current remaining after addition of ChTX and $CdCl_2$ (2) from control (1), $I_{K(Ca)}$ can be isolated as seen in (**B**). Again no significant blockade of $I_{K(Ca)}$ is observed (p > 0.05, n = 5). (**C-D**) Families of currents

were obtained by 10 mV steps from a holding potential of −80 mV (n = 5). (**E**-**F**) The I/V relationships for both peak (circles) and late (squares) I_K are shown in both the presence (open symbols) and absence (closed symbols), of 1 μM κ-ACTX-Hv1c, respectively. This curve was plotted using equation **1**, section **5**.**6**. Data is expressed as mean ± SEM. As seen, currents were not inhibited by 1 μM κ-ACTX-Hv1c at each potential tested and there was no shift in the threshold of activation (n = 5).

6.1.9 Effect of κ-ACTX-Hv1c on *pSlo* currents expressed in HEK293 cells

Confirmation of the specific molecular target of κ-ACTX-Hv1c was shown by the inhibition of *pSlo* currents expressed in HEK293 cells. As discussed in section **5**.**4**, the construct containing the encoding region for the α-subunit of the large-conductance $K_{(Ca)}$ ($BK_{(Ca)}$) channel isolated from the American cockroach *Periplaneta americana* (*pSlo*) was cloned into the expression vector pcDNA3.1. This plasmid, which also carries the G418 resistance gene, was stagnently expressed in HEK293 cells. Successful expression of the coding region for *pSlo* was determined by the ability to produce a large outward current upon depolarisation of the membrane using whole-cell patch clamping. The recording conditions including voltage-protocols are outlined in section **5**.**4**.

Stepping the voltage from a holding potential of −90 mV to +40 mV elicits a large outward current with a small peak component followed by a late current that persists until completion of the test pulse. Sensitivity of the current to partially reversible blockade by TEA-Cl (10 mM) and charybdotoxin (1 μM), was 84.1 ± 1.5%, and 80.1 ± 2.1 % respectively, thus confirming the current was $I_{K(Ca)}$ mediated (Fig **6**.**10A** & **B** n = 12). No significant shift in the voltage dependence of half maximal activation ($V_{1/2}$) was observed in the presence ($V_{1/2}$ = 22.6 ± 1), or absence ($V_{1/2}$ = 22.8± 2), of TEA (10 mM, p > 0.05, paired Student's tTest, n = 12). Likewise, ChTX (1 μM) failed to significantly alter $V_{1/2}$ in the presence ($V_{1/2}$ = 28.6 ± 1), or absence ($V_{1/2}$ = 27.8± 2), of ChTX (1 μM, p > 0.05, paired Student's tTest, n = 12, Fig **6**.**10C** & **D**). Strong, but incomplete blockade of *pSlo* channel

currents by TEA-Cl (10 mM) and ChTX (1 µM), was previously reported by Derst *et al*, 2003.

Addition of TEA-Cl (10 mM) at the conclusion of each experiment was undertaken as a positive control. In addition, experiments performed on un-transfected HEK293 cells produced no significant outward current when recorded under the same conditions (data not shown, $n = 3$).

This current does not show the large characteristic initial peak component seen when recording wild-type $I_{K(Ca)}$ (see section **6**.**1**.**7**). This is likely due to the lack of the auxiliary channel subunits. Addition of 300 nM κ-ACTX-Hv1c caused a significant inhibition of 58.7 ± 8.7 % with partial reversibility upon superfusion for up to 10 minutes with toxin-free external solution (Fig **6.11A** & **B**, $p < 0\ 05$ paired Student's *t*-test, $n = 5$). Analysis of the concentration-response relationship for doses between 1 nM and 3 µM revealed an IC_{50} value for inhibition of late current (measured at the end of the +40 mV test pulse) of 240.5 ± 1.08 nM (Fig **6.11E**, $n = 5$). This value represents an 83-fold increase in IC_{50} value for inhibition of wild-type $I_{K(Ca)}$, but is comparable to the 158 nM IC_{50} reported for ChTX on *pSlo* currents (Derst *et al* 2003). Families of *pSlo* channel currents were elicited by 10 mV steps from a holding current of –90 mV to a maximum of +80 mV, recorded in both the absence (Fig **6.11C**), and presence, of 300 nM κ-ACTX-Hv1c (Fig **6.11D**, $n = 5$). Analysis of the *I/V* relationship (Fig **6.11F**) revealed only a minor voltage-dependent blockade of late current that was partially reversible. In addition there is no significant shift in the voltage of half maximal activation ($V_{1/2}$ = 26.1 ± 1.3 mV and 24.7 ± 2.3 mV, in the presence of toxin, $p > 0.05$, paired Student's *t*Test, $n = 5$). By plotting the normalized late current remaining in the presence of 300 nM κ-ACTX-Hv1c versus time revealed a τ_{on} value of 133.2 ± 9.7 seconds. In addition, current amplitude was measured during a washout period with toxin-free solution, that revealed a τ_{off} value of 387 ± 24.6 seconds (Fig **6.11G**, $n = 5$). This current failed to return to control levels despite a wash out period of up to 10 minutes indicating partial reversibility of the toxin-channel interaction (data not shown).

These results confirm that κ-ACTX-Hv1c indeed inhibits insect $I_{K(Ca)}$ by the selective blockade of $BK_{(Ca)}$ channels. This is despite a 83-fold reduction in IC_{50} compared to the wild type possibly indicating that interaction of the toxin to the channel is aided by the presence of auxiliary β-subunits.
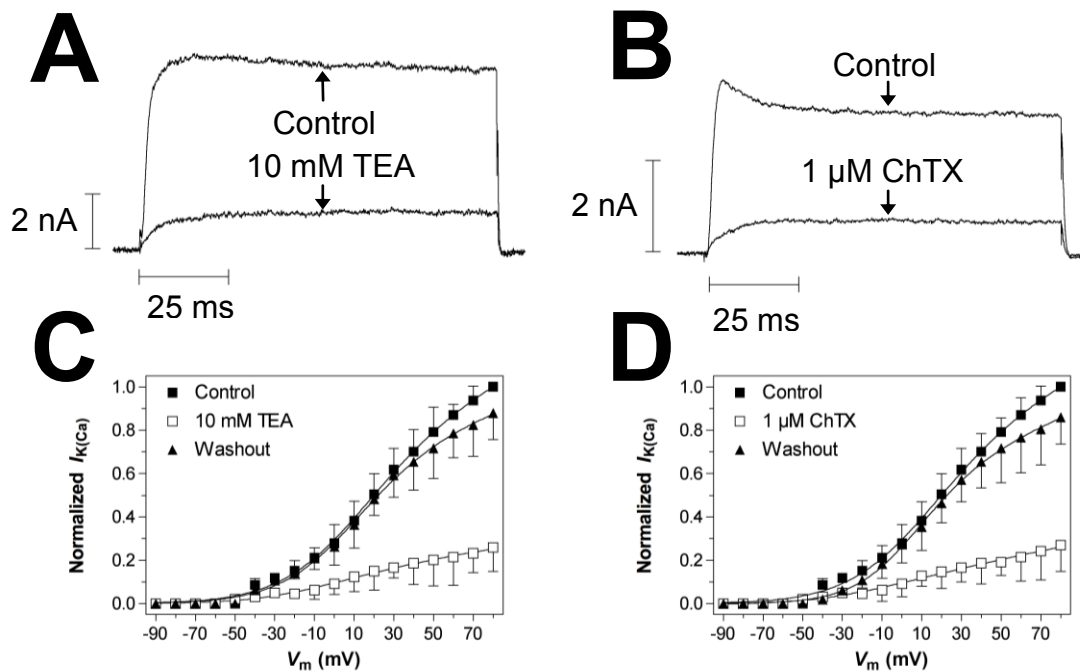
Fig 6.10: Inhibition of *pSlo* currents by TEA (10 mM) and ChTX (1 μM). (**A** & **B**) $I_{K(Ca)}$ were obtained by a 100 ms voltage step to +40 mV from a holding potential of –90 mV. Addition of 10 mM TEA inhibited $I_{K(Ca)}$ by 84.1 ± 1.5 % with partial reversibility (*n* = 12). Likewise addition of ChTX (1 μM) inhibited $I_{K(Ca)}$ by 80.1 ± 1.2 % with partial reversibility (*n* = 12). The *I*/*V* relationships for late I_K is shown in both the presence and absence of TEA (**C**,10 mM), or ChTX (**D**, 1 μM), respectively. As seen, currents are inhibited at each potential tested, there was also no significant shift in $V_{1/2}$ (*p* > 0.05, paired Student's *t*-test, *n* = 12).

A

Control

Washout

300 nM κ-ACTX-Hv1c

2 nA

25 ms

B

Control

10 nM κ-ACTX-Hv1c

1 μM κ-ACTX-Hv1c

1 nA

25 ms

C

Control

2 nA

25 ms

D

300 nM κ-ACTX-Hv1c

2 nA

25 ms

E

IC$_{50}$ = 240 nM

% Block $I_{K(Ca)}$

[κ-ACTX-Hv1c] (M)

F

Normalized late $I_{K(ca)}$

■ Control
□ 300 nM κ-ACTX-Hv1c
▲ Washout

V_m (mV)

G

Normalized late $I_{K(Ca)}$

τ_{on} = 133.2 sec

τ_{off} = 387 sec

Time (s)

H

Norm. Block (I_{toxin}/I_{cont})

○ 300 nM κ-ACTX-Hv1c

V_m (mV)
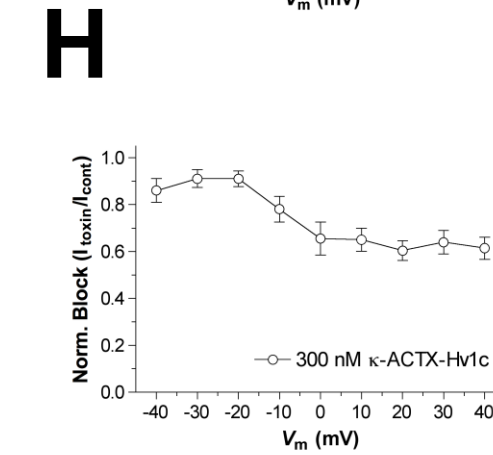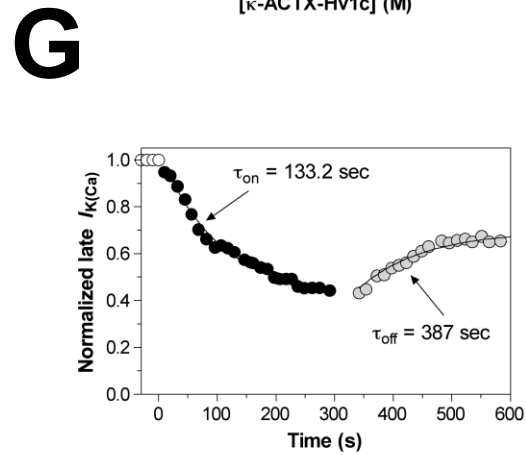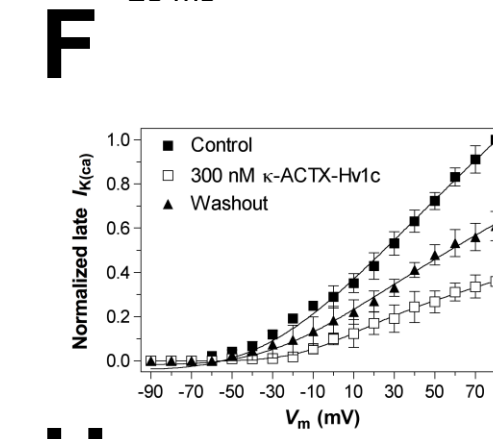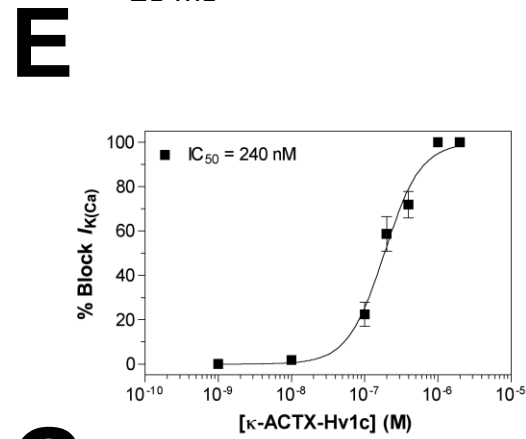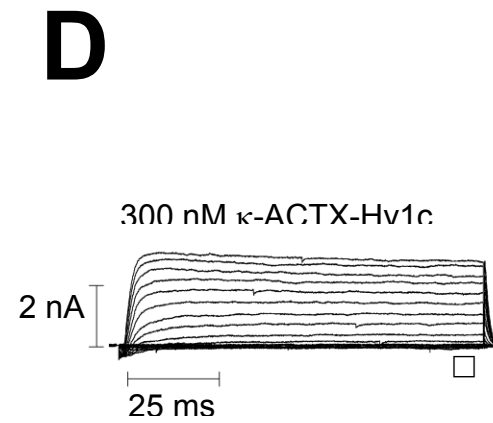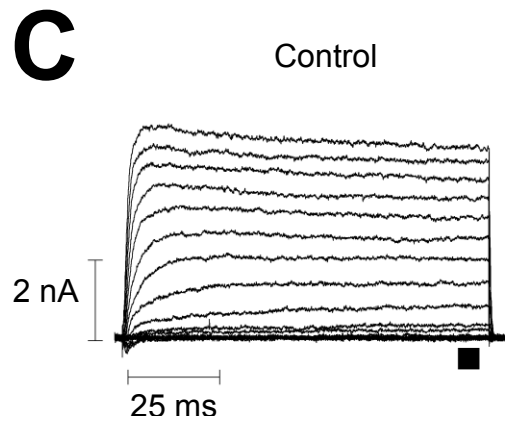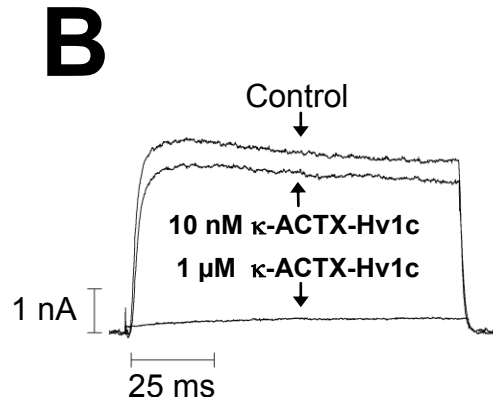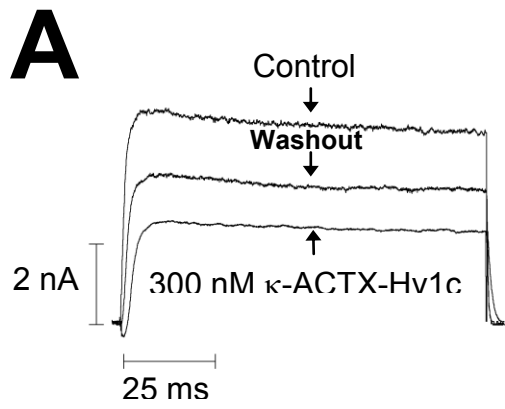
Fig 6.11: Inhibition of *pSlo* currents by κ-ACTX-Hv1c. (**A**) $I_{K(Ca)}$ were obtained by a 100 ms voltage step to +40 mV from a holding potential of –90 mV. Addition of 300 nM κ-ACTX-Hv1c inhibited $I_{K(Ca)}$ by 58.7 ± 8.7 % with partial reversibility. (**B**) Increasing concentrations of κ-ACTX-Hv1c further inhibited $I_{K(Ca)}$ with complete inhibition of current at concentrations above 1 μM. (**C-D**) Families of currents were obtained by 10 mV steps from a holding potential of –80 mV (*n* = 5). (**E**) Concentration-dependent block of *pSlo* currents by κ-ACTX-Hv1c reached a maximum at concentrations above 1 μM. (**F**) The *I/V* relationships for late I_K is shown in both the presence (□) ,and absence (■) of 300 nM κ-ACTX-Hv1c respectively. As seen, currents are inhibited by 300 nM κ-ACTX-Hv1c at each potential tested there was also no shift in $V_{1/2}$ (*n* = 5). (**G**) A plot of the time-course for inhibition of $I_{K(Ca)}$ by 300 nM κ-ACTX-Hv1c revealed values for τ_{on} and τ_{off} as 133 ± 10 and 387 ± 25 seconds respectively (*n* = 5). (**H**) Voltage-dependence of fractional block by 300 nM κ-ACTX-Hv1c (●) as compared to control. Similar to ChTX the fractional block of $I_{K(Ca)}$ by κ-ACTX-Hv1c reduces as voltage increases. Refer to section **5.6** for the equations for dose-response and *I/V* analysis. All data are expressed as mean ± SEM.

6.1.10 Effect of κ-ACTX-Hv1c on *dSlo* currents expressed in HEK293 cells

The large-conductance K_{Ca} (BK_{Ca}) channel, α-subunit (*dSlo*) was isolated from the fruit fly *Drosophila melanogaster* by Adelman *et al* 1992. *dSlo* currents were obtained by transfecting HEK293 cells with the construct containing the *dSlo* coding region cloned into the expression vector pcDNA3.1, which also carries the G418 resistance gene, as detailed in section **5**.**4**.**1**. Stepping the voltage from a holding potential of –90 mV to +40 mV elicits an outward sustained current that closely resembles that of *pSlo* currents. Unlike the block of *pSlo* currents, at concentrations up to 1 μM, ChTX fails to inhibit *dSlo* currents (data not shown, *n* = 5). In contrast *dSlo* currents could be reversibly inhibited (74.2 ± 3.4 %), by addition of TEA-Cl (10 mM), (Fig **6.12A**, *n* = 12). Addition of 3 μM κ-ACTX-Hv1c produced a minor, yet significant blockade of the current (17.9 ± 1.6 %) without reversibility (Fig **6.12A**, *p* < 0.05 paired Student's *t*-test, *n* = 5). This blockade was further increased at a concentration of 10 μM (26.7 ± 1.5 %), (Fig **6.12B**, *p* < 0.05 paired Student's *t*-test, *n* = 5). Due to a limited supply of κ-ACTX-Hv1c it

was not possible to use concentrations above 10 µM. Therefore the IC_{50} value could not be determined, however it would be > 10 µM. Families of currents were elicited by stepping the voltage in 10 mV steps from a holding voltage of –90 mV to +40 mV, recorded in both the absence (Fig **6**.**12C**), and presence (Fig **6**.**12D**), of 3 µM κ-ACTX-Hv1c. Analysis of the *I*/*V* relationship (Fig **6.12E**) revealed a voltage-independent blockade of late current without reversibility, in addition there is no significant shift in the voltage-dependence of activation (*p* > 0.05, paired Student's-*t*-test, *n* = 5).

Like ChTX the lack of activity against *dSlo* (as compared to *pSlo*) is mirrored by κ-ACTX-Hv1c. This indicates that only subtle variations in the structure of Slo channels can produce significant changes in phyla-selectivity (see discussion).
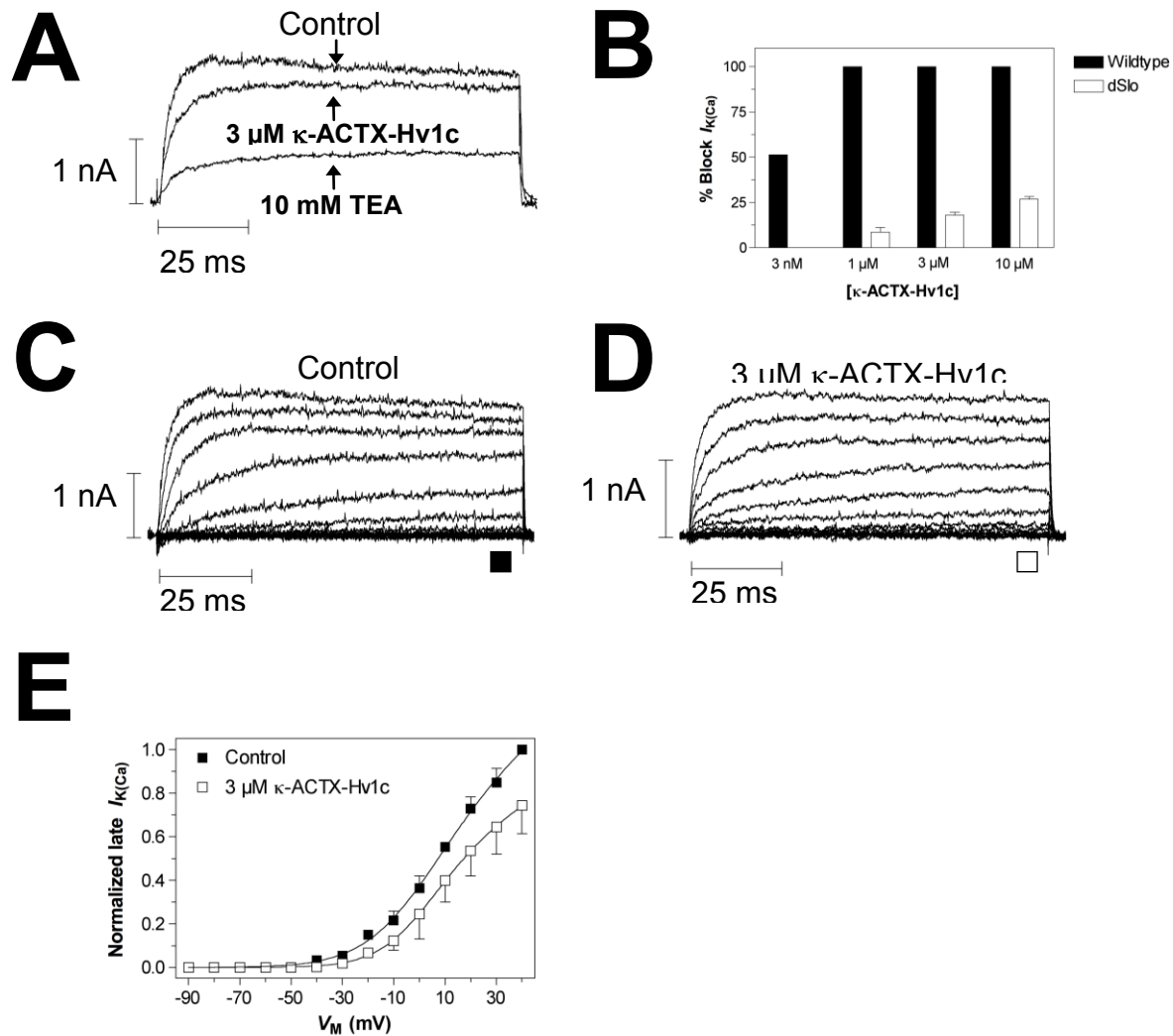
Fig 6.12: κ-ACTX-Hv1c fails to significantly inhibit *dSlo* channels. (**A**) $I_{K(Ca)}$ were obtained by a 100 ms voltage step to +40 mV from a holding potential of –90 mV. Addition of 3 μM κ-ACTX-Hv1c inhibited $I_{K(Ca)}$ without reversibility, in contrast total $I_{K(Ca)}$ could be reversibly inhibited by 10 mM TEA (74.2 ± 3.4 %) ($p < 0.05$, $n = 5$). (**B**) In comparison to inhibition of *pSlo* channel currents, complete block of *dSlo* channel current by κ-ACTX-Hv1c was not achieved at concentrations up to 10 μM. (**C**-**D**) Families of currents were obtained by 10 mV steps from a holding potential of –90 mV ($n = 5$). (**E**) The *I/V* relationships for late I_K is shown in both the presence (◇), and absence (■), of 3 μM κ-ACTX-Hv1c respectively. This curve was plotted using equation **2** in section **5**.**6**. Data is expressed as mean $\pm$ SEM. As seen, currents are inhibited by 3 μM κ-ACTX-Hv1c at each potential tested ($n = 5$).

6.1.11 Effect of κ-ACTX-Hv1c on *mSlo* currents expressed in HEK293 cells

Similar to the recording of *pSlo* and *dSlo* currents, *mSlo* currents were obtained by expression of the α-subunit of the calcium-activated potassium channel (BK_{Ca} channel) from mice in HEK293 cells. Currents were produced by stepping the membrane potential from a holding level of –90 mV to +40 mV for 100 ms. Similar to *pSlo* and *dSlo* a large outward, maintained current occurs that is reversibly inhibited by addition of 10 mM TEA-Cl (87.6 ± 2.6%, Fig **6**.**13A**, *n* = 10). Addition of 3 μM κ-ACTX-Hv1c produced a significant, yet minor inhibition of current (39.4 ± 4.8 %) that partially reversed after 10 minute perfusion with toxin-free solution (Fig **6**.**13A**, p < 0.05, paired Student's *t*-test, *n* =5). The inhibition of *mSlo* currents was dose-dependent and reached 44.6 ± 4.6 % block at a concentration of 10 μM (Fig **6**.**13B**, *n* = 5). The recording conditions and voltage protocols used were the same as those used for *pSlo* and *dSlo* and are outlined in section **5**.**4**.

Due to a limited supply of κ-ACTX-Hv1c it was not possible to use concentrations above 10 μM. The IC_{50} value could not be determined but was estimated to be by slight extrapolation of the concentration-response curve to be ~ 9.8 μM. In contrast, κ-ACTX-Hv1c blocked insect *pSlo* channels at nanomolar concentrations, showing a 41-fold selectivity for this channel over *mSlo*, supporting the phyla-specific toxicity of this toxin.

Families of currents were elicited by stepping the voltage in 10 mV steps from a holding potential of –90 mV to +40 mV, recorded in both the absence (Fig **6**.**13C**), and presence (Fig **6**.**13D**), of 3 μM κ-ACTX-Hv1c. Analysis of the *I*/*V* relationship (Fig **6.13E**) revealed a voltage-independent blockade of late current with partial reversibility, in addition there is no significant shift in the voltage-dependence of activation (*p* > 0.05, paired Student's *t*-test, *n* = 5).
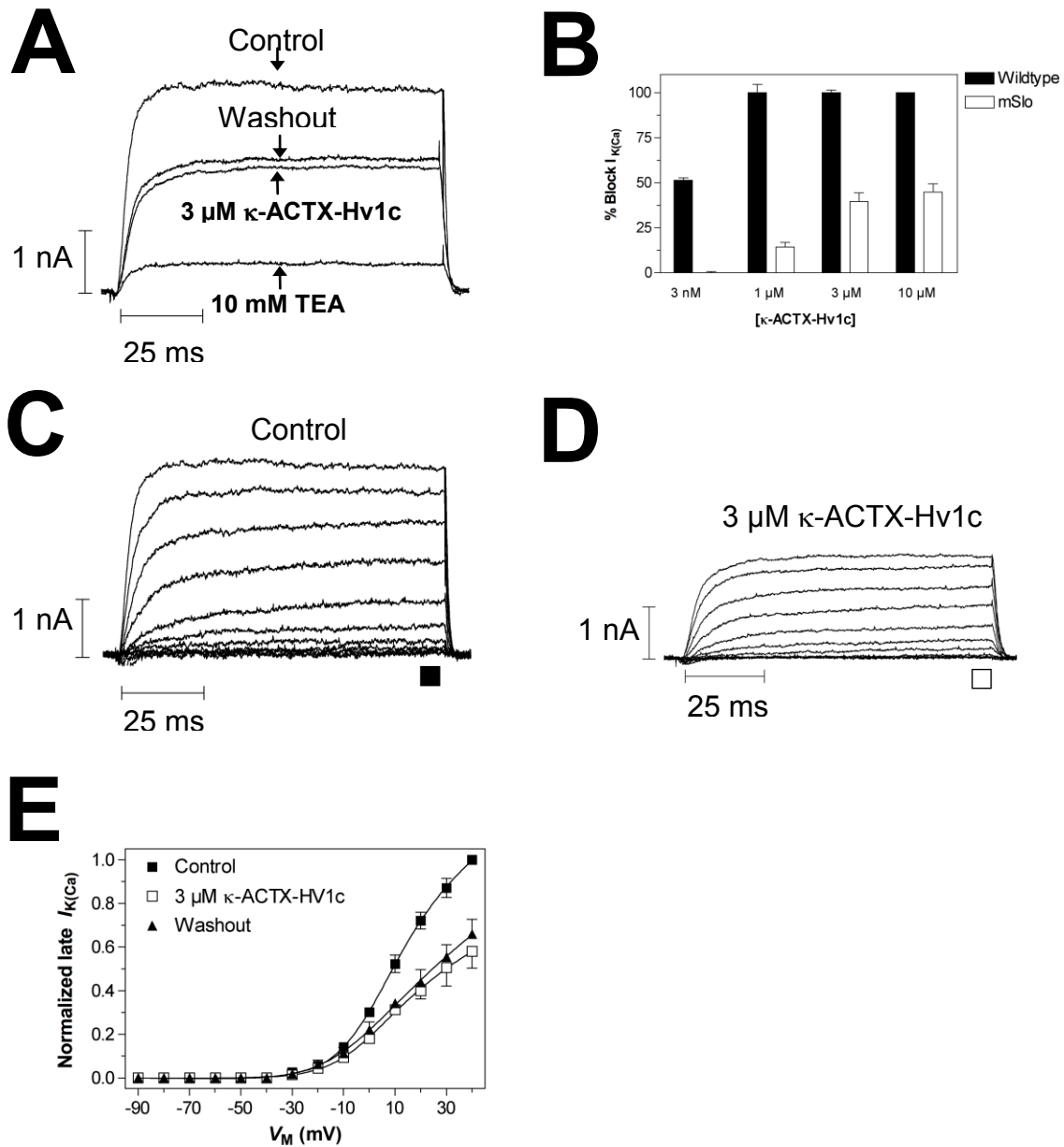
Fig 6.13: κ-ACTX-Hv1c significantly inhibits *mSlo* channels. (**A**) *mSlo* channel currnts were obtained by a 100 ms voltage step to +40 mV from a holding potential of –90 mV. Addition of 3 µM κ-ACTX-Hv1c inhibited *mSlo* channel currents with minimal reversibility, in addition currents could be inhibited by 10 mM TEA (87.6 ± 2.6 %, *n* = 10). (**B**) By comparison to inhibition of $I_{K(Ca)}$ in

DUM neurons (wild-type), complete block of *mSlo* channel currents by κ-ACTX-Hv1c was not achieved at concentrations up to 10 μM. (**C**-**D**) Families of currents were obtained by 10 mV steps from a holding potential of –90 mV (*n* = 5). (**E**) The *I/V* relationships for late *mSlo* channel currents is shown in both the presence (☐), and absence (■), of 3 μM κ-ACTX-Hv1c respectively. This curve was fitted using equation **1** in section **5**.**6**. Data is expressed as mean ± SEM. As seen, currents are inhibited by 3 μM κ-ACTX-Hv1c at each potential tested, in addition no shift in the voltage-dependence of activation was seen (*n* = 5).

6.2: Effect of alanine-scanning mutants of κ-ACTX-Hv1c on DUM neuron K_{Ca} channels

6.2.1 Preface

Mapping of the key functional residues of κ-ACTX-Hv1c using site-directed mutagenesis produced the first complete map of the bioactive surface of the toxin and revealed that the entire κ-ACTX-Hv1c pharmacophore is restricted to 7 residues that form a bipartite patch on one surface of the toxin (Maggio and King, 2002b). However, the primary pharmacophore or hot spot is restricted to just 5 residues (Arg^8, Tyr^{31}, Pro^9 and the Cys^{13}-Cys^{14} vicinal disulfide), as alanine mutants of these toxins (except Cys^{13}-Cys^{14}) were non-functional. The remaining 2 residues (Ile^2 and Val^{29}) are less critical for toxin activity and are thought to represent 'gasket' residues that prevent bulk solvent entering the binding site. This study was undertaken by assessing the activity of the toxins when injected into houseflies (*Musca domestica*) thus allowing the quantitative determination of toxicity as compared to the wild-type toxin.

However the primary pharmacophore was obtained by testing a series of alanine mutants in lethality assays in house flies. Thus there exists the possibility that any reduction in activity by mutation of the pharmacophore is due to a reduction in bioavailability of the toxin in the insect (ie reduced absorption or increased biotransformation). Accordingly we wished to initially confirm that pharmacokinetic issues did not contribute to a loss of activity for alanine mutants

of Arg[8], Tyr[31], Pro[9] or Val[29].   Ile[2] was not investigated further as it is not conserved in all κ-ACTX-1 family members (refer to section **4.1**). Furthermore, the two cysteine residues that form the vicinal disulfide were excluded from the scanning mutagenesis because it was previously shown that the vicinal disulfide is critical for toxin function (Wang *et al*, 2000) with a 425-fold reduction in house fly lethality (Maggio and King, 2002a) and hence mutation of either residue is certain to be highly deleterious.

Recording of $I_{K(Ca)}$ was performed by using whole-cell patch clamping of DUM neurons from the American cockroach *Periplaneta americana*. All mutants used in this investigation were assumed to be correctly folded by comparing far UV CD spectra of the wild type and mutant recombinant toxins. However a small loss of intensity in the positive CD band over the region 224-238 nm in the Y31A and P9A mutants was observed. However it was concluded that the small spectral changes are due to loss of the Tyr[31] side-chain chromophore in the Y31A and an increase in the solvent accessibility of the nearby Tyr[31] residue with P9A (Maggio and King, 2002b).

The activity of the mutant toxins was examined using DUM neurons, rather than *pSlo*-expressing HEK293 cells, for two reasons. First, it is possible that an as yet unknown subunit modulates the pharmacology of BK_{Ca} blockers on insect *Slo* channels [17], evident from the higher potency of ChTx on native neurons [14]. Second, the lower potency of the wild-type toxin on *pSlo* channels would necessitate testing of relatively high concentrations of the mutants to determine their IC_{50} values

6.2.2 R8A mutant

Substitution of an alanine for Arg[8] (R8A) produced a mutant toxin that in effect substitutes the large positively charged (polar) side-chain of arginine, for the small non-polar side-chain of alanine. Therefore if the length, polarity or positive charge of the amino acid side-chain in position 8 is critical for activity and or

binding to the target, then the R8A mutant should be relatively non-functional. Indeed when $I_{K(Ca)}$ was recorded under the conditions described in section **6.1.7**. R8A fails to inhibit $I_{K(ca)}$ at doses upto 3 µM (Fig **6**.**14A**). Analysis of the concentration-response relationship (Fig **6.24**) revealed IC_{50} values of 3.77 ± 0.02 µM and 3.39 ± 0.05 µM for peak and late $I_{K(Ca),}$ respectively (*n* = 5). This represents a 1614-fold reduction in activity for late current as compared to the wild-type toxin (Fig **6.25**). In comparison the LD_{50} in houseflies of R8A was 98-fold lower then the wild-type toxin, as determined by the insect toxicity bioassay (Fig **6.25**, Maggio and King 2002b). *I*/*V* analysis shows that blockade of $I_{K(Ca)}$ was not due to voltage-dependent shifts in activation shift in the voltage-dependence of activation (*p* > 0.05, paired Student's *t*-test, *n* = 5, Fig **6**.**14B**).

This result confirms the importance of the Arg^8 side-chain for blockade and or binding to the channel.

6.2.3 Y31A mutant

The substitution of alanine for Tyr^{31} (Y31A) produced a mutant toxin that removed the polar and weakly acidic hydroxyl-linked benzene ring of tyrosine. Therefore if the size, polarity or chemical reactivity (due to the attached hydroxyl group) of the amino-acid side-chain at position 31 is critical for activity and/or binding to the target, then the Y31A mutant should be relatively non-functional. Indeed when $I_{K(Ca)}$ was recorded under the conditions described in section **6.1.7**. Y31A failed to inhibit $I_{K(Ca)}$ at doses below 1 µM. Indeed complete inhibition of $I_{K(Ca)}$ was not achieved at concentrations of Y31A upto 3 µM (Fig **6**.**14C** & **D**). Due to the limited supply of the mutant toxin, higher concentrations could not be tested. Analysis of the concentration-response relationship (Fig **6.24**) revealed estimated IC_{50} values of 24.8 ± 0.05 µM and 45.1 ± 0.12 µM for peak and late $I_{K(Ca)}$ respectively. This represents a >10 000-fold reduction in activity for late current as compared to the wild-type toxin (Fig **6.25**). In comparison the LD_{50} of Y31A was 162-fold lower then the wild-type toxin, as determined by the insect toxicity bioassay (Fig **6.25**, Maggio and King 2002b). *I*/*V* analysis shows that

blockade of $I_{K(Ca)}$ was not due to a voltage-dependent shift in the voltage-dependence of activation ($p > 0.05$, paired Student's t-test, $n = 5$, data not shown).

As expected these results confirm the importance of the Tyr[31] side-chain for blockade and or binding to the channel. Possibly the reactive hydroxyl group is implicated in the hydrogen bonding of the toxin to the target, alternatively the benzene ring may act to directly occlude the channel. To further probe the interaction of the Tyr[31] side-chain with the target other alternative substitutions were to be used.
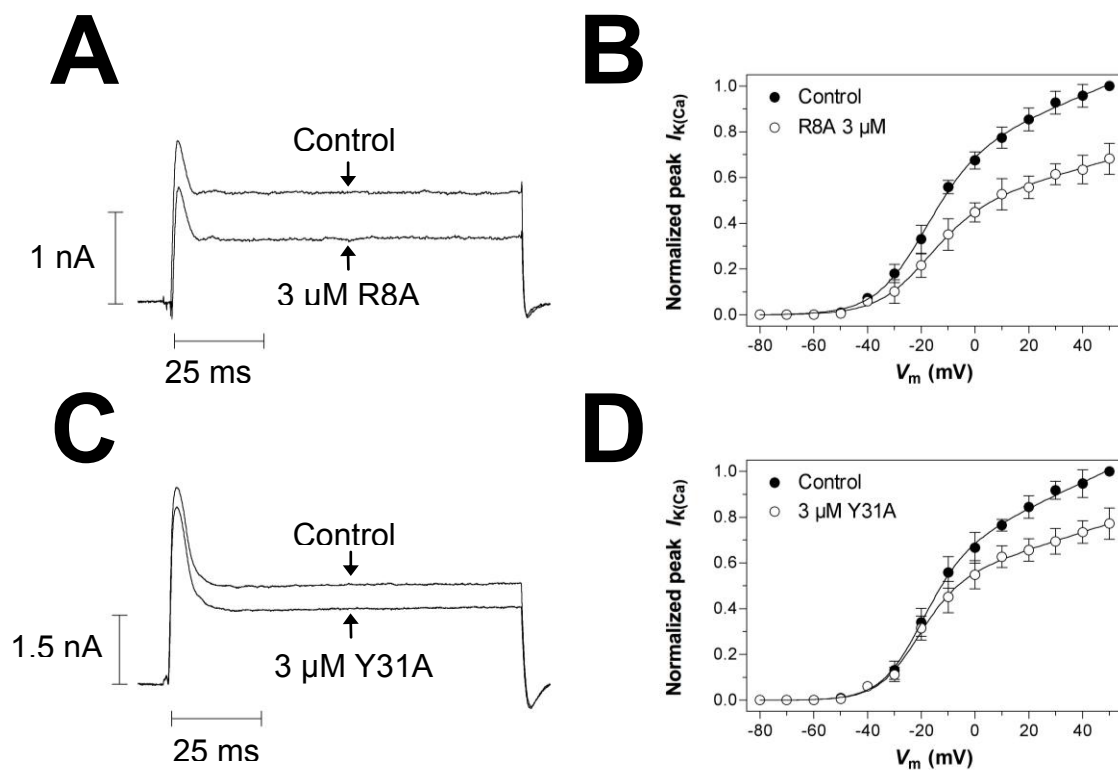
Fig 6.14: The mutant κ-ACTX-Hv1c constructs R8A & Y31A block K_{Ca} channels in cockroach DUM neurons. (**A**) Addition of 3 μM R8A inhibited both peak and late $I_{K(Ca)}$ with no significant reversibility (p > 0.05, $n = 3$). (**B**) As shown by the peak I/V graph, 3 μM R8A inhibited these currents at all potentials tested with no washout observed, in contrast to wild-type toxin. (**C**) Addition of 3 μM Y31A inhibited both peak and late $I_{K(Ca)}$ with no significant reversibility (p > 0.05, $n = 3$).

Currents were induced by stepping the potential to +40 mV from a holding potential of −80 mV. (**D**) As shown by the peak I/V graph, 3 μM Y31A inhibited these currents at all potentials tested with no washout observed, in contrast to wild-type toxin. The concentration-response curves for

R8A and Y31A are shown in figure **6**.**24**. Refer to section **5**.**6** for the equations for concentration-response and *I*/*V* analysis. Data is expressed as mean ± SEM.

6.2.4 P9A mutant

Substitution of alanine for Pro[9] (P9A) produced a mutant toxin that maintained the side-chain at position 9 as being small and non-polar. However the alanine side-chain is smaller and hydrophobic unlike proline, which is larger and hydrophilic because its side-chain is bonded to the backbone nitrogen as well as to the α-carbon.

Therefore if the size and possibly the chemical reactivity of the amino acid side-chain in position 9 is critical for activity and or binding to the target, then the P9A mutant should be less functional with an increased IC_{50} as compared to the wild-type toxin. Indeed when $I_{K(ca)}$ is recorded under the conditions described in chapter **5**, table **5**.**1**, 300 nM P9A irreversibly inhibits both peak and late $I_{K(ca)}$ by 55 ± 6.3 % and 54.3 ± 6.6 %, respectively (Fig **6**.**15A**, *n* =5). Analysis of the dose-response relationship (Fig **6**.**15B**) revealed IC_{50} values of 233 ± 0.03 nM and 287.1 ± 1.42 nM for peak and late $I_{K(Ca)}$, respectively (*n* = 5). This represents a ~ 100-fold reduction in activity for late current as compared to the wild-type toxin (Fig **6**.**25**). In comparison, the LD_{50} of P9A was 269-fold lower then the wild-type toxin, as determined by the insect toxicity bioassay (Fig **6**.**25**, Maggio and King 2002b).

Families of currents were elicited by stepping the voltage in 10 mV steps from a holding voltage of –80 mV to +50 mV, recorded in both the absence (Fig **6**.**15C**) and presence (Fig **6**.**15D**) of 300 nM P9A. Analysis of the *I*/*V* relationship for both peak (Fig **6**.**15E**) and late (Fig **6**.**15F**) $I_{K(Ca)}$ revealed a voltage-independent blockade of current without reversibility, in addition there is no significant shift in the voltage-dependence of activation ($p > 0.05$, paired Student's *t*-test, *n* = 5).

As expected these results confirm the importance of the Pro[9] side-chain for blockade and/or binding to the channel. Possibly the hydrophilic nature and/or

size of the proline side-chain enhances binding of the toxin to the target, by allowing the side-chain to move closer to the channel binding region.
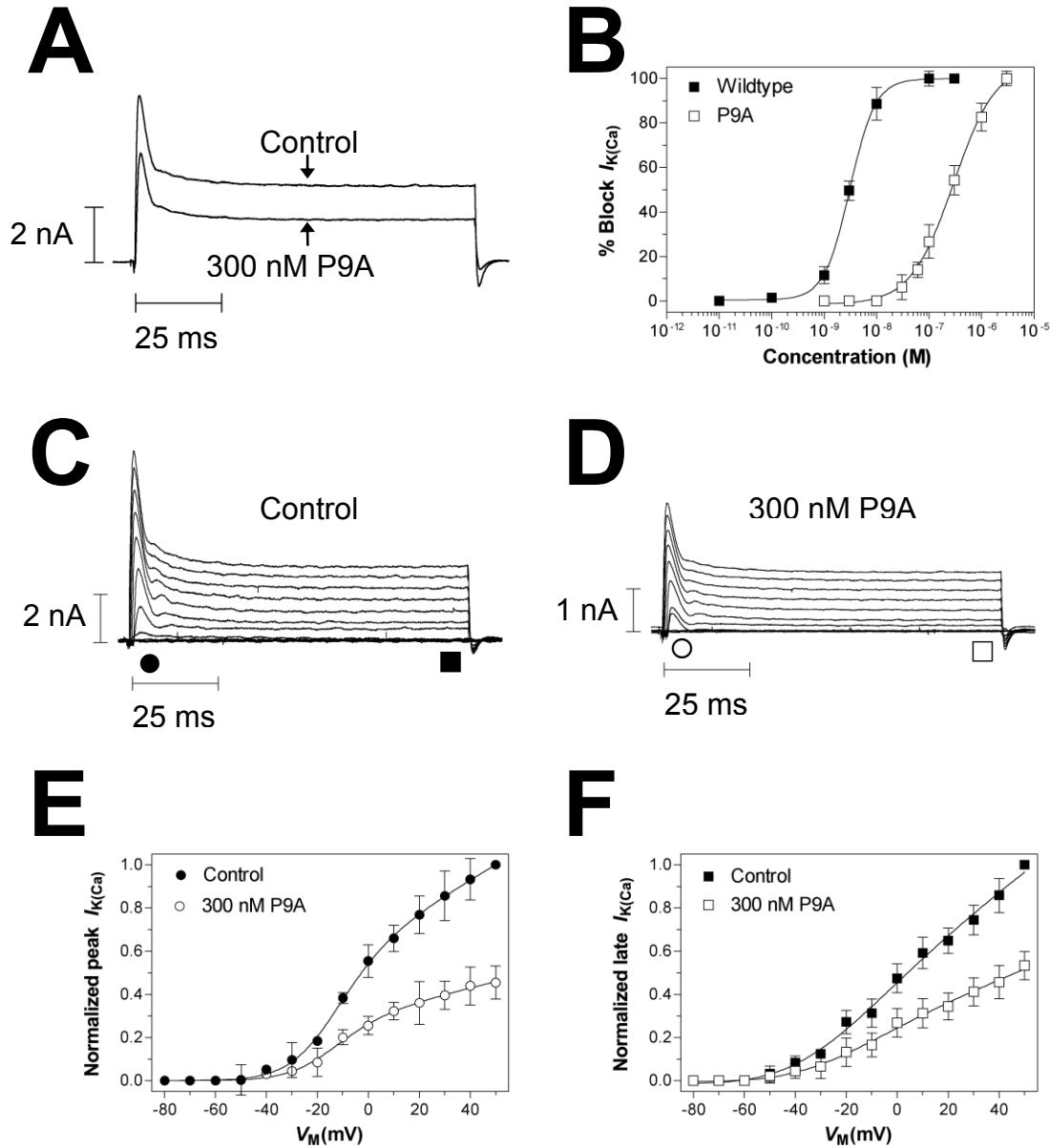
Fig 6.15: The mutant κ-ACTX-Hv1c construct P9A blocks K_{Ca} channels in cockroach DUM neurons. (**A**) Addition of 300 nM P9A inhibited both peak and late $I_{K(Ca)}$ with no significant reversibility ($p > 0.05$, $n = 4$). Currents were induced by stepping the potential to +40 mV from a holding potential of –80 mV. (**B**) The dose-response curve for inhibition of both late wild-type (κ-ACTX-Hv1c) (■), and late P9A (□), $I_{K(Ca)}$ revealed IC_{50} values of 2.9 and 290 nM, respectively. Families of currents were elicited by 10 mV depolarisation steps from –80 to +40 mV, in both the

absence (**C**), and presence (**D**), of 300 nM P9A (n = 4). As shown by the peak (**E**) and late (**F**) I/V graphs, 300 nM P9A inhibited these currents at all potentials tested with no washout observed, in contrast to wild-type toxin. Refer to section **5.6** for the equations for dose-response and I/V analysis. Data is expressed as mean $\pm$ SEM.

6.2.5 V29A

By substitution of alanine for Val[29] (V29A) produced a mutant toxin that preserves the non-polar, hydrophobic nature of the side-chain at position 29. The only difference being that valine has a larger un-reactive side chain compared to alanine and thus is thought to aide the interaction of the wild-type toxin to the target by excluding bulk-solvent from the binding site (Maggio and King, 2002). Activity of V29A was assessed on insect $I_{K(Ca)}$ as described above. 100 nM V29A irreversibly inhibited both peak and late $I_{K(ca)}$, by 95.6 $\pm$ 5.5 % and 94.5 $\pm$ 6.5 %, respectively (Fig **6.16A**, n =5). Analysis of the concentration-response relationship (Fig **6**.**16B**) revealed IC_{50} values of 17.3 $\pm$ 0.4 nM and 17.7 $\pm$ 2.3 nM for peak and late $I_{K(Ca)}$, respectively (n = 5 for all concentrations tested). This represents a 7.5-fold reduction in activity for block of the late $I_{K(Ca)}$ as compared to the wild-type toxin (Fig **6**.**25**). In comparison the LD_{50} of V29A was 13-fold lower than the wild-type toxin, as determined by the insect toxicity bioassay (Fig **6**.**25**, Maggio and King 2002b). Families of currents were elicited by stepping the voltage in 10 mV steps from a holding voltage of –80 mV to +50 mV, recorded in both the absence (Fig **6**.**16C**), and presence (Fig **6.16D**), of 100 nM V29A. Analysis of the I/V relationship for both peak (Fig **6.16E**) and late (Fig **6.16F**) $I_{K(Ca)}$ revealed a blockade of current without reversibility, in addition there is no significant shift in the voltage-dependence of activation (p <0.05, paired Student's t-test, n = 5).

These results show unsurprisingly that Val[29] plays a less critical role in the activity of the toxin.
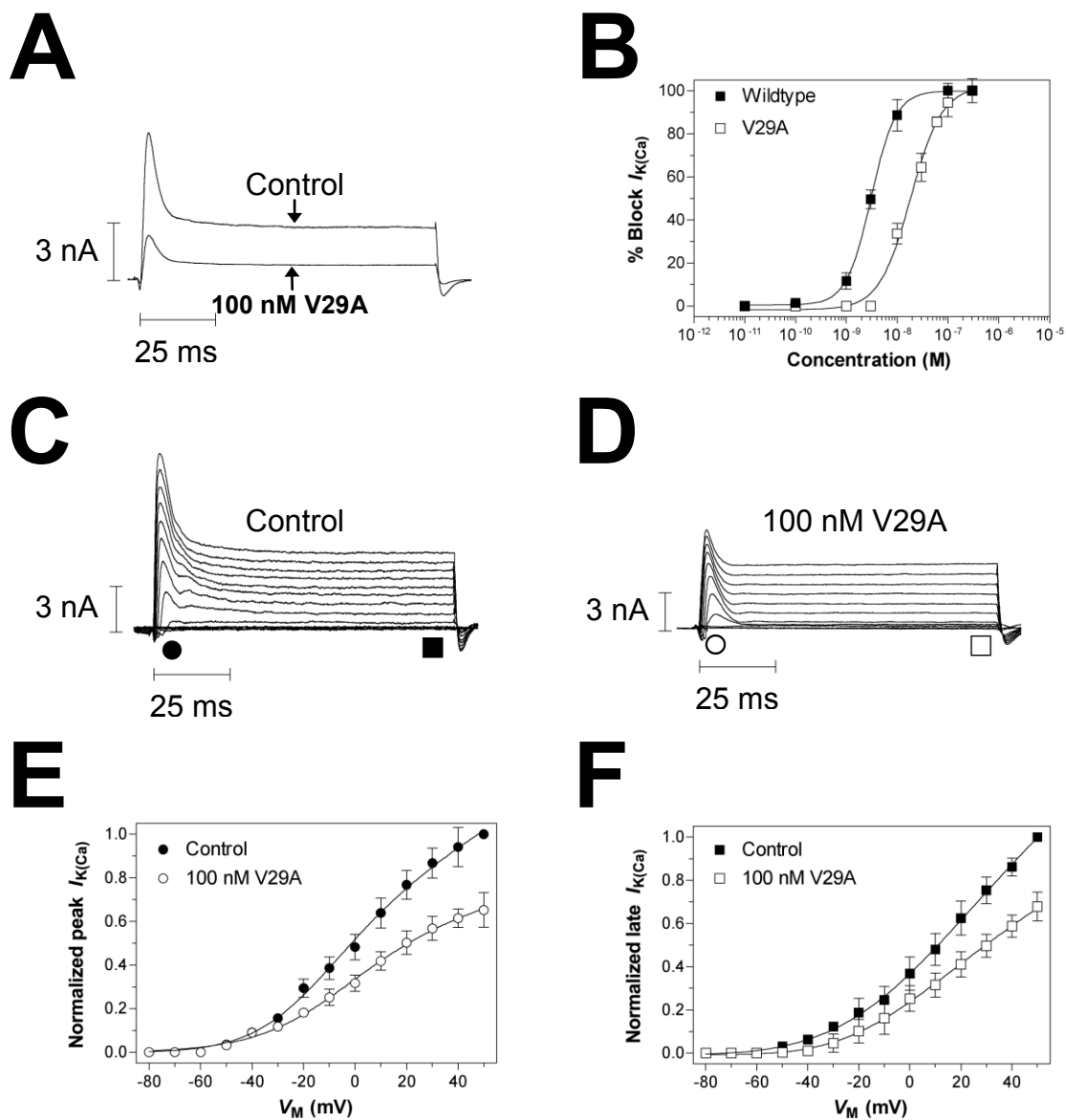
Fig 6.16: The mutant κ-ACTX-Hv1c construct V29A blocks K_{Ca} channels in cockroach DUM neurons. (**A**) Addition of 100nM V29A inhibited both peak and late $I_{K(Ca)}$ with no significant reversibility (p > 0.05, *n* = 4). Currents were induced by stepping the potential to +40 mV from a holding potential of –80 mV. (**B**) The dose-response curve for inhibition of both late wildtype (κ-ACTX-Hv1c) (■), and late V29A (□), $I_{K(Ca)}$ revealed IC_{50} values of 2.9 and 2.15 nM, respectively. Families of currents were elicited by 10 mV depolarisation steps from –80 to +40 mV, in both the absence (**C**) and presence (**D**) of 100 nM V29A (*n* = 4). As shown by the peak (**E**) and late (**F**) *I*/*V* graphs, 100 nM V29A inhibited these currents at all potentials tested with no significant difference in the voltage-dependence of activation. Refer to section **5.6** for the equations for dose-response and *I*/*V* analysis. Data is expressed as mean ± SEM.

6.3: Determining the chemical features of the toxin pharmacophore: functional role of Arg^8

6.3.1 Preface

To further probe the functional relevance of these residues and to investigate the role of individual chemical moieties in toxin activity a panel of additional mutants were constructed and their IC$_{50}$ values for inhibition of DUM neuron $I_{K(Ca)}$ was determined. Again all mutants were properly folded as judged from their CD spectrum as compared to the recombinant wild type toxin. Firstly the functional role of Arg^8 the only charged residue in the pharmacophore was investigated. This was done by construction of R8E, R8K, R8H and R8Q mutants. Within the insectophore of κ-ACTX-Hv1c, Arg^8 represents the only charged side-chain and therefore may substitute for the key Lys residue present in sea anemone, conotoxin, and scorpion toxins interacting with K$_{Ca}$ and K$_v$ channels (Goldstein and Miller, 1993; Terlau *et al*, 1999; Anderson *et al*, 1988; Duplais *et al*, 1997). Arg^8 could interact with the target channel in a number of ways: (i) via an electrostatic interaction with a negatively charged group on the channel, (ii) via a hydrophobic interaction between the alkyl chain and a corresponding hydrophobic group on the channel, (iii) hydrogen bonding via the bifurcated δ-guanidinium group, or (iv) some combination of these interactions. By using the mutants mentioned above, determination of the nature of the toxin-channel interaction could be closely investigated.

6.3.2 R8E mutant

If the interaction of the positively charged side-chain for the critically important Arg^8 to the target were by electrostatic force, substitution by the negatively

charged side-chain of glutamic acid would negate interaction with the target. Indeed at doses up to 3 µM, R8E inhibited peak and late $I_{K(Ca)}$ by 30.45 ± 6.7 % and 28.5 ± 5.7 % respectively (Fig **6.17A**, $n = 4$). The IC_{50} values for peak and late $I_{K(Ca)}$ were 5.23 ± 0.4 µM, and 5.54 ± 0.6 µM, respectively. This gives a 2237-fold reduction for blockade of $I_{K(Ca)}$ as compared to the wild-type toxin. In comparison the LD_{50} of R8E was 270-fold lower then the wild-type toxin, as determined by the insect toxicity bioassay (Fig **6.22**, Maggio and King 2002b). Also, R8E failed to alter the threshold of activation of $I_{K(Ca)}$ by analysis of the I/V relationship (Fig **6.17B**, $p > 0.05$, paired Student's t-test, $n = 4$).

6.3.3 R8Q

Similar to R8E, substitution of the critically important Arg^8 by glutamine (R8Q) was also considerably less active than wild-type toxin (Fig **6.17C**). This is not unexpected given the polar nature of the R8Q mutant. The calculated IC_{50} values for inhibition of both peak and late $I_{K(Ca)}$ were, 3.51 ± 0.45 µM and 4.1 ± 0.29 µM, respectively ($n = 4$). This represents a 1505-fold reduction in blockade of $I_{K(Ca)}$ as compared to the wild-type toxin (Fig **6.25**). Also, R8Q failed to alter the threshold of activation of $I_{K(Ca)}$ by analysis of the I/V relationship (Fig **6.17D**, $p > 0.05$, paired Student's t-test, $n = 4$). Due to similarly large detrimental effects on activity seen with both the R8E and R8A mutants this result confirms that the interaction of Arg^8 to the target is not simply by electrostatic interaction
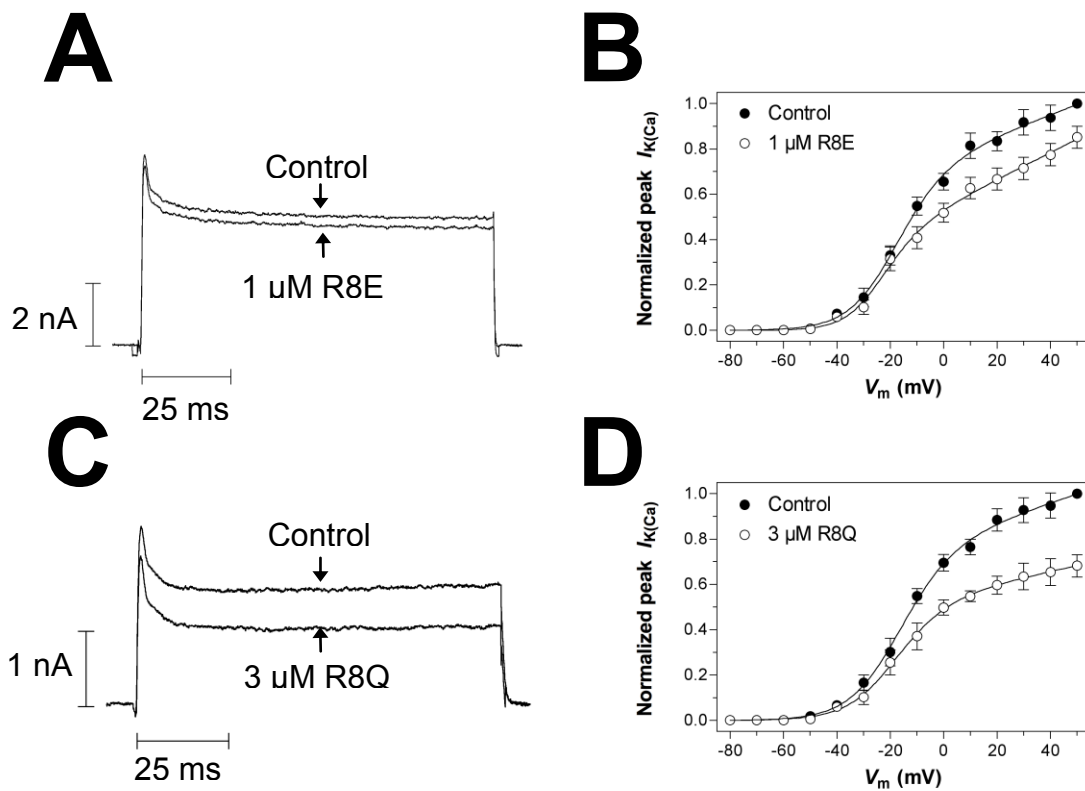
Fig 6.17: The mutant κ-ACTX-Hv1c constructs R8E & R8Q block K_{Ca} channels in cockroach DUM neurons. (**A**) Addition of 3 μM R8E inhibited both peak and late $I_{K(Ca)}$ with no significant reversibility (p > 0.05, *n* = 3). (**B**) As shown by the peak *I/V* graph, 3 μM R8E inhibited these currents at all potentials tested with no washout observed, in contrast to wild-type toxin. (**C**) Addition of 3 μM R8Q inhibited both peak and late $I_{K(Ca)}$ with no significant reversibility (p > 0.05, *n* = 3). Currents were induced by stepping the potential to +40 mV from a holding potential of –80 mV. (**D**) As shown by the peak *I/V* graph, 3 μM R8Q inhibited these currents at all potentials tested with no washout observed, in contrast to wild-type toxin. The concentration-response curves for R8E and R8Q are shown in figure **6.24**. Refer to section **5.6** for the equations for concentration-response and *I/V* analysis. Data is expressed as mean ± SEM.

6.3.4 R8K

Replacing the Arg[8] side-chain with a slightly shorter Lys (R8K) side chain maintains the positive charge. Indeed, addition of 300 nM R8K causes a non-reversible inhibition of $I_{K(Ca)}$ by 33.8 ± 4.2 % and 36.1 ± 4.3 % for peak and late

$I_{K(Ca)}$, respectively (Fig **6**.**18A**, n =5). Analysis of the dose-response relationship (Fig **6**.**18B**) revealed IC_{50} values of 528 ± 13 nM and 560 ± 15 nM for peak and late $I_{K(Ca)}$, respectively (n = 5 for all concentrations tested). This represents a 226-fold reduction in activity for late current as compared to the wild-type toxin (Fig **6**.**22**). In comparison the LD_{50} of R8K was 30.8-fold lower then the wild-type toxin, as determined by the insect toxicity bioassay (Fig **6**.**25**, Maggio and King 2002b). Families of currents were elicited by stepping the voltage in 10 mV steps from a holding voltage of –80 mV to +50 mV, recorded in both the absence (Fig **6**.**18C**) and presence (Fig **6**.**18D**) of 300 nM R8K. Analysis of the I/V relationship for both peak (Fig **6**.**18E**) and late (Fig **6**.**18F**) $I_{K(Ca)}$ revealed no significant shift in the voltage-dependence of activation (p > 0.05, paired Student's t-test, n = 5).

A

B

C

D

E

F

Fig 6.18: The mutant κ-ACTX-Hv1c construct R8K blocks K_{Ca} channels in cockroach DUM neurons. (**A**) Addition of 30 nM R8K inhibited both peak and late $I_{K(Ca)}$ ($p > 0.05$, $n = 4$). Currents were induced by stepping the potential to +40 mV from a holding potential of –80 mV. (**B**) The dose-response curve for inhibition of both late wildtype (κ-ACTX-Hv1c) (■), and late R8K (□), $I_{K(Ca)}$ revealed IC_{50} values of 2.9 and 655 nM respectively. Families of currents were elicited by 10 mV depolarisation steps from –80 to +40 mV, in both the absence (**C**), and presence (**D**), of 30 nM R8K ($n = 4$). As shown by the peak (**E**), and late (**F**), I/V graphs, 30 nM R8K inhibits these

currents at all potentials tested with no significant washout observed. Refer to section **5.6** for the equations for dose-response and *I*/*V* analysis. Data is expressed as mean ± SEM.

6.3.5 R8H mutant

To test the importance of the arginine δ-guanido group for target binding, the arginine was substituted with histidine (R8H) whose imidazole moiety is a close mimic. Addition of 30 nM R8H inhibited both peak and late $I_{K(Ca)}$ by 66.8 ± 4.8 % and 60.8 ± 7.8 %, respectively (Fig **6.19A**, *n* = 5). Analysis of the dose-response relationship (Fig **6.19B**) revealed IC_{50} values of 19 ± 3.4 nM and 21.6 ± 4.1 nM for peak and late $I_{K(Ca)}$, respectively (*n* = 5 for all concentrations tested). This represents a 8.2-fold reduction in activity for late current as compared to the wild-type toxin (Fig **6.25**). In comparison the LD_{50} of R8H was 4.5-fold lower then the wild-type toxin, as determined by the insect toxicity bioassay (Fig **6.25**, Maggio and King 2002b). Families of currents were elicited by stepping the voltage in 10 mV steps from a holding voltage of –80 mV to +50 mV, recorded in both the absence (Fig **6.19C**) and presence (Fig **6.19D**) of 30 nM R8H. Analysis of the *I*/*V* relationship for both peak (Fig **6.19E**), and late (Fig **6.19F,**) $I_{K(Ca)}$ revealed no significant shift in the voltage-dependence of activation (*p* > 0.05, paired Student's *t*-test, *n* = 5).
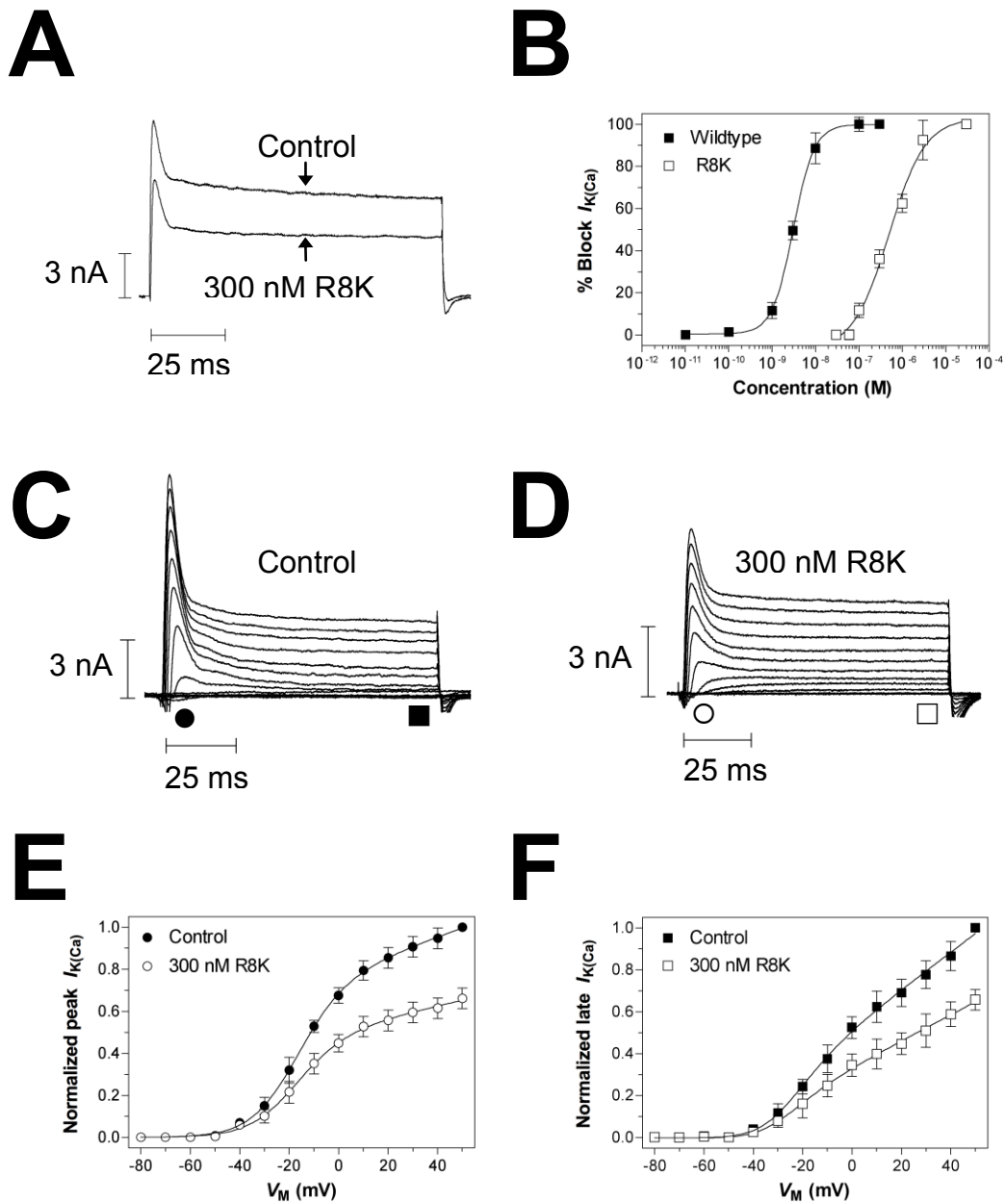
A

B

C

D

E

F
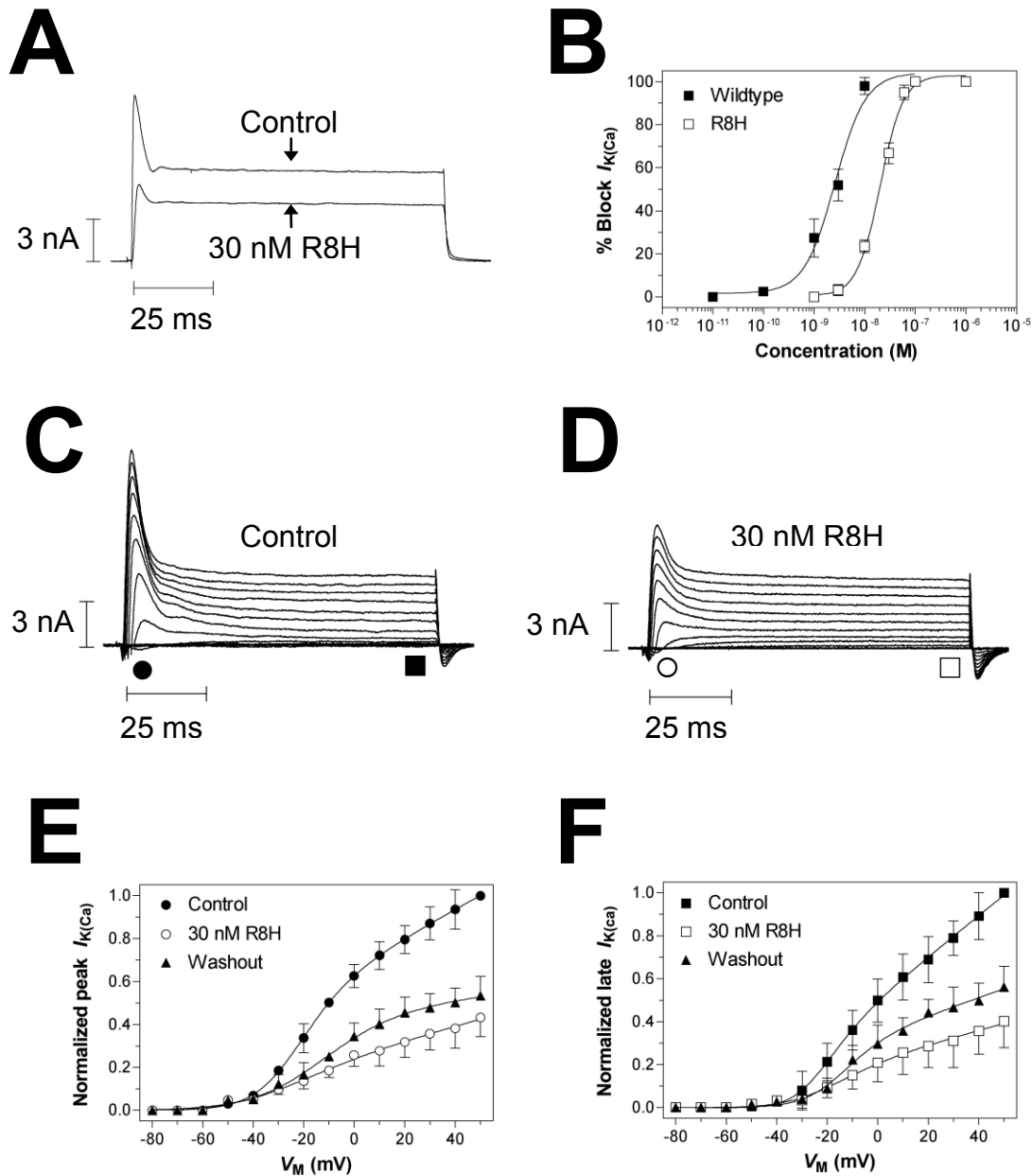
Fig 6.19: The mutant κ-ACTX-Hv1c construct R8H blocks K_{Ca} channels in cockroach DUM neurons. (**A**) Addition of 30 nM R8H inhibits both peak and late $I_{K(Ca)}$ with partial reversibility ($p < 0.05$, $n = 4$). Currents were induced by stepping the potential to +40 mV from a holding potential of −80 mV. (**B**) The concentration-response curve for inhibition of both late wild-type (κ-ACTX-Hv1c) (■) and late R8H (□) $I_{K(Ca)}$ revealed IC_{50} values of 2.9 and 23.8 nM respectively. Families of currents were elicited by 10 mV depolarisation steps from −80 to +40 mV, in both the absence (**C**), and presence (**D**), of 30 nM R8H ($n = 4$). As shown by the peak (**E**), and late (**F**), I/V graphs, 30 nM R8H inhibits these currents at all potentials tested with no significant shift in the voltage-

dependence of activation ($p > 0.05$ paired Student's t-test, $n = 4$). Refer to section **5.6** for the equations for dose-response and I/V analysis. Data is expressed as mean $\pm$ SEM.

6.4: Determining the chemical features of the toxin pharmacophore: functional role of Tyr[31]

6.4.1 Preface

The next step in elucidating the interaction of κ-ACTX-Hv1c with the insect $K_{(Ca)}$ channel was to probe the features of the critically important Tyr[31] residue. It has previously been shown that the hydroxyl group of Tyr[31] is expendable by replacing it with Phe (Maggio and King, 2002b). In order to probe the importance of the ring structure at this position we determined the IC_{50} for inhibition of $I_{K(Ca)}$ with mutants that replaced Tyr[31] with Val, Leu, Trp and Phe respectively.

6.4.2 Y31V mutant

Replacement of the aromatic ring of Tyr[31] with the smaller hydrophobic side-chain of valine saw a large >10 000-fold reduction in IC_{50} value for inhibition of $I_{K(Ca)}$ as compared to the wild-type toxin. This large decrease in activity was remarkable given only a 2.9-fold loss of lethality in the fly assay (Fig **6.25**). At doses up to 3 µM Y31V inhibited both peak and late $I_{K(Ca)}$ by 12.0 ± 4.5 % and 10.1 ± 5.5 %, respectively (Fig **6.20A**,$n = 4$). Doses above 3 µM were not tested given the limited amount of material available. Furthermore, analysis of the I/V relationship for both peak and late $I_{K(Ca)}$ revealed no significant shift in the voltage-dependence of activation (Fig **6.20B**, $p > 0.05$, paired Student's t-test, $n = 4$). Val[29] was previously suggested to be a gasket residue responsible for shielding the toxin-binding surface from bulk solvent (Maggio and King, 2002b). The κ-ACTX-Hv1c structure implies that proper spatial orientation of the side-

chains of Val[29] and Tyr[31] are influenced by intermolecular van der Waals interactions between these side-chains. Spatial repositioning of these side-chains may allow water molecules to permeate the binding surface and destabilize the toxin-target interaction.
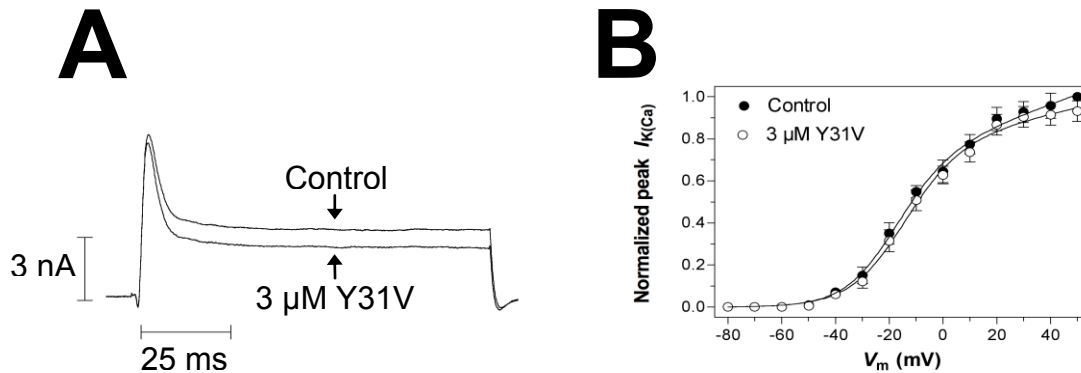
Fig 6.20: The mutant κ-ACTX-Hv1c construct Y31V blocks K_{Ca} channels in cockroach DUM neurons. (**A**) Addition of 3 μM Y31V inhibited both peak and late $I_{K(Ca)}$ with no significant reversibility ($p > 0.05$, $n = 4$). (**B**) As shown by the peak I/V graph, 3 μM Y31V inhibited these currents at all potentials tested with no washout observed, in contrast to wild-type toxin. Currents were induced by stepping the potential to +40 mV from a holding potential of –80 mV. The concentration-response curves for Y31V is shown in figure **6.24**. Refer to section **5.6** for the equations for concentration-response and I/V analysis. Data is expressed as mean ± SEM.

6.4.3 Y31L mutant

Addition of 300 nM Y31L inhibited both peak and late $I_{K(Ca)}$ by 59.6 ± 6.5 % and 55.65 ± 6.6 %, respectively (Fig **6.21A**, n = 4). Analysis of the dose-response relationship (Fig **6.21B**) revealed IC_{50} values of 237 ± 12 nM and 265 ± 14 nM for peak and late $I_{K(Ca)}$ respectively ($n = 5$ for all concentrations tested).

Similar to valine, substitution of Tyr[31] for leucine (Y31L) resulted in a large 101-fold reduction in IC_{50} value by inhibition of $I_{K(Ca)}$ as compared to the wild-type toxin. This compared favourably with a 22-fold reduction in LD_{50} value as determined by the insect bioassay (Fig **6.25**, Maggio and King 2002b). Families of currents were elicited by stepping the voltage in 10 mV steps from a holding voltage of –80 mV to +50 mV, recorded in both the absence (Fig **6.21C**), and

presence (Fig **6.21D**), of 300 nM Y31L. Analysis of the I/V relationship for both peak (Fig **6.21E**), and late (Fig **6.21F**), $I_{K(Ca)}$ revealed no significant shift in the voltage-dependence of activation ($p > 0.05$, paired Student's t-test, $n = 5$). Given, the reduced size of the side-chains of Leu and Val it is apparent that these substitutions compromise local interactions and form a leak in the gasket that probably allows water to access the binding site.

Fig 6.21: The mutant construct Y31L blocks K_{Ca} channels in cockroach DUM neurons. (**A**) Addition of 300 nM Y31L inhibited both peak and late $I_{K(Ca)}$ with no significant reversibility ($p > 0.05$, $n = 4$). Currents were induced by stepping the potential to +40 mV from a holding potential of −80 mV. (**B**) The concentration-response curve for inhibition of both late wild-type (κ-ACTX-Hv1c) (■) and late Y31L (□) $I_{K(Ca)}$ revealed IC_{50} values of 2.9 and 265 nM respectively. Families of currents were elicited by 10 mV depolarisation steps from −80 to +40 mV, in both the absence

(**C**), and presence (**D**), of 300 nM Y31L (n = 4). As shown by the peak (**E**) and late (**F**) I/V graphs, 300 nM Y31L inhibits these currents at all potentials tested with no significant washout observed. Refer to section **5**.**6** for the equations for dose-response and I/V analysis. Data is expressed as mean $\pm$ SEM.

6.4.4 Y31F mutant

As previously shown in housefly lethality tests the hydroxyl group of the critical Tyr[31] is expendable by replacing it with phenylalanine (Maggio and King, 2002b). This was confirmed, as addition of 10 nM Y31F inhibited both peak and late $I_{K(Ca)}$ by 74.5 $\pm$ 7.5 % and 70.44 $\pm$ 8.6 %, respectively (Fig **6.22A**, n = 4). Analysis of the dose-response relationship (Fig **6.22B**) revealed IC_{50} values of 6.2 $\pm$ 1.4 nM and 6.7 $\pm$ 2.1 nM for peak and late $I_{K(Ca)}$ respectively (n = 5 for all concentrations tested)

This represents a mere 2.6-fold reduction in IC_{50} value by inhibition of late $I_{K(Ca)}$ as compared to the wild-type toxin and was very similar to the 1.8-fold reduction in LD_{50} value as determined by the insect bioassay (Fig **6.25**, Maggio and King 2002b). Families of currents were elicited by stepping the voltage in 10 mV steps from a holding voltage of –80 mV to +50 mV, recorded in both the absence (Fig **6.21C**), and presence (Fig **6.21D**), of 10 nM Y31F. Analysis of the I/V relationship for both peak (Fig **6.21E**), and late (Fig **6.21F**), $I_{K(Ca)}$ revealed a voltage-independent blockade of current with minor yet significant reversibility (p < 0.05, paired Student's t-test, n = 5). In addition there is no significant shift in the voltage-dependence of activation (p > 0.05, paired Student's t-test, n = 5).
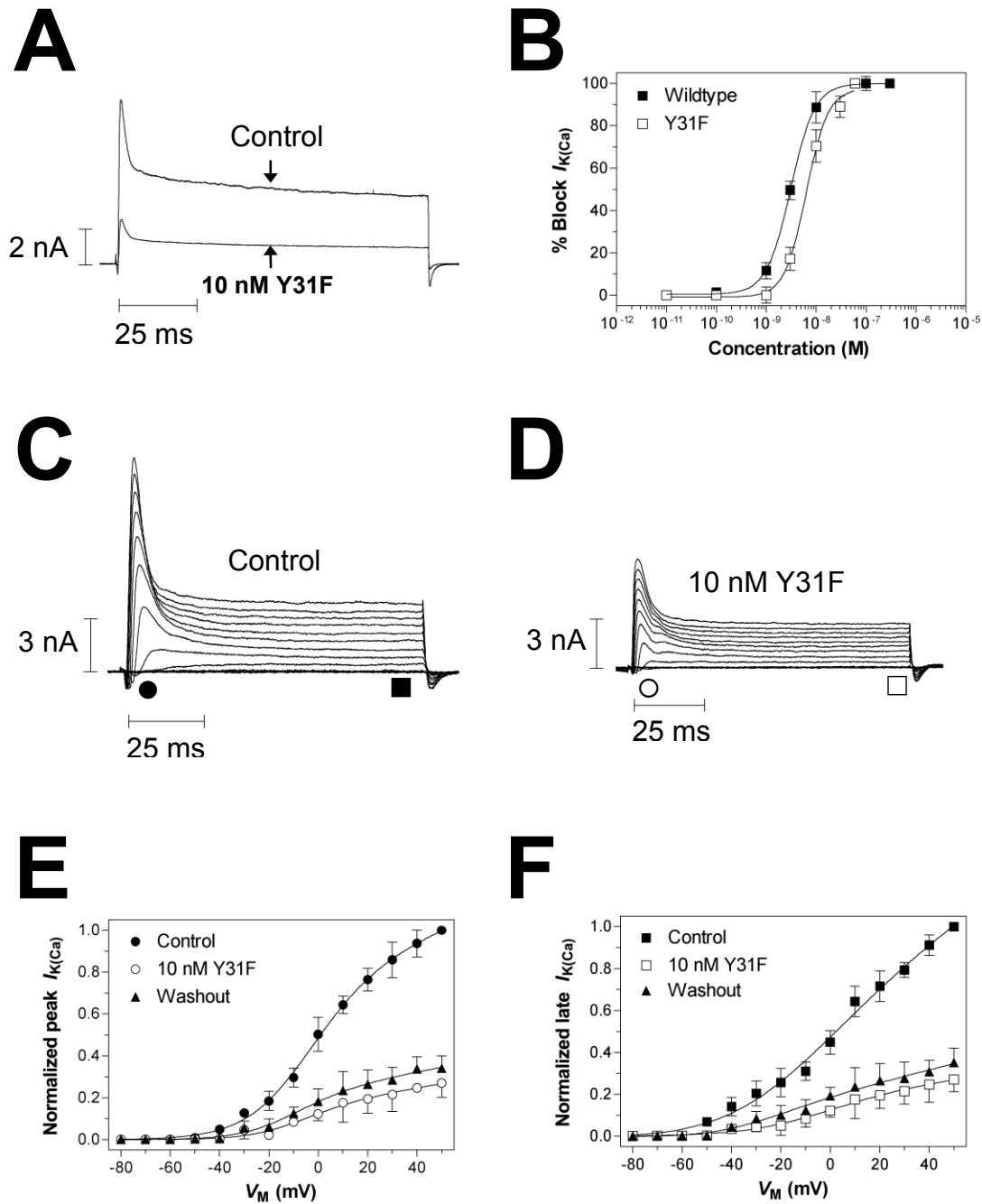
Fig 6.22: The mutant κ-ACTX-Hv1c construct Y31F blocks K_{Ca} channels in cockroach DUM neurons. (A) Addition of 10 nM Y31F inhibits both peak and late $I_{K(Ca)}$ with no significant reversibility ($p > 0.05$, $n = 4$). Currents were induced by stepping the potential to +40 mV from a holding potential of –80 mV. (B) The dose-response curve for inhibition of both late wildtype (κ-ACTX-Hv1c) (■) and late Y31F (□) $I_{K(Ca)}$ revealed IC_{50} values of 2.9 and 6.7 nM respectively. Families of currents were elicited by 10 mV depolarisation steps from –80 to +40 mV, in both the

absence (**C**) and presence (**D**) of 10 nM Y31F (*n* = 4). As shown by the peak (**E**) and late (**F**) *I*/*V* graphs, 10 nM Y31F inhibits these currents at all potentials tested with partial washout observed. Refer to section **5**.6 for the equations for dose-response and *I*/*V* analysis. Data is expressed as mean ± SEM.

6.4.5 Y31W

If the hydrophobic ring structure of the Tyr^{31} side-chain is the critical moiety for interaction with the target, then we would expect that substitution with tryptophan would display a comparable wild-type activity. As previously mentioned substitution with the progressively less bulky hydrophobes Val, Leu, (and Ala) resulted in a decrease in the potency of K_{Ca} channel block. In contrast substitution with phenylalanine that differs only by the absence of a hydroxyl group, mirrored the activity of the wild-type toxin. This confirmed that the hydroxyl group is not essential for interaction with the target. Addition of 30 nM Y31W inhibited both peak and late $I_{K(Ca)}$ by 29.1 ± 2.4 % and 26.8 ± 8.9 %, respectively (Fig **6.23A**, *n* = 4). Analysis of the dose-response relationship (Fig **6.23B**) revealed IC_{50} values of 42 ± 4 nM and 41 ± 5 nM for peak and late $I_{K(Ca)}$ respectively (*n* = 5 for all concentrations tested). This represents a mere 18.1-fold reduction in IC_{50} value by inhibition of late $I_{K(Ca)}$ as compared to the wild-type toxin and was very similar to the 4.7-fold reduction in LD_{50} value as determined by the insect bioassay (Fig **6.25**, Maggio and King 2002b). Families of currents were elicited by stepping the voltage in 10 mV steps from a holding voltage of –80 mV to +50 mV, recorded in both the absence (Fig **6.23C**), and presence (Fig **6.23D**), of 30 nM Y31W. Analysis of the *I*/*V* relationship for both peak (Fig **6.23E**), and late (Fig **6.23F**), $I_{K(Ca)}$ revealed a voltage-independent blockade of current with minor yet significant reversibility, in addition there is no significant shift in the voltage-dependence of activation (*p* > 0.05, paired Student's *t*-test, *n* = 5).
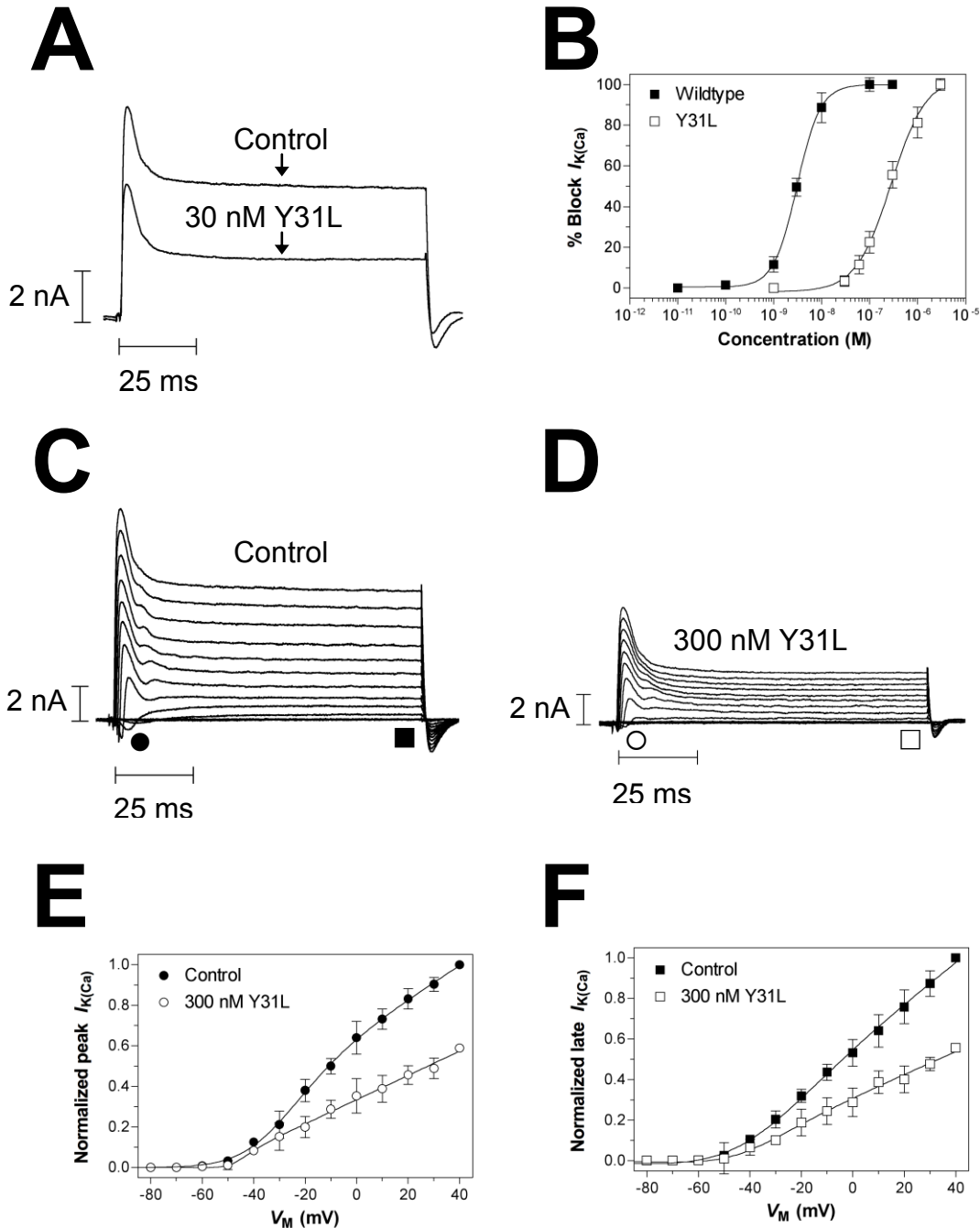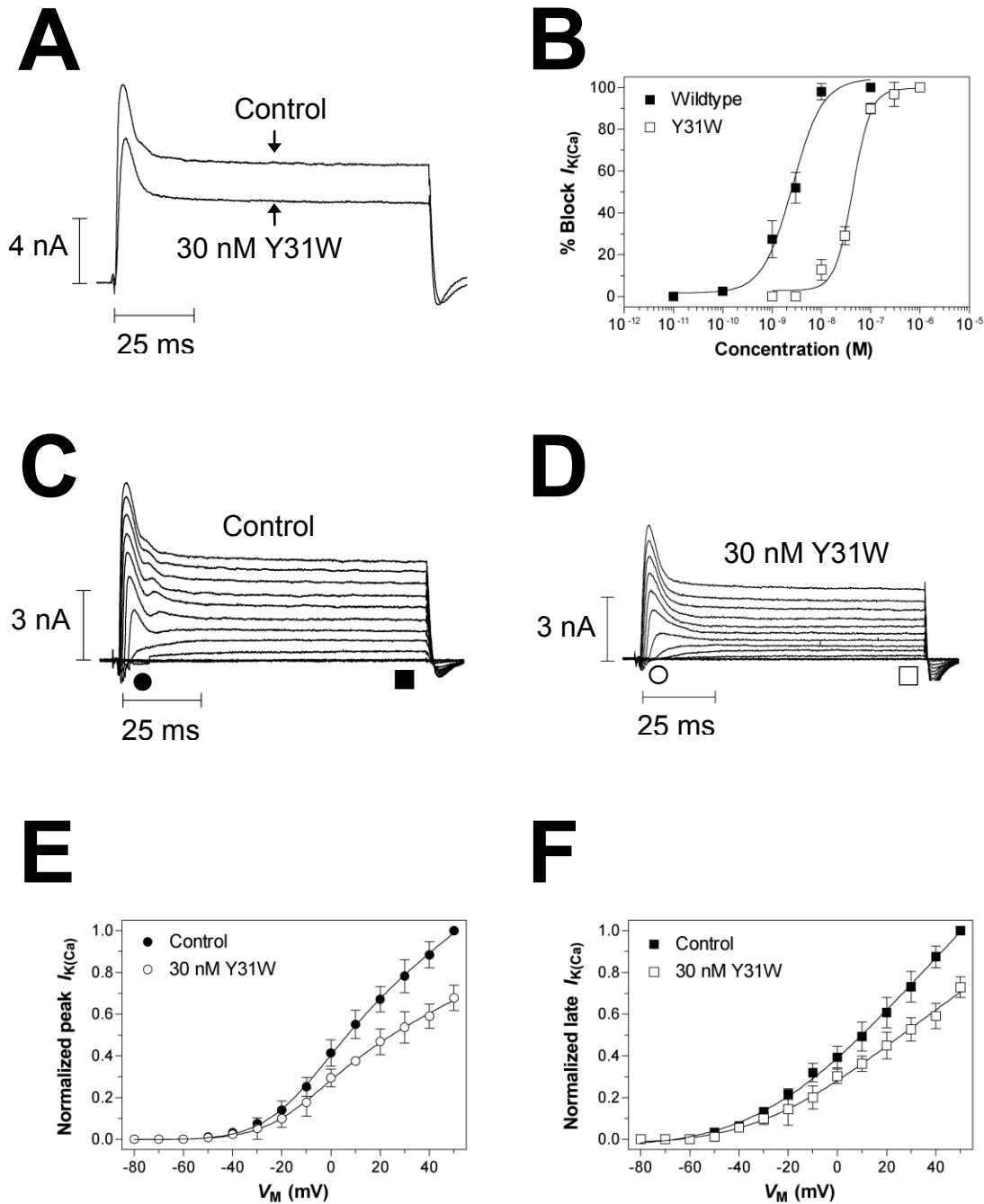
Fig 6.23: The mutant construct Y31W blocks K_{Ca} channels in cockroach DUM neurons. (**A**) Addition of 30 nM Y31W inhibits both peak and late $I_{K(Ca)}$ with no significant reversibility ($p > 0.05$, paired Student's t-test, $n = 4$). Currents were induced by stepping the potential to +40 mV from a holding potential of –80 mV. (**B**) The dose-response curve for inhibition of both late wild-type (κ-ACTX-Hv1c) (■) and late Y31W ☐) $I_{K(Ca)}$ revealed IC_{50} values of 2.9 and 40.7 nM respectively. Families of currents were elicited by 10 mV depolarisation steps from –80 to +40 mV, in both the

absence (**C**), and presence (**D**), of 30 nM Y31W (n = 4). As shown by the peak (**E**), and late (**F**), *I*/*V* graphs, 30 nM Y31W inhibits these currents at all potentials tested with no significant washout observed. Refer to section **5**.**6** for the equations for dose-response and *I*/*V* analysis. Data is expressed as mean $\pm$ SEM.
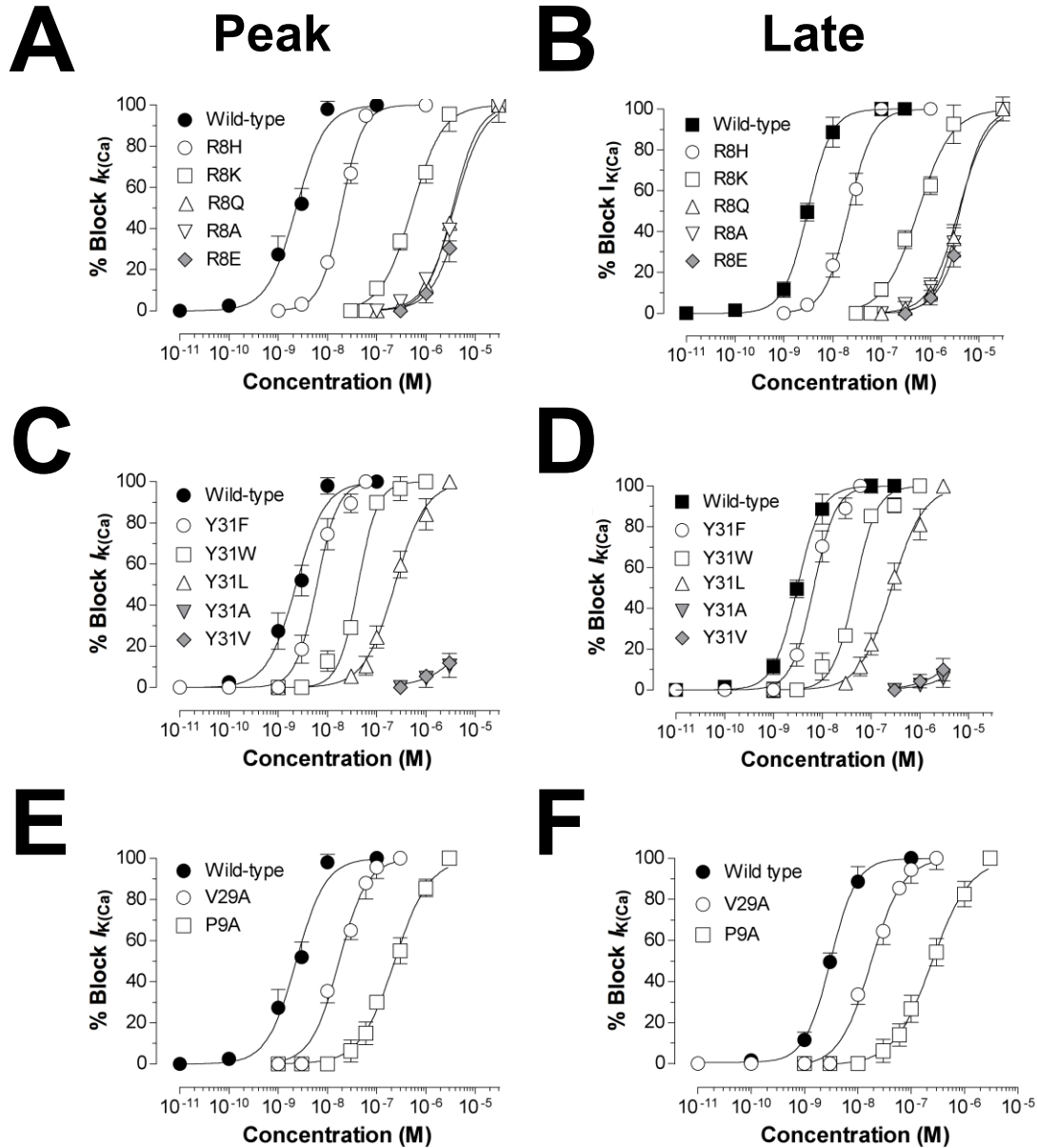
Fig 6.**24**: Concentration-response curves for recombinant κ-ACTX-Hv1c mutants on cockroach DUM neuron $I_{K(Ca)}$. Concentration-response curves for inhibition of peak (**A**), and late (**B**), $I_{K(Ca)}$ by R8H, R8H, R8Q, R8A and R8E. (**B**) Concentration-response curves for inhibition of peak (**C**), and late (**D**), $I_{K(Ca)}$ by Y31F, Y31W, Y31L, Y31A and Y31V. Dose-response curves for inhibition of peak (**E**) and late (**F**) $I_{K(Ca)}$ by V29A and P9A.
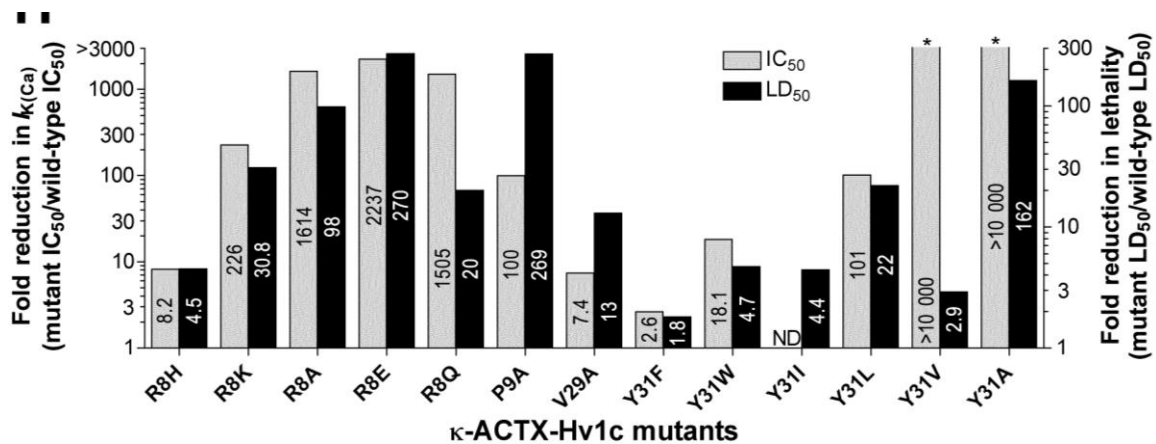
Fig 6.25: Comparison of fold-reductions in DUM neuron $I_{K(Ca)}$ IC$_{50}$ (left-hand *y*-axis, light bars) and house fly LD$_{50}$ (right-hand *y*-axis, dark bars). For comparison, data for the fold-reductions in house fly LD$_{50}$ for R8A, R8E, P9A, Y31F and Y31A are included (Maggio & King, 2002b). *Mutants Y31V and Y31A have IC$_{50}$ values estimated to be ≥ 10 µM.

It would be apparent that cockroach DUM neuron BK$_{Ca}$ channels are distinct from BK$_{Ca}$ channels found in *Musca domestica.* Therefore it would not be surprising that a difference in the affinity of κ-ACTX-Hv1c for cockroach DUM neuron BK$_{Ca}$ and *M. domestica* BK$_{Ca}$ channels exists. This is shown by the marked differences in the lethality assay and electrophysiological assay discussed as part of this project. Furthermore it is difficult to reconcile the two very different assays as they differ in terms of bioavailability, the likelihood of *in vivo* degradation, and possible pH variance at the binding site. These two assays are shown together to determine if a correlation between the assays exists, and as is apparent that is not the case.

-

CHAPTER 7

RESULTS

7.1: DETERMINATION OF THE TARGET SITE FOR THE 'HYBRID' TOXIN FW178

7.1.1 Preface

The prototypic 'hybrid' family member FW178 has been shown to be the most potent insecticidal atracotoxin yet discovered (G.F. King and B. Sollod, personal communication). However, elucidation of the 3D structure of FW178 provides little insight into the target of the toxin. Mapping of the pharmacophore of FW178 using alanine-scanning mutagenesis has been performed and revealed 4 critical residues (Gln^8, Pro^9, Asn^{28} and Val^{34}) and 2 less critical residues (Thr^{33} and Tyr^{36}). Remarkably, the pharmacophores of κ-ACTX-Hv1c, ω-ACTX-Hv1a, and FW178 can be overlaid with a high degree of superposition of key functional residues, despite the variations in tertiary structure folding. Therefore, does FW178 share the same target as κ-ACTX-Hv1c (insect K_{Ca} channels) or ω-ACTX-Hv1a (insect Ca_V channels) or both? The aim of this section of the project was to identify the site and mode of action of FW178 in order to solve this quandary.

-

7.1.2 Vertebrate Toxicity of the 'hybrid' toxin FW178

To determine if the 'hybrid' toxin FW178 was insect-selective it was tested in an *in vitro* mammalian nerve-muscle preparation. The toxin was applied to the chick biventer cervicis nerve-muscle preparation, as described in section **5**.**5**. Following a period of steady indirectly-stimulated the preparation was challenged with the cholinergic agonists ACh (1 mM), CCh (20 µM) and KCl (40 mM) (Fig **7**.**1A**).
1 µM FW178 was then added to the bath solution and indirectly stimulated twitch contractions were followed over a 1 hr timecourse The addition of the toxin failed to alter resting tension in the muscle, twitch tension, nor induce muscle fasciculations (Fig **7**.**1B**, *n* = 3). Furthermore no significant change was observed in the measured responses to the cholinergic agonists following incubation with FW178 (Fig **7**.**1C** & **D**, *n* = 3, $p > 0.05$, Wilcoxon signed-rank test).

A

ACh (1 μM)   CCh (20 μM)   KCl (40 mM)

1 g

2 min

B

↑
1 μM FW178

C

ACh (1 μM)   CCh (20 μM)   KCl (40 mM)

D

% Control Amplitude

ACh   CCh   KCl

-
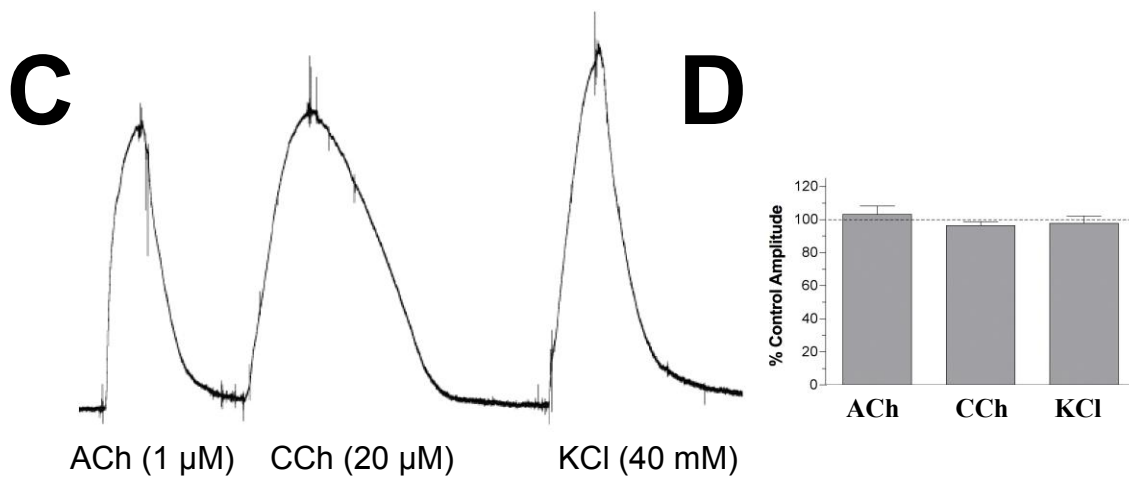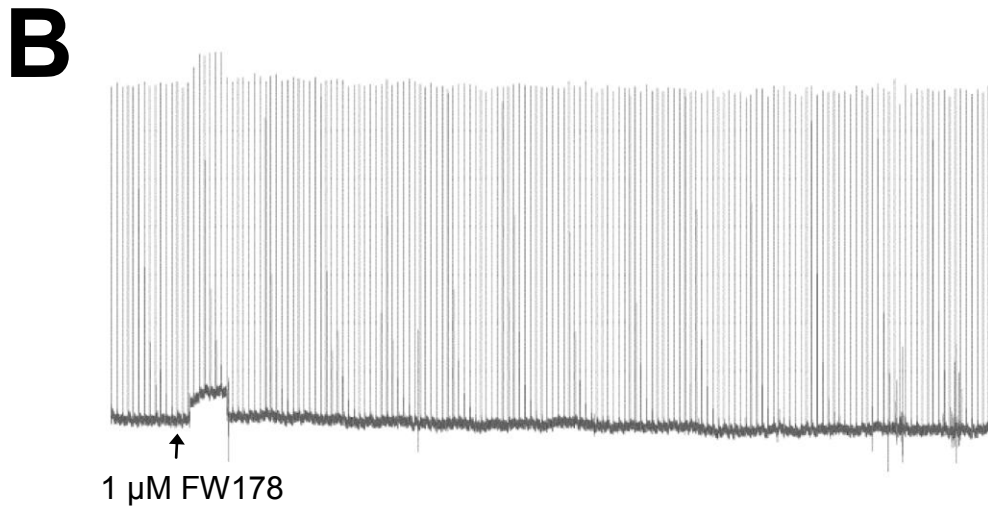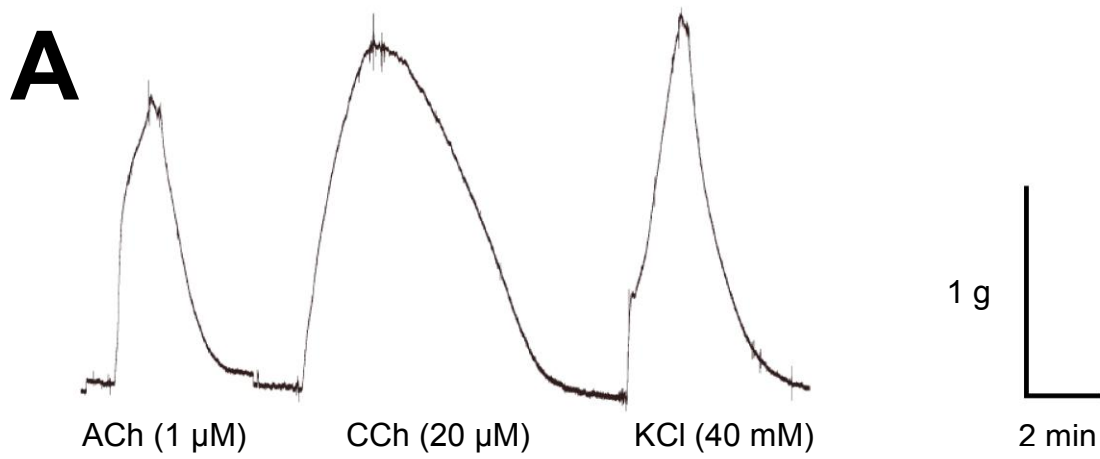
Fig 7.1: Typical responses of the isolated chick biventer nerve-muscle preparation to 1 µM FW178. Acetylcholine (ACh), carbachol (CCh) and potassium chloride (KCl) were applied to the preparation for 30 seconds (60 seconds for Cch) prior to, and after, exposure to 1 µM F☐☐☐☐ in the absence of electrical stimulation. (**A**) Control responses to the exogenously applied agonists. (**B**) Note the lack of fasciculations, maintained contracture or change in twitch tension seen in the presence of the toxin. (**C**) Responses elicited by the muscle to the exogenously applied agonists following F☐☐☐☐ exposure. Scale is the same as in panel A. (**D**) Summary of responses to the exogenously applied agonists following exposure to 1 µM F☐☐☐☐. Data are presented as a percentage of control amplitude (dashed line). No significant difference is seen when compared to the control (n = 3, p > 0.05 Wilcoxon signed-rank test). Data is expressed as mean $\pm$ SEM.

7.1.3 Effect of the 'hybrid' toxin FW178 on insect Na$_V$ channels

Sodium currents (I_{Na}) were recorded under voltage-clamp conditions in acutely dissociated dorsal unpaired median (DUM) neurons of the American cockroach *Periplaneta americana*, as described in section **5**.1. By stepping the membrane potential from –80 mV to –10 mV a large inward rapidly inactivating sodium current was observed (Fig **7**.**2A**). All currents were recorded in the presence of known Ca$_V$ channel blockers Cd^{2+} (1 mM), verapamil (0.01 mM) and NiCl$_2$ (0.1 mM), as well as known K$_V$ and K$_{Ca}$ channel blockers TEA-Cl (20 mM) and 4-AP (5 mM) (Grolleau and Lapied, 1995a). Addition of 150 nM TTX always totally abolished this current thus confirming it was carried by Na$_V$ channels. Addition of 1 µM FW178 failed to significantly alter peak amplitude or inhibit inactivation of I_{Na} (p > 0.05, paired Student's t-test, n = 5). Families of I_{Na} were elicited by stepping the voltage in 10 mV steps from a holding voltage of –80 mV to +70 mV, recorded in both the absence (Fig **7**.**2C**), and presence (Fig **7.2D**), of 1 µM FW178. Analysis of the I/V relationship (Fig **7.2B**) revealed no significant blockade of peak I_{Na} or shift in the voltage-dependence of activation (p > 0.05, paired Student's t-test, n = 5). The equation for this curve fit is detailed in section **5.6**. There was no difference in the calculated reversal potential (V_{rev}) for sodium of +49.6 mV (using the Nernst equation), compared to the measured values of +52.2 $\pm$ 1.1 mV and +51.6 $\pm$ 2.0 mV in the absence and presence of the toxin,

-

respectively. This indicates that the toxin did not alter Na$_V$ channel ion selectivity (Fig **7**.**2B**).
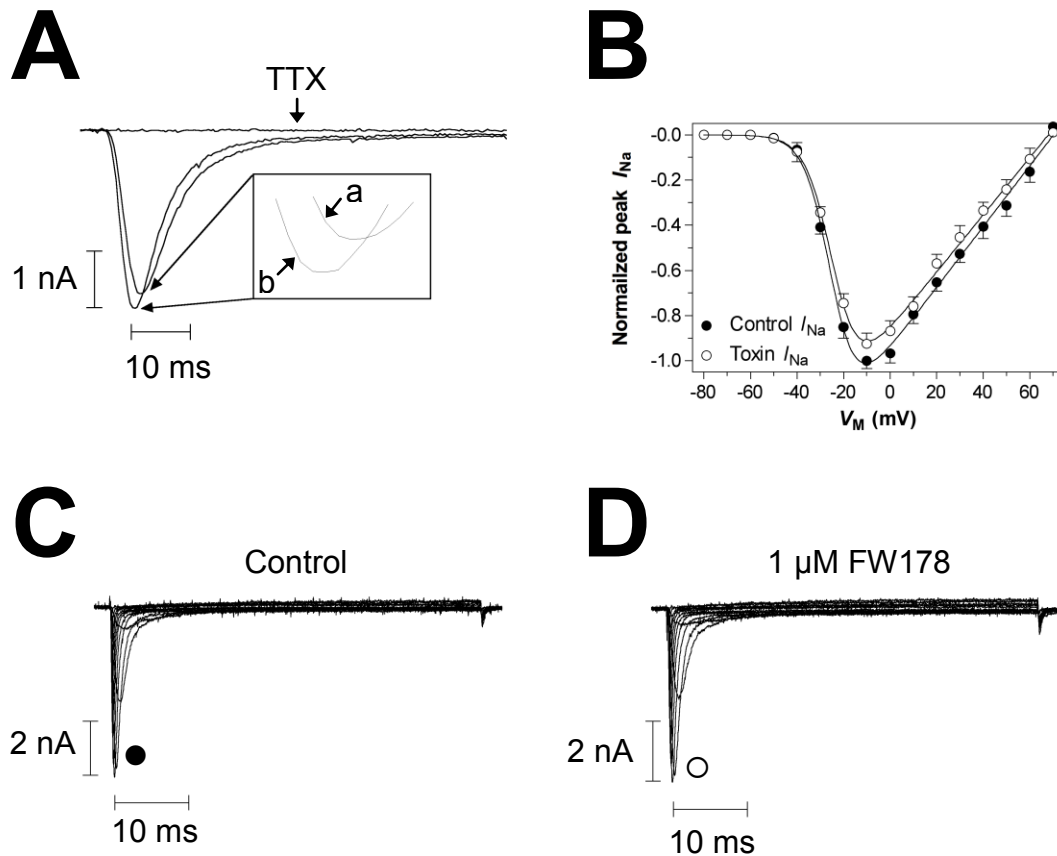
Fig 7.**2**: Effects of 'hybrid' toxin FW178 on Na$_V$ channels in cockroach DUM neurons. (**A**) Superimposed typical current traces showing lack of effect of 1 μM FW178 on I_{Na} currents that were obtained by a 50 ms step to +10 mV from a holding potential of –80 mV. The inset shows an enlarged view of the peak current in the presence (**b,**) and absence (**a**), of the toxin. This current could be completely abolished by addition of 150 nM TTX, thus proving the current was carried by Na$_V$ channels (n = 5) (**B**) The I/V relationship is shown in both the presence (○), and absence (●), of 1 μM FW178. As seen, there is no shift in the threshold of activation or reversal potential (V_{rev}) by addition of the toxin. (**C**-**D**) Families of currents were obtained by 10 mV steps, in the absence (**C**) and presence (**D**) of 1μM FW178 from a holding potential of –80 mV (n = 5) (see section **5**.**1**.**9** & **5**.**1**.**10** for further details). Data is expressed as mean ± SEM.

-

7.1.4 Effect of the 'hybrid' toxin FW178 on insect Ca_V channels

Ca_V channel currents (I_{Ca}) were recorded under the same conditions as those used for testing κ-ACTX-Hv1c as detailed in section **5**.**1**.**9**. Stepping the membrane potential from –90 mV to –10 mV a large inward current is elicited. This current has an initial peak (or transient) component followed by a non-inactivating (or maintained) component still present at the end of the 100 ms test pulse (Fig **7.3A**). All currents were recorded in the presence of the Na_V channel blocker TTX (150 nM), whilst any potassium current was absent due to the lack of potassium in either the external or internal solutions.

Addition of 1 mM $CdCl_2$ always totally abolished this current thus confirming it was carried by Ca_V channels. Addition of 1 μM FW178 significantly inhibited both peak and late current by 66.7 $\pm$ 4.9 % and 61.4 $\pm$ 6.2 %, respectively (n = 4). Examination of the concentration-response curve reveals that blockade of current is concentration-dependent with an IC_{50} value for inhibition of peak I_{Ca} as 409 $\pm$ 15 nM (Fig **7.3B**).

To characterise any alterations in the voltage-dependence of activation by FW178 on insect I_{Ca}, the voltage was increased using 10 mV steps from –90 mV to +50 mV. Families of currents between –60 mV and +50 mV were recorded in both the absence (Fig **7.3C**), and presence (Fig **7.3D**), of 1 μM FW178. The normalized peak current for each voltage step (I/V) was then plotted both in the absence and presence of the toxin for both 1 μM (Fig **7.3E**), and 300 nM (Fig **7.7F**), FW178. Analysis revealed a consistent block of current at all voltages tested thus confirming that inhibition of I_{Ca} by Fw178 is not voltage-dependent nor was there a shift in $V_{1/2}$..

No significant reversibility is seen following 10 minute washout period with toxin free solution after exposure to FW178 (p > 0.05, paired Student's t-test, n = 5). Finally plotting the normalized late current remaining in the presence of 1 μM FW178 versus time revealed a τ_{on} value of 74.5 seconds.

A

1 mM Cd^{2+}

1 μM FW178

Control

1 nA

25 ms

B

● IC$_{50}$ 409 ± 14.9

% Block of I_{Ca}

[FW178] (M)

C

Control

1 nA

25 ms

D

1 μM FW178

1 nA

25 ms

E

Normalized peak I_{Ca}

● Control
○ 300 nM Toxin

V_M (mV)

F

Normalized peak I_{Ca}

● Control
○ 1 μM Toxin

V_M (mV)

G

Toxin (1 μM)

Normalized peak I_{Ca}

τ_{on} = 74.5 sec

Time (s)

-
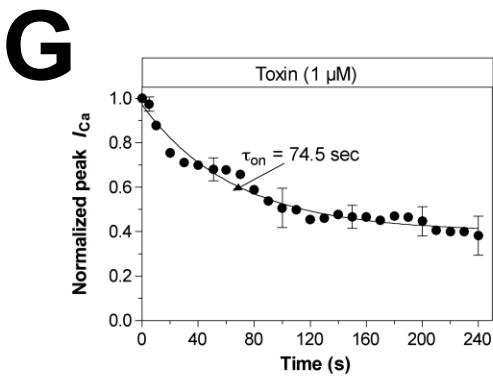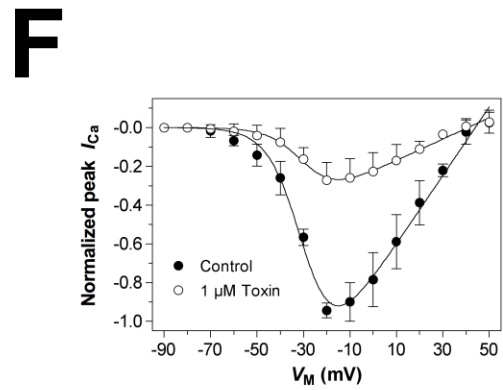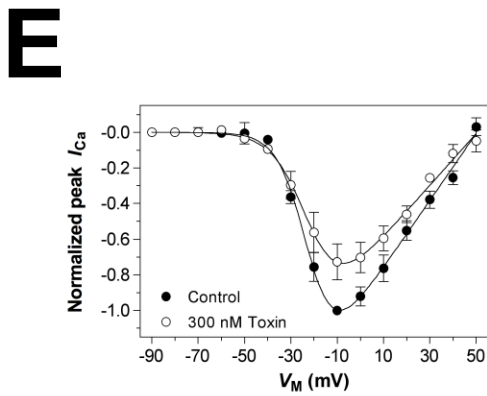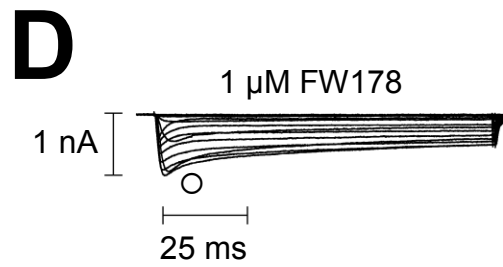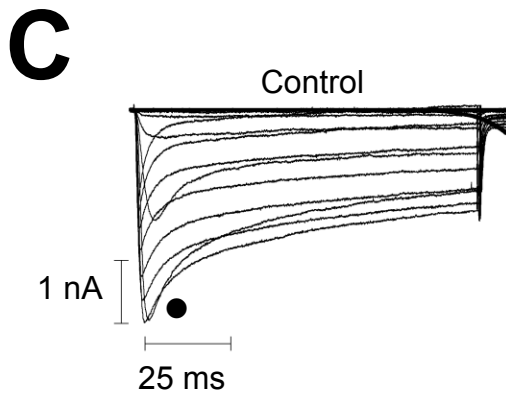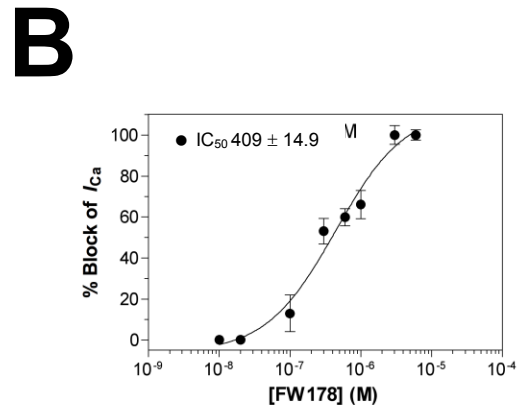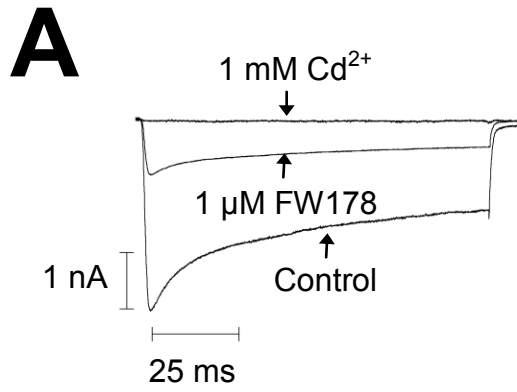
Fig 7.3: The 'hybrid' toxin FW178 blocks Ca_V channels in cockroach DUM neurons. (**A**) Addition of 1 µM Fw178 inhibits both peak and late I_{Ca} without significant reversibility ($p > 0.05$, $n = 5$). Currents were induced by stepping the potential to -10 mV from a holding potential of –90 mV. (**B**) The dose-response curve for inhibition of peak (●) I_{Ca} revealed an IC_{50} value of 409 ± 15 nM. Families of currents were elicited by 10 mV depolarisation steps from –90 to -10 mV, in both the absence (**C**),and presence (**D**), of 1 µM FW178 ($n = 5$). As shown by the peak I/V graphs for 300 nM FW178 (**E**), and 1 µM FW178 (**F**), inhibition of current by toxin (○) as compared to control (●) is seen at all potentials tested (**G**) A plot of the time-course for inhibition of I_{Ca} by 1 µM FW178 revealed a τ_{on} value of 74.5 ± 11.7 ($n = 5$). Refer to section **5**.6 for the equations for dose-response and I/V analysis. Data is expressed as mean ± SEM.

7.1.5 Effect of the 'hybrid' toxin FW178 on insect $K_{(A)}$ and $K_{(DR)}$ channels

Despite showing that the 'hybrid' toxin FW178 targets insect Ca_V channels it was necessary to confirm that the toxin did not also target insect potassium channel subtypes, especially given that the pharmacophore of FW178 overlaps with κ-ACTX-Hv1c. Currents were therefore recorded in the presence of TTX (150 nM) and Cd^{2+} (1 mM) to block Na_V and Ca_V channels, respectively. Given that the presence of Cd^{2+} does not completely inhibit K_{Ca} channels, ChTX (30 nM) was also included in the external solution. Under these conditions outward current represent only the 'A-type' ($K_{(A)}$) and delayed-rectifier ($K_{(DR)}$) potassium channel subtypes. Stepping the voltage from a holding level of –80 mV to +40 mV elicits a large maintained outward current that persists until conclusion of the step pulse (Fig **7**.4A). Addition of 1 µM FW178 failed to inhibit total I_K ($n = 5$). Furthermore, addition of the antagonists TEA-Cl (50 mM) and 4-AP (5 mM), totally abolished all outward current (data not shown, $n = 4$). This indicates that the observed current was carried only by potassium ions. The normalized late (Fig **7**.4B) I/V relationship was then plotted in both the absence (v) and presence (□) of 1 µM FW178. Presence of the toxin consistently failed to inhibit late current at all voltages tested within the range of –50 mV to + 40 mV ($p > 0.05$, $n = 5$). The equation for this curve fit is detailed in chapter **5**, section **6**. Furthermore no

-

change in the voltage-dependence of activation is seen in the presence of the toxin (n = 5). Families of outward currents were obtained by increasing the voltage from a holding level of –80 mV to +40 mV in 10 mV increments, in both the absence (Fig **7**.**4C**) and presence (Fig **7**.**4D**) of 1 µM FW178 (n = 5).

Interestingly when ChTX was absent from the external solution, addition of 1 µM FW178 elicited a small, yet significant inhibition of late I_K by 11.4 $\pm$ 3.4 % (Fig **7**.**5**). This response indicates that FW178 may also target $I_{K(Ca)}$ as well as I_{Ca}. However the full extent of the response was masked due to the presence of Cd^{2+} to block Ca_V channels but FW178 most likely inhibited some $I_{K(Ca)}$.

Therefore to test the action of FW178 against insect $K_{(Ca)}$ channels, HEK293 cells expressing the α-subunit of the BK channel from *Periplaneta americana* (*pSlo*) were used.
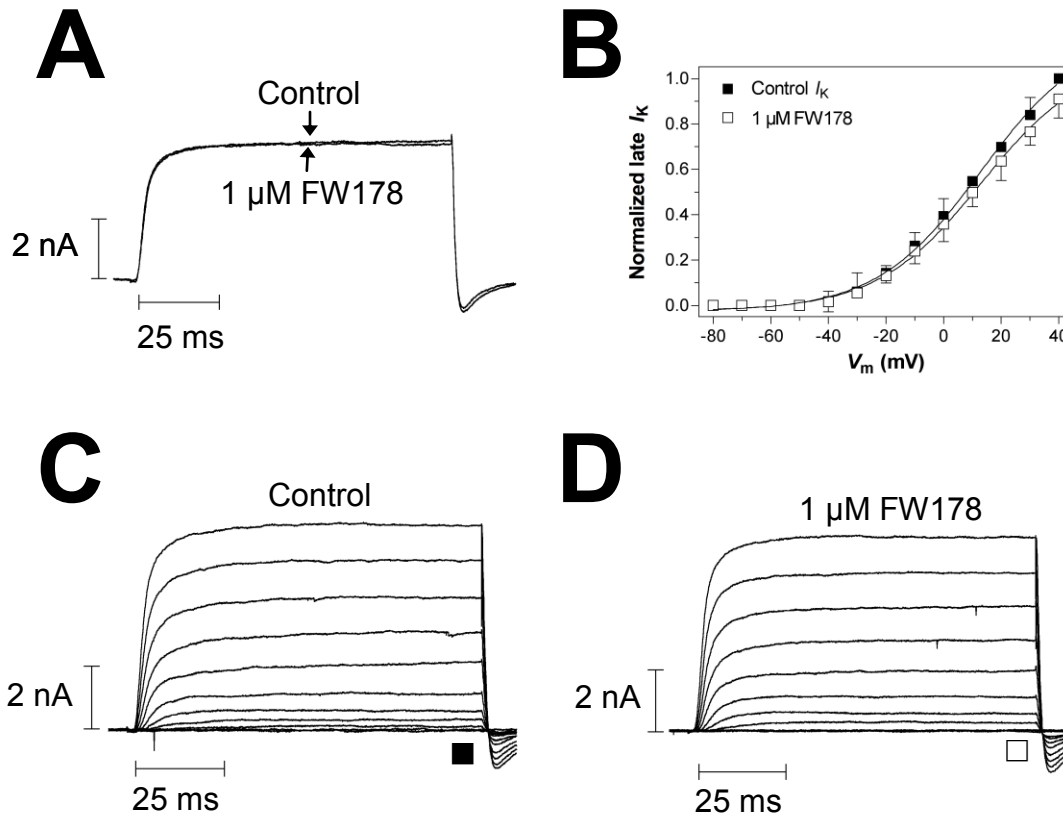
Fig 7.4: Effects of 'hybrid' toxin FW178 on macroscopic K_V channels comprising $I_{K(A)}$ and $I_{K(DR)}$ in cockroach DUM neurons. (**A**) Superimposed typical current traces showing lack of effect of 1 µM FW178 on total $I_{K(A)}$ and $I_{K(DR)}$ currents that were obtained by a 100 ms step to +40 mV from a holding potential of –80 mV. This current was recorded in the presence of 150 nM TTX, 1 mM Cd^{2+} and 30 nM ChTX, thus revealing only $I_{K(A)}$ and $I_{K(DR)}$. In addition, this current could be completely abolished by addition of 50 mM TEA and 1 mM 4-AP (data not shown) (*n* = 5). The *I/V* relationship is shown in both the presence (□) and absence (■) of 1 µM FW178 (**B**). As seen, there is no shift in the threshold of activation or voltage-dependence of activation following addition of the toxin. Refer to section **5**.**6**.for the equation for the *I/V* analysis. Families of currents were obtained by 10 mV steps in the absence (**C**), and presence (**D**), of 1µM FW178 from a holding potential of –80 mV (*n* = 5). Data is expressed as mean ± SEM.
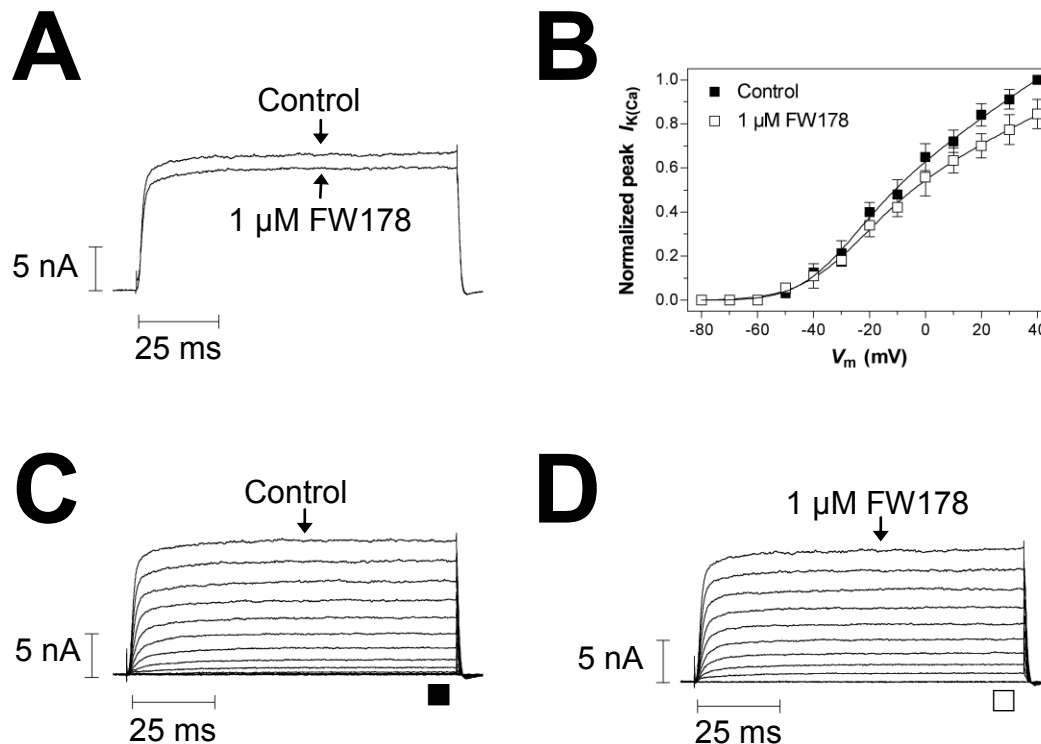
Fig 7.5: Block of K_V channel currents by the 'hybrid' toxin FW178 in the absence of ChTX. (**A**) Superimposed typical current traces showing block (11.4 $\pm$ 3.4 %), of I_K recorded in the absence of ChTX by 1 μM FW178 ($p < 0.05$, paired Student's t-test, $n = 3$). Currents were obtained by a 100 ms step to +40 mV from a holding potential of –80 mV. This current was recorded in the presence of 150 nM TTX, 1 mM Cd^{2+} and 5 mM 4-AP, thus revealing only $I_{K(DR)}$ and a partial $I_{K(Ca)}$ ($n = 3$). Given the lack of block on $I_{K(DR)}$ and $I_{K(A)}$ (refer Fig **7**.4), 1 μM FW178 must block $I_{K(Ca)}$. (**B**) The I/V relationship is shown in both the presence ($\square$) and absence ($\blacksquare$) of 1 μM FW178. As seen, there is no shift in the threshold of activation or voltage-dependence of activation following addition of the toxin. Refer to section **5**.**6**.for the equation for the I/V analysis. Families of currents were obtained by 10 mV steps in the absence (**C**), and presence (**D**), of 1μM FW178 from a holding potential of –80 mV ($n = 3$). Data is expressed as mean $\pm$ SEM.

7.1.6 Effect of the 'hybrid' toxin FW178 on *pSlo* currents expressed in HEK293 cells

FW178 blocks insect Ca_V channels in a concentration-dependent manner. In addition, the toxin most likely inhibits insect K_{Ca} channels, given a lack of activity on 'A-type' and delayed rectifier K_V channel subtypes. Given with the selective

-

inhibition of K_{Ca} by κ-ACTX-Hv1c and topologically similar pharmacophores it is likely that FW178 also blocks *pSlo* channels in DUM neurons.

To examine the effects of FW178 on insect $I_{K(Ca)}$, stably transfected HEK293 expressing the α-subunit of the K_{Ca} channel from the American cockroach *Periplaneta americana* (*pSlo*), were used. Refer to section **5.4.2** for further details. Successful expression of the coding region for *pSlo* was determined by the ability to produce a large outward current upon depolarisation of the membrane. The recording conditions including voltage-protocols are outlined in chapter **5** & table **5.5**. Stepping the voltage from a holding potential of –90 mV to +40 mV elicits a large outward current with a small peak component followed by a late current that persists until completion of the test pulse. Sensitivity of the current to partially reversible blockade by TEA-Cl (10 mM) and charybdotoxin (1 µM), was $84.1 \pm 1.5\%$, and $80.1 \pm 2.1\ \%$ respectively, thus confirming the current was $I_{K(Ca)}$ mediated (n = 12). Addition of TEA-Cl (10 mM) at the conclusion of each experiment was undertaken to act as a positive control.

Addition of 600 nM FW178 caused $46.2 \pm 6.6\ \%$ inhibition of current remaining at the end of the test pulse (Fig **7.6A**, n = 5). Analysis of the concentration-response relationship for doses between 10 nM and 10 µM revealed an IC_{50} value for inhibition of late current of 671 ± 7 nM (Fig **7.6B**, n = 5). Families of currents were elicited by 10 mV steps from a holding current of –90 mV to a maximum of + 80 mV, recorded in both the absence (Fig **7.6C**), and presence (Fig **7.6D**), of 600 nM FW178 (n = 5). Analysis of the I/V relationship (Fig **7.6E**) revealed a voltage-independent blockade of late current that was partially reversible, in addition there is no significant shift in the voltage-dependence of activation (p > 0.05, paired Student's t-test, n = 5). By plotting the normalized late current remaining in the presence of 600 nM FW178 versus time revealed a τ_{on} value of 165 seconds. In addition, the remaining current was measured during a wash out period with toxin free solution that revealed a τ_{off} value of 416 seconds (Fig **7.6F**, n = 5). This block of current was only partially reversible and failed to return to control levels despite a wash out period of up to 15 minutes (data not shown).

-

FW178 represents the first insect-selective atracotoxin to target two distinct voltage-gated ion channels, namely Ca_V and $K_{(Ca)}$. As a result FW178 has been renamed hybrid-ACTX-Hv1 to reflect its ability to inhibit both I_{Ca} and $I_{K(Ca)}$.

A

Control

600 nM FW178

1 µM FW178

2 nA

25 ms

B

IC_{50} = 671 nM

% Block $I_{K(Ca)}$

[FW178] (M)

C

Control

2 nA

25 ms

D

600 nM FW178

1 nA

25 ms

E

■ Control
□ 600 nM FW178
▲ Washout

Normalized $I_{K(Ca)}$

V_m (mV)

F

Toxin (1 µM)   Washout

τ_{on} = 165 sec

τ_{off} = 416 sec

Normalized late $I_{K(Ca)}$

Time (s)

-
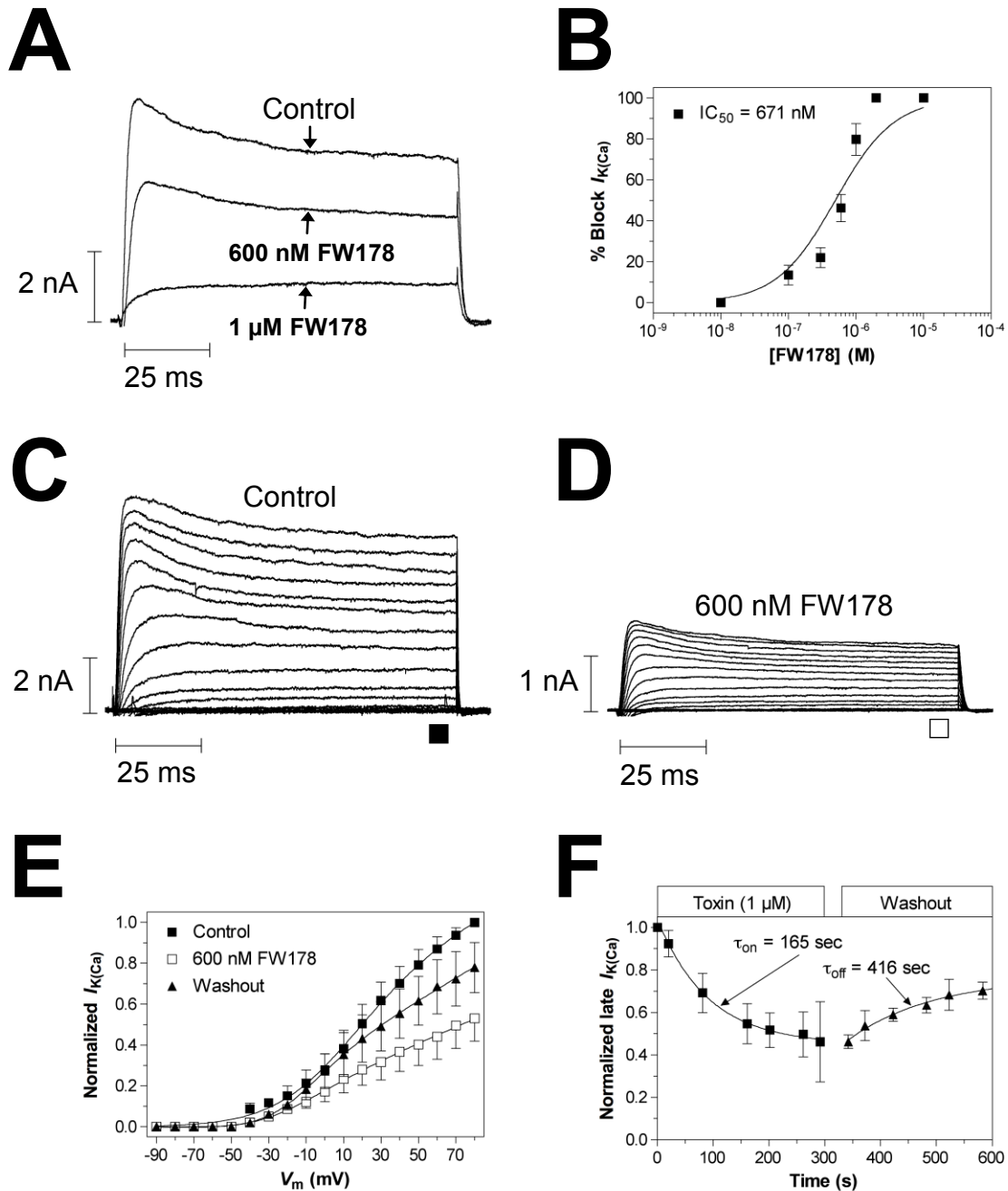
Fig 7.**6**: Inhibition of *pSlo* currents by the 'hybrid' toxin FW178. (**A**) $I_{K(Ca)}$ were obtained by a 100 ms voltage step to +40 mV from a holding potential of –90 mV. Addition of either 600 nM or 1 µM FW178 inhibited $I_{K(Ca)}$ with partial reversibility (refer to panel **E**). (**B**) Concentration-response curve for inhibition of $I_{K(Ca)}$ revealed an IC_{50} value of 671 ± 7 nM. (**C**-**D**) Families of currents were obtained by 10 mV steps from a holding potential of –90 mV in the presence (**D**), and absence (**C**), of 600 nM toxin (*n* = 5). (**E**) The *I/V* relationships for late *pSlo* currents is shown in both the presence (▢), and absence (■), of 600 nM FW178, respectively. As seen *pSlo* currents were inhibited by 600 nM FW178 at each potential tested but there was no shift in the threshold of activation (*n* = 5). (**F**) A plot of the time-course for inhibition of *pSlo* currents by 600 nM FW178 revealed values for τ_{on} and τ_{off} as 165 and 416 seconds respectively (*n* = 5). Refer to section **5**.**6**.for the equations for dose-response and *I/V* analysis. Data is expressed as mean ± SEM.

CHAPTER 8

DISCUSSION

Preface

The κ-ACTXs are a unique family of excitatory peptide toxins that contain a rare vicinal disulfide bond. Despite significant interest in this class of peptides as bioinsectides (Tedford *et al* 2004, Maggio *et al*, 2005), their molecular target has until now proven elusive.

This thesis demonstrates that κ-ACTX-Hv1c is a high-affinity, specific blocker of insect BK_{Ca} channels. κ-ACTX-Hv1c reversibly suppressed $I_{K(Ca)}$ in cockroach DUM neurons in a concentration-dependent manner with a IC_{50} of 2 nM. In contrast, κ-ACTX-Hv1c had no effect on cockroach I_{Na}, I_{Ca} nor other insect K_V channel currents, such as $I_{K(DR)}$ or $I_{K(A)}$ (*Shaker*-like). Furthermore, κ-ACTX-Hv1c blocked insect *pSlo* channels at nanomolar concentrations, showing a 41-fold selectivity for this channel over *mSlo*, supporting the phyla-specific toxicity of this toxin.

8.1 What is the molecular target of κ-ACTX-Hv1c

Minimizing the potential cross-resistance to newly developed insecticides requires they act on unique targets or novel sites on existing targets. The screen that was employed to elucidate the target site for κ-ACTX-Hv1c was whole-cell patch clamping of Dorsal Unpaired Median (DUM) neurons from the American cockroach *Periplaneta americana*. This insect cell model was chosen as it

processes a variety of well-characterised ion channel types (Grolleau and Lapied 2000), including a number of classical insecticide targets. These include the classical voltage-dependent sodium (Na_v), both high and low-voltage activated calcium (Ca_V) and five-types of K_V channels (namely, the delayed-rectifier K_{DR}, 'A-type' K_A, the sodium-actived K_{Na}, the calcium-activated K_{Ca} and the inward-rectifier K_{IR}). Due to this diverse repertoire of voltage-dependent ion channels that are present in DUM neurons any activity by κ-ACTX-Hv1c should be easily detected. The insect-specificity and excitatory phenotype of κ-ACTX-Hv1c is reminiscent of a subclass of β-scorpion toxins that target insect Na^+ channels (Cestéle *et al*, 2003) and the initial 3D structure of κ-ACTX-Hv1c closely resembled the excitatory Na^+ channel modulator δ-ACTX-Hv1a also from *Hadronyche versuta.* These toxins exert their excitatory effect by altering the channel inactivation kinetics, resulting in prolonged action potentials (Nicholson *et al* 1994;1998). In contrast to these toxins κ-ACTX-Hv1c displayed no effect on the amplitude or kinetics of TTX-sensitive I_{Na} at concentrations as high as 1 μM (Fig. **6**.**1**). Further, κ-ACTX-Hv1c failed to alter the voltage-dependence of activation of sodium currents (Fig. **6.1B**). This result confirms that κ-ACTX-Hv1c does not exert its lethal effect through interaction with insect TTX-sensitive Na^+ channels. Unlike ω-ACTX-1 or –2 toxins, κ-ACTX-Hv1c failed to significantly block I_{Ca} with no differences in peak current amplitude between control and toxin at any of the voltages tested (Fig **6.2**). In addition there was no shift in the voltage dependence of activation (or activation threshold) in the presence of κ-ACTX-Hv1c. This result may not be all that surprising given that κ-ACTX-Hv1c does not show high structural similarity to ω-ACTX-Hv1a or ω-ACTX-Hv2a that both target insect calcium channels. Furthermore the excitatory phenotype of κ-ACTX-Hv1c is in contrast to the biphasic excitatory/depressant paralysis of ω-ACTX-Hv1a (Chong *et al* 2006) or depressant paralysis of ω-ACTX-Hv2a (Wang *et al* 2001).

It should be mentioned that the Na_V and Ca_V channel subtypes tested as part of this investigation only encompassed those from *P. americana* DUM neurons and

did not provide evidence that κ-ACTX-Hv1c does not target Na_V and Ca_V channel subtypes from other phyla. Given that phyla-specific variations do exist, further studies on Na_V and Ca_V channel subtypes needs to be undertaken. Furthermore κ-ACTX-Hv1c needs to be tested against Na_V and Ca_V channel subtypes from other insect orders. These may include field cricket (*Gryllus bimaculatus*, Orthoptera), giant neurons or honeybee (*Apis mellifera* Hymenoptera), Kenyon cells (Kloppenburg and Hörner, 1998; Schäfer *et al*, 1994).

The next likely target for κ-ACTX-Hv1c was the insect potassium channel, given that the critically important Arg^8 and Tyr^{31} residues overlay extremely well with the Lys-Tyr/Phe dyad of the potassium channel toxins BgK and agitoxin 2 (Fig **4.2C**).

In contrast to the lack of activity on Ca_V and Na_V channels, 1 μM κ-ACTX-Hv1c reduced both the peak and late whole-cell outward I_K (Fig. **6.3**). Presence of the toxin consistently inhibited both peak and late current at voltages tested. In contrast no change in the voltage-dependence of activation was seen for either peak or late current in the presence of κ-ACTX-Hv1c. Given that DUM neurons exhibit a variety of potassium channel subtypes, it was necessary to examine each in turn to identify which subtype(s) is targeted by κ-ACTX-Hv1c.

κ-ACTX-Hv1c failed to significantly inhibit $I_{K(DR)}$ at doses upto 1 μM. However addition of 1 μM κ-ACTX-Hv1c significantly inhibits $I_{K(A)}$ by 14.3 $\pm$ 4.6 % at voltages above +30 mV (Fig **6.4**), with no shift the voltage dependence of activation. Nevertheless, this modest blockade of $I_{K(A)}$ fails to explain the large inhibition of both peak and late macroscopic I_K, The $I_{K(Ca)}$ represents a large proportion of total I_K (personal observation n = >30) and therefore represents that most likely target for κ-ACTX-Hv1c. In fact, addition of κ-ACTX-Hv1c caused a dose-dependent equipotent block of both late-sustained and fast-transient $I_{K(Ca)}$ with IC_{50} values of 2.1 nM and 1.8 nM respectively. These actions occurred in the absence of any significant changes in the voltage-dependence of K_{Ca} channel activation or alterations in the degree of block at higher doses (Fig **6.7**). This data provides evidence against κ-ACTX-Hv1c interacting with the voltage sensor

region. However, the further that κ-ACTX-Hv1c penetrates into the voltage field of the membrane to block the pore the greater the degree of voltage dependent block. Given that ChTX should produce a voltage-dependent block these combined effects of κ-ACTX-Hv1c and ChTX addition are difficult to differentiate and therefore it is impossible to determine if κ-ACTX-Hv1c has a voltage dependent action on $I_{K(Ca)}$.

Thus unlike other spider toxins targeting K_v channels (Swartz 2007) κ-ACTX-Hv1c appears to be a channel blocker not a gating modifier. κ-ACTX-Hv1c therefore represents the first spider toxin that selectively targets insect high-conductance Ca^{2+}-activated potassium (BK_{Ca}) channels, also known as slowpoke (*Slo*) channels.

8.2 κ-ACTX-Hv1c targets insect BK_{Ca} channels

To confirm the specific action of κ-ACTX-Hv1c, expression of the clone for the *Periplaneta americana* slo channel (*pSlo*) was achieved in human embroyonic kidney (HEK293) cells. In the presence of κ-ACTX-Hv1c, I_K was inhibited in a concentration-dependent manner revealing an IC_{50} of 240 nM. Although this was considerably higher than for the native BK_{Ca} channel in DUM neurons, the loss of potency parallels that seen with ChTx, with an increase from 1.9 nM to 158 nM (Derst *et al* 2003). This is no doubt due to the absence of a modulatory β-subunit which has been previously shown to cause a 50-fold increase in the affinity of ChTx for the α-subunit of human *hSlo* channels (Hanner *et al*, 1997). In support, the activation kinetics of the native $I_{K(Ca)}$ in DUM neurons were much more rapid than *pSlo* channel currents (Derst *et al* 2003), similar to the more rapid onset and inactivation of currents when mammalian *Slo* channels are expressed in association with β2 and β3 subunits (Xia *et al*, 2003; Wallner *et al*, 1999; Lingle *et al*, 2001). However, no homologs of mammalian β subunits are present in *Drosophila* and *C. elegans* (Littleton and Ganetzky, 2000) and *dSlo* currents are

not functionally affected by coexpression with a mammalian β1-subunit (Wallner *et al* 1996). Nevertheless, modulation of the gating of *dSlo* channels has been observed when co-expressed with Slob ('*Slowpoke* binding protein') a 60 kDa *Drosophila* protein (Schopperle *et al*, 1998). Unfortunately no pharmacological studies have been performed with ChTx on *Slo* channels co-expressing Slob and therefore the β-subunit associating with *pSlo* channels remains unidentified. Until the putative regulatory subunits associated with *pSlo* have been identified the native phenotype cannot be reconstituted. In turn the influence that these subunits have on the affinity of κ-ACTX-Hv1c for *pSlo* channels cannot be determined. Despite this the phyla-specificity of κ-ACTX-Hv1c has been proven as it has been shown to inhibit *pSlo* but does not inhibit native rat BK$_{Ca}$ channels in DRG neurons nor *mSlo* channels expressed in HEK293 cells.

Despite the fact that the *Slo* gene encoding BK$_{Ca}$ channels is highly conserved throughout evolution, insect and mammalian *Slo* channels nonetheless display minor mutations in their pore regions (Fig **8.1**). Importantly the critical residues for binding and action of ChTx are believed to be situated between the pore region and both flanking transmembrane segments S5 and S6 channels (Anderson *et al* 1998)
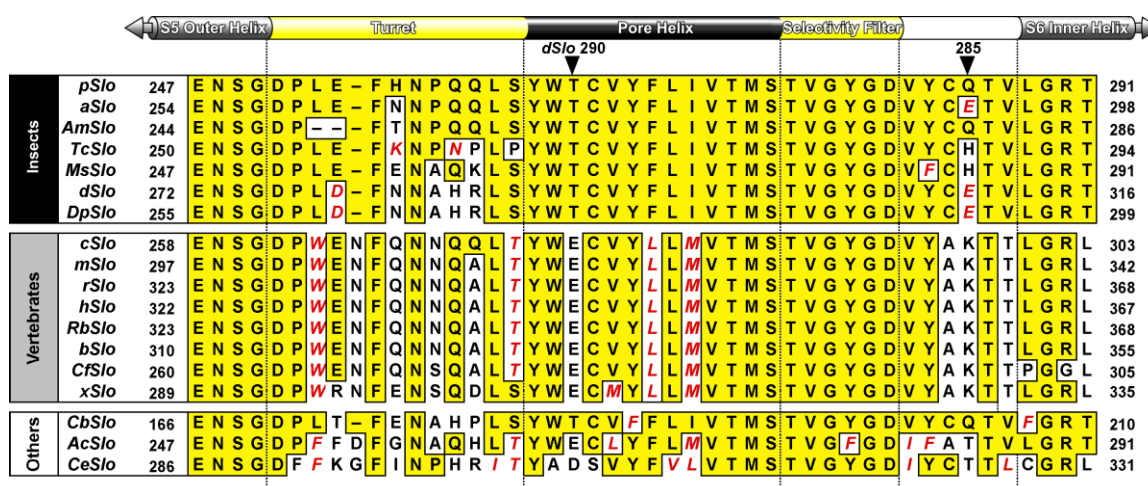
Figure **8.1:** Alignment of the pore region of vertebrate and invertebrate *Slo* channels. This alignment is restricted to the pore region located between

transmembrane segments S5 and S6. Sequences are from insects (*Periplaneta americana, p*; *Anopheles gambiae*, *a*; *Apis mellifera*, *Am*; *Tribolium castaneum*, *Tc*; *Manduca sexta*, *Ms*; *Drosophila melanogastor*, *d;* and *D. pseudoobscura*, *Dp*), vertebrates (chicken, *c*; mouse, *m*; rat, *r*; human, *h*; rabbit, *Rb*; bovine, *b*; *Canis familiaris*, *Cf;* and *Xenopus laevis*, x), marine invertebrates (*Cancer borealis*, *Cb;* and *Aplysia californica*, *Ac*) and *Caenorhabditis elegans* (*Ce*). Identical residues are boxed in gray while conservative substitutions are in gray italic text. Arrowheads denote residues important for ChTx binding (see text for details).

Moreover, single point mutations in this region can significantly modulate α-KTx 1 toxin affinity (Wallner *et al*, 1999; Lingle *et al*, 2001). Table **8**.**1** summarizes the ability of κ-ACTX-Hv1c and ChTx to block various mammalian and insect BK_{Ca} channels. It is clear from the IC_{50} values that ChTx more potently blocks mammalian *Slo* channels (36 and 7.4 nM for *hSlo* and *mSlo*, respectively) than insect *Slo* channels (158 nM and > 5 µM for *pSlo* and *dSlo*, respectively (Wallner *et al*, 1999; Lingle *et al*, 2001). However this selectivity can be reversed as shown, using a T290E mutant of *dSlo* (Lingle *et al*, 2001) or Q285K mutant of *pSlo* (Wallner *et al*, 1999), to become more ChTx-sensitive. Therefore, it appears only subtle variations in the structure of *Slo* channels within the pore region can produce significant changes in phyla-selectivity, sufficient to explain the insect selectivity of κ-ACTX-Hv1c.

Table 8.1. Phyletic-selectivity of κ-ACTX-Hv1c and ChTX for K_{Ca} channels

Channel	IC$_{50}$ value (nM)	
	κ-ACTX-Hv1c	ChTX[a]
Insect		
Native cockroach DUM neuron BK$_{Ca}$	2.3	1.9*, 1.4 [c]
pSlo	240	158 [c]
dSlo	>10 000	5 800 [d]
Mammalian		
Native rat DRG neuron BK$_{Ca}$	>1 000	<100 [b]
hSlo	ND [e]	36 [d]
mSlo	9776	7.4 [d]
Phyletic selectivity (mSlo/pSlo IC$_{50}$)	41	0.047

[a] Data from [b]Scholz *et al*, 1998, [c]Derst *et al*, 2003, [d]Myers and Stampe, 2000, and present study*.
[e] ND, not determined.

Table **8**.**1** summarizes the ability of κ-ACTX-Hv1c and ChTX to block various mammalian and insect BK$_{Ca}$ channels. It is clear from the IC$_{50}$ values that ChTX more potently blocks mammalian *Slo* channels (36 and 7.4 nM for *hSlo* and *mSlo*, respectively) than insect *Slo* channels (158 nM and >5 M for *pSlo* and *dSlo*, respectively) (Derst *et al* 2003, Myers and Stampe, 2000). However this selectivity can be reversed as shown using a T290E mutant of *dSlo* (Myers and Stampe, 2000) or Q285K mutant of *pSlo* (Derst *et al*, 2003) to become more ChTX-sensitive. Therefore, it appears that only subtle variations in the structure of *Slo* channels can produce significant changes in phyla-selectivity. In contrast, -ACHTX-Hv1c blocked insect *pSlo* channels at nanomolar concentrations, showing a 41-fold selectivity for this channel over *mSlo*, supporting the phyla-specific toxicity of this toxin. Interestingly κ-ACTX-Hv1c, like ChTX and IbTX (Meera *et al*, 1997, Adelman *et al*, 1992), failed to potently block *dSlo* channel with the IC$_{50}$ >10 μM. Given the sequence identity in the pore region of *mSlo* with those of *rSlo* and *hSlo*, one might expect no effect of κ-ACTX-Hv1c on *rSlo* and *hSlo*.

8.3 Interaction of the pharmacophore with the channel target

Determination of protein-protein binding interfaces reveal that many interacting proteins contain a hot spot surrounded by carefully positioned residues whose main function is to exclude water from the binding surface (Cole and Warwicker, 2002). These 'gasket' residues that encircle the pharmacophore hot spot serve as a watertight seal to prevent bulk solvent from destabilizing protein-protein interactions. Somewhat surprising is that the chemical nature of these gasket residues seems to be relatively broad. Side chains with at least a methyl group (Ala) are usually large enough to maintain the integrity of the seal (Cole and Warwicker, 2002). Although mutation of Ile^2 was not assessed as part of this thesis, previous studies have shown that mutating Ile^2 to Ala caused only a 6.6-fold decrease in insecticidal activity, whereas deleting Ile^2 (N-terminal truncation mutant, Maggio and King, 2002a) resulted in a 70-fold drop in activity. This would be expected if Ile^2 served as a sealing residue as the Ala mutation would maintain the seal, whereas deletion would result in bulk solvent accessing the binding site thus reducing insecticidal activity (Maggio, 2006). In addition, mutating Val^{29} to Ala resulted in a 7.5-fold decrease in IC_{50} (Fig **6**.**16** & **6.25**), as compared to a 13-fold drop in insecticidal activity. The positioning of Val^{29} on the opposite edge of the central 'hot-spot' residues suggests it serves a similar role to Ile^2 in sealing the hot spot from bulk solvent.

Mutation of Pro^9 to Ala caused a 100-fold reduction in IC_{50} as compared to the wild-type toxin (Fig **6.15** & **6.25**). In comparison the insecticidal activity of P9A was 269-fold lower then the wild-type toxin. This raised the possibility that the observed reduction in activity was due to an induced structural perturbation rather than loss of the proline side chain. The spectral change induced by the P9A mutant results in just a slight reduction of maximum intensity at 224 nm. Therefore the reduction in activity of this mutant is likely due to the loss of the proline side chain rather than a structural perturbation (Maggio, 2006).

As expected these results confirm the importance of the Pro[9] side-chain for blockade and or binding to the channel. Possibly the hydrophilic nature and/or size of the proline side-chain enhances binding of the toxin to the target, by allowing the side-chain to move closer to the channel binding region.

8.3.1 The role of the critical arginine

Non-selective K_{Ca} channel blockers such as ChTX are believed to block the pore of the K_{Ca} channel via a Lys residue. Indeed all K_V channel blockers appear to utilise Lys in their functional dyad (Dauplais *et al*, 1997). Within the pharmacophore of κ-ACTX-Hv1c, Arg[8] represents the only charged side chain and there is a noticeable absence of a Lys residue. Nevertheless, Arg[8] may substitute for Lys and interact with the target channel in a number of ways: (i) via a strong electrostatic interaction with a negatively charged group on the channel, (ii) hydrogen bonding via the δ-guanido group, (iii) a hydrophobic interaction between the alkyl chain and a corresponding hydrophobic group on the channel, (iv) some combination of these interactions. Firstly to test the contribution of the positively charged δ-guanido group, an R8E mutant whose CD spectrum was consistent with proper folding was employed. The negative charge on the Glu resulted in a dramatic decrease in toxin activity (2237-fold) (Fig **6.17** & **6.25**), implying that the positively charged δ-guanido group significantly contributes to target binding through an electrostatic interaction. Furthermore if Arg[8] makes an ionic interaction with a negatively charged group on the target, then the R8E mutation would be expected to reduce potency even more then the R8A mutation as it will introduce repulsive electrostatic interactions. Importantly the R8E fold reduction in IC_{50} was only 1.4-fold lower then the R8A mutant. This most likely indicates that Arg[8] does indeed interact with a negatively charged group on the target via the positively charged δ-guanido group.

In order to determine the importance of the spatial position of the amine groups Arg[8] was mutated to Lys and His respectively and their effect on $I_{K(Ca)}$ IC_{50} was determined. Replacing the Arg[8] side chain with the slightly shorter Lys side chain

maintains the positive charge. If the interaction were solely electrostatic then the R8K mutation should maintain most if not all of the toxin activity. However this mutation resulted in a 226-fold reduction in IC_{50} (Fig **6**.**18** & **6.25**). The reduced activity of the R8K mutant indicates that either the positively charged amino group is not the sole interacting region of the wild-type δ-guanido group or the Lys residue cannot properly access the binding site. To test this Arg^8 was substituted with His which contains an aromatic ring which is a better mimic of the Arg δ-guanido group. However, the His side chain is much shorter than both Arg and Lys and is only partially charged at physiological pH. This mutant displayed a minor drop in IC_{50} (8.2-fold) compared with the Lys substitution (Fig **6**.**24**). From these results, it would appear that the charged amine on the Arg side chain is involved in binding, but the actual charge contributes negligible, if any, energy towards target binding. The activity of the R8H mutant also rules out the arginine alkyl chain as a key moiety. Having negated the contribution of the positive charge and the alkyl chain, the critical moiety of the arginine side chain must be the δ-guanido group. This is consistent with the R8H result since the imidazole side chain of histidine is a suitable analog of this moiety. Furthermore these results suggest that the capacity of Arg^8 to act as a hydrogen bond donor/acceptor is as important as its ability to present a positive charge to the target. Hydrogen-bonding capacity alone is not sufficient for a high-affinity interaction with insect BK channels since an R8Q mutant is much less potent than R8K and R8H mutants and only slightly more potent than an R8A mutant.

In conclusion it would appear that the function of Arg^8 is to form a dual hydrogen bond with the target. Both the δ-guanido and imidazole moieties maintain activity because they contain two identically spaced nitrogen atoms that can serve as hydrogen donors. The slightly acidic pH of insect hemolymph (6.6-6.7) ensures that much of the histidine side chain (pKa ~6.04) has two protonated nitrogen atoms which can donate protons to hydrogen bonds (Bogan and Thorn, 1998). It is possible that Arg^8 forms hydrogen bonds with surface-exposed carbonyls in the pore region of the BK channel. The modest drop in activity of the R8H mutant (4.5-fold) may be attributed to the percentage of unprotonated imidazole groups,

which could donate only one hydrogen to the interaction. Consistent with dual hydrogen bond formation, the lysine ε-amine of the R8K mutant and the amide group of the R8Q mutant can donate only one hydrogen bond; thus binding is less energetically favourable as evidenced by the increase in the IC_{50} concentration of these mutants.

8.3.2 The role of the critical tyrosine

To determine the critical features of Tyr^{31}, this residue was mutated to the following residues: Phe, Val, Leu, Ala, or Trp and the corresponding IC_{50} values for inhibition of $I_{K(Ca)}$ was determined. The CD spectra were consistent with proper folding for all of the mutants. Unsurprisingly, the mutants that had large decreases in activity were Y31A (>10000-fold), Y31V (>10000-fold) and Y31L, which displayed a 101-fold drop in activity (Fig. **6.25**). It is surprising that the decrease in activity for Y31V was >10 000-fold considering the hydrophobic side chain of valine.   Perhaps the shorter less bulky β-carbon methyl group is insufficient to exclude bulk solvent from accessing the binding site.

The other two mutants (Y31F and Y31W) had minor 2- to 18-fold drops in activity (Fig. **6.25**) indicating that the hydroxyl group of Tyr^{31} is unimportant. Val^{29} was previously identified as a sealing residue responsible for shielding the toxin-binding surface from bulk solvent (section 3.4.1). The κ-ACTX-Hv1c structure implies that proper spatial orientation of the side chains of Val^{29} and Tyr^{31} are influenced by intermolecular van der Waals interactions between these side chains. Spatial repositioning of these side chains may allow water molecules to permeate the binding surface and destabilize the toxin-target interaction. The aromatic side chains of Phe and Trp may be suitable substitutes for the intermolecular interaction that the Tyr side chain normally makes with Val^{29}. The extended alkyl chain of a Leu residue lacks a branched carbon that can properly interact with the Val^{29} side chain. Thus, although the Y31L mutation does not significantly perturb the overall structure, compromising local interactions could form a leak in the gasket that allows water and other small molecules to access

the binding site. The fact that the critical Tyr^{31} can be replaced with Phe or Trp with minimal loss of activity indicates that it does not form a specific interaction with the target channel. We therefore conclude that the critical tyrosine interacts via a nonspecific hydrophobic interaction (eg the aromatic ring of Tyr^{31}). Any medium sized hydrophobic side chain that is aromatic or β-branched (eg. isoleucine) can emulate the interaction well enough to maintain toxic activity.

Besides Arg^{8} the other functionally critical residues in κ-ACTX-Hv1c are hydrophobic, including the vicinal disulfide. It would appear that hydrophobic interactions form a perimeter around the central Arg^{8} residue. Specific arrangements of hydrophobes around hydrogen bonds and/or electrostatic interactions of Arg^{8} would decrease the free energy of these interactions by decreasing the local dielectric

8.4 Model of κ-ACTX-Hv1c binding

Scorpion toxins from α-KTx subfamilies 1–3 block BK$_{Ca}$ channels in the vicinity of the selectivity filter, mainly via residues in their C-terminal *b*-hairpin (Stampe *et al*, 1994),. Despite its ability to block BK$_{Ca}$ channels, κ-ACTX-Hv1c has virtually no sequence homology with scorpion BK$_{Ca}$ blockers, particularly in the functionally critical *b*-hairpin region. Moreover, superposition of the 3D structure of κ-ACTX-Hv1c (Wang *et al*, 2000), with that of ChTX (Bontems *et al*, 1991), demonstrates that the backbone folds of the two toxins are significantly different. This raises the question of whether the two toxins interact in fundamentally different ways with insect BK$_{Ca}$ channels.

We previously speculated that the functional Lys-Tyr/Phe dyad that is largely conserved in toxins that target vertebrate K$_V$ channels (Dauplais *et al*, 1997), might also be present in κ-ACTX-Hv1c if Arg is considered a suitable substitute for Lys (Maggio and King, 2002). The "pseudo-dyad" of κ-ACTX-Hv1c is topologically similar to that of ChTX although the overlay is not as good as with the dyad of the K$_V$ channel blockers BgK and agitoxin 2 (Maggio and King, 2002). However, since we demonstrated in the present study that Lys is a poor

substitute for the functionally critical Arg^8 residue in κ-ACTX, this apparent similarity to the dyad of vertebrate K_V channel toxins is likely to be coincidental and not predictive of the mode of binding of κ-ACTX-Hv1c to insect BK_{Ca} channels.

Several lines of evidence suggest that κ-ACTX-Hv1c and ChTX engage BK_{Ca} channels via quite different molecular mechanisms. First, the pharmacophore of κ-ACTX-Hv1c is much smaller and involves far fewer residues than that of ChTX . Second, in contrast to ChTX and other toxins that target K_V channel (Goldstein and Miller, 1993; Terlau *et al*, 1999), the block of BK_{Ca} channels by κ-ACTX-Hv1c is significantly less voltage-dependent. This suggests that κ-ACTX-Hv1c does not bind as deeply into the extracellular mouth of the ion channel pore as these other toxins. This is likely due to the bifurcated δ-guanidinium group at the tip of the critical Arg^8 residue, which is much bulkier than the single amine moiety at the tip of the linear sidechain of the key Lys^{27} residue in ChTX. Consistent with this hypothesis, a K27R mutant of ChTx is 4-fold less potent on mammalian BK_{Ca} channels (Parks and Miller, 1992), and the voltage-dependency of block is significantly reduced compared with native toxin. Third, the ability of His, as opposed to Lys, to effectively substitute for Arg^8 in κ-ACTX-Hv1c suggests that factors other than electrostatic charge are also important at this position in the toxin pharmacophore. Hydrogen-bonding capacity might be critical, since the Arg guanido and His imidazole moieties contain two identically spaced nitrogens that can serve as hydrogen-bond donors/acceptors. It is possible that Arg^8 forms hydrogen bonds with surface-exposed carbonyls in the pore region of the BK_{Ca} channel. The combined evidence therefore suggests that these two toxins, although both derived from arachnid venoms, have evolved to interact in quite different ways with invertebrate BK_{Ca} channels.

The structural and mutagenesis results indicate that toxin binding is dictated largely by the hydrophobic sidechains of the pharmacophore forming a perimeter around the central Arg^8 residue. Specific arrangements of hydrophobes around hydrogen bonds and/or electrostatic interactions of Arg^8 would decrease the free

energy of these interactions by decreasing the local dielectric (Fernandez *et al* 2002; Fernandez and Scheraga, 2003). In turn the buried hydrogen bonds serve to decrease the entropy of the desolvating hydrophobic interactions and stabilize the overall toxin-target interaction. The exclusion of water from a binding interface is not atypical.

8.5 BK_{Ca} channels: a potential insecticide target?

A major bottleneck in the development of new insecticides has been the difficulty in identifying new molecular targets. Indeed, the vast majority of chemical insecticides are directed against one of five targets (four of which are ion channels) in the insect nervous system (Tedford *et al*, 2004a; Tedford *et al*, 2004b) . Although BK_{Ca} channels play important roles in the excitability of insect neurons and muscles (Singh and Wu, 1990), they have not been considered potential insecticide targets since no insect-selective ligands of these channels have previously been identified.

Evaluation of the effects of κ-ACTX-Hv1c on other insect specifi molecular targets such as neurotransmitter receptors eg. NACh & GABA/Cl$^-$, or key metabolic enzymes, eg. $sPLA_2$ & P450 would be important to confirm that the neurotoxic activity of κ-ACTX-Hv1c underlies the lethality of the toxin.

Interestingly, paxilline, a well-known mammalian BK_{Ca} channel blocker (McMillan *et al*, 2003), as well as several other structurally-related indole-diterpenes, are toxic to a wide range of insect genera (Li *et al* 2002;2005). In order to determine whether the insecticidal activity of these diterpenes might stem from their activity on BK_{Ca} channels, we examined their ability to block $I_{K(Ca)}$ in cockroach DUM neurons. Importantly, paxilline blocked both the fast-transient and late-sustained $I_{K(Ca)}$, with IC_{50} values of 17.1 and 16.0 nM (*n* = 7-9) respectively (data not shown). This supports our contention that inhibition of BK_{Ca} channels may contribute to their lethality to in insects and that insect BK_{Ca} channels might

therefore be potential insecticide targets.

Short-chain' scorpion α-KTx 1 family toxins, such as ChTx ($\square$-KTx 1.1) and iberiotoxin (IbTx, α-KTx 1.3), are frequently used as molecular tools to study BK_{Ca} channels. However, these toxins are poor leads for development of insecticides that block *invertebrate* BK_{Ca} channels since they have limited phyletic selectivity, with a tendency to be more active against vertebrate channels (Table 1). For example, ChTx blocks mammalian *Slo* channels (IC_{50} values of 36 and 7.4 nM for *hSlo* and *mSlo*, respectively) more potently than insect *Slo* channels (IC_{50} values of 158 nM and >5 $\square$M for *pSlo* and *dSlo*, respectively) (Derst *et al*, 2003, Myers and Stampe, 2000. In contrast, κ-ACTX-Hv1c is highly selective for insect BK_{Ca} channels: it blocks cockroach BK_{Ca} channels at low nanomolar concentrations and shows a 41-fold preference for *pSlo* over *mSlo* (Table 1). Since κ-ACTX-Hv1c is a pore blocker, and the pore regions of *mSlo*, *rSlo*, and *hSlo* are identical (see Fig. 7), we predict that κ-ACTX-Hv1c will also have little effect on *rSlo* and *hSlo* channels. Consistent with this hypothesis, κ-ACTX-Hv1c failed to inhibit BK_{Ca} currents in rat DRG neurons (which express *rSlo*) and it was previously shown that subcutaneous injection of κ-ACTX-Hv1c into newborn mice, at five times the LD_{50} dose in insects, fails to produce any overt signs of toxicity (Wang *et al*, 2000). Moreover, κ-ACTX-Hv1c failed to alter neurotransmission in an isolated chick biventer cervicis nerve-muscle preparation (Wang *et al*, 2000).

BK_{Ca} channels have been highly conserved throughout evolution, and therefore it may seem surprising that toxins can discriminate between invertebrate BK_{Ca} channels and their vertebrate counterparts. However, insect and mammalian *Slo* channels display several important differences in the pore region between the S5 and S6 transmembrane helices (Fig. 7), which is believed to be the primary site of interaction with ChTx, IbTx, and most likely κ-ACTX-Hv1c (Gao and Garcia, 2003). Remarkably, the phyletic selectivity of ChTx can be manipulated by a single point mutation in this region. For example, BK_{Ca} channels from fruit flies

and cockroaches become significantly more sensitive to ChTx, a vertebrate-specific BK_{Ca} blocker, when individual pore residues are mutated to that found in the corresponding position in vertebrate *Slo* channels; these mutants include T290E in *Drosophila dSlo* (Myers and Stampe, 2000) and Q285K in cockroach *pSlo* (Derst *et al*, 2003) (Fig **8**.**1**). Thus, the amino acid variation in the pore region of the BK_{Ca} channel appears sufficient to explain the insect selectivity of κ-ACTX-Hv1c.

8.6 Design of a novel chemical insecticide

κ-ACTX-Hv1c represents the first spider toxin that is a selective, high-affinity blocker of insect BK_{Ca} channels, and as such validates insect BK_{Ca} channels as potential insecticide targets. The insect specificity of κ-ACTX-Hv1c also recommends this toxin as a lead for the development of a novel chemical insecticide. Given that κ-ACTX-Hv1c is active against a wide range of insects, including dipterans, coleopterans, dictyopterans, orthopterans and lepidopterans (Wang *et al*, 2000; Maggio and King, 2002; Tedford *et al*, 2007), suggests that insecticides that target BK channels may have a wide application in the control of arthropod pests. A full alanine-scan mutagenesis of κ-ACTX-Hv1c has led to the first complete mapping of an insect-selective toxin bioactive surface. Given the detailed knowledge of the relative spatial orientation of the critical residues with respect to each other provides an avenue for the proper design of a small molecule mimetic that preserves toxin activity. As such, the spatially restricted pharmacophore residues (Fig **4**.**2B**) in κ-ACTX-Hv1c embody an amenable framework for the rational design of a small molecule mimetic. Given that κ-ACTX-Hv1c has a 870-fold higher selectivity for insect BK_{Ca} channels than ChTX, this epitope should provide a valuable template for the design of small-molecule insecticides that selectively target insect BK_{Ca} channels.

Study of invertebrate BK_{Ca} channels would be enhanced by the availability of a readily-available, high-affinity blocker that is devoid of activity on other ion

channels. While ChTx and κ-ACTX-Hv1c block cockroach BK_{Ca} channels with similar affinity, κ-ACTX-Hv1c offers several potential advantages as a research tool for invertebrate studies. First, in addition to its block of BK_{Ca} channels, ChTx also blocks K_V channels with moderate affinity (Gao and Garcia, 2003). In contrast, even at very high concentrations, κ-ACTX-Hv1c has very limited activity against K_V channels. Second, a bacterial expression system has been developed that allows recombinant

κ-ACTX-Hv1c to be produced cheaply and easily (Maggio and King, 2002). Third, since the binding epitope for κ-ACTX-Hv1c has been mapped, point mutants that could be used for negative controls can be readily produced using this bacterial expression system.

κ-ACTX-Hv1c is active against a diverse range of insect phyla (Tedford *et al*, 2007) and therefore insecticides that target this channel might find wide application in the control of arthropod pests. The molecular epitope on this peptide toxin that mediates its interaction with insect BK_{Ca} channels comprises only five spatially proximal residues (this study and Maggio and King, 2002)). Since κ-ACTX-Hv1c has 870-fold higher selectivity for insect BK_{Ca} channels than ChTx, this epitope should provide a convenient template for the rational design of small-molecule insecticides that selectively target insect BK_{Ca} channels.

CHAPTER 9

THE 'HYBRID' TOXIN FW178

Australian funnel-web spider venoms, like *Conus* venoms, contain peptides that cause both hyperexcitability and decreased neurotransmission in the nervous system of prey. *Conus* venom proteomes appear to be organized into groups of peptides (cabals), with different effects, that work in concert to achieve a particular toxic phenotype (Olivera and Cruz, 2001, Olivera, 2002). For example it was shown that a combination of two different *Conus* peptides, when injected into fish, acted synergistically to elicit an instantaneous tetanic paralysis, whereas a single component did not cause such a rapid immobilization (Terlau, 1996). These toxins then form 'cabals' such as the 'lightning-strike' (excitatory) cabal (κ-, δ-conotoxins) and 'motor' (depressant) cabal (α-, μ-, ψ- and ω-conotoxins).

It is likely that such 'cabals' exist in spider venoms, including atracotoxins. Indeed κ-ACTX-Hv1 and δ-ACTX-1 are likely to form an analogous 'lightning-strike' cabal to that found in conus venoms. Theses two toxins are likely to act synergistically to prolong AP duration and increase spontaneous repetitive firing (Grolleau *et at*, 2001; Windley M and Nicholson GMN personal communication). In regards to the use of these peptides for insecticidal drug development, it would appear that simultaneous application of a pair or group of synergistic toxins would likely have greater effect then use of a single peptide. Unfortunately, though, developing such a delivery system for multiple peptides would be more problematic. The ideal solution therefore, would be the use of a single peptide that acted synergistically on multiple targets. The evidence provided in this thesis appears to indicate that the hybrid toxin FW178 functions in this manner.

The 'hybrid' toxin FW178 is a unique toxin that shares little sequence homology with other known atracotoxin. Interestingly however the pharmacophore of FW178 (Fig **4.11**) does contain elements of the pharmacophore of ω-ACTX-Hv1a and κ-ACTX-Hv1c. overlays The electrophysiological studies undertaken demonstrated that FW178 blocks Ca_V currents in cockroach DUM neurons as well as $K_{(Ca)}$ currents carried by *pSlo* channels with IC_{50} values of 409 nM and 671 nM respectively. FW178 therefore blocks cockroach Ca_V currents with about the same potency as ω-ACTX-Hv1a, while blocks cockroach *pSlo* channels with about a 4-fold lower potency than κ-ACTX-Hv1c.

FW178 used in these studies has an LD_{50} of 38 ± 3 pmol/g when injected into *M. domestica* when compared to the LD_{50} values for ω-ACTX-Hv1a (86.5 ± 1.3 pmol/g) and κ-ACTX-Hv1c (91 ± 5 pmol/g). This makes FW178 at least two-fold more potent than any other atracotoxin isolated from Australian funnel-web spiders. Despite this, FW178 only blocks cockroach Ca_V channels with a similar potency to ω-ACTX-Hv1a, and blocks cockroach $K_{(Ca)}$ with 4-fold *less* potency than κ-ACTX-Hv1c. Therefore the striking potency of FW178 must result from a synergistic effect on insect Ca_V and $K_{(Ca)}$ channels.

This may not be surprising given these channels are in fact physically associated in the membrane (Grunnet and Kaufman, 2004, Liu *et al*, 2004) and recent evidence suggests they are physiologically coupled (Spafford *et al*, 2005).

Not only does FW178 directly block the pore of insect $K_{(Ca)}$ channels, FW178 also enhances this action by indirectly reducing current through these channels by blocking the inward flow of calcium through Ca_V channels, thus resulting in a decrease in intracellular Ca^{2+} levels. As a result, $K_{(Ca)}$ channels fail to adequately function, rendering FW178 lethal. Therefore, FW178 appears to be synergistically acting on these two targets. This mode of action is supported by the excitatory phenotype induced upon injection into the housefly, *Musca domestica*, that is also observed following injection of κ-ACTX-Hv1c (Wang *et al*,

2000) and initially following injection of ω-ACTX-Hv1a or ω-ACTX-Ar1a (Chong *et al*, 2007).

FW178 appears to be insect-selective as it is lethal in *M. domestica*, has been shown to target Ca_V and BK_{Ca} channels in *P. Americana* and yet fails to modulate pre-synaptic and post-synaptic activity in the isolated chick biventer nerve-muscle preparation. However for insect-selectivity to be confirmed it is necessary to perform further *in vivo* and *in vitro* assays. This could include intracerebroventricular injections in newborn BALB/c mice or rat vas deferens bioassay. Furthermore the insect-selectivity of FW178 could only be confirmed by assessing activity against the mammalian analogs of *pSlo*, namely *mSlo* and *hSlo* as well as Ca_V channels from rat dorsal root ganglion.

Virus-expressed toxins can be synergistic with chemical pesticides by targeting different sites on the same channel. For example, the killing speed of recombinant baculovirus expressing scorpion toxin AaIT was further increased in the presence of low doses of pyrethroid (Popham *et al*, 1998).

Recently the coexpression of κ-ACTX-Hv1c and ω-ACTX-Hv1a in AcMNPV baculovirus has resulted in a decrease in the ET_{50} (time to 50% paralysis/death) of *H. virescens* larvae, as compared to expression of each toxin individually (Maggio, 2006). This proves that targeting distinct sites simultaneously enhances insecticidal activity.

In turn AcMNPV has been engineered to encode the insect-selective neurotoxin AaIT isolated from the venom of the scorpion *Androctonus australis*. Apon expression in the host this peptide produces neurological responses similar to that evoked by pyrethroid insecticides. It has been shown to be orally infective to the most economically important group of lpidopteran pests, the notuids which include genera such as *Heliothis, Trichoplusia* and *Spodoptera*. Finally the engineering of AcMNPV to express the key enzyme juvenile hormone esterase isolated from the cotton bollworm has proven highly effective (Inceoglu *et al*,

2000). This ability to use the insects own genes for control is particularly attractive environmentally.

The construction and apparent success of these genetically engineered baculoviruses represent a considerable advance in the continuing effort to develop a viable baculovirus for use as a pest control agent. The development of a more effective, faster-acting baculovirus could provide a novel agent for the pesticide arsenal including unique mode of action for combating resistant or selected pests.

The synergistic effects of low molecular mass substances with neurotoxins has been reported extensively by Ineoglu *et al* 2003, Wullschleger *et al*, 2004;2005. It has been shown that histamine and taurine facilitate the neurotoxic activity of CSTX-1 from *Cupiennius salei*. Accordingly it has been hypothesised that μ-agatoxins, which are disulfide-short peptides modifying Na_V channels, enhance the short-term action of α-agatoxins (acylpolyamines). The use of 'spreading factors' namely, cytolytic and enzymatic cofactors with neurotoxic peptides appears to enhance prey lethality. By using a combination of 'spreading factor' and neurotoxin expression in baculoviruses, may reduce the time to kill of the virus.

FW178 represents the first known dual-target self-synergizing spider toxin. This inherent ability makes FW178 an ideal insecticide not only because dual target synergy can provide an increased potency, but also in addition, simultaneous targeting of two ion channels drastically reduces the chance of insects evolving target-site resistance simultaneously in two distinct ion channels. Thus the hybrid toxin FW178 is an excellent lead compound for the development of a novel insecticide.

CHAPTER 10

REFERENCES

Achenbach H, Walther C and Wicher D (1997). Octopamine modulates ionic currents and spiking in dorsal unpaired median (DUM) neurons. *NeuroReport*. **8**: 3737-3741.

Adams ME, Bindakos VP, Hasegawa L and Venema VJ (1990). ω-agatoxins: Novel calcium channel antagonists of two subtypes from funnel-web spider (*Agelenopsis aperta*) venom. *Journal of Biological Chemistry*. **265**: 861-867.

Alessandri-Haber N, Lecoq A, Gasparini S, Granger-Macmath G, Jacquet G, Harvey AL, de Mederios C, Rowen EG, Gola M, Ménez A and Crest M (1999). Mapping the functional anatomy of BgK on $K_V1.1$, $K_V1.2$ and $K_V1.3$. Clues to design analogs with enhanced selectivity. *Journal of Biological Chemistry*. **274**: 35653-35661.

Albuquerque EX, Daly JW and Witkop B (1971). Batrachotoxin: Chemistry and pharmacology. *Science*. **172**: 995-1002.

Amat C, Lapied B, French AS and Hue B (1998). Na^+-dependent neuritic spikes initiate Ca^{2+}-dependent somatic plateau action potentials in insect dorsal paired median neurons. *Journal of Neurophysiology*. **80**: 2718-2726.

Anderson CS, Mackinnon R, Smith C and Miller C (1988). Charybdotoxin block of single Ca^{2+}-activated K^+ channels. Effects of channel gating, voltage, and ionic strength. *Journal of General Physiology*. **91**: 317-333.

Armstrong CM (1981). Sodium channels and gating currents. *Physiological Review*. **61**: 644-682.

Atkinson RK, Howden MEH, Tyler MI and Vonarx EJ (1993). Insecticidal toxins derived from funnel web (*Atrax* or *Hydronyche*) spiders. International patent application PCT/AU93/00039.

Atkinson RK, Vonarx EJ and Howden MEH (1996). Effects of whole venom and venom fractions from several Australian spiders, including *Atrax* (*Hadronyche*) species, when injected into insects. *Comparative Biochemistry and Physiology*. **114C:** 113-117.

Baell, JB, Harvey AJ and Norton RS (2002). Design and synthesis of type-III mimetics of ShK toxin. *Journal of Computer Aided Molecular Design*. **16**: 245-262.

Barchi RL (1988). Probing the molecular structure of the voltage-dependent sodium channel. *Annual Review of Neuroscience*. **11**: 455-495.

Benoit E, Legrand AM and Doboid Jm (1986). Effects of ciguatoxin on current and voltage-clamped frog myelinated nerve fibre. *Toxicon*. **24**: 357-364.

Benquet P, Le Guen J, Dayanithi Y, Pichon Y and Tiaho F(1999). ω-Aga-IVA-sensitive (P/Q)-type and –resistant (R-type) high-voltage activated Ca^{2+} currents in embryonic cockroach brain neurons. *Journal of Neurophysiology*. **82**: 2284-2293.

Benzinger GR, Kyle JW, Blumenthal KM and Hanck DA (1998). A specific interaction between the cardiac sodium channel and site-3 toxin anthopleurin. *Journal of Biological Chemistry*. **273**: 80-84.

Bergvinson D and Garcia-Lara S (2004). Genetic approaches to redusing losses of stored grain to insects and diseases. *Current Opinions in Plant Biology*. **7**: 480-485.

Bernard C, Corzo G, Mosbah A, Nakajima T and Darbon H (2001). Solution structure of Ptu1, a toxin from the assassin bug *Peirates turpis* that blocks the voltage-sensitive calcium channel N-type. *Biochemistry*. **40**: 12795-12800.

Bezanilla F and Armstrong CM (1972). Negative conductance caused by entry of sodium and cesium ions into the potassium channels of squid axons. *Journal of General Physiology*. **60**: 588-608.

Bezanilla F and Armstrong CM (1977). Inactivation of the sodium channel. I Sodium channel experiments. *Journal of General Physiology*. **70**: 549-566.

Bindakos VP and Adams ME (1989). ω-Aga-I: A presynaptic calcium channel antagonist from venom of the funnel-web spider, *Agelenopsis aperta*. *Journal of Neurobiology*. **20**: 171-188.

Bindakos VP, Venema VJ and Adams ME (1991). Differential antagonism of transmitter release by subtypes of the ω-agatoxins. *Journal of Neurophysiology*. **66**: 590-601.

Birinyi-Strachan LC (2002). The electrophysiology of Pacific-ciguatoxin-1 and Australian spider toxins. PhD Thesis, University of Technology, Sydney.

Blatz AL and Magleby KL (1986). Single apamin-blocked Ca^{2+}-activated K^+ channels of small conductance in cultured rat skeletal muscle. *Nature*. **323**: 718-720.

Bogan A and Thorn K (1998). Anatomy of hot spots in protein interfaces. *Journal of Biological Chemistry*. **280**: 1-9.

Bonning BC and Hammock BD (1996). Development of recombinant baculoviruses for insect control. *Annual Reviews in Entomology*. **41:** 191-210.

Bontems F, Roumestand C, Gilquin B, Ménez A and Toma F (1991). Refined structure of charybdotoxin: common motifs in scorpion toxins and insect defensins. *Science* **254**: 1521–1523.

Branton WD, Kolton YN Jan YN and Jan LY (1997). Neurotoxins from *Plectreurys* spider venom are potent presynaptic blockers in *Drosophila*.. *Journal of Neuroscience.* **7**: 4195-4200.

Bravo A, Gill SS and Soberón M (2007). Mode of action of *Bacillus thuringiensis* Cry and Cyt toxins and their potential for insect control. *Toxicon*. **49**: 423-435.

Brogdon WG and McAllister JC (1998). Insecticide resistance and vector control. *Emerging Infectious Disease*. **4**: 605-613.

Brown MR, Sheumack DD, Tyler MI and Howden MEH. (1988). Amino acid sequence of versutoxin, a lethal neurotoxin from the venom of the funnel-web spider *Atrax versutus. Biochemical Journal*. **250:** 401-405.

Brunet B (1996). *Spiderwatch: a guide to Australian spiders*, Reed Books, Melbourne, Australia.

Cahalan MD (1975). Modification of sodium channel gating in frog myelinated nerve fibers by *Centruroides sculpturatus* scorpion venom. *Journal of Physiology*. **244**: 511-534.

Carlini CR and Grossi-de-Sa MF (2002). Plant toxic proteins with insecticidal properties. A review on their potentialities as bioinsecticides. *Toxicon*. **40**: 1515-1539.

Catterall WA, Ray R and Morrow CS (1976). Membrane potential dependent binding of scorpion toxin to action potential Na^+ ionophore. *Proceedings of the National Academy of Sciences of the USA*. **73**: 2682-2686.

Catterall WA (1977). Activation of the action potential Na^+ ionophore by neurotoxins. An allosteric model. *Journal of Biological Chemistry*. **252**: 8667-8676.

Catterall WA (1979). Binding of scorpion toxin to receptor sites associated with sodium channels in frog muscle. *Journal of General Physiology*. **74**: 375-391.

Catterall WA (1980). Neurotoxins that act on voltage-sensitive sodium channels in excitable membranes. *Annual Review of Pharmacology and Toxicology*. **20**: 15-42.

Catterall WA (1988). Structure and function of voltage-sensitive ion channels. *Science*. **242**: 50-61.

Catterall WA (1992). Cellular and molecular biology of voltage-gated sodium channels. *Physiological Reviews*. **72**: S15-48.

Catterall WA (2000). From ionic currents to molecular mechanisms: The structure and function of voltage-gated sodium channels. *Neuron*. **26**: 13-25.

Catterall WA (2001). Structural biology: A 3D view of sodium channels. *Nature*. **409**: 988-989, 991.

Cestèle S, Qu Y, Rogers JC, Rochat H Scheuer T and Catterall WA (1998). Voltage sensor-trapping enhanced activation of sodium channels by beta scorpion toxin bound to the S3-S4 loop in domain II. *Neuron*. **21**: 919-931.

Cestèle S and Catterall WA (2000). Molecular mechanisms of neurotoxin action on voltage-gated sodium channels. *Biochimie*. **82**: 883-892.

Chahine M, Chen LQ, Fotouhi N, Walsky R, Fry D, Santarelli V, Horn R and Kallen RG (1995). Characterizing the mu-conotoxin biding site on voltage-sensitive sodium channels with toxin analogues and channel mutations. *Receptors and Channels*. **3**: 161-174.

Chakraborty S (1999). Biological pesticides: Bugs that reduce chemical pesticide use. *Australasian Science*. **June**: 22-24.

Chamberlain D and Stewart, CNJ (1999). Transgene escape and transplastomics. *Nature Biotechnology*. **17**: 330-331.

Chandler WK, Hodgkin AL and Meves H (1965). The effect of changing the internal solution on sodium inactivation and related phenomena in giant axons. *Journal of Physiology*. **180**: 821-836.

Chandy KG, DeCoursey TE, Fischbach M, Tala N, Cahalan MD and Gupta S (1986). Altered K^+ channel expression in abnormal T lymphocytes from mice with the lpr gene mutation. *Science*. **233**: 1197-1200.

Chen YH, Li MH, Zhang Y, He LL, Yamada Y, Fitzmaurice A, Shen Y, Zhang H, Tong L and Yang J (2004). Structural basis of the α_1-β subunit interaction of voltage-gated Ca^+ channels. *Nature*. **429**: 675-680.

Chong Y, Hayes JL, Sollod B, Wen S, Wilson D, Hains P, Hodgson WC, Broady KW, King GF and Nicholson GM (2007). The ω-atracotoxins: Selective blockers of insect M-LVA and HVA calcium channels.

Christie MJ, North RA, Osborne PB, Douglass J and Adelman JP (1990). Heteropolymeric potassium channels expressed in *Xenopus* oocytes from cloned subunits. *Neuron*. **4**: 405-411.

Chu P-J, Robertson HM and Best PM (2001). Calcium channel γ subunits provide insight into the evolution of this gene family. *Gene*. **280**: 37-48.

Cohen SA and Barchi RL (1993). Voltage-dependent sodium channels. *International Review of Cytology*. **137C:** 55-103.

Cole C and Warwicker J (2002).Side-chain conformational entropy at protein-protein interfaces. *Protein Science*. **11**: 2860-70.

Conti F, De Felice LJ and Wanke E (1975). Potassium and sodium ion current noise in the membrane of the squid giant axon. *Journal of Physiology*. **248**: 45-82.

Courand F, Rochat H and Lissitzki S (1978). Binding of scorpion and sea anemone neurotoxins to a common site related to the action potential Na^+ ionophore in neuroblastoma cells *Biochemistry and Biophysical Research Community*. **83**: 1525-1530.

Craik DJ, Daly NL and Waine C (2001). The cysteine knot structure of ion channel toxins and related polypeptides. *Toxicon*. **36**: 1573-1583.

Crawley MJ (1999) Bollworms, genes and ecologists. *Nature.* **400**: 501-502.

Crossman AR, Kerkut GA, Pitman RM and Walker RJ (1971). Electrically excitable nerve cell bodies in the central ganglia of two insect species *Periplaneta americana* and *Schistocerca gregaria*. Investigation of cell geometry and morphology by intracellular dye injection. *Comparative Biochemistry and Physiology*. **40A**: 579-594.

Cruz LJ, Gray WR, Olivera BM, Zeikus RD, Kerr L, Yoshikami D and Moczydlowski E (1985). *Conus geographus* toxins that discriminate between neuronal and muscle sodium channels. *Journal of Biological Chemistry*. **260**: 9280-9288.

Cui J, Cox DH and Aldrich RW (1997). Intrinsic voltage dependence and Ca^{2+} regulation of *mSlo* large conductance Ca-activated K^+ channels. *Journal of General Physiology*. **109**: 647-673.

Daly JC and Murray DAH (1988) Evolution of resistance to pyrethroids in *Helicoverpa armigera* (Hübner) (Lepidoptera: Noctuidae) in Australia. *Journal of Economic Entomology*. **81:** 984-988.

Dauplais M, Lecoq A, Song J, Cotton J, Jamin N, Gilquin B, Roumestand C, Vita C, de Medeiros CLC, Rowan EG, Harvey AL and Ménez A (1997). On the

convergent evolution of animal toxins. *Journal of Biological Chemistry*. **272**: 4302-4309.

De Jongh KS, Warner C and Catterall WA (1990). Subunits of purified calcium channels. α_1 and δ are encoded by the same gene. *Journal of Biological Chemistry*. **265**: 14738-14741.

Derst, C, Messutat S, Walther C, Eckert M, Heinemann H and Wicher D (2003). The large conductance Ca^{2+}-activated potassium channel (*pSlo*) of the cockroach *Periplaneta americana*: structure, localization in neurons and electrophysiology. *European Journal of Neuroscience*. **17**: 1197-1212.

De Waard M, Gurnett CA and Campbell KP (1996). Structural and functional diversity of voltage-activated calcium channels. *Ion Channels*. **4**: 41-87.

Doering CJ and Zamponi GW (2003). Molecular pharmacology of high voltage-activated calcium channels. *Journal of Bioenergetics and Biomembranes*. **35**: 491-505.

Dolphin AC (2003). β subunits of voltage-gated calcium channels. *Journal of Bioenergetics and Biomembranes*. **35**: 599-620.

Dong K (1997). A single amino acid change in the *para* sodium channel protein is associated with knockdown-resistance (kdr) to pyrethroid insecticides in German cockroach. *Insect Biochemistry and Molecular Biology*. **27**: 93-100.

Doyle DA, Cabral JM, Pfuetzner RA, Kuo A, Gulbis M, Cohen SL, Chait BT and Mackinnon R (1998). The structure of the potassium channel: Molecular basis of K^+ conduction and selectivity. *Science*. **280**: 69-77.

Dryden MW, Broce AB and Moore WE (1993). Severe flea infestation in diary calves. *J. Am. Veterinary Medical Association*. **203**: 1448-1452.

Dryer SE (1994). Na^+-activated K^+ channels: a new family of large-conductance ion channels. *Trends in Neuroscience*. **17**: 155-160.

Dunbar SJ and Pitman RM (1985). Unitary currents recorded from the soma of identified cockroach neurones using the patch-clamp technique. *Journal of Physiology*, *London*. **367**: 88P.

Dymond GR and Evans PD (1979). Biogenic amines in the nervous system of the cockroach, *Periplaneta americana*: association of octopamine with mushroom bodies and dorsal unpaired median (DUM) neurones. *Insect Biochemistry*. **9**: 535-545.

Eckert M, Rapus J, Nürnberger A and Penzlin H (1992). A new specific antibody reveals octopamine-like immunoreactivity in cockroach ventral nerve cord. *Journal of Comparative Neurology*. **322**: 1-15.

Eitan M, Fowler E, Herman R, Duval A, Pelhate M and Zlotkin E (1990). A scorpion venom neurotoxin paralytic to insects that affects sodium channel inactivation: purification, primary structure and mode of action. *Biochemistry*. **29**: 5941-5947.

Elia AJ and Gardner DR (1990). Some morphological and physiological characteristics of an identifiable dorsal unpaired median neurone in the

metathoracic ganglion of the cockroach *Periplaneta americana*. *Comparative Biochemistry and Physiology*. **95C**: 55-62.

Elkins T, Ganetzky B and Wu CF (1986). A *Drosophila* mutation that eliminates a calcium-dependent potassium current. *Proceedings of the National Academy of Sciences of the USA*. **83**: 8415-8419.

Evans PD (1985). Octopamine. In Kerkut GA, Gilbert LI (ed). *Comprehensive Insect Physiology, Biochemistry and* Pharmacology. **11**. Pergamon Press Oxford, pp 499-529.

Feng ZP, Doering CJ, Winkfein RJ, Beedle AM, Spafford JD and Zamponi GW (2003). Determinants of inhibition of transiently expressed voltage-gated calcium channels by ω-conotoxins GviA and MVIIA. *Journal of Biological Chemistry*. **278**: 20171-20178.

Fernandez A, Sosnick TR and Colubri A (2002). Dynamics of hydrogen bond desolvation in protein folding. *Journal of Molecular Biology*. **321**: 659-675.

Fernandez A and Scheraga HA (2003). Insufficiently dehydrated hydrogen bonds as determinants of protein interactions. *Proceedings of the National Academy of Sciences of the USA*. **100**: 113-118.

Fletcher JI, Chapman BE, Mackay JP, Howden MEH and King GF (1997a). The structure of versutoxin (δ-ACTX-Hv1a) provides insight into the binding of site 3 neurotoxins to the voltage-gated sodium channel. *Structure*. **5**: 1525-1535.

Fletcher JI, Smith R, O'Donoghue SI, Nilges M, Connor N, Howden MEH, Christie MJ and King GF (1997b). The structure of a novel insecticidal neurotoxin ω-atracotoxin-HV1, from the venom of an Australian funnel web spider. *Nature Structure Biology*. **4**: 559-566.

Fuhrman FA (1967). Tetrodotoxin. *Scientific American*. **217**: 60-71.

Gao YD and Garcia ML (2003). Interaction of agitoxin2, charybdotoxin and iberiotoxin with potassium channels: selectivity between voltage-gated and Maki-K channels. *Proteins*. **52**: 146-154.

Galvez A, Gimenez-Gallego G, Reuben JP, Roy-Contancin L, Feigenbaum P, Kaczorowski GJ and Garcia ML (1990). Purification and characterization of a unique, potent, peptidyl probe for the high conductance calcium-activated potassium channel from venom of the scorpion *Buthus tamulus*. *Journal of Biological Chemistry*. **265**: 11083-11090.

Ganetzky B (2000). Genetic analysis of ion channel dysfunction in *Drosophila*. *Kidney International*. **57**: 766-771.
Garcia ML, Galvez A, Garcia-Calvo M, King VF, Vazquez J and Kaczorowski GJ (1991). Use of toxins to study potassium channels. *Journal of Bioenergetics and Biomembranes*. **23**: 615-646.

Ghatta S, Nimmagadda D, Xu X and O;Rourke S (2005). Large-conductance calcium-activated potassium channels: Structural and functional implications. *Pharmacology and Therapeutics*. **110**: 103-116.

Gimenez-Gallego G, Navia MA, Reuben JP, Katz GM, Kaczorowski GJ and Garcia ML (1988). Purification, sequence, and model structure of charybdotoxin, a potent selective inhibitor of calcium-activated potassium channels. *Proceedings of the National Academy of Sciences of the USA*. **85**: 3329-3333.

Ginsberg BL and Warriner J (1960). The isolated chick biventer-cervicis nerve-muscle preparation. *British Journal of Pharmacology*. **15**: 410-411.

Goh JW and Pennefather PS (1987). Pharmacological and physiological properties of the after-hyperpolarization current of bullfrog ganglion neurones. *Journal of Physiology*. **394**: 315-330.

Goldin AL (2002). Evolution of voltage-gated Na$^+$ channels. *Journal of Experimental Biology*. **205**: 575-584.

Goldstein SA and Miller C (1993). Mechanism of charybdotoxin block of a voltage-gated K$^+$ channel. *Biophysical Journal*. **65**: 1613-1619.

Goldstein SA, Price LA, Rosenthal DN, Pausch MH (1996). ORK1, a potassium-selective leak channel with two pore domains cloned from *Drosophila melanogaster* by expression in *Saccharomyces cerevisiae*. *Proceedings of the National Academy of Sciences of the USA*. **93**: 13256-13261.

Goodman CS and Spitzer NC (1981a). The mature electrical properties of identified neurons in grasshopper embryos. *Journal of Physiology*, *London*. **313**: 385-403.

Gordan D and Zlotkin E (1993). Binding of an ∝-scorpion toxin to insect sodium channels is not dependent on membrane potential. *FEBS Letters*. **315**: 125-128.

Gordan D (1997). Molecular biology v-gated ionic channels: Structure-function relationships. In: *Principles of Medical Biology*, Volume 7A. Membranes and Cell signalling, pp 245-305.

Gordon D, Gilles N, Betrand D, Molgó J, Nicholson GM, Sauviat MP, Bwnoit E, Shichor I, Lotan I, Gurevitz M, Kallen RG and Heiniemann SH (2002). Scorpion toxins differentiate among neuronal sodium channel subtypes: Nature's guide for design of selective drugs. In: Ménez A, ed. Perspectives in Molecular Toxinology: John Wiley & Sons; 215-238.

Gray MR (1987). Distribution of the funnel-web spiders. In: *Toxic Plants and Animals: a Guide for Australia*, 1st Ed pp 313-321 (Covacevich J, Davie P and Pearn J, Eds) Queensland: Queensland Museum.

Grishin EV (1998). Black widow spider toxins: The present and the future. *Toxicon*. **36**: 1693-1701.

Grolleau F and Lapied B (1994). Transient Na+-activated K+ current in beating pacemaker isolated adult neurosecretory cells (DUM neurones). *Neuroscience Letters*. **167**: 46-50.

Grolleau F and Lapied B (1995a). Separation and identification of multiple potassium currents regulating the pacemaker activity of insect neurosecretory cells (DUM neurons). *Journal of Neurophysiology*. **73**: 160-171.

Grolleau F and Lapied (1995b). Evidence for the contribution of a novel low voltage-activated Ca^{2+} current in regulating pacemaker activity of insect neurosecretory cells. *Journal of Physiology*, (*London*). **489**: 67P.

Grolleau F and Lapied B (1996). Two distinct low-voltage-activated Ca^{2+} currents contribute to the pacemaker mechanism in cockroach dorsal unpaired median neurons. *Journal of Neurophysiology*. **76**: 963-976.

Grolleau F, Lapied B, Buckingham SD, Mason WT and Sattelle DB (1996). Nicotine increases [Ca^{2+}]$_i$ and regulates electrical activity in insect neurosecretory cells (DUM neurons) via an acetylcholine receptor with 'mixed' nicotinic-muscarinic pharmacology. *Neuroscience Letters*. **220**: 142-146.

Grolleau F and Lapied B (2000). Dorsal unpaired median neurones in the insect central nervous system: towards a better understanding of the ionic mechanisms

underlying spontaneous electrical activity. *Journal of Experimental Biology*. **203**: 1633-1648.

Grunnet M and Kaufman WA (2004). Co-assembly of big conductance Ca^{2+}-activated K^+ channels and L-type voltage-gated Ca^{2+} channels in rat brain. *Journal of Biological Chemistry*. **279**: 36445-36453.

Gubler, DJ (1998). Resurgent vector-borne diseases as a global health problem. *Emerging Infectios Disease*. **4**: 442-450.

Gundel M, Möbius P and Wicher D (1996). Different types of dorsal unpaired median (DUM) neurons in a cockroach abdominal ganglion. In *Göttingen Neurobiology Report* (ed. N. Elsner and H. U. Schnitzler), p. 606. Göettingen: Georg Thieme Verlag.

Gunning RV, Balfe ME and Easton CS (1992) Carbamate resistance in *Helicoverpa armigera* (Hübner) (Lepidoptera: Noctuidae) in Australia. *Journal of the Australian Entomological Society*. **31:** 97-103.

Gunning RV and Easton CS (1994) Endosulfan resistance in *Helicoverpa armigera* (Hübner) (Lepidoptera: Noctuidae) in Australia. *Journal of the Australian Entomological Society*. **33:** 9-12.

Guy HR and Seetharamulu P (1986). Molecular model of the action potential sodium channel. *Proceedings of the National Academy of Sciences of the USA*. **83**: 508-512.

Guy HR and Conti F (1990). Pursuing the structure and function of voltage-gated channels. *Trends in Neuroscience*. **13**: 201-206.

Habermann E (1972). Bee and wasp venoms. *Science*. **177**: 314-322.

Habermann E (1984). Apamin. *Pharmacology and Therapeutics*. **25**: 255-270.

Hagiwara S, Ozawa S and Sand O (1975). Voltage clamp analysis of two inward current mechanisms in the egg cell membrane of a starfish. *Journal of General Physiology*. **65**: 617-644.

Hamill OP, Marty A, Neher E, Sakmann B and Sigworth F (1981). Improved patch-clamp techniques for high-resolution current recording from cells and cell-free membrane patches. *European Journal of Physiology*. **391**: 85-100.

Hanner M, Schmalhofer WA, Munjos P, Knaus HG, Kaczorowski and Garcia ML (1997). The β-subunit of the high-conductance calcium-activated potassium channel contributes to the high-affinity receptor for charybdotoxin. *Proceedings of the National Academy of Sciences of the USA*. **94**: 2853-2858.

Hartshorne RP and Catterall WA (1981). Purification of the saxitoxin of the sodium channel from rat brain. *Proceedings of the National Academy of Sciences of the USA*. **78**: 4620-4624.

Hartshorne RP, Messner DJ, Coppersmith JC and Catterall WA (1982). The saxitoxin receptor of the sodium channel from rat brain. Evidence for two non-identical beta subunits. *Journal of Biological Chemistry*. **257**: 13888-13891.

Hasson A, Fainzilber M, Gordon D, Zlotkin E and Spira ME (1993). Alteration of sodium currents by new peptide toxins from the venom of *Molluscivorous Conus* snail. *European Journal of Neuroscience*. **5**: 56-64.

Heine M and Wicher D (1998). Ca^{2+} resting current and Ca^{2+}-induced Ca^{2+} release in insect neurosecretory neurons. *NeuroReport* **9**: 3309-3314.

Hermann A and Erxleben C (1987). Charybdotoxin selectively blocks small Ca-activated K channels in *Aplysia* neurons. *Journal of General Physiology*. **90**: 27-47.

Hille B (1971). The hydration of sodium ions crossing the nerve membrane. *Proceedings of the National Academy of Sciences of the USA*. **68**: 280-282.

Hille B (1972). The permeability of the sodium channel to metal cations in myelinated nerve. *Journal of General Physiology*. **59**: 637-658.

Hille B (1992). *Ionic Channels ofr Excitable Membranes* (ed. B Hille). Massachusetts: Sinauer. 607P.

Hirschberg B, Rovner A, Lieberman M and Patlak J (1995). Transfer of twelve charges is needed to open skeletal muscle Na^+ channels. *Journal of General Physiology*. **106**: 1053-1068.

Hodgkin AL and Huxley AF (1952). A quantitative description of membrane current and its application to conduction and excitability in nerve. *Journal of Physiology*. **117**: 500-544.

Holly JR, Popham, Yonghong w and Miller LK (1997). Genetic improvement of *Helicoverpa* zea nuclear polyhedrosis virus as a biopesticide. *Biological Control*. **10**: 83-91.

Hoover K, Herrmann R, Moskowitz, H, Bonning BC, Duffy SS, McCutchen BF and Hammock BD (1996). The potential of recombinant baculoviruses as enhanced bioinsecticides. *Pesticide Outlook*. **7**(3): 21-27.

Hoyle G (1974). A function for neurons (DUM) neurosecretion on skeletal muscle of insects. *Journal of Experimental Zoology*. **189**: 401-406.

Hoyle G and Dagan D (1978). Physiological characteristics and reflex activation of DUM (octopaminergic) neurons of locust metathoracic ganglion. *Journal of Neurobiology*. **9**: 59-79.

Huang JMC, Wu CH and Baden DG (1984). Depolarizing action of redtide dinoflagellate brevetoxin on axonal membranes. *Journal of Pharmacology and Experimental Therapeutics*. **299**: 615-621.

Hwang DF, Tai KP, Chueh CH, Lin LC and Jeng SS (1991). Tetrodotoxin and derivatives in several species of the gastropod Naticidae. *Toxicon*. **29**: 1019-1024.

Inceoglu AB, Kamita SG, Hinton AC, Huang Q, Severson TF, Kang B-d and Hammock BD (2000). Recombinant baculoviruses for insect control. *Pest Management Science*. **57**: 981-987.

Inceoglu B, Lango J, Jing J, Chen L, Doymaz F, Pessah IN and Hammock BD (2003). One scorpion, two venoms: prevenom of *Parabuthus transvaalicus* acts as an alternative type of venom with distinct mechanism of action. *Proceedings of the National Academy of Sciences of the USA*. **100**: 922-927.

Isom LL and Catterall WA (1996). Na$^+$ channel subunits and Ig domains. *Nature*. **383**: 307-308.

Isom LL (2001). Sodium channel β-subunits: Anything but auxiliary. *The Neuroscientist*. **7**: 42-53.

Jiang Y, Pico A, Cadene M, Chait BT and Mackinnon R (2001). Structure of the RCK domain from the *E. coli* K$^+$ channel and demonstration of its presence in the human BK channel. *Neuron*. **29**: 593-601.

Jover E, Courand F and Rochat H (1980). Two types of scorpion neurotoxins characterized by their binding to two separate receptor sites on rat brain synaptosomes. *Biochemistry and Biophysics Research Communications*. **95**: 1607-1614.

Jonas P, Vogel W, Arantes EC and Giglio JR (1986). Toxin gamma of the scorpion *Tityus serrulatus* modifies both activation and inactivation of sodium permeability of nerve membrane. *European Journal of Physiology*. **407**: 92-99.

Kalapothakis E, Penaforte CL, Beláro PSL, Romano-Silva MA, Cruz JS, Prado MM, Gulmareaes P, Gomez MV and Prado VF (1998). Cloning of cDNAs encoding neurotoxic peptides from the spider Phoneutria nigriventer. Toxicon. 36: 1843-1850.

Kellenberger S, West JW and Catterall WA (1997) Molecular analysis of the putitive inactivation particle in the inactivation gate of brain type IIA Na$^+$ channels. *Journal of General Physiology*. **36**: 12554-125549.

Kim JL, Konishi S, Iwai H, Kohno T, Gouda H, Shimada I, Sato K and Arata Y (1995). Three-dimensional solution structure of the calcium channel antagonist ω-agatoxin-IVA; consensus molecular folding of calcium channel blockers. *Journal of Molecular Biology*. **250**: 659-671.

King G, Tedford H and Maggio F (2002). Structure and function of insecticidal neurotoxins from Australian funnel-web spiders. *Journal of Toxicology*-toxin reviews. **21**: 359-389.

King GF, Escoubas P and Nicholson GM (2008). Peptide toxins that selectively target insect Na$_V$ and Ca$_V$ channels. *Channels*. **2**: 1-17.

King GF (2007). Modulation of insect Ca$_V$ channels by peptidic spider toxins. *Toxicon*. **49**: 513-530.

Kloppenburg P and Hörner M (1998). Voltage-activated currents in identified giant interneurons isolatd from adult crickets *Gryllus bimaculatus*. *Journal of Experimental Biology*. **201**: 2529-2541.

Kobayashi K, Sasaki T, Sato K and Kohno T (2000). Three-dimensional solution structure of ω-conotoxin TxVII, an L-type calcium channel blocker. *Biochemistry*. **39**: 14761-14767.

Koradi R, Billeter M and Wüthrich K (1996). MOLMOL: a program for display and analysis of macromolecular structures. *Journal of Molecular Graphics*. **14**: 51-55.

Kostyuk PG (1999). Low-voltage activated calcium channels: Achievements and problems. *Neuroscience*. **92**: 1157-1163.

Krezel A, Kasibhatla C, Hidalgo P, Mackinnon R and Wagner G (1995). Solution structure of the potassium channel inhibitor agitoxin-2: caliper for probing channel geometry. *Protein Science*. **4**: 1478-1489.

Lapied B, Malecot CO and Pelhate M (1989). Ionic species involved in the electrical activity of single adult aminergic neurons isolated from the sixth abdominal ganglion of the cockroach *Periplaneta americana*. *Journal of Experimental Biology*. **144**: 535-550.

Lapied B, Le Corronc H and Hue B (1990a). Sensitive nicotinic and mixed nicotinic-muscarinic receptors in insect neurosecretory cells. *Brain Research*. **533**: 132-136.

Lapied B, Malecot CO and Pelhate M (1990b). Patch-clamp study of the properties of the sodium current in cockroach single isolated adult aminergic neurons. *Journal of Experimental Biology*. **151**: 387-404.

Lapied B, Stankiewicz M, Grolleau F, Rochat H, Zlotkin E and Pelhate M (1999). Biophysical properties of scorpion α-toxin-sensitive background sodium channel contributing to the pacemaker activity in insect neurosecretory cells (DUM neurons). *European Journal of Neuroscience*. **11**: 1449-1460.

Latorre R, Oberhauser A, Labarca P and Alvarez (1989). Varieties of calcium-activated potassium channels. *Annual Review of Physiology*. **51**: 385-399.

Lesage F, Guillemare E, Fink M, Duprat F, Lazdunski M, Romey G and Barhanin J (1996). A pH-sensitive yeast outward rectifier K^+ channel with two pore domains and novel gating properties. *Journal of Biological Chemistry*. **271**: 4183-4187.

Leung HT, Branton WD, Phillips HS, Jan L and Byerly L (1989). Spider toxins selectively block calcium currents in *Drosophila*. *Neuron*. **3**: 767-772.

Lew MJ, Flinn JP, Pallaghy PK, Murphy R, Whorlow SL, Wright CE, Norton RS and Angus JA (1997). Structure-function relationships of ω-conotoxin GVIA. *Journal of Biological Chemistry*. **272**: 12014-12023.

Li C, Gloer JB, Wicklow DT and Dowd PF (2002). Thiersinines A and B: novel antiinsectan indole diterpenoids from a new fungicolous *Penicillium* species (NRRL 28147). *Organic Letters*. **4**: 3095-3098.

Li C, Gloer JB, Wicklow DT and Dowd PF (2005). Antiinsectan decaturin and oxalicine analogues from *Penicillium thiersii*. *Journal of Natural Products*. **68**: 319-322.

Linford NJ, Cantrell AR, Qu Y, Scheuer T and Catterall WA (1998). Interaction of batrachotoxin with the local anesthetic receptor site in transmembrane segment IVS6 of the voltage-gated sodium channel. *Proceedings of the National Academy of Sciences of the USA*. **95**: 13947-13952.

Lingle CJ, Zeng XH, Ding JP, and Xia XM (2001). Inactivation of BK channels mediated by the NH_2 terminus of the β3b auxiliary subunit involves a two-step mechanism: possible separation of binding and blockade. *Journal of General Physiology.* **117**: 583–606.

Little MJ, Wilson H, Zappia C, Cestèle S, Tyler MI, Martin-Eauclaire M-F, Gordon D and Nicholson GM (1998a). δ-Atracotoxins from Australian funnel-web spiders compete with scorpion α-toxin binding on both rat brain and insect sodium channels. *FEBS Letters*. **439:** 246-252.

Little MJ, Zappia C, Gilles N, Connor M, Tyler MI, Martin-Eauclaire M-F, Gordon D and Nicholson GM (1998b). δ-Atracotoxins from Australian funnel-web spiders compete with scorpion α-toxin binding but differentially modulate alkaloid toxin activation of voltage-gated sodium channels. *Journal of Biological Chemistry*. **273:** 27076-27083.

Littleton JT and Ganetzky B (2000). Ion channels and synaptic organization: analysis of the *Drosophila* genome. *Neuron*. **26**: 35-43.

Liu YB, Tabashink BE, Dennehy TJ, Patin AL and Bartlett AC (1999). Development time and resistance to *Bt* crops. *Nature*. **400**: 519.

Liu G, Shi J, Yang L, Luxiang C, Park SM, Cui J and Marx SO (2004). Assembly of a Ca^{2+}-dpendent BK channel signaling complex by binding to β2 adrenergic receptor. *European Molecular Biology Organization*. **23**: 2196-2205.

Losey JE, Rayor LS and Carter ME (1999). Transgenic pollen harms monarch larvae. *Nature*. **399**: 214.

Loughney K, Kreber R and Ganetsky B (1989). Molecular analysis of the *para* locus, a sodium channel gene in *Drosophila*. *Cell*. **58**: 1143-1154.

Mackinnon R, Heginbotham L and Abramson T (1990). Mapping the receptor site for charybdotoxin, a pore-blocking potassium channel inhibitor. *Neuron*. **5**: 767-771.

Mackinnon R (1991). Using mutagenesis to study potassium channel mechanisms. *Journal of Bioenergetics and Biomembranes*. **23**: 647-663.

Mackinnon R, Cohen SL, Kuo A, Lee A and Chait BT (1998). Structural conservation in prokaryotic and eukaryotic potassium channels. *Science*. **280**: 106-109.

Maeda S and Hammock BD (1993). Recombinant baculoviruses expressing foreign genes for insect pest control. In: *Pest Control with Enhanced Environmental Safety.* (Duke SO, Menn JJ and Plimmer JR, Eds) pp. 281-297, American Chemical Society, Washington, DC., USA.

Maggio F and King GF (2002a). Role of the structurally disordered N- and C-terminal residues in the Janus-faced atracotoxins. *Toxicon*. **40**: 1355-1361.

Maggio F and King (2002b). Scanning mutagenesis of a Janus-faced atracotoxin reveals a bipartite surface patch that is essential for neurotoxic function. *Journal of Biological Chemistry*. **277**: 22806-22813.

Maggio F, Sollod BL, Tedford HW and King GF (2005). Spider toxins and their potential for insect control. In *Comprehensive Molecular Insect Science* (Gilbert LI. Iatrou K & Gill SS, eds). Pp 221-238. Elsevier.

Maggio F (2006). PhD Thesis. Department of Molecular, Microbial and Structural Biology, University of Connecticut Health Center, Farmington, Connecticut USA.

McCutchen BF, Choudary PV, Crenshaw R, Maddox D, Kamita SG, Palekar N, Volrath S, Fowler E, Hammock BD and Maeda S (1991). Development of a recombinant baculovirus expressing an insect-selective neurotoxin: potential for pest control. *Bio/Technology*. **9**: 848-852.

McMillian LK, Carr RL, Young CA, Astin JW, Lowe RG, Parker EJ, Jameson GB, Finch SC, Miles CO, McManus OB, Schmalhofer WA, Garcia ML, Kaczorowski GJ, Goetz M, Tkacz JS and Scott B (2003). Molecular analysis of two cytochrome P450 monooxygenase genes required for paxilline biosynthesis in *Penicillium paxilli* and effects of paxilline intermediates on mammalian maki-K ion channels. *Molecular Genetics and Genomics*. **270**: 9-23.

Mebs D and Schmidt K. Occurrence of tetrodotoxin in the frog *Atelopus oxyrhynchus*. *Toxicon*. **27**: 819-822.

Meera P, Waller M, Jiang Z and Toro L (1996). A calcium switch for the functional coupling between alpha (hslo) and beta subunits (KV, Ca beta) of maxi K channels. *FEBS Letters*. **382**: 84-88.

Meera P, Wallner M, Song M and Toro L (1997). Large conductance voltage- and calcium-dependent K$^+$ channel, a distinct member of voltage-dependent ion channels with seven N-terminal transmembrane segments (S0-S6), an extracellular N terminus, and an intracellular (S9-S10) C terminus. *Proceedings of the National Academy of Sciences of the USA*. **94**: 14066-14071.

Menzler S, Bikker JA, Suman-Chauhan N and Horwell DC (2000). Design and biological evaluation of non-peptide analogous of ω-conotoxin MVIIA. *Bioorganic & Medicinal Chemistry Letters*. **10**: 345-347.

Miller C, Moczydloski E, Latorre R and Phillpis M (1992). Charybdotoxin, a protein inhibitor of single Ca^{2+}-acdtivated K^+ channels from mammalian skeletal muscle. *Nature*. **313**: 316-318.

Moczydlowski E and Latorre R (1983). Gating kinetics of Ca^{2+}-activated potassium channels from rat muscle incorporated into planar lipid bilayers: evidence for two voltage-gated Ca^{2+} binding reactions. *Journal of General Physiology*. **82**: 511-542.

Moczydlowski E, Olivera BM, Gray WR and Strichartz GR (1986). Discrimination of muscle and neuronal sodium channel subtypes by binding competition between [³H]saxitoxin and μ-conotoxins. *Proceedings of the National Academy of Sciences of the USA*. **83**: 5321-5325.

Morais-Cabral JH, Zhou Y and MacKinnon R (2001). Energetic optimization of ion conduction rate by the K^+ selectivity filter. *Nature*. **414**: 37-42.

Moscardi F (1999). Assessment of the application of the baculoviruses for control of Lepidoptera, *Annual Reviews in Entomology*. **44:** 257-289.

Myers MP and Stampe P (2000). A point mutation in the maxi-K clone *dSlo* forms a high affinity site for charybdotoxin. *Neuropharmacology*. **39**: 11-20.

Nadasdi L, Yamashiro D, Chung D, Tarczy-Homoch K, Adriaenssens P and Ramchandran J (1995). Structure-activity analysis of a conus peptide blocker of N-type neuronal calcium channels. *Biochemistry*. **34**: 8076-8081.

Narahashi T, Moore JW and Scott WR (1964). Tetrodotoxin blockage of sodium conductance increase in lobster giant axons. *Journal of General Physiology*. **47**: 965-974.

Narahashi T (1974). Chemicals as tools in the study of excitable membranes. *European Journal of Physiology*. **399** 813-889.

Nasonkin, I, Alikasifoglu A, Ambrose C, Cahill P, Cheng M, Sarniak A, Egan M and Thomas PM (1999). A novel sulfonylurea receptor family member expressed in the embryonic *Drosophila* dorsal vessel and tracheal system. *Journal of Biological Chemistry*. **274**: 29420-29425.

Nichols CG and Lopatin AN (1997). Inward rectifier potassium channels. *Annual Review of Physiology*. **59**: 171-191.

Nicholson GM, Willow W, Howden ME and Narahashi T (1994). Modification of sodium channel gating and kinetics by versutoxin from the Australian funnel-web spider *Hydronyche versuta*. *European Journal of Physiology*. **428**: 400-409.

Nicholson GM, Walsh R, Little MJ and Tyler MI (1998). Characterisation of the effects of robustoxin, the lethal neurotoxin from the Sydney funnel-web spider *Atrax robustus*, on sodium channel activation and inactivation. *European Journal of Physiology*. **436**: 117-126.

Nicholson GM, Little M and Birinyi-Strachan L (2004). Structure and function of δ-atracotoxins: lethal neurotoxins targeting the voltage-gated sodium channel. *Toxicon*. **43**: 587-599.

Nicholson GM (2007). Insect-selective spider toxins targeting voltage-gated sodium channels. *Toxicon*. **49**: 490-512.

Noda M, Shimuzu S, Tanabe T, Takai T, Kayano T, Ikeda T, Takahashi H, Nakayama H, Kanaoka Y, Minamino N, Kangawa K, Matsuo H, Raftery M, Hirose T, Inayama S, Hayashida H, Miyata T and Numa S (1984). Primary structure of Electrophorous electricus sodium channel deduced from cDNA sequence. *Nature*: **312**: 121-127.

Noda M, Ikeda T, Kayano T, Suzuki H, Takeshima H, Kurasaki M, Takahashi H and Numa S (1986). Existence of distinct sodium channel messenger RNAs in rat brain. *Nature*: **320**: 188-192.

Noda M, Suzuki H, Numa S and Stühmer W (1989). A single point mutation confers tetrodotoxin and saxitoxin insensitivity on the sodium channel II. *FEBS Letters*. **259**: 213-216.

Norton R and Pallaghy P (1998). The cysteine knot structure of ion channel toxins and related polypeptides. *Toxicon*. **36**: 1573-1583.

Novotny V, Basset Y, Miller SE, Weiblen GD, Bremer B, Cizek L and Drozd P (2002). Low host specificity of herbivorous insects in a tropical forest. *Nature*. **416**: 841-844.

Oerke E-C and Dehne H-W (2004). Safeguarding production-losses in major crops and the role of crop production. *Crop Protection*. **23**: 275-285.

Oliveria BM, River J, Scott JK, Hilyard DR and Cruz LJ (1991). Conotoxins. *Journal of Biological Chemistry*. **266**: 22067-22070.

Olivera BM, Miljanich GP, Ramachandran J and Adams ME (1994). Calcium channel diversity and neurotransmitter release: The ω-conotoxins and ω-agatoxins. *Annual Review of Biochemistry*. **63**: 823-867.

Olivera BM and Cruz LJ. Conotoxins, in retrospect (2001). *Toxicon*. **39**: 7-14.

Olivera BM (2002). Conus venom peptides: Reflections from the biology of Clades and Species. *Annual review of ecological systems*. **33**: 25-47.

Pallaghy PK, Alewood D, Alewood PF and Norton RS (1997). Solution structure of robustoxin, the lethal neurotoxin from the funnel-web spider A*trax robustus*. *FEBS Letters.* **419:** 191-196.

Park CS and Miller C (1992). Interaction of charybdotoxin with permeant ions inside the pore of a K$^+$ channel. *Neuron*. **9**: 307-313.

Pelhate M, Pichon Y and Beadle DJ (1990). Cockroach axons and cell bodies: Electrical activity. In *Cockroaches as Models for Neurobiology: Applications in Biomedical Research* (ed. I Huber, EP Masler and BR Rao), pp 131-148. Boca Raton, FL: CRC Press.

Popham HJR, Li Y and Miller LK (1998). Genetic improvement of a Helicoverpa zea nuclear polyhedrosis virus as a biopesticide. *Biological Control.* **10**: 83-91.

Possani LD, Selisko B and Gurrola GB (1999). Structure and function o scorpion toxins affecting K$^+$ channels. *Perspectives in Drug Discovery and Design.* **15**: 15-40.

Price M, Lee SC and Deutsch C (1989). Charybdotoxin inhibits proliferation and interleukin 2 production in human peripheral blood lymphocytes. *Proceedings of the National Academy of Sciences of the United States of America*. **86**: 10171-10175.

Ramaswami M and Tanouye MA (1989). Two sodium-channel genes in *Drosophila*: implications for channel diversity. *Proceedings of the National Academy of Sciences (USA)*. **86**: 2079-2082.

Rauer H, Lanigan MD, Pennington MW, Aiyar J, Ghanshani S, Cahalan MD and Norton RS (2000). Structure-guided transformation of charybdotoxin yields an analog that selectively targets Ca^{2+}-ativated over voltage-gated K^+ channels. *Journal of Biological Chemistry*. **275**: 1201-1208.

Raymond V and Lapied (1999b). Hyperpolarized-activated inward potassium and calcium-sensitive chloride currents in beating pacemaker insect neurosecretory cells (dorsal unpaired median neurons). *Neuroscience*. **93**: 1207-1218.

Raymon-Delpech V, Matsuda K, Sattelle BM, Rauh JJ and Sattelle DB (2005). Ion channels: molecular targets of neuroactive insecticides. **5**: 119-133.

Rogawski MA (1985). The A-current: how ubiquitous a feature of excitable cells is it?. *Trends in Neurosciences*. **8**: 214-219.

Rogers JC, Qu Y, Tanada TN, Scheuer T and Catterall WA (1996). Molecular determinants of high affinity binding of α-scorpion toxin and sea anemone toxin in the S3-S4 extracellular loop in domain IV of the Na^+ channel α-subunit. *Journal of Biological Chemistry*. **271**: 15950-15960.

Roush RT and Shelton AM (1997). Assessing the odds: The emergence of resistance to *Bt* transgenic plants. *Nature Biotechnology*. **15**, 816-817.

Rudy B (1988). Diversity and ubiquity of K channels. *Neuroscience*. **25**: 729-749.

Sato K, Ishida Y, Wakamatsu K, Kato R, Honda H, Ohizumi Y, Nakamura H, Ohya M, Lancelin JM and Kohda D (1991). Active site of μ-conotoxin GIIIA,

apeptide blocker of muscle sodium channels. *Journal of Biological Chemistry*. **266**: 16989-16991.

Sato S, Nakamura H, Ohizumi Y, Kobayashi J and Hirata Y (1983). The amino acid sequences of homologous hydroxyproline-containing myotoxins from the marine snail *Conus geographus* venom. *FEBBS Letters*. **155**: 77-280.

Sato K, Ishida Y, Wakamatsu K, Kato K, Honda H, Ohizumi Y, Nakamura H, Ohya M, Lancelin JM, Kohda D and Inagaki F (1991). Active site of mμ-conotoxin GIIIA, a peptide blocker of muscle sodium channels. *Journal of Biological Chemistry*. **266**: 16989-16991.

Schäfer S, Rosenboom H and Menzel R (1994). Ionic currents of Kenyon cells from the mushroom body of the honeybee. *Journal of Neuroscience*. **14**: 4600-4612.

Schantz EJ (1986). Chemistry and biology of saxitoxin and related toxins. *Annuals of the New York Academy of Sciences*. **479**: 15-23.

Schopperle WM, Holmqvist MH, Zhou Y, Wang J, Wang Z, Griffith LC, Keselman I, Kusinitz F, Dagan D and Levitan IB (1998).Slob, a novel protein that interacts with the slowpoke calcium-dependent potassium channel. *Neuron .***20**: 565-573.

Schweitz H, Stansfeld CE, Bidard JN, Fagni L, Maes P and Lazdunski M (1989). Charybdotoxin blocks dendrotoxin-sensitive voltage-activated K$^+$ channels. *FEBS Letters*. **250**: 519-522.

Sheets ME, Kyle Jw, Kallen RG and Hanck DA (1999). The Na channel voltage sensor associated with inactivation is localized to the external charged residues of domain IV, S4. *Biophysical Journal*. **77**: 747-757.

Sheumack DD, Claassens R, Whiteley NM and Howden MEH (1985). Complete amino acids sequence of a new type of lethal neurotoxin from the venom of the funnel-web spider *Atrax robustus. FEBS Letters*. **181:** 154-156.

Sigworth FJ (1980). The conductance of sodium channels under conditions of reduced current at the node of Ranvier. *Journal of Physiology*. **307**: 131-142.

Singh S and Wu CF (1990). Properties of potassium currents and their role in membrane excitability in *Drosophila* larval muscle fibres. *Journal of Experimental Biology*. **152**: 59-76.

Skinner WS, Dennis PA, Li SP and Quistad GB (1992). Identification of insecticidal peptides from venom of the trapdoor spider, *Aptostichus schlingeri* (Ctenizidae) *Toxicon*. **30**(9), 1043-1050.

Sollod B (2006). From venoms to insecticides: exploring the structure, function, and evolution of peptide toxins found in the venom of Australian funnel-web spiders. PhD Thesis, Department of Molecular, Microbial and Structural Biology, University of Connecticut Health Center, Farmington, Connecticut USA.

Song W, Liu Z, Tan J, Nomura Y and Dong K (2004). RNA editing generates tissue-specific sodium channels with distinct gating properties. *Journal of Biological Chemistry*. **279**: 32554-32561.

Spafford JD, Dunn T, Smit AB, Syed NI and Zamponi GW (2005). *In vitro* characerization of L-type calcium channels and their contribution to firing behaviour in invertebrate respiratory neurons. *Journal of Neurophysiology*.

Stampe P, Kolmakova-Partensky L and Miller C (1994). Intimations of K^+ channel structure from a complete functional map of the molecular surface of charybdotoxin. *Biochemistry* **33**: 443–450.

Stoya G, Agricola H, Eckert M and Penzlin H (1989). Investigations on the innervation of the oviduct muscle of the cockroach, *Periplaneta americana* (L.). *Zoologie Jahrbuch Physiologie*. **93**: 75-86.

Strong PN, Weir SW, Beech DJ, Hiestand P and Kocher HP (1989). Effects of potassium channel toxins from *Leiuris quinbquestriatus hebraeus* venom on responses to cromakalin in rabbit blood vessels. *British Journal of Pharmacology*. **98**: 817-826.

Sutherland SK (1990). Treatment of arachnid poisoning in Australia. *Australian Family Physician.* **19**: 47-61.

Swartz KJ (2007). Tarantula toxins interacting with voltage sensors in potassium channels. *Toxicon*. **49**: 213-230.

Szeto TH, Birinyi-Strachan LC, Smith R, Connor M, Christie MJ, King GF and Nicholson GM (2000). Isolation and pharmacological characterisation of δ-atracotoxin-Hv1b, a vertebrate-selective sodium channel toxin. *FEBS Letters*. **470**(3): 293-9.

Tanaka Y and Washio H (1988). Morphological and physiological properties of the dorsal unpaired median neurons of the cockroach metathoracic ganglion. *Comparative Biochemistry and Physiology*. **91A**: 37-41.

Tedford HW, Fletcher JI and King GF (2001). Functional significance of the β-hairpin in the insecticidal neurotoxin ω-atracotoxin-Hv1a. *Journal of Biological Chemistry*. **276**: 26568-26576.

Tedford HW, Gilles N, Ménez A, Doering CJ, Zamponi GW and King GF (2004a), Scanning mutagenesis of ω-atracotoxin-Hv1a reveals a spatially restricted

epitope that confers selectivity against insect calcium channels. *Journal of Biological Chemistry*. **279**: 44133-44140.

Tedford HW, Sollod BL, Maggio F and King GF (2004b). Australian funnel-web spiders: master insecticide chemists. *Toxicon*. **43**: 601-618.

Tedford HW, Maggio F, Reenan RA and King GF (2007). A model genetic for testing the *in vivo* function of peptide toxins. *Peptides*. **28**: 51-56.

Tempel BL, Papazian DM, Schwartz TL, Jan YN and Jan LY (1987). Sequence of a probable potassium channel component encoded at *Shaker* locus of *Drosophila*. *Science*. **237**: 770-775.

Terlau H, Heineman SH, Stühmer W, Imoto K and Numa S (1991). Mapping the site of block by tetrodotoxin and saxitoxin on sodium channel II. *FEBS Letters*. **293**: 93-96.

Terlau H (1996). Stratergy for rapid immobilization of prey by a fish-hunting marine snail. *Nature*. **381**: 148-151.

Terlau H, Boccaccio A, Olivera BM and Conti F (1999). The block of *Shaker* K^+ channels by κ-conotoxin PVIIA is state dependent. *Journal of General Physiology*. **114**: 125-140.

Thomas MV (1984). Voltage-clamp analysis of a calcium-mediated potassium conductance in cockroach (*Periplaneta americana*) central neurones. *Journal of Physiology*, *London*. **350**: 159-178.

Tian L, Coghill LS, Macdonald SH, Armstrong DL and Shipston MJ (2003). Leucine zipper domain targets cAMP-dependent protein kinase to mammalian BK channels. *Journal of Biological Chemistry*. **278**: 8669-8677.

Timpe LC, Schwarz TL, Tempel BL, Papazian DM, Jan YN and Jan LY (1988). Expression of functional potassium channels from Shaker cDNA in *Xenopus* oocytes *Nature*. **331**: 143-145.

Triggle DJ (1999). The pharmacology of ion channels: with particular reference to voltage-gated Ca^{2+} channels. *European Journal of Pharmacology*. **375**: 311-325.

Tsunoda S and Salkoff L (1995). Genetic analysis of *Drosophila* neurons: Shal, Shaw and Shab encode most embryonic potassium currents. *Journal of Neuroscience*. **15**: 1741-1754.

Valdivia HH, Smith JS, Martin BM, Coronado R and Possani LD (1988). Charybdotoxin and noxiustoxin, two homologous peptide inhibitors of the K^+ (Ca^{2+}) channel. *FEBS Letters*. **226**: 280-284.

Van Petegem F, Clarke KA, Chatelain FC and Minor DL Jr (2004). Structure of a complex between a voltage-gated calcium channel β-subunit and an α-subunit domain. *Nature*. **429**: 671-675.

Venema VJ, Swiderek KM, Lee TD, Hathaway GM and Adams ME (1992). Antagonism of synaptosomal calcium channels by subtypes of ω-agatoxins. *Journal of Biological Chemistry*. **267**: 2610-2615.

Wadman, M (1997) Dispute over insect resistance to crops. *Nature*. **388:** 817.

Wallner M, Meera, P and Toro L. (1996) Determinant for δ-subunit regulation in high-conductance voltage-activated and Ca^{2+}-sensitive K^+ channels: an

additional transmembrane region at the N terminus. *Proceedings of the National Academy of Sciences of the USA* **93**: 14922–14927

Wang SY and Wang GK (1998). Local anesthetic block of batrachotoxin-resistant muscle Na$^+$ channels. *Molecular Pharmacology*. **54**: 389-396.

Wang X-H, Smith R, Fletcher JI, Wilson H, Wood CJ, Howden MEH and King GF (1999). Structure-function studies of ω-atracotoxin, a potent antagonist of insect voltage-gated calcium channels. *European Journal of Biochemistry.* **264:** 488-494.

Wang X-H (2000a). Discovery and characterization of insecticidal neurotoxins from Australian funnel-web spider venom. PhD Thesis, University of Sydney, Australia.

Wang X-H, Smith R, Connor M, Maciejewski MW, Howden, MEH, Nicholson GM, Christie MJ and King GF (2000b). Discovery and characterization of a family of insecticidal neurotoxins with a rare vicinal disulfide bridge. *Nature Structural Biology*. **7**(6)**:** 505-513.

Wang X-H, Connor M, Wilson D, Wilson HI, Nicholson GM, Smith R, Shaw D, Mackay JP, Alewood PF, Christie MJ and King GF (2001). Discovery and structure of a potent and highly specific blocker of insect calcium channels. *Journal of Biological Chemistry*. **276**: 40306-40312.

Warmke JW, Reenan RA, Wang P, Qian S, Arena JP, Wang J, Wanderler D, Liu K, Kaczorowski GJ, Van der Ploeg LH, Ganetzky B and Cohen CJ (1997). Functional expression of *Drosophila para* sodium channels. Modulation by the membrane protein TipE and toxin pharmacology. *Journal of General Physiology*. **110**: 119-133.

Wei A, Solaro C, Lingle C and Salkoff L (1994). Calcium sensitivity of BK-type K_{Ca} channels determined by a separate domain. *Neuron*. **13**: 671-681.

Wei A, Jegla T and Salkoff L (1996). Eight potassium channel families revealed by the *C. elegans* genome project. *Neuropharmacology*. **35**: 805-829.

West JW, Patton DE, Scheuer T, Wang W, Goldin AL and Catterall WA (1992). A cluster of hydrophobic amino acid residues required fast sodium channel inactivation. *Proceedings of the National Academy of Sciences of the USA*. **89**: 10910-10914.

Wicher D, Walther C and Penzlin H (1994). Neurohormone D induces ionic current changes in cockroach central neurones. *Journal of Comparative Physiology*. **174A**: 507-515.

Wicher D and Penzlin H (1997) Ca^{2+} currents in central insect neurones: electrophysiological and pharmacological properites. *Journal of Neurophysiology*. **77**: 186-199.

Wicher D and Penzlin H (1998). ω-Toxins affect Na^+ currents in neurosecretory insect neurons. *Receptors and Channels*. **5**: 355-366.

Wicher D and Reuter G (1993). Neurohormone D increases the intracellular Ca^{2+} level in cockroach neurones through a Cd^{2+}-sensitive Ca^{2+} influx. *Neuroscience Letters*. **159**: 13-16.

Wood JN and Baker (2001). Voltage-gated sodium channels. *Current Opinion in Pharmacology*. **1**: 17-21.

Wullschleger B, Kuhn-Nentwig L, Tromp J, Kämpfer U, Schaller J, Schürch S and Nentwig W (2004). CSTX-13, a highly synergistically acting two-chain neurotoxic

enhancer in the venom of the spider *Cupiennius salei* (Ctenidae). *Proceedings of the National Academy of Sciences of the USA*. **101**: 11251-11256.

Wullschleger B, Nentwig W and Kuhn-Nentwig L (2005). Spider venom: enhancement of venom efficacy mediated by different synergistic strategies in *Cupiennius salei*. *Journal of Experimental Biology*. **208**: 2115-2121.

Xia XM, Ding JP and Lingle CJ (2003). Inactivation of BK channels by the NH_2 terminus of the $\beta 2$ auxiliary subunit: an essential role of a terminal peptide segment of three hydrophobic residues. *Journal of General Physiology*. **121**: 125-148.

Xu CQ, Brone B, Wicher D, Bozkurt O, Lu WY and Huys I (2004). BmBKTx1, a novel Ca^{2+}-activated K^+ channel blocker purified from the Asian scorpion *Buthus martensi* Karsch. *Journal of Biological Chemistry*. **279**: 34562-34569.

Yamasuto T, Nagal H, Yasumura D, Michishita959,j T, Endo A, Yotsu M and Kotaki Y (1986). Interspecies distribution and possible origin of terodotoxin. *Annuals of the New*. *York*. *Academy of*. *Sciences*. **479**: 44-51.

Yanagawa Y, Abe T and Satake M (1986). Blockade of [^{3}H] lysine-tetrodotoxin binding to sodium channel proteins by conotoxin GIII. *Neuroscience Letters*. **64**: 7-12.

Young L, Jernigan RL and Covell DG (1994). A role for surface hydrophobicity in protein-protein recognition. *Protein Science*. **3**: 717-729.

Zagotta WN, Hoshi T and Aldrich RW (1989). Gating of single Shaker potassium channels in *Drosophila* muscle and in *Xenopus* oocytes injected with Shaker mRNA. *Proceedings of the National Academy of Sciences of the USA*. **86**: 7243-7247.

Zhou XB, Arntz C, Kamm S, Motejilek K, Sausbier U and Wang GX (2001). A molecular switch for specific stimulation of the BKCa channel by cGMP and cAMP kinase. *Journal of Biological Chemistry*. **276**: 43239-43245.

Zhu S, Darbon H, Dyason K, Verdonck F and Tytgat J (2003). Evolutionary origin of inhibitor cystine knot peptides. *FASEB*. **17**: 1765-1767.

Zilberberg N, Froy O, Loret E, Cestèle S, Arad D, Gordon D and Gurevitz M (1997). Identification of structural elements of a scorpion α-neurotoxin important for receptor site recognition. *Journal of Biological Chemistry*. **272**: 14810-14816.